Fractional Calculus Based Methods and Models to Characterize Diffusion in the Human Body

Methoden en modellen op basis van fractionele calculus voor de karakterisering van de diffusie in het menselijk lichaam

Dana Copot

Promotoren: prof. dr. ir. C.-M. Ionescu, em. prof. dr. ir. R. De Keyser
Proefschrift ingediend tot het behalen van de graad van
Doctor in de ingenieurswetenschappen: biomedische ingenieurstechnieken

UNIVERSITEIT GENT

Vakgroep Elektrische Energie, Metalen, Mechanische Constructies en Systemen
Voorzitter: prof. dr. ir. L. Dupré
Faculteit Ingenieurswetenschappen en Architectuur
Academiejaar 2017 - 2018

ISBN 978-94-6355-114-4
NUR 950
Wettelijk depot: D/2018/10.500/32

Ghent University
Faculty of Engineering and Architecture
Department of Electrical Energy, Metals,
Mechanical Constructions and Systems

Promotor: Prof. Dr. Ir. Clara Ionescu
Co-Promoter Prof. Dr. Ir. Robin De Keyser

Ghent University
Faculty of Engineering and Architecture

Department of Electrical Energy, Metals, Mechanical Constructions and Systems
Technologiepark 914, B-9052 Ghent, Belgium

Members of the exam committee:

Chairman:
Prof. Dr. Ir. Patrick De Baets - Faculty of Engineering and Architecture, UGent

Secretary:
Dr. Ir. Annelies Coene - Faculty of Engineering and Architecture, UGent

Examination committee:
Prof. Dr. Ir. Antonio Visioli - Brescia University, Italy
Prof. Dr. Ir. J. Tenreiro Machado - Polytechnic Institute of Porto, Portugal
Prof. Dr. Ir. Pascal Verdonck - Faculty of Engineering and Architecture, UGent
M.D. Martine Neckebroek - University Hospital Ghent, Belgium

Other Members:
Prof. Dr. Ir. Clara Ionescu - Faculty of Engineering and Architecture, UGent
Prof. Dr. Ir. Robin De Keyser - Faculty of Engineering and Architecture, UGent

Thesis submitted for the title of
Doctor of Biomedical Engineering
Academic year 2017-2018

Acknowledgement

When I have started my PhD five years ago, I did not know exactly where this journey will lead me. Along the way, I have met a lot of people who guided me on my journey and show the right path to follow. In this respect, I would like to acknowledge them for their contributions.

Firstly, I would like to express my sincere gratitude to my promoters Prof. Clara Ionescu and Prof. Robin De Keyser for the continuous support during my PhD. I would like to thank them for their patience, motivation, and immense knowledge. Without their guidance and numerous opportunities they have offered to me during these years, this book would not exist. I want to thank Prof. Clara Ionescu, who was not just my promoter but she was my mentor, my friend, my role model. During these years she always inspired and motivated me to never give up and she always encouraged and supported me to go further.

Besides my promoters, I would like to thank to M.D. Martine Neckebroek from Ghent University Hospital for the interesting and useful discussions, and for having the patience and good-will to help me with the preparation of the ethical committee files for clinical trials. Additionally, I thank all the members of the jury for their interest and for reading this dissertation.

I would like to thank to my colleagues, who provided a friendly atmosphere during many hours of work, but also for taking part in the measurement campaign for testing the latest technology developed in our research group. Also, many thanks to my friends, Ir. Adelina and Ir. Zuf, for making time to come to the lab to participate in the measurement campaign.

I would like to thank to my husband for always being there for me, especially during difficult times. Also, many thanks to my parents and sisters, who encouraged me to go further whenever the light at the end of the tunnel seemed un-existent. I would also like to thank to my little daughter Sofia (2 months old) because thanks to her now I can give a definition of pain.

This dissertation presents research results which were financially supported by the following grants: FWO Research Project: Development of a generic patient parameterizable model to describe pain-relief levels during general anesthesia, project nr. G026514N, 2014-2017. FWO Research Project: Detection and Validation of changing viscoelastic effects in the respiratory system with disease, project nr. G008113N, 2013-2016.

Ghent, April 2018
Dana Copot

Table of Contents

List of Tables

List of Figures

List of Symbols

Defined in Chapter 2:

- T_{in} - Heating temperature at front of the wall
- P_{in} - Heat flux at front of the wall
- T_{out} - Heating temperature at back of the wall
- P_{out} - Output heat flux
- A, B, C, D - Matrix coefficients
- λ - Thermal conductivity
- a - Thermal diffusivity
- ρ - Mass density
- c - Specific heat
- S_w - Cross-section of the wall
- L - Surface length
- α - Recursive factor
- m - Fractional operator

Defined in Chapter 3:

- P - Pressure
- Q - Flow
- P_0 - End expiration
- $1/C$ - Elastance
- V - Volume
- R - Resistance
- I - Inertia

- ν - Poisson coefficient
- μ - Viscosity
- ρ - Density
- l - Length of the airway tube
- $M1$ - Modulus of Bessel function of order 1
- ϵ_1 - Phase angle
- δ - Womersley parameter
- r - Wall radius
- h - Wall thickness
- Re - Resistance in first airway
- Ce - Compliance in first airway
- γ - Ratio of resistances/total level
- χ - Ratio of compliances/total level
- K - Gain factor
- n - Fractional order operator
- Z_n - Inverse of admittance
- G_r - Tissue damping
- H_r - Tissue elastance
- η_r - Tissue hysteresivity
- T - Nonlinear index
- r_1 - Inner radius
- r_2 - Outer radius
- R_i - Resistance of cell i
- C_i - Compliance of cell i
- P_i - Pressure profile along cell face
- N - Total number of cells
- c - Specific heat

- Y_t - Total admittance
- λ - Thermal conductivity

Defined in Chapter 5:

- q_1, q_2, q_3, q_3 - Drug amount in compartment 1, 2 and 3
- V_1, V_2, V_3 - Volume of compartment 1, 2, 3
- $U(t)$Infusion rate
- Cl_1, Cl_2, Cl_3 - Clearance in compartment 1, 2, 3
- lbm - Lean body mass
- C_e - Effect site concentration
- K_{ij} - drug transfer frequency from $i^{th}$to j^{th} compartment
- E_0 - Effect before surgery
- E_{max} - Maximum effect
- C_{50} - Drug amount at half maximal effect
- γ - Patient sensitivity parameter
- n - Fractional order operator
- h - Sampling period
- τ - Escape rate
- θ - Drug ratio
- μ - Rate parameter

Defined in Chapter 6:

- n - Fractional order operator
- R_0 - High-frequency resistor
- R_∞ - Low-frequency resistor
- τ_α - Relaxation time
- V_0 - Voltage amplitude
- Θ - Phase angle
- $D^n(j\omega)^n$ - Weyl derivative

- β - Imaginary part of fractional operator
- α^* - Real part of fractional operator
- D - Diffusion coefficient
- k - Clearance rate
- λ - Tortuozity
- α - Porosity

List of Acronyms

Defined in Chapter 1:

$COPD$	Chronic obstructive pulmonary disease
ECG	Electrocardiogram
FO	Fractional order
LDE	Linear partial equations

Defined in Chapter 4:

BP	Blood pressure
BPS	Behavioral pain scale
$BPRS$	Behavioral pain rating scale
$CPOT$	Critical care pain observational tool
HR	Heart rate
ICU	Intensive care unit
LOC	Level of consciousness
NIH	National institute for health
NOL	Nociception level
NRS	Numerical rating scale
$NVPS$	Nonverbal pain scale
$PAIN$	Pain assessment and intervention notation
$PBAT$	Pain behavior assessment tool
PPI	Pain pupillary index
PRD	Pupillary reflex dilatation
SC	Skin conductance
SCR	Skin conductance response
VAS	Visual analogue scale
VRS	Verbal rating scale

Defined in Chapter 5:

$ADME$	Absorption, Distribution, Metabolism, Elimination
BIS	Bispectral index
FDE	Fractional differential equations
ODE	Ordinary differential equation
PK	Pharmacokinetics
$PK-PD$	Pkarmacokinetics-pharmacodynamics

Defined in Chapter 6:

ECF	Extracellular fluid
EEG	Electroencephalogram
CPE	Constant phase element
GCT	Gate control theory
$GCPE$	Generalized constant phase element
K	Potassium
MRI	Magnetic resonance imaging
Na	Sodium

Nederlandse samenvatting –Summary in Dutch–

Fractionele calculus kan beschouwd worden als een veralgemening van klassieke afgeleiden en integralen, waarbij de orde nu ook niet-geheel kan zijn. Principes en methodes uit de fractionele calculus zijn ook van nut voor systemen die kunnen worden gemodelleerd door fractionele differentiaalvergelijkingen (die dus afgeleiden van niet-gehele orde bevatten). Dit worden fractionele-orde (FO) systemen genoemd en ze zijn nuttig om een atypisch gedrag (bijvoorbeeld diffusie) van dynamische systemen te karakteriseren. Voor een gehele-orde systeem varieert de magnitude in de Bode karakteristiek met een geheel veelvoud van 20 $dB/decade$ ($\pm$20 dB/dec, $\pm$40 dB/dec, ...) en de fase met een geheel veelvoud van 90° ($\pm$ 90°, $\pm$180 °, ...). Voor een FO systeem met een fractionele orde n varieert de magnitude met $n \cdot 20$ dB/dec en evenzo zal de fase varieren met $n \cdot 90°$.

Dynamische systemen die op een natuurlijke wijze aan de hand van fractionele orde modellen kunnen beschreven worden vertonen specifieke kenmerken, zoals visco-elasticiteit, diffusie en een fractale structuur. Het ademhalingssysteem is hiervan een ideaal voorbeeld. Hoewel de visco-elastische en diffuse eigenschappen van het ademhalingssysteem reeds intensief werden onderzocht, werd de fractale structuur tot nog toe genegeerd. Een van de redenen is wellicht dat de luchtwegen geen perfecte symmetrie vertonen, dus niet echt voldoen aan een van de voorwaarden om een typisch fractale structuur te zijn. Toch kan men een zekere mate van recurrentie herkennen in de modellen die worden gebruikt voor het beschrijven van de luchtwegenstructuur. In dit proefschrift zal de fractionele calculus toegepast worden om de gasdiffusie in de menselijke longen te modelleren en om de geneesmiddelendiffusie in het menselijk lichaam te karakteriseren.

Het ademhalingsstelsel bezit de drie hierboven opgesomde eigenschappen en er is geen enkele reden waarom men een van deze zou moeten negeren. Bovendien wordt in het geval van aandoeningen de visco-elasticiteit beinvloed door veranderingen op cellulair niveau die ook de oorzaak zijn van lokale vernauwingen en afsluitingen, die dan op hun beurt een invloed hebben op zowel de structuur van het luchtwegenstelsel als op de diffusieoppervlakte. Als een specifiek model (bv. een elektrisch analogon) van de luchtwegen zou bestaan, dan zou dit kunnen gebruikt worden voor simulatiedoeleinden, zowel bij gezonde als bij pathologische gevallen.

In de alveoli van zoogdierlongen diffundeert zuurstof door verschillen in partile druk over het alveolaire capillaire membraan. De longen hebben een grote

diffusieoppervlakte om dit gasuitwisselingsproces te vergemakkelijken. Eigenlijk kan de verspreiding van om 't even welke grootheid die kan worden beschreven door de diffusievergelijking of door een *random walk* model (bijvoorbeeld concentratie, warmte, enz.) diffusie worden genoemd. Verschillende factoren zoals pathologien, lichaamsbeweging en een ongebruikelijke omgeving, kunnen de gasuitwisseling in de longen beperken (d.w.z. de zuurstof beperken die de longen binnendringt). Bij sommige ziekten, zoals emfyseem en interstitile longziekte, wordt het capillaire bed verminderd, wat resulteert in een verminderde tijd beschikbaar voor bloedoxygenatie. Bij longoedeem en interstitile fibrose kan daarentegen de bloed-gas barrire abnormaal worden verdikt wat dan de diffusiecapaciteit vermindert. In dit proefschrift wordt de relatie bestudeerd tussen wiskundige modellen voor diffusie enerzijds en niet-invasieve metingen van de longfunctie anderzijds.

De tweede toepassing van diffusie die in dit proefschrift wordt behandeld is de verspreiding van medicijnen in het menselijk lichaam. Ten behoeve van het regelen van anesthesie kan wiskundige modellering van medicijndiffusie erg nuttig zijn om het mechanisme van medicijnafgiftesystemen beter te begrijpen. De beschrijving van medicijntransport in het menselijk lichaam stelt ons in staat om enerzijds het mechanisme te begrijpen en om anderzijds een kwantitatieve voorspelling te doen van de effecten van formulering en verwerkingsparameters op de resulterende medicijnafgiftekinetiek. De grootste uitdaging bij de ontwikkeling en optimalisatie van geautomatiseerde systemen voor toediening van geneesmiddelen is het bereiken van een optimale geneesmiddelenconcentratie op de plaats van actie. Om het optimale concentratie-tijd profiel op de plaats van actie te hebben, moet de afgifte van het geneesmiddel zo nauwkeurig mogelijk worden geregeld.

Drie componenten bepalen de algemene anesthesietoestand van de patint: hypnose (gebrek aan bewustzijn, gebrek aan geheugen), analgesie (gebrek aan pijn) en neuromusculaire blokkade (gebrek aan beweging). In de literatuur zijn verschillende schema's voor het induceren en handhaven van hypnose en neuromusculaire blokkade voorgesteld. Deze twee deelcomponenten van anesthesie zijn momenteel tot voldoende rijpheid gekomen om hen te integreren in n enkel platform voor klinische anesthesie. Hypnotische en opiode (pijnstillende medicatie) bijwerkingen resulteren in veranderingen in andere biosignalen zoals hartslag, ademhalingssnelheid, gemiddelde arterile druk, gas in- en uitademingspercentages, lichaamstemperatuur, enz. Binnen het anesthesie-paradigma is de detectie en het kwantificeren van pijn - via een objectieve meting die wordt ondersteund door een wiskundig model - nog steeds een ontbrekend stuk in de puzzel (ondanks enkele monitoren die recent op de markt beschikbaar gekomen zijn, bv. Medstorm, Medasense, Algiscan). Op zich is pijn een zeer complex proces, waarbij een groot aantal chemische, fysische en elektrische subprocessen betrokken zijn, allemaal gebundeld in n grootschalig systeem.

In dit proefschrift zijn de eerste stappen gezet in de richting van enerzijds een sensor om het pijnniveau op een objectieve manier te meten en anderzijds een model om mathematisch de signaalroutes van nociceptor-excitatie te modelleren. Het resultaat is de ANSPEC-PRO monitor, die op een niet-invasieve manier de pijn meet door middel van huidimpedantie. Het prototype is op dit moment alleen

gevalideerd bij wakkere vrijwilligers met zelf-geinduceerde nociceptor-excitatie (d.w.z. mechanische pijnstimuli). Deze eerste resultaten moeten het pad effenen naar een compleet regelplatform voor algemene anesthesie door middel van zijn drie componenten: hypnose, analgesie en neuromusculaire blokkade.

Dit proefschrift is als volgt gestructureerd:

In Hoofdstuk 1 wordt een korte geschiedenis van fractionele calculus beschreven evenals het gebruik ervan in de biomedische ingenieurstechnieken.

Hoofdstuk 2 behandelt de diffusietheorie in poreuze media. De inleidende concepten over diffusie voorgesteld in dit hoofdstuk worden verder in het proefschrift toegepast bij het modelleren van diffusie in de longen en bij geneesmiddelendiffusie in het menselijk lichaam.

In Hoofdstuk 3 wordt gedetailleerd beschreven hoe de principes en methodes uit de fractionele calculus gebruikt kunnen worden voor de modellering van het ademhalings-systeem. De diffusieconcepten worden besproken vanuit het perspectief van gasuitwisseling in de longen en met betrekking tot de wijze waarop de diffusiefactor de voortgang van ziektes benvloedt.

In Hoofdstuk 4 wordt een geleidelijke overgang van het modelleren van diffusie in de longen naar het modelleren van geneesmiddelendiffusie voorgesteld. Een gedetailleerde beschrijving van de bestaande methodes en tools voor pijnbeoordeling samen met hun voor- en nadelen wordt voorgesteld. Dit hoofdstuk leidt tot het besluit dat er geen mathematisch-fysiologisch gebaseerd model beschikbaar is voor de beschrijving van de nociceptieve route. Deze uitdaging wordt verder behandeld in hoofdstukken 5 en 6.

Hoofdstuk 5 introduceert het gebruik van diffusieprocessen voor de karakterisatie van de werking van een geneesmiddel. Om de evolutie van de geneesmiddelen in het menselijk lichaam te beschrijven worden er compartimentele farmacokinetische en farmaco-dynamische modellen gebruikt. In dit hoofdstuk wordt een analyse van atypische diffusie gellustreerd en wordt het farmaco-kinetisch model herzien.

In Hoofdstuk 6 worden de eerste stappen gezet in de richting van een mathematisch model voor nociceptie en een geconcentreerd fractionele orde model wordt afgeleid. Dit model werd gevalideerd met metingen uitgevoerd met de recentste technologie voor pijnbeoordeling. De resultaten bekomen voor de pijnevaluatie bij een groep van vrijwilligers worden weergegeven.

De besluiten van dit doctoraatsproefschrift worden voorgesteld in Hoofdstuk 7.

English summary

Fractional calculus is a generalization of classical integer-order integration and differentiation (non-integer) order operators. Tools from fractional calculus can be also used for general systems that can be modeled by fractional differential equations containing derivatives of non-integer order. These are called fractional order systems they are useful to characterize anomalous behavior (e.g. diffusion) of dynamical systems. In the case of an integer order system, the magnitude varies with an integer multiple of 20 dB/dec ($\pm 20 dB/dec$, $\pm 40 dB/dec$, etc) and the phase with an integer multiple of 90° (± 90°, ± 180°). In the case of fractional order systems, the magnitude varies with $n \cdot 20 dB/dec$ and the phase will vary with $n \cdot 90$ ° (n is the fractional order operator).

Dynamical systems whose model can be approximated in a natural way using FO terms, exhibit specific features, such as viscoelasticity, diffusion and a fractal structure; hence the respiratory system is an ideal application for FO models. Although viscoelastic and diffusive properties were intensively investigated in the respiratory system, the fractal structure was ignored. Probably one of the reasons is that the respiratory system does not pose a perfect symmetry, hence failing to satisfy one of the conditions for being a typical fractal structure. Nonetheless, some degree of recurrence has been recognized in the airway generation models.

The respiratory system poses all three properties enumerated above and there is no reason why one should ignore either one of them. Moreover, with pathology, viscoelasticity is affected by changes at the cellular level, narrowing or occluding the airway, which in turn affects both the structure of the airway distribution, as well as the diffusion area. If a specific model (e.g. an electrical analogue) of the respiratory tree would exist, it would allow simulation studies in both healthy and pathology scenarios.

In the alveoli of mammalian lungs, due to differences in partial pressures across the alveolar-capillary membrane, oxygen diffuses out. Lungs contain a large surface area to facilitate this gas exchange process. Finally, the spreading of any quantity that can be described by the diffusion equation or a random walk model (e.g. concentration, heat, etc.) can be called diffusion. Several factors such as: pathologies, exercise and unusual environment can limit the gas exchange in the lungs (i.e. limit the O_2 entering the lungs). In some diseases such as emphysema and interstitial lung disease, the capillary bed is reduced resulting in a decreased time available for blood oxygenation. In pulmonary edema and interstitial fibrosis, instead, the blood-gas barrier may be thickened abnormally and the diffusing capacity reduced. In this thesis a relation to diffusion in the lungs by means of

mathematical modeling and non-invasive measurements is being proposed.

The second application of diffusion considered in this thesis is drug diffusion. From the point-of-view of regulating anesthesia, mathematical modeling of drug diffusion can be very useful to better understand the mechanism of drug delivery systems. Therefore, the description of drug transport into the human body can be highly beneficial and allows us to understand the insight of the mechanism and to do quantitative prediction of the effects of formulation and processing parameters on the resulting drug release kinetics. The major challenge in the development or optimization of automated drug delivery systems is to achieve optimal drug concentration at the site of action. In order to have the optimal concentration-time-profile at the site of action the release of the drug must be controlled as accurately as possible.

Three components define the general anesthesia state of patient: hypnosis (lack of awareness, lack of memory), analgesia (lack of pain) and neuromuscular blockade (lack of movement). In literature several schemes to induce and maintain hypnosis and neuromuscular blockade have been proposed. These two aspects of anesthesia are now mature for integration in a single environment. Hypnotic and opioid (analgesic medication) side-effects mark changes in other biosignals as heart rate, respiratory rate, mean arterial pressure gas in- and ex-piratory percentages, body temperature, etc. Until recently, within the anesthesia regulation paradigm, detecting and quantifying pain with an objective measure supported by means of a mathematical model is still a missing piece in the puzzle, despite the few available monitors available just recently on the market (e.g. Medstorm, Medasense, Algiscan). As such, pain is a complex process, involving a manifold of chemical, physical and electrical sub-processes all sequenced in a systemic context.

In this thesis the first steps towards a sensor to measure the pain level in an objective manner and a mathematical model to characterize nociception pathway have been made The result is the ANSPEC-PRO monitor, non-invasively measuring pain by means of skin impedance. The prototype has been validated at this moment only in awake volunteers with self-induced nociceptor excitation (i.e. mechanical pain stimuli). These first results will enable the next steps towards a complete regulatory dynamic system for controlling general anesthesia by means of its all three components: hypnosis, analgesia and neuromuscular blockade.

A brief description of the thesis outline is given hereafter.

In **Chapter 1** a brief history of fractional calculus and its application in several domains is given. The use of fractional calculus in field of biomedical engineering is also introduced.

Chapter 2 addresses the theoretical preliminaries of diffusion phenomena in porous media. Tools from this chapter will be further employed for the particular cases investigated in this thesis.

In **Chapter 3** a detailed description on the use of fractional calculus tools to model the respiratory system is discussed. The diffusion concepts are discussed from the perspective of gas exchange in the lungs and how the diffusing factor influences the progress of disease.

In **Chapter 4** a soft transition from modeling diffusion in the lungs to mod-

eling drug diffusion is presented. Here, a detailed description of the existing methods and tools for pain assessment along with their advantages and disadvantages is given. From this chapter we have concluded that no mathematically-physiologically based model to characterize the nociceptor pathway is available. This challenge is further addressed in Chapter 5 and 6.

Chapter 5 introduces the use of diffusion processes to characterize drug effect. To describe the evolution of drugs in the human body the compartmental pharmacokinetic-pharmacodynamic models are used. In this chapter an analysis of the anomalous diffusion is illustrated and a revisited pharmacokinetic model is presented.

In **Chapter 6** the first steps towards a mathematical model of nociception are taken and a fractional order model is derived. This model has been validated on measurements performed with the latest technology for pain assessment followed by the obtained results. The conclusions of this thesis are presented in **Chapter 7**.

1 Introduction

1.1 Brief History of Fractional Calculus

Fractional calculus (FC) is an extension of ordinary calculus with more than 300 years of history. FC was initiated by Leibniz and L'Hospital as a result of a correspondence which lasted several months in 1695. The issue raised by Leibniz for a fractional derivative (semi-derivative, to be more precise) was an ongoing topic in decades to come. Subsequent references to fractional derivatives were made by Lagrange in 1772, Laplace in 1812, Lacroix in 1819, Fourier in 1822, Riemann in 1847, Green in 1859, Holmgren in 1865, Grunwald in 1867, Letnikov in 1868, Sonini in 1869, Laurent in 1884, Nekrassov in 1888, Krug in 1890, Weyl in 1919, and others [1, 2].

It is interesting to note that simultaneously with these initial theoretical developments, first practical applications of fractional calculus can also be found [3]. Abel's solution had attracted the attention of Joseph Liouville, who made the first major study of fractional calculus. Probably the most useful advance in the development of fractional calculus was due to a paper written by G.F. Bernhard Riemann. Unfortunately, the paper was published only posthumously in 1892. Seeking to generalize a Taylor series in 1853, Riemann derived different definition that involved a definite integral and was applicable to power series with non-integer exponents. The earliest work that ultimately led to what is now called the Riemann-Liouville definition appears to be the paper by N. Ya. Sonin in 1869 where he used Cauchy's integral formula as a starting point to reach differentia-

tion with arbitrary index. A. V. Letnikov extended the idea of Sonin a short time later in 1872 [4]. Both tried to define fractional derivatives by utilizing a closed contour. Starting with Cauchy's integral formula for integer order derivatives.

Grunwald and Letnikov provided the basis for another definition of fractional derivative which is also frequently used today. Today, the Grunwald-Letnikov definition is mainly used for derivation of various numerical methods with finite sum to approximate fractional derivatives. Among the most significant modern contributions to fractional calculus are those made by the results of M. Caputo in 1967 [5]. One of the main drawbacks of Riemann-Liouville definition of fractional derivative is that fractional differential equations with this kind of differential operator require a rather strange set of initial conditions. Caputo [5] reformulated the more classic definition of the Riemann-Liouville fractional derivative in order to use classical initial conditions, the same one needed by integer order differential equations.

1.2 Fractional Calculus in Biomedical Engineering

Fractal time series analysis, and implicitly fractional calculus, have been used to improve the modeling accuracy of many phenomena in natural sciences [6]. The fractional order derivative model is appropriate for modeling complex dynamics, eg. ions undergoing anomalous diffusion in dielectrics. Fractional order models are a generalizations of the classical integer order models. The net advantage is that fractional differ-integration enables the inclusion of memory and hereditary properties in models for processes governed by diffusion in all its aspects (i.e. sub-diffusion, classical and super-diffusion).

The complexity of all living systems is expressed in the structure and function of each cell and tissue. Thus, the biological functions of cardiac muscle, articular cartilage and the spinal cord, for example, are embedded in the three-dimensional structure of each tissues cells, extracellular matrix, and overall anatomical organization. In the heart, tight electrical contacts between cardiac cells ensure that the pacemaker signals are distributed sequentially to the atria and ventricles; in the knee, the multiple layers within hyaline cartilage distribute transient loads by the rapid movement of ions and water; while in the axons of the spinal cord, sensory input and reflexes are expressed via electrical signals action potentials that are directed through complex neural networks.

For many physiological systems (e.g., action potential propagation, blood oxygenation, and feedback control of insulin secretion) linear differential equation (LDE) models are highly successful. These models provide the basis for our understanding of normal physiological homeostatis, as well as the changes in system dynamics that bring on or are the consequences of disease. Physiological models describe events both at the molecular level (ion transport, gas diffusion, vesicle

formation) and at the organ level (e.g. blood clearance, oxygen uptake, etc.). The extent to which a fractional order model will span multiple scales (the nanoscale, microscale, mesoscale, and macroscale) is based on an underlying presumption that fractional derivatives can capture features of complex tissue structure. Current work in fractional calculus is directed at answering the questions of where and when such models are valid. However, the multiscale patterns observed in muscle fibers, tendon and nerve fibers provide a structural rationale for the hypothesis that multiscale structure is effectively encoded in fractional order operations.

The extension of linear systems to include fractional order theory requires learning a new mathematical tool; a tool with which there are substantial issues associated with identifying the appropriate initial conditions and in selecting the proper definition of fractional integration to be used for a given problem [7, 8]. Relaxation processes are common in cells and tissues. Therefore, it should not be surprising to see that fractional calculus can play an important role in describing the input-output behavior of biological systems The physical foundations for this behavior may be sought in the fractal or porous structure of the system components or in the physical characteristics of its surfaces and interfaces. Much work [9] is ongoing to develop a direct link between fractal models of molecules, surfaces, and materials and the fractional kinetics or dynamics of the resulting behavior (polymerization electrochemical reactions, viscoelastic relaxation).

A major attribute of fractional dynamic models is that they interpolate between the known integer order behavior by extending the transfer function models from rational algebraic functions of the Laplace transform parameter s to non-rational functions $f(s)$ involving fractional powers of s^{α}. This is an approach that extends the traditional Laplace transform methods of linear systems analysis [10]. Hence, the fractional dynamics hypothesis is accessible to the engineer and scientist through both Laplace and Fourier techniques (for $s = j\omega$ where $j = \sqrt{-1}$ and ω is the angular frequency in rad/s).

Diffusion plays an important role in many processes in living organism, is a key feature in the course of drug distribution in the human body. The research performed in the last decades suggest diffusion processes can deviate from Fick's first law. They can be either faster (super-diffusion) either slower (sub-diffusion) processes [11, 12]. This new approach of diffusion processes is described as anomalous diffusion. In biomedical literature several datasets have been characterized by power-laws [13], gamma functions or fractal kinetics [11, 12], and their use has been justified by the presence of the anomalous diffusion. It has been shown that fractional calculus is an alternative theory that can describe this anomalous behavior [11–13]. In the past many attempts to model the diffusion process have been made and fractional order models have been shown to well-characterize these processes. The last decade has shown an increased interest in the research community to employ parametric model structures of fractional order (FO) for analyzing

nonlinear biological systems [11, 12, 14, 15]. The advantage of using tools from fractional calculus over the standard integer order modeling approaches is that it can describe very well the inherent abnormal or heavy tail decay processes.

1.3 Contributions of this thesis

In this thesis the diffusion process will be addressed from the perspective of two applications: diffusion of gas exchange in the lungs and drug diffusion. Diffusion is of fundamental importance in many disciplines of physics, chemistry and biology. It is well known that the fractional operator $\frac{d^{0.5}}{dt^{0.5}} \longleftrightarrow s^{0.5}$ appears in several types of problems [16, 17]. The transmission lines or the heat flow are examples where the half-operator is the fundamental element. Diffusion is in fact part of transport phenomena, being one of the essential partial differential equations of mathematical physics. Molecular diffusion is generally superimposed on, and often masked by, other transport phenomena such as convection, which tend to be much faster. However, the slowness of diffusion can be the reason for its importance. Transport due to diffusion is slower over long length scales: the time it takes for diffusion to transport matter is proportional to the square of the distance. In cell biology, diffusion is the main form of transport for necessary materials such as amino acids within cells. Metabolism and respiration rely in part upon diffusion in addition to active processes.

In the alveoli of mammalian lungs, due to differences in partial pressures across the alveolar-capillary membrane, oxygen diffuses out. Lungs contain a large surface area to facilitate this gas exchange process. Finally, the spreading of any quantity that can be described by the diffusion equation or a random walk model (e.g. concentration, heat, etc.) can be called diffusion. Several factors such as: pathologies, exercise and unusual environment can limit the gas exchange in the lungs (i.e. limit the O_2 entering the lungs). In some diseases such as emphysema and interstitial lung disease, the capillary bed is reduced resulting in a decreased time available for blood oxygenation. In pulmonary edema and interstitial fibrosis, instead, the blood-gas barrier may be thickened abnormally and the diffusing capacity reduced. If the diffusion coefficient decreases, oxygen diffusion is impeded and as a consequence the rise in partial pressure when oxygen enters a red blood cell is slowed down. In both situation, the partial pressure of oxygen may not reach that of alveolar gas before the end of the pulmonary capillary.

Diffusion in lungs can be also stressed by a decrease of the alveolar oxygen partial pressure, e.g. when the subject reaches high altitude or breathes a low oxygen mixture. In fact, this reduces the partial pressure difference responsible for driving the oxygen across the blood-gas barrier. Moreover, during exercise, the pulmonary blood flow increases, causing pulmonary capillary transit time to fall. For example, during severe exercise the time spent by the red cell in the pulmonary

capillaries may be brought down to as little as one-third, resulting in a reduced time for oxygenation. Despite this, in healthy subjects, breathing normal air, the fall in the end-capillary is generally not measurable. However, if the blood-gas barrier of the subject is considerably thickened by disease the difference between alveolar and end-capillary is noticeable. For instance, chronic obstructive pulmonary disease (COPD), defined by airflow limitation, is associated with an important reduction in physical activity. This leads to patient's disability an poor health-related quality of life. Diffusing capacity for carbon monoxide is a common clinical test that provides a quantitative measure of gas transfer in the lungs. A decrease in diffusing capacity (one of the first signs of disease progression) indicated arterial oxygen desaturation during exercise. In case of subjects with COPD a decrease in diffusing capacity poses a high risk for poor survival.

The main contribution on this first application is a relation to diffusion in the lungs by means of mathematical modeling and non-invasive measurements. The main results are presented in Chapter 3.

The second application of diffusion considered in this thesis is drug diffusion. From the point-of-view of regulating anesthesia, mathematical modeling of drug diffusion can be very useful to better understand the mechanism of drug delivery systems. Therefore, the description of drug transport into the human body can be highly beneficial [18–20] from two points-of-view: (i) allows you to understand the insight of the mechanism and (ii) allows you to do quantitative prediction of the effects of formulation and processing parameters on the resulting drug release kinetics. The major challenge in the development or optimization of automated drug delivery systems is to achieve optimal drug concentration at the site of action. In order to have the optimal concentration-time-profile at the site of action the release of the drug must be controlled as accurately as possible.

Diffusion phenomena has been extensively investigated in the last years in the field of drug delivery systems. One of the most common methods to describe the diffusion phenomena of drug in the human body is the compartmental modeling. This analysis is based on mathematical models, typically in the form of systems of ordinary differential equations that are widely used to characterize the time of uptake and elimination of a drug. Diffusion represents a key process in the uptake of drugs by the human body. Processes such as membrane permeability, dissolution of solids and dispersion in cellular matrices are considered to be governed by diffusion [12, 15]. It has been observed that faster processes (*super-diffusion*) or slower processes (*sub-diffusion*) can be modeled by fractional-order derivatives with an order greater or less than 1, respectively. It has been shown that differential equations with fractional derivatives and integrals describe anomalous diffusion more accurately [21, 22].

The main contribution on the second application investigated in this thesis is a proof that pharmacokinetic-pharmacodynamic drug diffusion models are charac-

terized by memory effects. This justifies the use fractional order tools to model these processes. The results obtained are presented in Chapters 5 and 6.

1.4 Thesis outline

In this thesis the use of fractional calculus tools with applications to respiratory system and nociception pathway modeling is addressed. The outline of the thesis is presented hereafter:

In **Chapter 1** a brief history of fractional calculus and its application to several domains is given. Next, a more detailed description on the use of these tools in biomedical engineering is provided. In this chapter the importance and the advantages of using fractional calculus tools to describe complex phenomena (e.g. diffusion) is introduced. The main contributions of this thesis along with the related list of publication are also given.

In **Chapter 2** the preliminaries on diffusion theory are presented. Here, the mathematical concepts and definition of diffusion through porous media are addressed. Based on the focus of this thesis, three modelling approaches are considered: i) longitudinal diffusion, spherical diffusion and molecular diffusion. Theoretical concepts introduced in this chapter, will be further used to characterize diffusion of gas in human lung and drug diffusion in the human body.

In **Chapter 3** a detailed description on the use of fractional calculus tools to model the respiratory system is addressed. The diffusion concepts are discussed from the perspective of gas exchange in the lungs and how the diffusing factor influences the progress of disease. Based on the theory presented in previous chapter a fractional order impedance model has been derived. First, the impedance for one alveolus has been simulated followed by a network of alveoli. The main contribution in this chapter is a first link between diffusion phenomena in the lungs and chronic obstructive pulmonary disease, by means of mathematical models. Parameters such as tissue damping (reflecting the capacity for energy absorption) and tissue hysteresivity have been used to investigate if there is a link between changes in small airways and the diffusion phenomena.

In **Chapter 4** a soft transition from modeling diffusion in the lungs to modeling drug diffusion is presented. Here, a detailed description of the existing methods and tools for pain assessment along with their advantages and disadvantages is given. In clinical practice, the most used tool for pain assessment (for communicative patients) are the numerical and visual rating scales. For the non-communicative patients several attempts to develop a tool to evaluate pain have been made. Despite the advances in pain research and management, the assessment of pain in an objective way (for both cases, communicative and non-communicative patients) remains a challenge. In the last years, a few devices

have been developed towards an objective assessment of pain, but there is not enough clinical validation of these devices and therefore they are not part of the daily clinical routine. Moreover, from this chapter we have concluded that no mathematically-physiologically based model to characterize the nociceptor pathway is available. This challenge is further addressed in Chapter 5 and 6.

In **Chapter 5** an introduction on the use of diffusion processes to characterize drug effect is given. To describe the evolution of drugs in the human body the compartmental pharmacokinetic-pharmacodynamic models are used. In this chapter a preliminary step towards a nociceptor pathway model is presented. Understanding and characterizing the drug transport (diffusion) in the human body allows us to understand the insight of the diffusion process and provides us a way to predict the effects on the drug release kinetics. When a drug (for pain relief) is given to a patient the nociception is inhibited. Understanding phenomena such as drug uptake, distribution and elimination will give extra insight which can be further used in developing a mathematical model of nociception. In this chapter an analysis of the anomalous diffusion is illustrated and a revisited pharmacokinetic model is presented.

In **Chapter 6** the first steps towards a mathematical model of nociception are taken and a fractional order impedance model is derived. For validation purposes an in-house prototype device for continuous measurement of skin impedance has been developed. This custom-made device allows us to excite the skin with an multisine as an input signal (i.e. sending in a voltage) and measuring the corresponding output (i.e. the current). A brief description of the device is given in Appendix A. In this chapter four mathematical models have been investigated (i.e. Cole-Cole impedance model, non-parametric impedance model, interlaced zero-pole impedance model and the developed lumped fractional order impedance model) and validated using the developed device for pain assessment.

In **Chapter 7** the conclusions of this thesis are presented followed by the future perspectives beyond this doctoral thesis.

1.5 Publications

Here a selected list of publications (directly related to the research presented in this thesis) is given. The publications where tools from modeling, identification and control of dynamical systems are employed is given in Appendix D.

Publications in international journals (A1)

1. C.M. Ionescu, A. Lopes, **D. Copot**, J.A.T. Machado, J. Bates. The Role of Fractional Calculus in Modelling Complex Phenomena and Underlying Structure in Biology, Communications in Nonlinear Science and Numerical Simulation, 51, 141-159, 2017.
2. **D. Copot**, R. De Keyser, J. Juchem, C.M. Ionescu, Fractional order impedance model to estimate glucose concentration: in vitro analysis. Acta Polytechnica Hungarica, 14(1), 207-220, 2017.
3. **D. Copot**, C.M. Ionescu, R. De Keyser. Structural changes in the COPD lung and related changes in diffusion mechanism, PLOS ONE Journal, 12(5), doi.org/10.1371/journal.pone.0177969, 2017.
4. **D. Copot**, R. Magin, R. De Keyser, C.M. Ionescu, Data-driven modelling of drug tissue trapping using anomalous kinetics, Chaos, Solitons and Fractals, 102, 441-446, 2017.
5. C. Ionescu, **D. Copot**, Monitoring respiratory impedance by wearable sensor device: protocol and methodology, Biomedical Signal Processing and Control, 56-62, 2017
6. I. Assadi, A. Charef, **D. Copot**, R. De Keyser, T. Bensouici, C.M. Ionescu, Evaluation of respiratory impedance properties by means of fractional order models, Biomedical Signal Processing and Control, 34, 206-213, 2017.
7. **D. Copot**, R. De Keyser, E. Derom, M. Ortigueira, C.M. Ionescu. Reducing bias in fractional order impedance estimation for lung function evaluation, Biomedical Signal Processing and Control, 39, 74-80, 2018.
8. **D. Copot**, C.M. Ionescu, Pain monitoring tools: a systematic review, Journal of Clinical Monitoring and Computing, 2018, submitted.
9. **D. Copot**, C.M. Ionescu, Models for nociception stimulation and memory effects in awake and aware healthy individuals, IEEE Transactions on Biomedical Engineering, 2018, submitted.
10. **D. Copot**, C.M. Ionescu, Prototype and methodology for non-invasive nociception stimulation and related pain assessment in awake individuals, IEEE Transactions on Measurements and Instrumentaion, 2018, submitted.

Publications in international journals (A2)

1. C.M. Ionescu, **D. Copot**, R. De Keyser, Three compartmental model for Propofol diffusion during general anesthesia, Journal of Discontinuity, Nonlinearity and Complexity, 2(4), 357-368, 2013.

2. **D. Copot**, C.M. Ionescu, Objective Pain Assessement: How far are we?, E Cronicon Anesthesia Journal, Special Issue on Critical Care and Importance of Anaesthesia for Pain Relief, SI 01, 11-14, 2018.

3. **D. Copot**, C.M. Ionescu, A fractional order controller for delay dominant systems. Application to a continuous casting line, Journal of Applied Nonlinear Dynamics, in print.

Books

1. D. Copot and C.M. Ionescu, Automated Drug Delivery in Anaesthesia where are we?, Elsevier, September 2019.

Chapter in books

1. A. Chevalier, **D. Copot**, C.M. Ionescu, J.A.T. Machado, R. De Keyser, Emerging Tools for Quantifying Unconscious Analgesia: Fractional Order Impedance Models. Discontinuity and Complexity in Nonlinear Physical Systems, series: Nonlinear Systems and Complexity, vol 6., Eds. Machado J.A. Tenreiro, Baleanu Dumitru, Luo Albert C.J, 135-149, 2014.

2. **D. Copot**, Diffusion in small airways, Lung Function testing in the 21st Century (Elsevier) - Biomedical Engineering Series, May 2018.

3. C. Muresan, **D. Copot**, Methods for extracting lung function information from time-based signals, Lung Function testing in the 21st Century (Elsevier) - Biomedical Engineering Series, May 2018.

Editor of Books

1. Member in the Editorial Board, C.M. Ionescu, **D. Copot**, C. Copot, A. Chevalier, R. De Keyser. Book of Abstracts of International Conference on Fractional Signals and Systems with CDRom proceedings ISBN 978-90-9027744-8, 2013.

2. Guest Editor, L. Kovacs, **D. Copot** Special Issue on The importance of modeling, analysis and control in both industrial and clinical application, Acta Polytechnica Hungarica, 14(1), 2017.

Publications in international conferences (P1)

1. A. Chevalier, **D. Copot**, C.M. Ionescu, R. De Keyser. Fractional Order Impe-dance Models as Rising Tools for Quantification of Unconscious Analgesia. 21th Mediterranean Conference on Control and Automation, 25-28 June, Crete, Greece, 206-212, 2013.

2. **D. Copot**, A. Chevalier, C.M. Ionescu, R. De Keyser. A Two-Compartment Fractional Derivative Model for Propofol Diffusion in Anesthesia, IEEE Multi-Conference on Systems and Control, 28-30 August, Hyderabad, India, 264-269, 2013.

3. C. Ionescu, **D. Copot**, R. De Keyser. Parameterization Through Fractional Calculus of the Stress-Strain Relation in Lungs. European Control Conference, Strasbourg, France, 24-27 June, 510-515, 2014.

4. C.M. Ionescu, **D. Copot**, C. Copot, R. De Keyser, Bridging the gap between modelling and control of anesthesia: an ambitious ideal, International Conference on Fractional Differentiation and its Applications, Catania, Italy, 23-25 June, 2014.

5. **D. Copot**, C.M. Ionescu, R. De Keyser, Modelling drug interaction using a fractional order pharmacokinetic model, International Conference on Fractional Differentiation and its Applications, Catania, Italy, 23-25 June, 2014.

6. **D. Copot**, C.M. Ionescu. Drug delivery system for general anesthesia: where are we? IEEE International Conference on Systems, Man and Cybernetics, San Diego, CA, USA, 5-8 October, 2452-2457, 2014.

7. C.M. Ionescu, **D. Copot**, R. De Keyser. A fractional order impedance model to capture the structural changes in lungs, IFAC World Congress, Cape Town, South Africa, 24-29 August, 5363-5368, 2014.

8. **D. Copot**, C.M. Ionescu, R. De Keyser. Relation between fractional order models and diffusion in the body, IFAC World Congress, Cape Town, South Africa, 24-29 August, 9277-9282, 2014.

9. R. De Keyser, **D. Copot**, C.M. Ionescu, Estimation of patient sensitivity to drug effect during Propofol hypnosis. IEEE International Conference on Systems, Man, and Cybernetics (SMC), Hong Kong, China, 10-13 October, 2487-2491, 2015.

10. **D. Copot**, R. De Keyser, C.M. Ionescu, In vitro glucose concentration estimation by means of fractional order impedance models, IEEE International Conference on Systems, Man, and Cybernetics (SMC), Budapest, Hungary, 9-12 October, 2711-2716, 2016.

11. C.M. Ionescu, **D. Copot**, R. De Keyser, Modelling for control of depth of hypnosis - a patient friendly approach, IEEE International Conference on Systems, Man, and Cybernetics (SMC), Budapest, Hungary, 9-12 October, 2653-2658, 2016.

12. **D. Copot**, C. Muresan, R. De Keyser, C.M. Ionescu, Fractional order modeling of diffusion processes: a new approach for glucose concentration estimation, International Conference on Automation, Quality and Testing, Robotics, Cluj-Napoca, Romania, 19-21 May, 407-712, 2016.

13. C.M. Ionescu, **D. Copot**, R. De Keyser, Modelling Doxorubicin effect in various cancer therapies by means of fractional calculus, American Control Conference, Boston, USA, 6-8 July, 1283-1288, 2016.

14. **D. Copot**, C.M. Ionescu, Guided Closed Loop Control of Analgesia: Are We There Yet?, IEEE International Conference on Intelligent Engineering Systems, Larnaca, Cyprus, 20-23 October, 137-142, 2017 (best paper award).

15. C.M. Ionescu, **D. Copot**, On the use of fractional order PK-PD models, European Workshop on Advanced Control and Diagnosis, Lille, France, 17-18 July, 2017.

16. **D. Copot**, R. De Keyser, L. Kovacs, C.M. Ionescu, Towards a cyber-medical system for drug assisting devices, European Workshop on Advanced Control and Diagnosis, Lille, France, 17-18 July, 2017.

17. C.M. Ionescu, **D. Copot**, R. De Keyser, Anesthesiologist in the Loop and Predictive Algorithm to Maintain Hypnosis While Mimicking Surgical Disturbance, 20th World Congress of the International Federation of Automatic Control (IFAC), 9-14 July, Toulouse, France, 15080-15085, 2017.

18. **D. Copot**, C.M. Ionescu, R. De Keyser, Patient specific model based induction of hypnosis using frcational order control, 20th World Congress of the International Federation of Automatic Control, 9-14 July, 15097-15102, 2017.

19. **D. Copot**, M. Neckebroek, C.M. Ionescu, Hypnosis Regulation in Presence of Saturation, Surgical Stimulation and Additional Bolus Infusion, 3rd IFAC Conference on Advances in Proportional-Integral-Derivative Control, Ghent, Belgium, 9-11 May, 2018, accepted.

20. C.M. Ionescu, **D. Copot**, M. Neckebroek, C. Muresan, Anesthesia regulation: towards completing the picture, International Conference on Automation, Quality and Testing, Robotics, Cluj-Napoca, Romania, 24-26 May, 2018, accepted.

Publications in international conferences (C1)

1. C.M. Ionescu, **D. Copot**, R. De Keyser. Respiratory impedance model with lumped fractional order diffusion compartment. IFAC Fractional Differentiation and Applications, 4-6 February, Grenoble, France, 255-260, 2013.

2. **D. Copot**, A. Chevalier, C.M. Ionescu, R. De Keyser. Drug diffusion through cell membrane as a step towards modeling pain relief during anesthesia, International Conference on Mathematical methods in engineering, July 22-26, Porto, Portugal, 150-156, 2013.

3. C.M. Ionescu, **D. Copot**, C. Copot, R. De Keyser. Bridging the gap between modelling and control of anesthesia: a ticklish task. International Conference on Fractional Differentiation and its Applications, Catania, Italy, 23-25 June 2014.

4. **D. Copot**, C.M. Ionescu, R. De Keyser, Modelling drug interaction using a fractional order pharmacokinetic model. International Conference on Fractional Differentiation and its Applications, Catania, Italy, 23-25 June 2014.

5. C.M. Ionescu, **D. Copot**, H. Maes, G. Vandersteen, R. De Keyser. Structural and functional changes occurring during growth of the respiratory system can be quantified and classified. International Conference on Bio-Inspired Systems and Signal Processing, 3-6 March, Loire Valley, France, 110-115, 2014.

6. **D. Copot**, A. Chevalier, C.M. Ionescu, R. De Keyser, Non-invasive Pain Sensor Development for Advanced Control Strategy of Anesthesia: A Conceptual Study. International Conference on Biomedical Electronics and Devices, 3-6 March, Loire Valley, France, 95-101, 2014.

7. **D. Copot** , C.M. Ionescu, R. De Keyser. Remifentanil pharmakokinetics: a fractional order modeling approach, European Nonlinear Dynamics Conference, Vienna, Austria, 6-10 July 2014.

8. **D. Copot**, R. De Keyser, C.M. Ionescu. Drug interaction between Propofol and Remifentanil in individualized drug delivery systems. 9th IFAC Symposium on Biological and Medical Systems (BMS), 31 August -2 September, Berlin, Germany, 64-69, 2015.

9. **D. Copot**, C.M. Ionescu, R. De Keyser, Towards an assistive drug delivery system for general anesthesia. 34th Benelux Meeting on System and Control, 24-26 March, Lommel, Belgium, 2015, (abstract).

10. **D. Copot**, R. De Keyser, C. Ionescu, Identification and performance analysis of a fractional order impedance model for various test solutions, International Conference on Fractional Differentiation and its Applications, July 18 - 20, Novi Sad, Serbia, 2016.

2

Preliminaries on Diffusion

This Chapter introduces the necessary definitions and mathematical preliminaries on diffusion phenomena through porous media. The use of fractional calculus tools to model diffusion processes is also introduced. The theoretical aspects addressed here are the basis for the remainder of this thesis.

2.1 Fractional order modelling of diffusion through porous media

Most of the natural laws of physics (e.g. Newton's law, Maxwell's law, Fick's law, Fourier's law) are stated in terms of partial differential equations (PDE). These laws characterize the physical phenomenon by means of balance (energy, mass, heat) equations. The basic process in the diffusion phenomenon is the movement of fluid (or ions, or air) from a zone with a higher density (concentration, pressure) to one of lower. In a diffusion process or a chemical reaction Fick's law provides a linear relationship between the flux of molecules and the chemical potential difference. Likewise, there is a direct relation between the heat flux and the temperature difference in a thermally conducting slab, as expressed by Fourier's law. For example, diffusion of gases between the air in the lungs and blood takes place from a region with a higher concentration to one with a lower concentration. As the difference in concentration increases also the diffusion rate is increasing. Material properties of tissue arise from nanoscale and microscale architecture of sub-cellular, cellular and extracellular networks. Previous works concerning diffu-

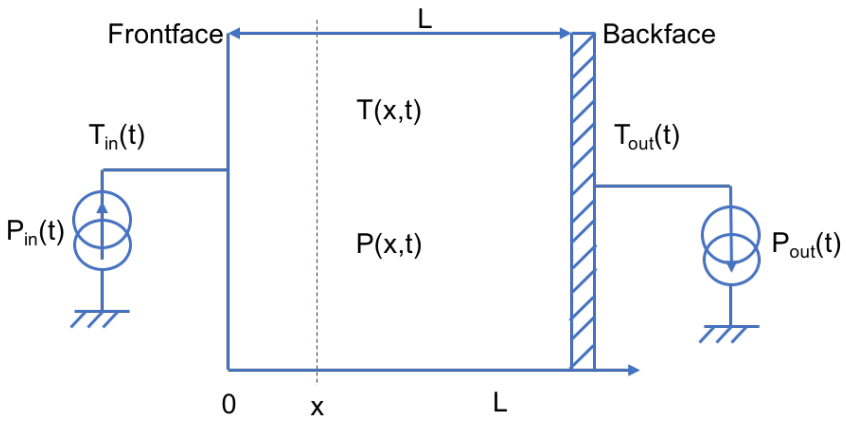

Figure 2.1: Schematic representation of diffusion through a wall.

sion modelling using fractional calculus approach have already shown the ability of such models to estimate with good accuracy the frequency behavior from time data acquisitions [16, 17, 23, 24]. In the following sections three modelling approaches are addressed.

2.1.1 Longitudinal diffusion modelling

Let us consider the problem which consists in computing the heating temperature $T_{in}(t)$ at the front face of a wall where a random heat flux $P_{in}(t)$ is applied. Heating temperature $T(x,t)$ is assumed to be uniform on any plane parallel to the front and back face (see Figure 2.1). The dimensions of the wall are characterized by its section S_w and thickness L. Let $P(x,t)$ be the flux passing through the wall at abscissa x. $T(x,t)$ and $P(x,t)$ satisfy the following heat diffusion equations:

$$\frac{\partial T(x,t)}{\partial t} = a\frac{\partial^2 T(x,t)}{\partial x^2} \tag{2.1}$$

$$P(x,t) = -\lambda S_w \frac{\partial T(x,t)}{\partial x} \tag{2.2}$$

with:

- λ - thermal conductivity ($Wm^{-1}\ ^oC^{-1}$),
- $a = \lambda/\rho c$ - thermal diffusivity ($m^2\ s^{-1}$),
- ρ - mass density (kgm^{-3}),
- c - specific heat ($J\ kg^{-1}\ ^oC^{-1}$).

Let $T_{out}(t)$ be the back face temperature and $P_{out}(t)$ the output flux. We write $T_{in}(s)$, $P_{in}(s)$ and $T_{out}(s)$, $P_{out}(s)$ the Laplace transforms of $T_{in}(t)$, $P_{in}(t)$ at $x = 0$ and $T_{out}(t)$, $P_{out}(t)$ at $x = L$. One can model the wall using a thermal quadrupole relating the inputs ($T_{in}(s)$, $P_{in}(s)$) to the outputs ($T_{out}(s)$, $P_{out}(s)$) [25]:

$$\begin{bmatrix} T_{in}(s) \\ P_{in}(s) \end{bmatrix} = \begin{bmatrix} A & B \\ C & D \end{bmatrix} * \begin{bmatrix} T_{out}(s) \\ \phi_{out}(s) \end{bmatrix} \tag{2.3}$$

where the matrix coefficients A, B, C, D characterize the heat transfer phenomenon in the wall. By applying the Laplace transform to (2.1) and (2.2), one obtains:

$$sT(x,s) - T(x,0) = a\frac{\partial^2 T(x,s)}{\partial x^2} \tag{2.4}$$

$$P(x,s) = -\lambda S_w \frac{\partial T(x,s)}{\partial x} \tag{2.5}$$

Assuming the longitudinal temperature profile is initially constant at time $t = 0$:

$$T(x,0) = 0, 0 < x < L \tag{2.6}$$

The solution set of the second order spatial differential equation (2.4) is given by:

$$T(x,s) = L_1(s)cosh(\delta x) + L_2 \sin h(\delta x) \tag{2.7}$$

with $\delta = \sqrt{s/a}$. Using (2.5) and (2.7) and considering the boundary conditions yields to:

$$\begin{array}{l} T_{in}(s) = \cos h(\delta L)T_{out}(s) + \frac{1}{\lambda S_w}\frac{\sin h(\delta L)}{\delta}P_{out}(s) \\ P_{in}(s) = \lambda S_w \delta \sin h(\delta L)P_{out}(s) \end{array} \tag{2.8}$$

Hence the wall thermal matrix coefficients are given by:

$$\begin{array}{l} A = D = \cos h(\delta L) \\ B = \frac{1}{\lambda S_w}\frac{\sin h\delta L}{\delta} \\ C = \lambda S_w \delta \sin h(\delta L) \end{array} \tag{2.9}$$

If we consider the experiment where the back-face temperature is kept constant (i.e. $T_{out}(s) = 0$), the transfer function which can be interpreted as thermal impedance is:

$$Z_w(s) = \frac{T_{in}(s)}{P_{in}(s)} = \frac{B}{D} = \frac{L}{\lambda S_w}\frac{tanh(\lambda L)}{\delta L} = \frac{L}{\lambda S_w}\frac{\tan h(\sqrt{\frac{s}{a}}L)}{(\sqrt{\frac{s}{a}}L)} \tag{2.10}$$

The static gain of that transfer function corresponding to the thermal resistance R_{thw} has the following expression:

$$\lim_{s\to 0} Z_s(s) = \frac{T_f(s)}{P_{in}(s)} = R_{thw} = \frac{L}{\lambda S_w} \tag{2.11}$$

At high frequencies, the the wall behaves half order integrator:

$$\lim_{s\to\infty} Z_s(s) = \frac{\sqrt{a}}{\lambda S_w s^{0.5}} \tag{2.12}$$

2.1.2 Spherical diffusion modelling

Let us consider the problem which consists in computing the heating temperature $T_{in}(t)$ at the inner surface of a sphere of radius r_1 where the random heat flux $P_{in}(t)$ is applied. Heating temperature $T(r,t)$ is assumed to be uniform on any spherical slice of radius r (see Figure 2.2). Let $\phi(r,t)$ be the flux passing through the sphere at radius r. Assuming the heat conduction is isotropic, the heat diffusion is an unidirectional phenomenon governed by the following equations:

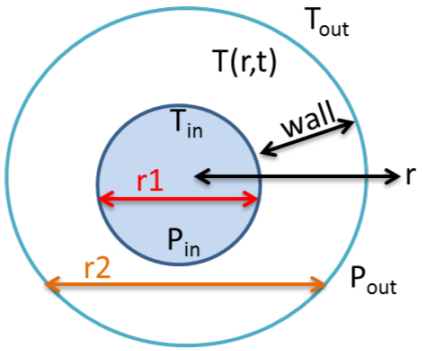

Figure 2.2: Schematic representation of diffusion through a sphere.

$$\frac{\partial T(r,t)}{\partial t} = a\left[\frac{\partial^2 T(r,t)]}{\partial r^2} + \frac{2}{r}x\frac{\partial T(r,t)}{\partial r}\right] \tag{2.13}$$

$$\phi(r,t) = -\lambda(4\pi r^2)\frac{\partial T(r,t)}{\partial r} \tag{2.14}$$

with λ; a; ρ and c defined in Section 2.1.1.

Let $T_{out}(t)$ be the outer temperature and $\phi_{out}(t)$ the output flux. We write the $T_{in}(s)$, $P_{in}(s)$ and $T_{out}(t)$, $\phi_{out}(t)$ the Laplace transforms of $T_{in}(t)$, $P_{in}(t)$ at $r = r_1$ and $T_{out}(t)$, $\phi_{out}(t)$ at $r = r_2$. One can model the wall using a quadrupole relating the inputs ($T_{in}(s)$, $P_{in}(s)$) to the outputs ($T_{out}(s)$, $\phi_{out}(s)$).

$$\begin{bmatrix} T_{in}(s) \\ P_{in}(s) \end{bmatrix} = \begin{bmatrix} A & B \\ C & D \end{bmatrix} * \begin{bmatrix} T_{out}(s) \\ \phi_{out}(s) \end{bmatrix} \tag{2.15}$$

where the matrix coefficients A, B, C and D characterize the heat transfer phenomenon in the sphere. Applying the Laplace transform to (2.13) and (2.14) provides:

$$sT(r,s) - T(r,0) = a\left[\frac{\partial T(r,s)}{\partial r^2} + \frac{2}{r}x\frac{\partial T(r,s)}{\partial r}\right] \tag{2.16}$$

$$\phi(r,s) = -\lambda(4\pi r^2)\frac{\partial T(r,s)}{\partial r} \tag{2.17}$$

Assuming the radial temperature profile is initially constant at time t=0:

$$T(r,0) = 0, r_1 < r < r_2 \tag{2.18}$$

The solution of the second order partial differential equation (2.16) is given by:

$$T(r,s) = r^{-0.5}x\big[L_1(s)I_{-0.5}(\delta r) + L_2(s)K_{-0.5}(\delta r)\big] \tag{2.19}$$

with $\delta = \sqrt{s}/a$.

$L_1(s)$ and $L_2(s)$ are constant of integration and $I_{-0.5}(x)$ and $K_{-0.5}(x)$ are modified Bessel functions of, respectively, first and second type given by [26]:

$$K_{-0.5}(x) = \big(\frac{\pi}{2x}\big)^{0.5}e^{-x} \tag{2.20}$$

$$I_{-0.5}(x) = \big(\frac{2}{\pi x}\big)^{0.5} \tag{2.21}$$

Considering the boundary conditions and using equations (2.19) and (2.17) the matrix terms A, B, C and D characterizing the heat transfer of the sphere can be determined [27]:

$$\begin{array}{l} A = \frac{r_1}{r_2}cosh(\delta(r_2-r_1)) - \frac{sinh(\delta(r_2-r_1))}{\delta r_1} \\ B = \frac{1}{4\pi r_1 r_2}\frac{sinh(\delta(r_2-r_1))}{\delta\lambda} \\ C = 4\pi r_2\lambda[1 - \frac{r_1}{r_2}cosh(\delta(r_2-r_1)) + (\lambda r_1 - \frac{1}{\lambda r_2})\frac{sinh(\delta(r_2-r_1))}{\delta r_1} \\ D = \frac{r_1}{r_2}cosh(\delta(r_2-r_1)) + \frac{sinh(\delta(r_2-r_1))}{\delta r_1} \end{array} \tag{2.22}$$

Considering that the heat flux $P_{in}(t)$ is applied uniformly to the inner spherical surface of radius r_1, the output temperature of the external spherical surface r_2 being kept constant ($T_{out}(s) = 0$), the following transfer function which can be interpreted as a thermal impedance is obtained:

$$Z_s(s) = \frac{T_{in}(s)}{P_{in}(s)} = \frac{B}{D} = \left(\frac{1}{4\pi r_1\lambda}\right)\frac{1}{1 + \sqrt{\frac{s}{a}}r_1\frac{1}{tanh(\sqrt{\frac{s}{a}}(r_2-r_1))}} \tag{2.23}$$

The thermal resistance R_{ths} is given by considering the static gain:

$$\lim_{s\to 0} Z_s(s) = \frac{T_{in}(s)}{\phi_{in}(s)} = T_{ths} = \frac{1}{4\pi\lambda}\left[\frac{1}{r_1} - \frac{1}{r_2}\right] \tag{2.24}$$

At high frequencies, the thermal impedance of the sphere behaves like a non-integer integrator whose order is equal to 0.5:

$$\lim_{s\to\infty} Z_s(s) = \frac{\sqrt{a}}{\lambda(4\pi r_i^2)s^{0.5}} \tag{2.25}$$

2.1.3 Molecular diffusion

In this section a general approach for modelling a system consisting of identical or different species is given. Through its alveolar nature, a specie consists of an orifice and a cavity. The orifice serves as hydraulic resistance or energy dissipater or dashpot. The cavity serves as pneumatic capacitance or energy tanks or spring. By analogy, a resistance-capacitance cell can represent the specie model.

Case of identical species: A first step considering identical species, the aim being to study the structuring effect of multiplicity. As all the species are identical (Figure 2.3), each specie absorbs same flow. The transition from one specie to N species shifts the model from a RC cell (Figure 2.3) to a new RC cell (Figure 2.4) whose resistance is N times lower than for a single specie (R/N) and has a capacitance N time higher than for a single specie (NC).

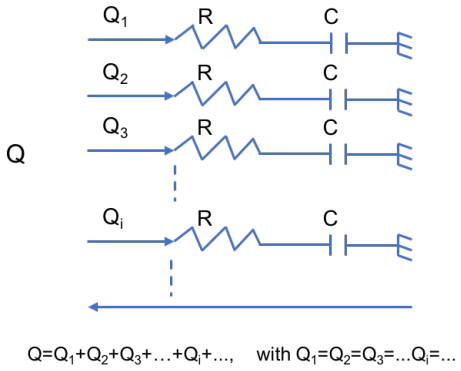

Figure 2.3: Schematic of a RC model for identical species.

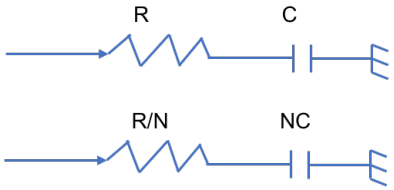

Figure 2.4: Transition from one specie to N species.

Case of different species: A second step consists in considering the different species (Figure 2.5), the aim being to study the structuring effect of difference associated with multiplicity. The species are differentiated through their orifices and cavities. Therefore, the resistance and capacitance characterizing them exhibits a constant ratio of the recursive factors (α and η). An RC cell network is character-

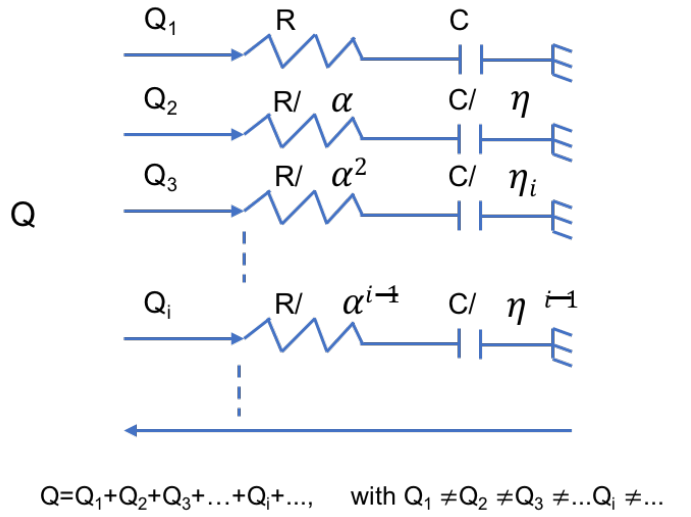

Figure 2.5: Schematic of a RC model for different species.

ized by an admittance ($Y(j\omega)$) given by (2.26) whose Bode diagram is shown in Figure 2.6

$$Y(j\omega) = j\omega \sum_i \frac{C_i}{1 + C_i R_i j\omega} \tag{2.26}$$

with $R_i = \frac{R}{\alpha_i}$ and $C_i = \frac{C}{\eta_i}$ with their recurrent ratios. As described in [28] the Bode diagrams can only take the average of asymptotic diagrams (Figure 2.6). From here also the idea of smoothing of the steps for gain and the crenels for the phase. The smoothing of the steps is represented by a gain smoothing line with the slope less than 20 dB/dec and with $0 < m < 1$. The smoothing of the crenels is characterized phase smoothing line with an order less than $\pi/2$ with $0 < m < 1$, with $m = log\alpha/log(\alpha\eta)$. Considering the studied system presented in Figure 2.7 and from Newton's second law one may write the following differential equation:

$$M\frac{dV(t)}{dt} + F(t) = 0 \tag{2.27}$$

where $V(t)$ is the speed of mass M and $F(t)$ is the dyke reaction force. If S is the flow section $V(t) = Q(t)/S$ and $F(t) = P(t)S$. Hence, the new differential

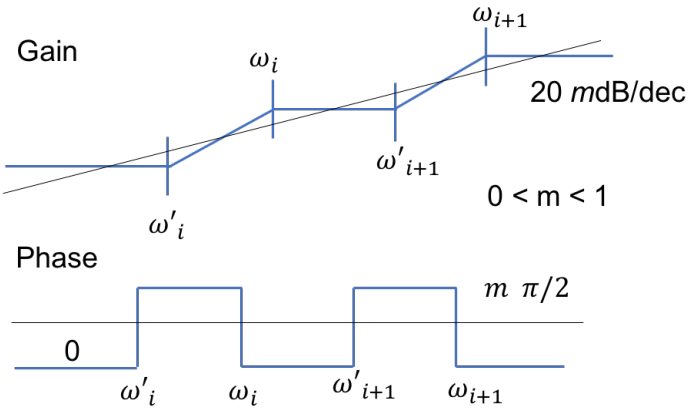

Figure 2.6: Smoothing of the Bode diagrams.

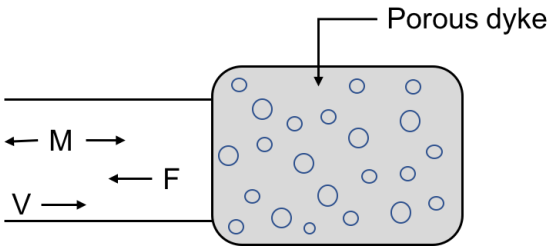

Figure 2.7: Study system.

equation with two variables $Q(t)$ and $P(t)$:

$$\frac{M}{S^2}\frac{dQ(t)}{dt} + P(t) = 0 \tag{2.28}$$

Finally, the water-dyke admittance can be described by the following equation:

$$Y(j\omega) = \frac{Q(j\omega)}{P(j\omega} = \left(\frac{j\omega}{j\omega_0}\right)^m \tag{2.29}$$

for which is deduced the symbolic equation:

$$Q(j\omega) = \frac{1}{\omega_0^m}(j\omega)^m P(j\omega) \tag{2.30}$$

which, in time domain, is expressed as:

$$Q(t) = \frac{1}{\omega_0^m}\left(\frac{d}{dt}\right)^m P(t) \tag{2.31}$$

This equation represents the (dynamic) model of the porous interface and indicates that the flow $Q(t)$ is proportional to the non-integer derivative of pressure $P(t)$.

2.2 Summary

This Chapter presented the theoretical aspects of diffusion processes. The theoretical aspects addressed in this chapter of the thesis are further employed to model the diffusion of gases in the lungs and drug diffusion in the human body. Diffusion in lungs is addressed in Chapter 3 and the tools presented in this chapter are employed to model the gas exchange phenomena. For this, the theory presented here is used in order to model a network of alveoli. Both cases (i.e. identical and different species/alveoli) presented in this section are used to model the diffusion process. Modelling of drug diffusion in the human body can be also modeled using the tools presented in this chapter. More specifically, in Chapter 5 the pharmacokinetic-pharmacodynamic model characterizing drug uptake and effect are based on theoretical aspects presented in this chapter.

3
Diffusion in the Lungs

In this Chapter the importance of gas diffusion through the respiratory membrane is investigated. The theory described in Chapter 2 is further employed in Section 3.4. First, the impedance of one alveolus has been simulated followed by a network of alveoli. The simulation results are then compared with measurements by means of derived parameters.

The main publications where this work has been presented are:

- **D. Copot**, C.M. Ionescu, R. De Keyser. Structural changes in the COPD lung and related changes in diffusion mechanism, PLOS ONE Journal, 12(5), doi.org/10.1371/journal.pone.0177969, 2017.
- **D. Copot**, C.M. Ionescu, R. De Keyser. Relation between fractional order models and diffusion in the body, IFAC World Congress, Cape Town, South Africa, 24-29 August, 9277-9282, 2014.
- C.M. Ionescu, **D. Copot**, R. De Keyser. A fractional order impedance model to capture the structural changes in lungs, IFAC World Congress, Cape Town, South Africa, 24-29 August, 5363-5368, 2014.

3.1 Lung mechanics

Breathing is essentially a mechanical process in which the muscles of the thorax and abdomen, working together under the control of the brain, produce the pressures required to expand the lung so that air is sucked into it from the environment. These pressures must be sufficient to overcome the tendencies of the lung and chest wall tissues to recoil, much like blowing up a balloon. Pressure is also required to drive air along the pulmonary airways, a system of branching conduits that begins at the mouth and ends deep in the lungs at the point where air and blood are close enough to exchange oxygen and carbon dioxide. The mechanical properties of the lungs thus determine how muscular pressures, airway flows, and lung volumes are related. The research field of lung mechanics is concerned with the study of these properties [29].

In a spontaneously breathing subject, a negative pressure is generated around the outside of the lungs by the respiratory muscles. This produces a flow of gas along the pulmonary airways in the direction of decreasing pressure. The blood-gas barrier is less than a micron thick, so it presents a very small impediment to the passage of gas molecules. It also has an extremely large surface area so that many gas molecules can cross it in parallel. The transport of oxygen and carbon dioxide across the blood-gas barrier occurs solely by passive diffusion. Gases always tend to move from regions of high partial pressure to regions of low partial pressure. The partial pressures of oxygen and carbon dioxide in the alveoli and the pulmonary capillary blood normally favor movement of oxygen into the blood and carbon dioxide into the alveoli. The blood-gas barrier that these gases must cross in the process is so large and so thin that sufficient numbers of gas molecules can move across it to meet the demands of life in a healthy lung. In some diseases, however, this ceases to be the case. The efficiency of gas exchange is thus tightly linked to the physical properties of the blood-gas barrier.

3.2 Gas Diffusion Through the Respiratory Membrane

There are about 300 million alveoli in the two lungs, and each alveolus has an average diameter of about 0.2 millimeter. The alveolar walls are extremely thin, and between the alveoli is an almost solid network of interconnecting capillaries. The thickness of the respiratory membrane occasionally increases for instance, as a result of edema fluid in the interstitial space of the membrane and in the alveoli so that the respiratory gases must then diffuse not only through the membrane but also through this fluid. Also, some pulmonary diseases cause fibrosis of the lungs, which can increase the thickness of some portions of the respiratory membrane. Because the rate of diffusion through the membrane is inversely proportional to

the thickness of the membrane, any factor that increases the thickness to more than two to three times the normal can interfere significantly with normal respiratory exchange of gases.

The diffusion coefficient for transfer of each gas through the respiratory membrane depends on the gass solubility in the membrane and, inversely, on the square root of the gass molecular weight. The rate of diffusion in the respiratory membrane is almost exactly the same as in water. Therefore, for a given pressure difference, carbon dioxide diffuses about 20 times as rapidly as oxygen. Oxygen diffuses about twice as rapidly as nitrogen. The pressure difference across the respiratory membrane is the difference between the partial pressure of the gas in the alveoli and the partial pressure of the gas in the pulmonary capillary blood. The partial pressure represents a measure of the total number of molecules of a particular gas striking a unit area of the alveolar surface of the membrane in unit time, and the pressure of the gas in the blood represents the number of molecules that attempt to escape from the blood in the opposite direction.

Diffusing Capacity for Oxygen. In the average young man, the diffusing capacity for oxygen under resting conditions averages 21 ml/min/mm Hg. In functional terms, means that the mean oxygen pressure difference across the respiratory membrane during normal, quiet breathing is about 11 mm Hg. Multiplication of this pressure by the diffusing capacity (11x21) gives a total of about 230 milliliters of oxygen diffusing through the respiratory membrane each minute;this is equal to the rate at which the resting body uses oxygen.

Diffusing Capacity for Carbon Dioxide. The diffusing capacity for carbon dioxide has never been measured because of the following technical difficulty: Carbon dioxide diffuses through the respiratory membrane so rapidly that the average Pco_2 in the pulmonary blood is not far different from the Pco_2 in the alveolithe average difference is less than 1 mm Hg and with the available techniques, this difference is too small to be measured. Nevertheless, measurements of diffusion of other gases have shown that the diffusing capacity varies directly with the diffusion coefficient of the particular gas. Because the diffusion coefficient of carbon dioxide is slightly more than 20 times that of oxygen, one would expect a diffusing capacity for carbon dioxide under resting conditions of about 400 to 450 ml/min/mm Hg and during exercise of about 1200 to 1300 ml/min/mm Hg.

In Figure 3.1 the gas exchange in the blood capillaries of the lungs and systemic circulation is shown. As a result of gas exchange in the lungs, the systemic arteries carry oxygenated blood with a relatively low carbon dioxide concentration. After the oxygen is unloaded to the tissues, the blood in the systemic veins has a lowered oxygen content and an increased carbon dioxide concentration.

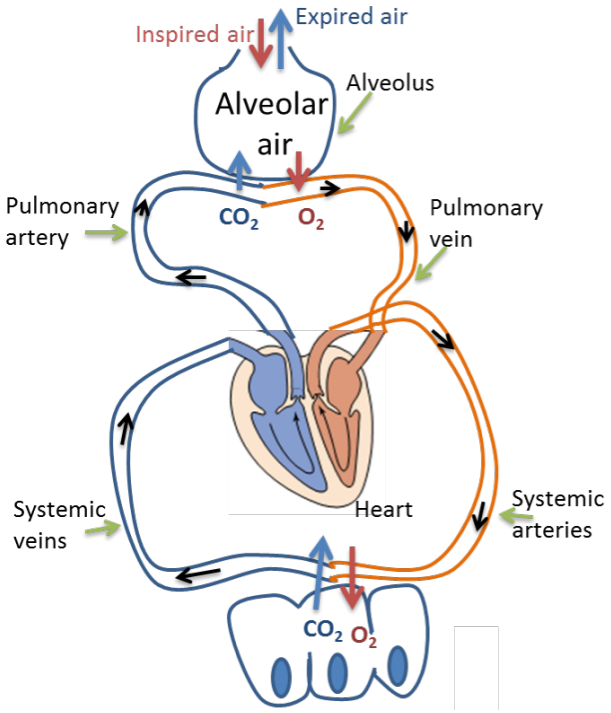

Figure 3.1: Gas exchange in the blood capillaries of the lungs and systemic circulation.

3.3 Structural changes in chronic obstructive pulmonary disease

COPD is often paired with emphysema and referred to as small airway disease [30, 31]. It features a prolonged time constant for lung deflation, due to increased resistance of the small conducting airways and increased compliance as a result of emphysematous destruction. The latter implies breaking the alveolar walls and disruption of the adjacent connective walls, inflammation and tissue mass enlargement. Density of the lung is decreased, with airspace enlargement and computer tomography scans have shown various degrees of heterogeneity in density of porous tissue with various degrees of obstruction [32].

Using a gross analogy to the Sierpinski triangle of various densities, as illustrated in Figure 3.2, we can enumerate the following changes in our impedance model as a result of airway remodelling in COPD:

- the R and C parameters, along with their corresponding recurrent ratios, will vary in different respiratory zones;

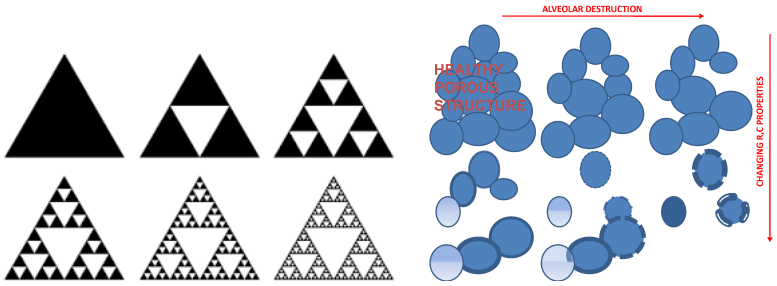

Figure 3.2: Classical Sierpinski triangle (left) and Sierpinski-like arrangement of alveolar areas with various degrees of density.

- the alveolar changes will affect the fractional order term value n;
- within respiratory zones, different such fractional order term values will exist;
- the porous structure of the network of alveoli will then contain multi-fractal spacial distribution and thus multi-fractal dynamics.

Fractal and multi-fractal analysis has been given lots of attention in medical applications [33]. Specifically for lung applications, dissimilarity principle has been applied to classify lung parenchyma based on image processing techniques [34], as well as pulmonary emphysema [35]. Airway remodelling has been correlated to fractal dimension in asthma [36], providing insight into space filling mechanism. Pulmonary embolism has been detected using multifractal analysis from lung scans and provided useful classification tool [37].

It is interesting to provide a correlation between changes in COPD at the alveolar level and fractional order impedance values evaluated in various degrees of obstruction. As COPD progresses, changes in the R, C parameters and structure of the alveolar network will affect the impedance and thus the lung function will change.

As the ratios of resistance and capacitance increase with various degrees of COPD obstruction (i.e. classified as GOLD2, GOLD3 and GOLD4, from mild to severe degree of obstruction), the fractional order term value n will vary. If the relative increase is the same, the value will remain unchanged. If resistance has absolute variance higher than capacitance, then the values of n will increase. Similarly, if capacitance has absolute variance higher than resistance, then the values of n will decrease.

The implications for damping are complex. Due to relative increase in compliance as a result of more empty spaces in the alveolar structure, damping will apparently decrease, but due to increased tissue density, the overall damping is

increasing. Notice that if alveolar surface is decreased with pathology, the time constant defined in previous section for the network will also increase. This is in line with the pathology of COPD which has long deflation periods. In conclusion, local structural changes are more important than the network spacial distribution in terms of impedance.

3.4 Diffusion at low frequencies

In the context of electrical analogy, one usually considers voltage as the equivalent for respiratory pressure (P) and current as the equivalent for airflow (Q). The pressure in function of time is the accumulation of these components with the trans-pulmonary pressure at end-expiration (P_0):

$$P(t) = \frac{1}{C}V(t) + R\frac{dV}{dt} + I\frac{d^2V}{dt^2} + P_0 \tag{3.1}$$

where elastance $(1/C)$ (the reciprocal of the compliance) is directly related to volume (V), the resistance (R) is related to airflow and the inertia (I) is related to accelerating particles. This equation represents the global relationship between airflow and pressure in the lungs. Its equivalent frequency domain form is the respiratory impedance as a function of oscillatory frequency [38].

This principle has been applied by means of Womersley theory and Navier-Stokes equations to elastic tubes preserving structure and morphology of the airways [39]. According to the seminal work of Weibel and Mandelbrot [40–42], the structure of the lungs can be roughly approximated by a recurrent dichotomous tree of 24 levels, leading to a rough approximation of 2^{24} alveolar ducts. At the end of each alveolar duct there is a porous bag called alveoli, which are grouped together like a lot of interlinked caves, rather than individual sacks.

A mathematical model of the respiratory tree up to 24th level has been proposed [39] and used in subsequent works in clinical studies [14]. The model is based on the geometrical parameters: radius and wall thickness (r, h), on the mechanical characteristics of the airway tube: complex elastic moduli (given by its modulus $(|E|)$ and angle(φ_E)) on the Poisson coefficient (ν_P), and on the air properties: viscosity and density (μ, ρ). Over the length ℓ of an airway tube, we have the corresponding definitions for electrical resistance:

$$R_e = \ell\frac{\mu\delta^2}{\pi r^4 M_1}\sin(\varepsilon_1), \tag{3.2}$$

and for electrical capacitance

$$C_e = \ell\frac{2\pi r^3(1-\nu_P^2)^2}{|E|\,h}\cos\varphi_E, \tag{3.3}$$

where, M_1 is the modulus of the Bessel function of order 1, ε_1 is the phase angle of the complex Bessel function of order 1, and $\delta = \sqrt{\omega\rho/\mu}$ the Womersley parameter.

We have shown that the geometry of the lungs leads to a piecewise fractal structure, whose electrical equivalent leads to a recurrent ladder network. The admittance of such network has the form:

$$Y_N(s) \cong \cfrac{1/R_{e1}}{1+\cfrac{1/R_{e1}C_{e1}s}{1+\cfrac{1/\gamma R_{e1}C_{e1}s}{\cdots\cfrac{\cdots}{1+\cfrac{1/\chi^{N-2}\gamma^{N-1}R_{e1}C_{e1}s}{1+1/\chi^{N-1}\gamma^{N-1}R_{e1}C_{e1}s}}}}} \tag{3.4}$$

with R_{e1} and C_{e1} denoting the resistance and compliance in the first airway (i.e. trachea), and γ the ratio of resistances per total levels, χ the ratio of compliances per total levels and s the Laplace operator. This continuous fraction expansion can be well-approximated for $N \to \infty$ airway levels by the compact form of admittance [43]:

$$Y_N(s) \cong \frac{1/R_{e1}}{K(\gamma,\chi)\cdot(1/R_{e1}C_{e1}s)^n} \tag{3.5}$$

with $K(\lambda,\chi)$ a gain factor depending on the values of the ratios and the fractional order n given by

$$n = \frac{\log(\gamma)}{\log(\gamma)+\log(\chi)} \tag{3.6}$$

Notice that the impedance, $Z_N(s)$ will be the inverse of the admittance. In the frequency domain, the fractional order will lead to a constant-phase behaviour, i.e. a phase-locking in the frequency range given by the convergence conditions [14, 43]. The lumped version of this model is the well-known constant-phase element model given by:

$$Z_{CP}(s_k) = R + I(s_k) + \frac{1}{C(s_k^\beta)} \tag{3.7}$$

where R (kPa s/L) and I (kPa s^2/L) denote the central airway resistance and inertance respectively, whereas the last term consists of a constant-phase element which can be split into a real and imaginary part, denoting tissue damping and tissue elastance. These two latter properties are defined as averaged over the frequency range evaluated by the lung function test [44–46].

$$\begin{aligned} G_r &= \frac{1}{C\omega_k^\beta}\cos(\beta\pi/2) \\ H_r &= \frac{1}{C\omega_k^\beta}\sin(\beta\pi/2) \\ \eta_r &= \frac{G_r}{H_r} \end{aligned} \tag{3.8}$$

and their ratio denotes the degree of heterogeneity present in the tissue [47]. This ratio is in fact a characterization of sources for nonlinear contributions in the respiratory dynamical properties. If changes in R are small, then any changes in G_r (kPa s$^{(1-\beta)}$/L) will represent changes in parenchyma or in very small airways. The memory effects are introduced via $s^{(1-\beta)}$ [16]. These effects are observed in materials with viscoelastic properties. Chronic changes in H_r (kPa s$^{(1-\beta)}$/L) reflect changes in the intrinsic mechanical properties of the parenchyma [48]. This parametric model has been shown to reliably estimate airway and tissue properties and its sensitivity to bronchodilatation in dogs at low frequencies has been assessed in [44]. The same model has been used to assess respiratory impedance in rats at low frequencies in [49]. The model has been used to evaluate respiratory impedance in healthy and sick patients [14, 47]. The reliability of the parameter estimates from model fitting to raw data has shown that the inertance I and the resistance R may contain a high degree of uncertainty , while the constant-phase term delivers a reliable estimate of peripheral tissue properties. The study also showed that the steep dependency on frequency at low frequencies in the real part of impedance is consistently fitted by the constant-phase model from (3.7) when compared to other models from literature.

In order to quantify the non-linear contributions the following index has been introduced [14]:

$$T = \frac{P_{even} + P_{odd}}{P_{exc}} \cdot \frac{U_{exc}}{U_{even} + U_{odd}} \tag{3.9}$$

where each variable represents the sum of the absolute values of all the contributions in the pressure and flow signals a non-excited frequencies (even and odd) and the odd excited frequencies. The index expresses the relative ration of the contributions at non-excited frequencies with respect to the contributions at the excited frequencies. For a detailed overview on filtering techniques applied to extract the contributions see [14, 50].

To allow a systematic approach, we need to use an impedance model of one alveolus which will be later used for analysis of alveolar sac structures and their respective properties in presence of remodelling effects.

Impedance of one alveolus: Let us assume a spherical alveolus characterized by an inner radius r_1 and an outer radius r_2. We may assume without loss of generality that heat conduction is anisotropic, heat diffusion is unidirectional and spherical coordinates can be used for modelling. Following the line of thought presented in [16, 17], approximating the spherical wall (i.e. difference between inner radius and outer radius) with many cells whose pressure is governed by:

$$\frac{dP_i}{dt} = \frac{1}{R_i C_i}(P_{i-1} - 2P_i + P_{i+1}) \tag{3.10}$$

with R_i and C_i representing the resistance and compliance properties of the cell

i and P_i pressure profile assumed uniformly distributed along the cell face. The thickness of each cell is then given by the relation: $h = r_2 - r_1/N$, with N the total number of cells and $0 \leq i \leq N$. Introducing $N_0 = r_1/h$, it follows that the radii of each cell is given by $r_i = (N_0 + i)h$. The surface of the cell becomes:

$$S_i = 4\pi r_i^2 = 4\pi h^2 (N_0 + i)^2 \tag{3.11}$$

and it follows that the resistance of each cell is given by:

$$R_i = \frac{h}{\lambda \cdot S_i} = \frac{1}{4\pi\lambda h(N_0 + i)^2} \tag{3.12}$$

where λ is the thermal conductivity (W m^{-1} ^{o} C^{-1}). The capacity per cell is defined as:

$$C_i = \frac{4}{3}\pi h^3 [3(N_0 + i)^2 + \frac{1}{4}]\rho c \tag{3.13}$$

with ρ mass density (kg m^{-3}) and c specific heat (J kg^{-1} ^{o}C^{-1}). The ladder network of series connected cells with resistance and capacity calculated in (3.12) - (3.13) in Laplace operator, provides the explicit impedance which can be evaluated over a range of frequencies. This can be either a ladder network made of recurrent elements, either one with same element values per cell. In our case, the latter applies since we assumed a homogeneous density of the alveolar wall.

Numerical simulation was performed using a linear state-space representation given in (3.14)-(3.15):

$$\begin{aligned} A_s(i, i-1) &= \frac{a}{h^2}\frac{(N_0 + i)^2}{(N_0 + i)^2 + \frac{1}{12}} \\ A_s(i, i) &= -\frac{a}{h^2}\frac{(N_0 + i)^2 + (N_0 + i + 1)^2}{(N_0 + i)^2 + \frac{1}{12}} \\ A_s(i, i-1) &= \frac{a}{h^2}\frac{(N_0 + i + 1)^2}{(N_0 + i)^2 + \frac{1}{12}} \end{aligned} \tag{3.14}$$

$$\begin{aligned} A_s(1, 1) &= \frac{a}{h^2}\frac{(N_0 + 1)^2}{\frac{N_0^2}{2} + \frac{N_0}{2} + \frac{1}{24}} \\ A_s(1, 2) &= \frac{a}{h^2}\frac{(N_0 + 1)^2}{\frac{N_0^2}{2} + \frac{N_0}{2} + \frac{1}{24}} \\ A_s(I, I-1) &= \frac{a}{h^2}\frac{(N_0 + I - 1)^2}{(N_0 + I - 1)^2 + \frac{1}{12}} \\ A_s(I, I) &= -\frac{a}{h^2}\frac{(N_0 + I - 1)^2 + (N_0 + 1)^2}{(N_0 + I - 1) + \frac{1}{12}} \end{aligned} \tag{3.15}$$

Network of alveoli: Air in the lungs passes terminal bronchi, enters respiratory bronchi and consequently reaches the alveolar ducts and alveoli. This may be interpreted as penetration of air through a porous material, i.e. lung tissue, whose density increases with distance. Figure 3.3 illustrates the aforementioned transport phenomenon. The material is assumed to be homogeneous, sponge-like, whereas every alveolus has same properties. This assumption corresponds to healthy lung tissue. Fractal properties have been applied to intergranullar materials

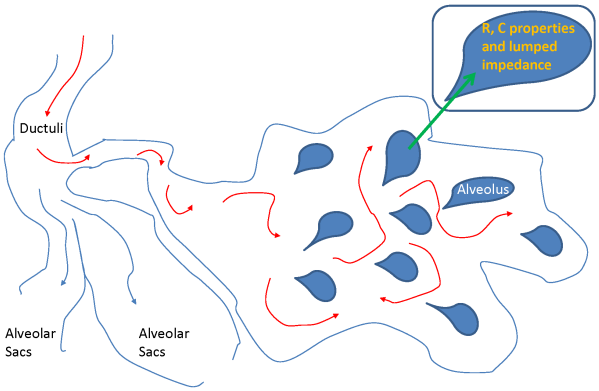

Figure 3.3: Conceptual view of air passing through a network of alveoli. In this picture, the airflow has to reach every alveolus characterized by its own resistance, capacitance and resulting lumped impedance.

for impedance models and sphere like geometry has been employed successfully to proof convergence to a fractional order impedance model [51, 52]. The structure of such porous materials has been modelled with fractional calculus tools and led to fractal dimensions between dimension 2 (surface) and 3 (volumetric). Depending on the density of the material, the values for fractal dimension changed accordingly. In the context of lung pathology, changes in density occur in emphysematous lungs. The fractional order impedance term values reflects these changes and thus we speculate it might be of interest to study this aspect.

To illustrate the effect of changes in structure in tissue lungs, we will first discuss the nominal conditions of healthy lung tissue. The tools we employ are similar as for one alveolus, equivalent ladder network models. Porous material is not necessary permeable, therefore the pores we consider in our model are not linked to each other, thus similar to alveolar sacs (dead-end). To enter these pores, the airflow must counteract resistance with dissipative energy and must inflate/deflate with an elastic capacitance which decreases the peak pressure for the same given volume of air. The flow entering from the main stem we assume equally divided

between the alveolar pores. Mandelbrot introduced the fractal character to porosity because of self-similarity principle [42]. In this context, we may employ recurrent ladder networks of parallel cells - each cell denoting an alveolus. Although Mandelbrot introduced fractality in porous materials as randomly distributed (si ze and location), due to the very compact structure of the lung ductuli we may consider this parallel arrangement of cells as deterministic [40].

3.5 Patients

The study includes 43 COPD diagnosed patients ($\geq$ 60 years) who came for periodic evaluation of their lung function at Ghent University Hospital, Belgium. The study group included: 18 subjects diagnosed with COPD-GOLD II; 15 subjects diagnosed with COPD-GOLD III and 10 subjects diagnosed with COPD-GOLD IV. Biometric and spirometric variables are listed in Table 3.1. Written informed consent was obtained from all participants. This study and the consent procedure was approved by the local ethical committee of Ghent University Hospital, Ethical advice number B670201111936.

-	COPD-GOLD II	COPD-GOLD III	COPD-GOLD IV
# Patients	18	15	10
Age (yrs)	71 $\pm$9.4	77$\pm$5.7	68$\pm$3.5
Height (m)	1.62$\pm$0.07	1.7 $\pm$0.087	1.66 $\pm$0.035
Weight (kg)	70.4 $\pm$10.59	78.5 $\pm$10.66	75.4 $\pm$13.64

Table 3.1: Biometric characteristics data for the subjects included in the study.

3.6 Results and discussion

Figure 3.4 depicts the impedance of an isolated alveolus with particular lung tissue parameters. These parameters are given below, with units as given above [53–55]:

$$\rho = 350; c = 5000; \lambda = 0.05; \tag{3.16}$$

It can be observed that the lumped impedance follows closely the explicit impedance in a limited frequency range. This interval will depend on the parameters (3.16). Notice that changes with disease at alveolar level will affect the cell elements (3.10), consequently will change the lumped impedance form and affect the fractional order operator. Using the impedance of an alveolus, we can now construct a network of alveoli. The origin of this impedance is not essential, as long as its form has the term in fractional order to help us understand changes with

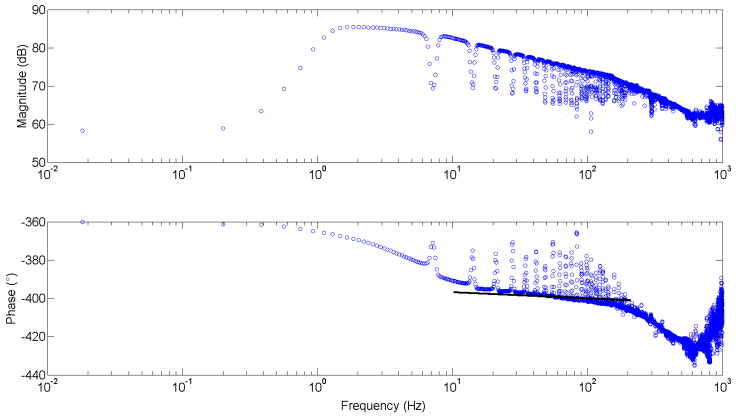

Figure 3.4: Explicit impedance for individual alveolus simulated with healthy lung parameters. Black thick line denotes the constant phase of the lumped impedance.

remodelling. Supposing that the flow is divided equally through the 5 alveolar sacs as in Figure 3.5, then all impedances are equal and receive the air-flow in parallel.

This allows us to write the following admittance equation:

$$Yt = Y1 + Y2 + Y3 + Y4 + Y5 \tag{3.17}$$

with $Yt = 1/Zt$ the total admittance and Y_i the admittances of each alveoli, with fractional order value $n = 0.5$. The total admittance will not change in phase, only in amplitude, dependent on the amount of alveoli we take into calculus of (3.17). In pathology, as explained before, the mechanical properties are altered as a result of remodelling and lead to different fractional order values. Structure of alveolar sacs also modifies, leading to various consistencies of network of alveoli, as conceptually illustrated in Figure 3.2. So if we consider that we have the same admittance form as in (3.17), but with the following elements:

$$\begin{aligned} &Y1 = Y2 = 1/Zs \\ &Y3 = Y4 = Y5 = 1/Zs" \\ &Zs(n = 0.5) \ \ and \ \ Zs" = Zs(n = 0.3) \end{aligned} \tag{3.18}$$

The phase will be altered, varying between $-0.3{*}90^o$ and $-0.5{*}90^o$. In COPD, we also have the breaking of alveolar walls, creating larger spaces. This will induce a different form of the admittance, as:

$$Yt = Y1 + Y2 + Y3 + \frac{1}{Z4 + Z5} \tag{3.19}$$

with the same $n = 0.5$ for $i = 1, 2, 3$ and $n = 0.3$ for $i = 4, 5$. This will also affect the phase of the total admittance, but the limit values will be the same as those

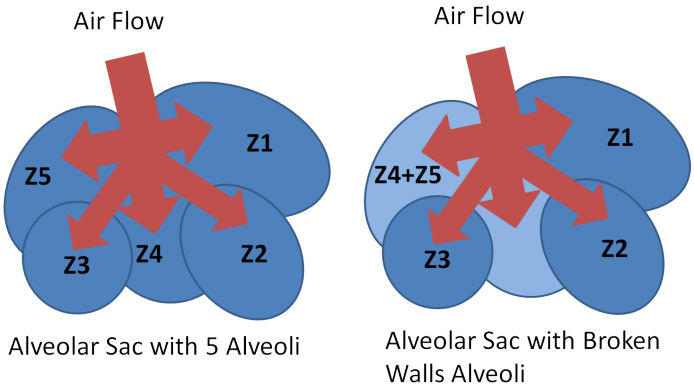

Figure 3.5: Schematic representation of an alveolar with 5 alveoli (left) and with broken alveoli (right)

from (3.18). This mathematical framework provides the necessary support for the multi-fractal dynamics exhibited by the lung parenchyma and much discussed in literature under the resulting property of self-organized critically system Phase dynamics and thus also phase transitions are direct result of remodelling effects as a self-defence mechanism of the respiratory system towards disease.

The result for the impedance obtained with (3.17) is depicted in Figure 3.6 and from (3.18) is depicted in Figure 3.7. It can be observed that the limit phase values

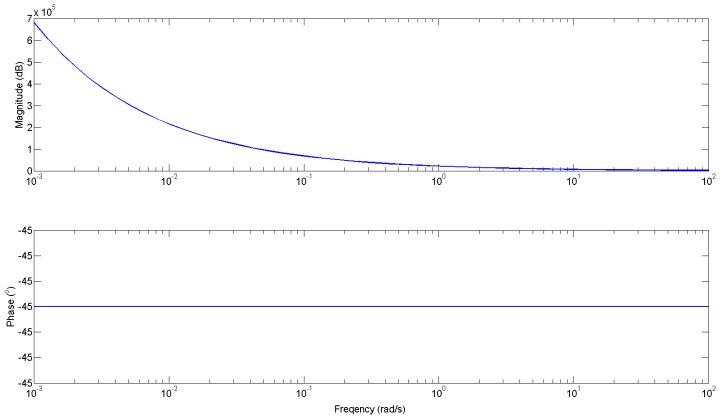

Figure 3.6: Impedance ($Zt = 1/Yt$) for all alveoli equal and $n = 0.5$ from (3.17).

are close to the expected values related from the fractional orders $(-30^o, -45^o)$. Finally, the result of the impedance with broken alveolar walls, as defined in (3.19)

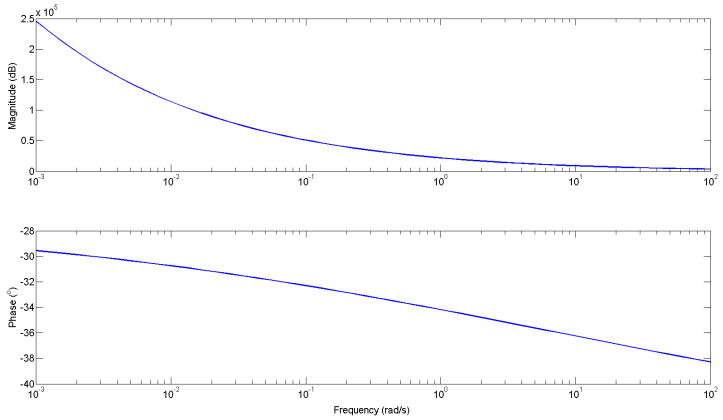

Figure 3.7: Impedance ($Zt = 1/Yt$) for mixed types of alveoli with impedances varying fractional orders $n = 0.3, n = 0.5$, as given in (3.18).

is given in Figure 3.8. As a general remark about all these simulation results, the magnitude values are unrealistically high. In reality, the very high alveolar surface (2^{24} alveolar sacs according to [40]) will reduce significantly the magnitude for a single sac. Here we used generic values to illustrate the effects of various changes occurring in such structures with pathology.

The simulation studies performed here suggest that the convergence of the fractional order in model from equation (3.7) has a structural origin and variations are directly related to structural changes. To our knowledge, such an analysis has not yet been reported in specialised literature.

Assuming initial conditions zero for both air flow and pressure the Laplace transform of (2.27) has the form in equation (2.30). This has similar form as the last term in equation (3.7) and combining these relations lead to:

$$Q(s) = \frac{\tau^n s^n}{1 + \tau^n s^n} \frac{Q_0}{s} \tag{3.20}$$

We have shown previously that such ladder networks converge to lumped form [14, 28]:

$$Y(s) \approxeq (\frac{s}{\omega})^n \tag{3.21}$$

with $n = r/(c + r)$ the fractional order term value dependent exclusively on the ratio of the alveolar parameters. This relation defines the admittance of air-alveolar interface. Changes in gas exchange area paired with disease evolution are related to the mass of air which can be involved in the ventilation process. This implies that the term in (3.20) has a time constant which is varying with the relative ratio between gas exchange surface and air mass. The damping factor of such a system

is independent on this term, but the natural frequency is inversely related to it via the following relation $\omega = 1/\tau$.

The natural frequency will increase for same surface with lower air mass, as expected in COPD patients. This is then always reflected by the balance of inertial and capacitive properties in these patients which tend to be equal at frequencies around 15 Hz and higher (in healthy, the resonant frequency is around 8Hz). In terms of respiratory impedance, the resonant frequency is where the negative part of the imaginary part of impedance (reactance) is equal to the positive part (i.e. crosses the zero line) [14, 38]. The damping factor is a parameter reflecting the

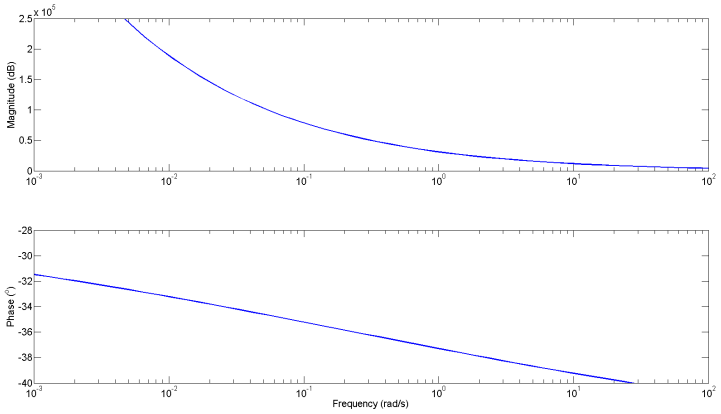

Figure 3.8: Impedance ($Zt = 1/Yt$) for broken alveolar walls and mixed types of alveoli with impedances varying fractional orders $n = 0.3, n = 0.5$, as given in (3.19).

capacity of the material for energy absorption. In the case of lung tissue damping is mostly characterize by viscoelasticity. The increased lung elastance in COPD due to more empty spaces in the alveolar structure will result in higher values of tissue damping than in healthy patients. The model from (3.20) has been used to mimic healthy and COPD patient by changing morphological parameter values in (3.12)-(3.13). This impedance was then fitted to the model in (3.7) to extract parameters from (3.8). The results are given in Figure 3.9 for tissue damping (G_r). It can be observed that as damping is increased, in COPD it relaxes as the alveolar walls are broken with COPD progress.

We do not have the possibility to measure non-invasively the impedance of the alveolar network. Instead, we employ the forced oscillation technique, a well-known lung function test broadly used to assess mechanical properties in lungs [38]. Figures 3.10-left and 3.10-right depict the boxplots for the tissue damping G_r and tissue hysteresivity η_r. Statistical analysis has been performed to identify if a significant difference between the group exists. Anova tests have been applied

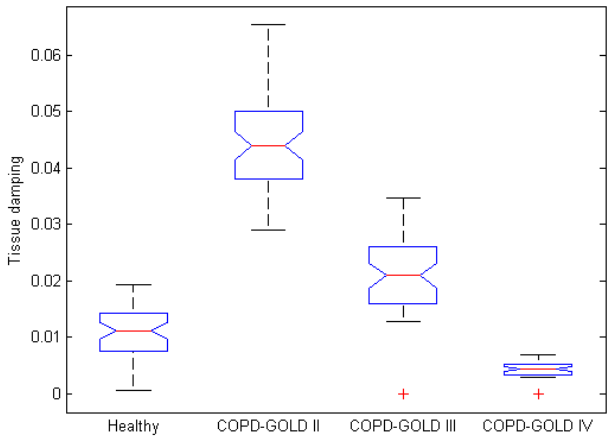

Figure 3.9: Simulated tissue damping (G_r) in: 1 - healthy, 2 - COPD-GOLD II, 3 - COPD-GOLD III and 4-COPD-GOLD IV (chronic obstructive pulmonary disease stage II, III and IV).

to the data and it has been observed a significant difference in tissue damping between the three groups: i.e. between: COPD-GOLD II and COPD-GOLD III; COPD-GOLD II and COPD-GOLD IV; COPD-GOLD III and COPD-GOLD IV. The p values identified for this case is lower than 0.01. Same analysis has been performed also for tissue hysteresivity and a p value lower than 0.05 has been identified.

The damping factor is a material parameter reflecting the capacity for energy absorption. In materials similar to polymers, as lung tissue properties are very much alike polymers, damping is mostly caused by viscoelasticity, i.e. the strain response lagging behind the applied stresses [45,46]. The loss of lung parenchyma (empty spaced lung), consisting of collagen and elastin, both of which are responsible for characterizing lung elasticity, is the leading cause of increased elastance in COPD. Damping will increase due to increased tissue density in places where alveolar walls are not broken.

Since pathology of COPD involves significant variations between inspiratory and expiratory air-flow, an increase in the hysteresivity coefficient η_r reflects increased inhomogeneities and structural changes in the lungs. In emphysematous lung, the caliber of small airways changes less than in the normal lung (defining compliant properties) and peripheral airway resistance may increase with increasing lung volume.

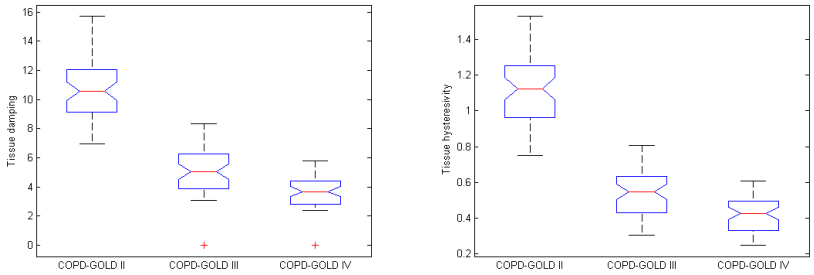

Figure 3.10: Left: Tissue damping (G_r); Right Tissue hysteresivity (η_r) in: 1 - COPD-GOLD II, 2 - COPD-GOLD III and 3 - COPD-GOLD IV (chronic obstructive pulmonary disease stage II, III and IV).

Based on our proposed derivations to obtain (3.5) and (3.20), the model from (3.7) has a strong theoretical basis linked to i) mechanical (resistance, elastance) properties of lung parenchyma, ii) structural layout (recurrent properties) and iii) tissue density (porous character). Alterations in these properties have an effect of the overall impedance parameters and these can now be linked to changes in small airways and alveolar levels. This in turn affects the degree of non-linearity in the tissue dynamics. The T index has been calculated for each group and the results obtained are presented in Figure 3.11-left.

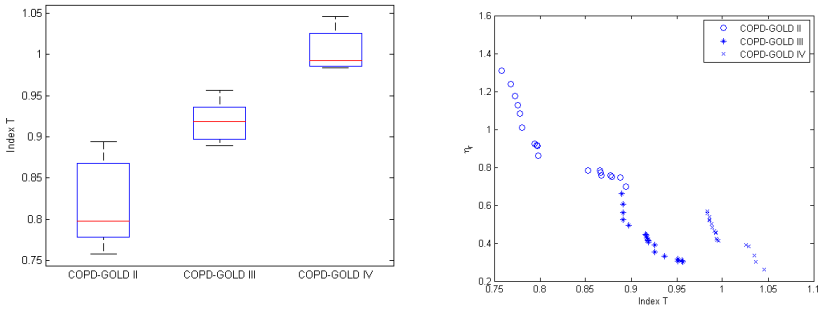

Figure 3.11: Left: Boxplot for the non-linear distortions in COPD-GOLD II, COPD-GOLD III and COPD-GOLD IV diagnosed groups. There is a significant difference between groups. Right: Relation between T index and the heterogeneity factor (η_n) is the evaluated COPD groups. 'o' denote COPD-GOLD II, '' denote COPD-GOLD III and 'x' denote COPD-GOLD IV.*

It can be noticed that there is a significant difference between the groups. From the results obtained we may conclude that the T index increases as COPD disease advances which is in line with prior rationale. Statistical analysis for the the T index in the measured group has been performed and the results obtained are reported in table 3.2.

Group	Min	Max	Mean	Std
COPD-GOLD II	0.7579	0.9840	0.8228	0.0488
COPD-GOLD III	0.8893	0.9568	0.9205	0.0229
COPD-GOLD IV	0.9836	1.0459	1.0019	0.0214

Table 3.2: Confidence intervals for the calculated T index in the measured groups. Std denotes standard deviation.

In Figure 3.11-right the evolution of the hysteresivity factor as a function of the T index is presented. The results obtained indicate that as COPD continues to deteriorate the alveolar walls the heterogeneity of the lungs will decrease as larger spaces occurs. However, the effects from changes at macromolecular level contribute to increased non-linear dynamics. The results indicate there exist a correlation between the T index and the heterogeneity factor (i.e. T increases ad the COPD disease advances). The added value of the T index is that it can be extracted directly from the measured signals without the necessity of (3.7).

3.7 Summary

In this chapter the importance of gas diffusion in patients with COPD disease has been investigated. A model of diffusion for COPD diagnosis does not exist and in this thesis a first step towards the development of such model has been taken. The proposed model has been simulated by means of numerical examples. The choice of number of alveoli was not based on any design specification but has been selected as a suitable number (either too low either too high) for the purpose of the study. The alveolar structure and morphology is drastically affected and thus plays an important role in determining the viscoelastic properties of lung parenchyma. Loss of alveolar surface area and dysfunction of the alveolar membrane as in emphysema lead to a decrease diffusion factor. Measurement of the diffusion factor can be of importance in (early) detection of COPD disease. Several methods to determine the diffusion factor have been investigated. Each method has its own advantages and limitation. The single breath method became the most generally accepted method.

In this chapter the available tools emerging from fractional calculus to model changes in COPD and to understand their effect on model parameters values have

been presented. The theoretical basis helps in understanding the interplay between all these structural and dynamical changes. The results obtained indicate that there is a direct relation between the T index and the heterogeneity in COPD lungs. A limitation of this study is that effects of decrease in vascularisation associated with broken alveolar walls are not investigated. This implies an augmentation of the model with complex mathematical description of diffusion phenomena. However, these are pertinent next steps in further developing the mathematical of fundaments respiratory mechanics. The obtained results are promising and is definitely worth to further investigate this hypothesis.

4

Towards a Pain Nociceptor Model

This chapter makes the soft transition from modeling diffusion in the lungs (Chapter 3) to modeling drug diffusion (Chapter 5). However, before investigating the use of diffusion models to characterize drug effect and uptake its necessity is addressed. Therefore, in this chapter the existing tools/methods/techniques and devices available to assess pain are presented. The contribution of this chapter to the remaining of the thesis is to indicate the gaps towards an objective pain assessment.

The publications related to this chapter are:

1. **D. Copot**, C.M. Ionescu, Objective Pain Assessement: How far are we?, E Cronicon Anesthesia Journal, Special Issue on Critical Care and Importance of Anaesthesia for Pain Relief, SI 01, 11-14, 2018,

2. **D. Copot**, C. Ionescu, Pain monitoring tools: a systematic review, Journal of Clinical Monitoring and Computing, 2018, submitted.

4.1 Introduction

Despite the importance of pain in medicine and biology, it is astonishing to discover that the word "pain" has been never defined satisfactorily.

- First definition states that *"pain is that sensory experience evoked by stimuli that injure or threaten to destroy tissue"* [56].

- Second definition describe pain as an abstract concept which refers to *1) a personal, private sensation of hurt; 2) a harmful stimulus which destroy the tissues; 3) a pattern of responses which operate to protect the organism from harm"* [57].

- Third definition is much better, but still falls short from being acceptable to all. Merskey et al. define pain as *an unpleasant sensory and emotional experience associated with actual or potential tissue damage, or described in terms of such damage* [58].

Pain is a highly personal experience and the patient is thus the best informant [59–62]. Pain is a multidimensional phenomenon that includes physiologic, sensory, affective, cognitive, behavioral, and sociocultural aspects. Several factors such as: age, race, gender etc. seem to modify patients' pain perception and reporting [63–66]. Despite modern techniques, pain remains a subjective experience and health care professionals have to rely on patients ratings [67]. Methods to accurately characterize patients pain level during unconsciousness are needed. For the case of intensive care unit there is no objective tool to evaluate the level of pain that the patient is experiencing.

Therefore, optimal pain assessment in intensive care units (ICU) is essential since it has been reported that 35% to 55% of nurses underrate patients pain [68, 69]. Moreover, in [70] has been reported that 64% of the patients did not receive any medications before or during painful procedures. In the SUPPORT (Study to Understand Prognoses and Preferences for Outcomes and Risks of Treatment) report [62], nearly 50% of patients reported pain, 15% reported moderately or extremely severe pain that occurred at least half of the time of the procedure, and nearly 15% were dissatisfied with their pain control. Inaccurate pain assessment and the resulting inadequate treatment of pain in critically ill adults can have significant physiologic consequences [71].

Hitherto, patient self-report is the best indicator of pain, e.g. using the numeric pain rating scale ranging from 0 to 10. However, many critically ill patients are unable to communicate effectively because of cognitive impairment, sedation, paralysis, or mechanical ventilation. Identification of the optimal pain scale in such patients is ongoing, and no single tool is universally accepted for use in the

non-communicative (anesthetized) patient [72, 73]. When a patient cannot express himself, observable indicators - both physiologic and behavioral - have been treated as pain-related indicators to evaluate pain level [74]. A more detailed description of the available tools is presented is given in section 2.

Therefore, there is a clear evidence that no accurate physiologic or clinical signs that can be used to objectively measure pain exists. Reliance on healthcare worker assessment of patient pain results in underestimation of the intensity of pain. According to the National Institutes for Health (NIH), patient self- reporting is the "most reliable indicator of the existence and intensity of pain" [75] Subjective pain measures that may need to be quantified include intensity, time course, quality, impact, and personal meaning. The ideal tool in the assessment of pain should include the identification of the presence of pain, as well as the progress of pain with time or treatment [76]. Also, this ideal tool should be applicable to any individual, regardless of psychologic, emotional, or cultural background. To that end, unidimensional pain scales have been developed. Because of their ease of use, these scales have become popular tools used to quantify pain relief and pain intensity. The most frequently used tools to assess acute pain are the numeric rating scale (NRS) and the visual analogue scale (VAS).

Although popular for study purposes, unidimensional pain scales have shortcomings. They were initially developed for use in experimental pain trials in which pain was limited and controlled. Clinical pain is different in the sense that it may become persistent, unbearable, and beyond the individual's control. It is also often associated with a strong emotional component not observed in the experimental setting. Pain scales tend to focus only on pain intensity, with increased risk of oversimplification of this complex experience. Furthermore, actual measurements are relative only to the individual being assessed. Identical stimuli applied to different individuals can yield to significantly different scores. Thus the numbers are simply estimates of the perception of the pain, based on past personal experience. Quantification of the experience requires the individual to abstract and quantify the sensation. The use of unidimensional pain scales is more appropriate in the setting of acute pain (caused by surgery, broken bone, burns, etc.) than chronic pain (e.g. headache, cancer pain, low back pain, etc.). Chronic pain is usually associated with other events such as degree of support and depression. The assessment of chronic pain often requires more complex evaluation tools.

Hence, pain is an subjective experience, and hitherto no objective tools exists to measure it. When possible, the existence and intensity of pain are measured by the patients self-report (i.e. conscious patients). Unfortunately, some patients cannot provide a self-report of pain either verbally, in writing, or by other means, such as finger span [77] or blinking their eyes to answer yes or no questions [78].

Effective management of analgesia in the ICU units requires an assessment of the needs of the patient, subjective and/or objective measurement of the key vari-

ables (such as pain, agitation, and level of consciousness), and titration of therapy to achieve specific targets [72, 79, 80]. It is important to admit that patient needs can differ depending on clinical circumstances, and that for any given patient therapeutic targets are likely to change over time. Thus, achieving patient comfort and ensuring patient safety, including avoidance of over- and under-dosage, relies on accurately measuring pain, agitation, sedation, and other related variables. This should be evaluated with validated tools that are easy to use, precise, accurate, and sufficiently robust to include a wide range of behaviors. From the point view of analgesia there is still a missing puzzle piece with respect to the existence of a objective pain measurement tool for general anesthesia. In this chapter a systematic review describing instruments/tools developed for pain measurement in conscious and unconscious patients will be reported.

4.2 Pain measurement during consciousness

Wide variation in the experience of chronic and neuropathic pain has led to the development of a broad range of pain measurement instruments. In general, pain measures can be classified into four groups: i) measures of pain intensity; ii) pain characteristics; iii) pain interference; iv) pain relief or global change. In addition, there are multiquestion measures to differentiate between types of pain (chronic and acute).

A first class of tools used for pain measurement include: NRSs, VASs, verbal rating scales (VRSs), percentage scale and graphical scales. In research and clinical settings, the above mentioned tools are being predominantly used to evaluate pain intensity. All tools produce good results as long as they are properly administered [83, 84] and all are highly correlated. These pain scales are reliable for multiple measurements within a single individual, but there is high variability among individuals with chronic pain. This variability makes it difficult to interpret the clinical importance of single pain measurements, but the change over time is a reliable and valid outcome for clinical trials. The improvement of pain assessment (expressed as a percent change to control for different baseline pain intensities) is highly correlated with his or her overall condition [86, 87].

Verbal rating scales typically consist of a series of verbal pain descriptors ordered from least to most intense (e.g., no pain, mild, moderate, or severe) [88]. Patients read the list and choose the word that best describes the intensity of their pain. A score of 0 is assigned to the descriptor with the lowest rank, a score of 1 is assigned to the descriptor with the next lowest rank, and so on. Numeric rating scales typically consist of a series of numbers ranging from 0 to 10 or 0 to 100 with endpoints intended to represent the extremes of the possible pain experience and labeled no pain and worst possible pain respectively. Patients choose the number that best corresponds to the intensity of their pain. Although VRSs and NRSs are

simple to administer and have demonstrated reliability and validity, the advantages associated with VASs and is the measurement instrument of choice when a unidimensional measurement of pain is required; however, this may not be true when assessing chronic pain in elderly patients. One study indicated that elderly patients make fewer errors on VRSs than on VASs.

A second class of pain measurement tools is based on questionnaire format. These tools are defined on a set of questions used to interrogate the patients about their pain. The clarity and specificity of the questions used will affect the reliability of the answers and the degree to which the questions relate to the process being studied-which is, their validity. Questionnaires are developed for one of the following purposes: to identify people with a specific condition within a population (discriminative), or to evaluate the change in a condition over time (evaluative). Although some scales aim to do both, the features that distinguish a specific condition are often not the best ones to follow over time. The format of each question contains several common elements, such as the condition being measured, the time frame, and modifiers of each, as needed. In Figure 4.1 an overview of the methods used for pain quantification in conscious patients is given.

4.3 Pain measurement during unconsciousness (e.g. general anesthesia)

Whereas routine pain assessment procedures can be used with ICU patients who are verbal, a substantial number of ICU patients may not be able to provide a self-report of the presence or intensity of their pain. The assessment of pain in these nonverbal critically ill patients poses numerous challenges. Research on the measurement of pain in critically ill adults who cannot self-report (referred to as nonverbal ICU patients) has emerged only within the past 2 decades. However, no measure of pain in nonverbal ICU patients is accepted as the gold standard. In this chapter six objective pain measures for use with nonverbal ICU patients and evaluation of the strengths and weaknesses of these measures will be discussed.

Objective pain measures are provided by observational instruments that can be categorized as either unidimensional or multidimensional. A unidimensional objective measure (eg, behavioral scale) may use a single domain (eg, facial expression) or several domains (eg, facial expression, body movements, sound, etc.) to evaluate a persons responses to pain. A multidimensional objective measure evaluates 2 or more pain dimensions (eg, behaviors, physiologic responses) and has several domains within each dimension. In the absence of self-report, unidimensional measures with multiple domains or multidimensional measures are the preferred tools to evaluate acute pain in nonverbal ICU patients [89].

The following unidimensional tools have been developed: Behavioral Pain

Scalar assessment tool	Definition	Strengths/Weakensses
Numerical Rating Scores	Numbers (0-10) with anchor descriptors are used to rate pain level or other symptoms: 0-no pain; 5-moderate; 10-worst pain	Good psychometric properties in measurement of change; ease of use **BUT** No intrinsic meaning to numbers
Verbal rating scales	VRS consists of a list of adjectives describing different levels of pain intensity: from 'no pain' to 'extremely intense pain	Commonly used measure in clinical assessment of pain and acute pain research models **BUT** People interpret words differently, especially across cultures
Visual Analog Scale	Fixed-lenght line (often 10 cm) and a mark is placed to indicate the level of pain. no pain (0 – 4 mm), mild pain (5– 44mm), moderate pain (45–74 mm), and severe pain (75– 100 mm)	Commonly used; good psycho metric properties **BUT** Requires visual presentation; no intrinsic meaning
Percentage scale	Numbers expressed as 0–100%	Used to indicate percentage change over time **BUT** No intrinsic value to specific Percentages
Graphical scales	Graphic presentation of response gradation (e.g., faces or colors)	Measure of pain in nonverbal adults or children **BUT** May not translate well across cultures
Pain measure questionnaire format	**Definition**	**Strengths/Weakensses**
Pain intensity	Measure of pain strength: worst pain; least pain; average pain; pain right now	Primary out come measure of most pain studies **BUT** Only one characteristic of pain; subjective perception of individual
Pain interference	Measure of the effect of pain on life activities: pain interference uses five items to characterize it: "mood", "enjoyment of life", "using your usual technique", "playing because of symptoms", and "playing as well as you would like". e.g. How much did pain interfere with your daily activities?	Supports pain intensity; measures the importance of the pain to the individual **BUT** Does not rank importance of the activity for the individual
Pain relief	Single question about the perception of change compared with a specific earlier time point	Measures individual's perception of efficacy of treatment over time **BUT** Does not always correlate with change in pain intensity; meaning may not be clear if used alone
Pain characteristics	Separate questions for describing multiple qualities of pain	Differentiates components and different types of pain **BUT** People's ability to differentiate pain types may be limited
McGill Pain Questionnaire	How strong is your pain? E.g. mild; discomfort; distressing; horrible; excruciating. Do the following items increase or decrease your pain? E.g. eating, heat, cold, no movement, movement, etc.	Provides a relatively rapid way of measuring subjective pain experience **BUT** Are difficult and time consuming to complete and demand a sophisticated literacy level

Figure 4.1: Pain measurement tools used for conscious patients.

Rating Scale (BPRS), Behavioral Pain Scale (BPS), Pain Behavior Assessment Tool (PBAT) and Critical-Care Pain Observational Tool (CPOT).

The BPRS is a unidimensional objective measure that assesses 4 behavioral domains: restlessness, tense muscles, frowning or grimacing, and patient sounds. Each domain contains 3 descriptors that indicate a progressive increase in pain severity and are scored on a scale that ranges from 0 (normal behaviors) to 3 (extreme pain behaviors). The total BPRS score (the sum of all domains scores) ranges from 0 (no pain) to 12 (most pain). Although the BPRS appears to possess satisfactory internal consistency, generalization of the BPRS findings [90–92] to nonverbal ICU patients is limited because it was tested in small homogeneous samples of post-anesthesia care unit (PACU) patients. In fact, patients with major complications and neurological problems were excluded from the studies. Moreover, the BPRS requires a patient to vocalize and to show discernible movements, which is limiting its use in a substantial percentage of nonverbal ICU patients who may be intubated, have an altered level of consciousness (LOC), unconscious patients or who have received neuromuscular blocking agents.

The BPS evaluates 3 behavioral domains (ie, facial expression, movements of upper limbs, compliance with ventilation). Each domain contains 4 descriptors that are rated on a 1 to 4 scale and the total BPS score can range from 3 (no pain) to 12 (most pain). Findings from 3 studies [90, 91, 93] suggest that the BPS is a valid and reliable measure for use in nonverbal ICU patients. However, attention to a number of factors would improve its clinical utility. First, the range of scores on the BPS (ie, 3 = no pain to 12 = most pain) should be revised so that a score of 0 reflects no pain behavior. Second, on the BPS, the lack of body movement equates with a pain-free state which is not most of the time the case for the ICU ward. **Moreover, during general anesthesia none of this tools can be used to evaluate pain during surgery for computerized closed loop drug titration.**

The PBAT unidimensional assessment tool was developed for a large-scale descriptive study of patients pain perceptions and behaviors associated with common hospital procedures in acute and critical care settings [94]. This tool consists of 3 behavioral domains with several descriptors within each domain (ie, facial expressions = 10 descriptors; body movement = 15 descriptors; verbal responses = 7 descriptors). The PBAT contains a number of features that enhances its clinical utility. The assessment procedure is simple (ie, mark the presence of a behavior) and not subject to interpretation. This approach contrasts with conventional objective pain measures that assign scores at the item level and use a sum score to indicate patients level of pain. To increase its applicability for use in nonverbal ICU patients, the tool requires modifications to the verbal response domain and the body movement domain because certain descriptors (eg, moaning, guarding, massaging) are not applicable in nonverbal patients with a decreased LOC. Additional evaluation is needed to confirm responsiveness of the PBAT to other sources

of acute pain, as well as to the administration of analgesics.

The CPOT is a unidimensional measure designed for use with intubated and nonintubated ICU patients. It evaluates four behavioral domains (ie, facial expressions, movements, muscle tension, ventilator compliance). Each CPOT domain is scored from 0 to 2, and the total score ranges from 0 (no pain) to 8 (most pain) [93]. However, the responsiveness of CPOT behaviors to painful stimuli in deeply sedated patients remains to be determined.

The following multidimensional tools have been developed: Pain Assessment and Intervention Notation (PAIN) Algorithm and Nonverbal Pain Scale (NVPS).

The PAIN Algorithm is a systematic pain assessment and management tool developed for research testing with critical care nurses. This tool consists of 3 parts: pain assessment; assessment of patients ability to tolerate opioids; and guidelines for analgesic treatment decisions and documentation. The pain assessment prompts nurses to observe the patient for the presence or absence of 6 behavioral domains (ie, facial expression, movement, posture, vocal sounds, pallor, perspiration) and 3 physiologic indicators (ie, heart rate (HR), blood pressure (BP), respiration). Then, the tool prompts nurses, based on their appraisal of these dimensions of pain, to rate the severity of the patients pain on a 0 (no pain) to 10 (most pain). The PAIN Algorithm may be a useful tool to standardize pain assessment and management in the ICU. However, the length of the tool limits its clinical utility [93]. Another limitation of this tool is that it does not standardize the measurements of behavioral and physiologic responses.

The NVPS includes 3 behavioral domains (ie, facial expression, body movement, guarding). Additionally, 4 physiologic domains were added based on a review of literature and grouped into 2 categories: Changes in vital sign over 4 hours and changes in skin color, warmth, and pupil dilation. Each NVPS domain is scored from 0 to 2 and the total score can range from 0 (no pain) to 10 (most pain). The NVPS has limited content validity and reliability as a pain measure for nonverbal ICU patients. First, certain NVPS behavioral descriptors such as smile or lying in normal position cannot be equated with a nonpainful state. Moreover, measurement of the physiologic indicators (eg, pupil dilation, perspiration) was not defined or standardized. In addition, the authors did not describe the rationale for their selection of vital sign parameters for pain (eg, respiratory rate increased by $>$10 breaths/min over 4 hours, SBP increased by $>$20 mm Hg over 4 hours).

Despite advances in pain research and management, the measurement of pain in nonverbal ICU patients remains an immense challenge for critical care clinicians. The dilemma of adequate versus inadequate pain management in these high-risk patients is largely attributed to the lack of vigorously tested valid and reliable pain measures. This critical review demonstrates that although 2 objective pain measures (ie, BPS, CPOT) showed validity and reliability, they have not received rigorous evaluation to consider them as a robust pain measure for use in

Pain measure questionnaire format	Definition	Strengths/Weakensses
Pain intensity	Measure of pain strength: worst pain; least pain; average pain; pain right now	Primary out come measure of most pain studies **BUT** Only one characteristic of pain; subjective perception of individual
Pain interference	Measure of the effect of pain on life activities: pain interference uses five items to characterize it: "mood", "enjoyment of life", "using your usual technique", "playing because of symptoms", and "playing as well as you would like". e.g. How much did pain interfere with your daily activities?	Supports pain intensity; measures the importance of the pain to the individual **BUT** Does not rank importance of the activity for the individual
Pain relief	Single question about the perception of change compared with a specific earlier time point	Measures individual's perception of efficacy of treatment over time **BUT** Does not always correlate with change in pain intensity; meaning may not be clear if used alone
Pain characteristics	Separate questions for describing multiple qualities of pain	Differentiates components and different types of pain **BUT** People's ability to differentiate pain types may be limited
McGill Pain Questionnaire	How strong is your pain? E.g. mild; discomfort; distressing; horrible; excruciating. Do the following items increase or decrease your pain? E.g. eating, heat, cold, no movement, movement, etc.	Provides a relatively rapid way of measuring subjective pain experience **BUT** Are difficult and time consuming to complete and demand a sophisticated literacy level

Figure 4.2: Pain measurement tools used to measure level of pain in non-communicative patients (i.e. unconsciousness).

nonverbal ICU patients. Although the discussed tools are mentioned as an objective way to measure pain, there is much room for improvement due to the fact that these tools are based on several domains and they are still depending on the experience of the nurse. Therefore, it cannot be claimed that with these tools the actual pain the patient is experiencing is being also the measured pain. In Figure 4.2 an overview of the available tools for pain assessment during unconsciousness is presented.

In conclusion, pain assessment is largely depended on the ability to rate personal subjective pain. Moreover, pain scales can be difficult to use during medical procedures. Several techniques have been developed for conscious and unconscious patients. For the first category (i.e. consciousness) most optimal tools for pain measurement are the VAS and NRS, but also the other techniques presented in this review are being used to evaluate pain level. For the second category (i.e. unconsciousness) several devices/tools have been developed in order to evaluate pain level. Even if effort has been made to develop an objective and individualized pain measurement device for unconscious/non-communicative patients there is no such tool is used in clinical practice. The first steps towards the development of such an objective pain assessment tool have been undertaken in this thesis.

4.4 Commercial Devices

In the last fifteen years the research effort on developing a device for objective measurement of pain has increased. As a result, nowadays there are three medical devices available on the market for pain assessment. Each of them is designed for a certain category of patients. A description of the available devices along with their advantages and disadvantages is given hereafter.

Med-Storm Pain Monitor is designed for infants, children and adults, with more focus on infants and children. This device is based on the measurement of skin conductance (SC) to monitor nociceptive stimulation, awareness and pain. Various methods of pain assessment in infants have been trialled in the search for objective, specific, physiologic measures of responses to pain. SC measured in the palm of the hand or on the plantar area of the foot may be one such measure. SC in these sites reflects the emotional sweating due to sympathetic nerve activity. The skin conductance response (SCR), which results from filling and reabsorption of sweat in the sweat glands, has previously been suggested to be the most sensitive SC parameter of sympathetic nerve activity in response to painful stimulation [95].

SC activity is caused by the release of sweat from the sweat glands upon activation of the sympathetic nervous system which in turn acts on muscarinic receptors in the sweat glands [96]. On cessation of this gland stimulation, fluid is reabsorbed from the ducts and the conductance decreases. This can be recorded as a ‘wave’

or a 'fluctuation' in electrodermal measurements [97], namely a SCR. SCR have a relatively steep onset and a flat recovery; that is, SCR rise time is shorter than recovery time. The steep onset represents the release of sweat from the secretory duct and the flat recovery is caused by the slower reabsorption of sweat within the duct.

In [95] the skin conductance variability between hospitalized infants at rest has been reported. The aim of the study was to investigate the hypothesis whether or not the SCR can be used as a parameter of stress [98, 99]. The outcome of the study indicated that the variability was higher for intra-patient variability than for inter-patient variability. The intra-patient variability was almost three times larger than inter-patient variability, i.e. 0.93 vs 0.27. The authors have reported that the observed variation in the heart rate implies problems with using heart rate as a physiological indicator for pain. They also indicated that although heart rate and oxygen saturation are considered sensitive indicators of pain, they lack of specificity. In this pilot study the authors intended to establish a baseline for SCR in hospitalized infants at rest. As the number of participants was small, further studies are required to determine the validity and reliability of the SC measurement as an added component to routine clinical pain monitoring device for critically ill infants.

The aim of the research performed in [98] was to investigate if the spontaneous SC activity can be used to measure the stress response to heel stick in premature infants. In this study twenty premature infants have been monitored. The outcome of this study indicates that the measurement of spontaneous SC activity showed stress responses to heel stick from at least 29 weeks age in healthy premature infants. The authors claim that the number and amplitude of the waves of spontaneous SC activity mirrors the response to sympathetic nervous system to the emotional state. From this study they also concluded that SC activity variables may be a useful tool for surveying stress responses to pain stimuli in premature infants. In a later a review on the capability of the SC to monitor pain and comparison to other physiological pain assessment tools in children and neonates has been reported [100]. In the intensive care units and at neonatal units the SCRs/sec showed a high sensitivity to monitor pain, but again, low specificity.

In [101] a comparison between the Wong-Baker Faces Scale (gold standard in clinical practice) versus SC has been investigated. In this study 150 children have been evaluated during routine care. The outcome of this study indicated that the self-reported pain score was significantly lower that the SC score. One of the limitations of the study is the lack of previous comparison between SC and Wong-Baker faces scale (see Figure 4.3). Another limitation is the difficulty to convert the SC data in a numerical scale that could be compared to Wong-Baker faces scale.

[1] http://wongbakerfaces.org/

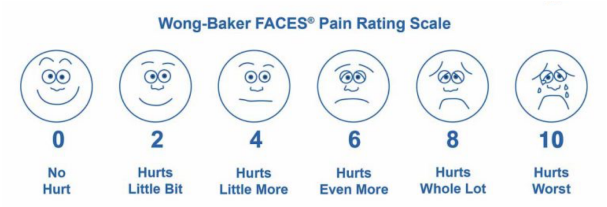

Figure 4.3: The Wong-Baker Faces Scale [1]

Med-Storm Pain Monitor™ system consists of a software that operates under Windows® together with a measuring unit and disposable sensors. The software has three different modes for different patient populations. In the anaesthesia mode it registers peaks/sec and area under curve. In the post-operative mode peaks/sec are recorded. In the infant mode peaks/sec are registered. When the research mode is selected, values of 'area huge peaks', 'area small peaks', 'peaks per second', 'average peak', 'average rise time' and 'signal quality' are displayed. When off-line, the software can be used to analyse recorded data. Recorded data can be exported to Microsoft Excel® . The electrodes are placed on the palm of the hand (adults) or around the foot (neonates). In Figure 4.4-left the measurement device is depicted and in Figure 4.4-right the variation of in skin conductance during three painful stimuli is presented.

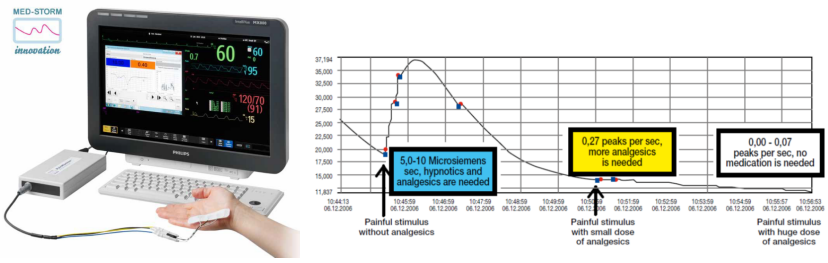

Figure 4.4: Med-Storm Pain Monitor [2]

[2] http://www.med-storm.com/

AlgiScan is a pain monitoring device based on pupillary reflex dilatation (PRD) and it has been developed for patient during anaesthesia In the last 20 years PRD has been studies as a potential marker for response to noxious stimulation in volunteers and surgical patients. Several studies have shown that in response to an incision or tetanic electrical stimulation of the skin, PRD monitoring permits the detection of a dramatic increase in pupil size, even during general anaesthesia [102–104]. In [103] a pilot study has been conducted in order to test the hypothesis whether or not the PRD can be used to assess noxious stimulation and analgesic effect in children undergoing anaesthesia. In [105] the performance of pupillometry to detect differences in PRD response to a standardised noxious stimulus during continuous infusion of Remifentanil has been investigated. The outcome of this study was a proof of concept that the method can perceive the effects of peripheral nerve block in patient receiving infusion of Remifentanil.

In [106] evaluation of the device in sedated patients has been investigated. In this study a comparison of the pupil size with heart rate, blood pressure and bispectral index has been performed. This study suggests that certain physiological reactions and pupil size changes may be potentially useful nociceptive indicators in ICU settings. However, this preliminary study does not suffice and further research is required in order to determine the clinical parameters of physiologic response change and evaluate the effects of opioids and sedatives on these responses.

In [107] a analysis on the objective assessment of the postoperative analgesia using the PRD method has been investigated. In this observational study pain intensity has been assessed by means of a VRS. Before and after drug administration to the patient, PRD has been measured. It has been noticed that the PRD index in the immediate postoperative period is significantly correlated with the VRS.

Figure 4.5: AlgiScan measurement device[3]

In Figure 4.5 the AlgiScan device is depicted along with a pain pupillary index (PPI) test. In this case the pupillary response to electrical stimulation indicates an insufficient level of analgesia for an surgical incision (i.e. PPI score 6/10).

[3] http://www.equip.nl/en/specialization/anesthesia/analgesia-monitor.html

MEDASENSE is another device based on a multi-parametric index for assessment of the presence and severity of pain. This technology combines the non-invasive probe incorporating 4 sensors (photoplethysmograph, galvanic skin response, temperature, and accelerometer). The finger probe continuously acquires physiological signals through four sensors. Several pain-related physiological parameters and derivatives are extracted and computed (heart rate, heart rate variability, pulse wave amplitude, skin conductance level, number of skin conductance fluctuations, temperature and more). Advanced machine learning algorithms identify the pain-related pattern and reflect the information on a scale where 0 represents no pain and 100 represents extreme pain - the nociception level (NOL) Index. NOL provides superior indication of the presence and severity of pain versus individual parameters (such as changes in heart rate and blood pressure). A figure of the device is given in Figure 4.6.

Figure 4.6: MEDASENSE measurement device[4]

Several studies have been published on the use and potential of this technology. In [108] a study on the development and validation of this method has been investigated. In this paper the NOL for patients undergoing anaesthesia has been reported. This study suggest a new index for non-invasive assessment of patient level of nociception during anaesthesia, based only on physiological parameters. In [109] the ability of the NOL to detect noxious stimuli during anaesthesia has been investigated. A comparison with heart rate and mean arterial pressure was performed. The results indicate that during nonnoxious event none of the parameters have changed. When incision took place an increase of the monitored parameters has been noticed. The outcome of this papers indicates that in contrast with heart rate and mean arterial pressure, the NOL was not affected by hemodynamic effects of Remifentanil. Another study [110] has investigated the abilities of NOL index and other measures of nociception to discriminate between noxious and nonnoxious stimuli, to progressively respond to graded stimuli and to respond to opioid administration. These studies suggest that the NOL index is a potential index to distinguish nonnoxious and graded noxious stimuli as well as the response to opioids.

[4] https://www.medasense.com/

The devices presented in this chapter have been evaluated mostly on sedated patients. Therefore, there is still much room for improvement. Although, clinically needed and theoretically promising, currently there is not enough evidence (i.e. clinical trials) to support the widespread use of any physiological sensors as ”objective” measures of pain. Another drawback is that none of these devices are based on mathematical interpretations/descriptions/models of pain.

4.5 Summary

In this chapter a detailed overview of the existing methods and devices available for pain assessment has been given. From here, one may conclude that the existing methods are subjective (i.e. based on patient feedback). With respects to the available devices two main conclusions can be drawn: 1) these devices are not yet employed in clinical settings as standard tools for pain assessment. This is due to the lack of large clinical trials but also, because each of them is for a certain class of patients. 2) none of them is based on a mathematically-physiologically based model. The challenges identified in this chapter are further exploited in the remaining of this thesis.

5

Pharmacokinetics-Pharmacodynamics Models of Drug Uptake and Drug Effect

In this chapter drug diffusion in the human body by means of compartmental models is presented. Fractional calculus tools are employed to characterize the profiles of drug concentration in each compartment.

The main publications where this work has been presented are:

- **D. Copot**, R. Magin, R. De Keyser, C. Ionescu, Data-driven modelling of drug tissue trapping using anomalous kinetics, Chaos, Solitons and Fractals, 102, 441-446, 2017.
- **D. Copot**, A. Chevalier, C.M. Ionescu, R. De Keyser. A Two-Compartment Fractional Derivative Model for Propofol Diffusion in Anesthesia, IEEE Multi-Conference on Systems and Control, Hyderabad, India, 28-30 August, 264-269, 2013.
- C.M. Ionescu, **D. Copot**, On the use of fractional order PK-PD models, European Workshop on Advanced Control and Diagnosis, Lille, France, 17-18 July, 1-12, 2017.

5.1 Introduction

Selecting appropriate models is a crucial step in capturing complex biological and physiological phenomena. Any choice of a model structure implies a simplified view of the interaction among the various elements that may characterise a dynamical system. In pharmacokinetics, a popular choice is that of compartmental models, due to their implicit simplicity and ease of understanding in relation to the mass balance equations and assumptions for uniform distribution, homogeneous transient times and immediate response to drug bolus administration [111]. Numerous works and decades of research have tailored their applicability for optimal drug delivery assist devices in several domains of medical applications, e.g. diabetes [112], cancer [113, 114], anaesthesia [115], immunodeficiency [116] and hormonal treatment [117].

Providing a best fit to data from observed drug concentration profiles implies the existence of some error tolerance intervals. Emerging tools from fractional calculus have proven useful to improve to a great degree the accuracy of dynamical models with respect to classical integer order modelling theory [118, 119]. The acceptance of these tools within the engineering community has led perhaps to a significant step forward in terms of data driven modelling and numerical simulation [120, 121]. However, their acceptance in clinical practice may require further tailoring for a better characterization of patient variability [122–124].

Compartmental models are a traditional tool for modelling drug pharmacokinetics (PK) in applications of general anaesthesia. The depth of anaesthesia regulatory problem consists of optimal calculation via such patient PK models of the amount of drug necessary to achieve a desired sedation level, irrespective of artefacts and disturbances [125]. Attempts to fractionalise PK compartmental models for anaesthesia have been done with simulated data. A net advantage however has not been shown, since secondary effects due to drug trapping were not accounted for at that time [126, 127].

Pharmacokinetic model gives information about the concentration profile of a drug as a function of time, in the body fluid (i.e. blood) as a result of a dose administration (e.g. bolus injection). Compartmental models seems to be widely used, while they provide a continuous description of the concentration that can serve as a input function for the pharmacodynamic part. In general, the pathway of a drug through the body can be separated into three distinct phases: uptake, distribution, and elimination.

Uptake: Different routes of administration produce variability in the rate of drug uptake and amount of drug delivered effectively to the body. Intravenous administration of a drug results in the entire dose entering the plasma immediately, although it must pass initially through the pulmonary circulation and some drugs (e.g. fentanyl) have significant take-up by the lungs [128].

Distribution: After intravenous administration of a drug, the peak blood concentration is determined by the dose, the rate of administration, and the cardiac output. With a high cardiac output, the effective volume of blood in which the drug is initially diluted is larger, leading to a lower peak concentration. A high cardiac output transports the drug fast to the vessel-rich tissues (including brain), and for highly lipid-soluble drugs, fast equilibration takes place, leading to a fast onset of action. Therefore, a low cardiac output leads to a higher initial peak concentration, because the drug is mixed with a smaller volume of blood during injection, though it will take longer to reach its target site [128]. All the aspects mentioned above explains why a smaller dose of induction agent is required in an elderly or shocked patient but may have a slower onset of action, while a young patient may require a much larger dose, but they will start to feel the effects more quickly.

Elimination: Full recovery depends on the removal of the drug from the body. Such elimination may result from excretion, metabolism, or a combination of of the two drugs. Large molecular weight drugs are often excreted in the bile, but most drugs are renally excreted. In order for the kidneys to handle lipid-soluble drugs, they need to be metabolized into a polar, water-soluble form. Most of this metabolism occurs in the liver and can be divided into two phases reactions. Phase one is the reaction which consist in oxidation, reduction, and hydrolysis, while in the second phase reaction consist in conjugating the resulting metabolites with sulphate, glucuronide, or other groups. For most drugs, elimination occurs in an exponentially declining manner, the rate of elimination being proportional to the plasma concentration, as the downstream end of the gradient remains at zero [128]. This system (i.e. the amount of drug being removed is a constant fraction in unit time rather than a constant amount) is known as first-order kinetics. The pharmacokinetic model represented in Figure 5.1 is represented traditionally by the following equations (5.1)-(5.4).

From the point-of-view of regulating anesthesia, mathematical modeling of drug diffusion can be very useful to better understand the mechanism of drug delivery systems. Therefore, the description of drug transport into the human body can be highly beneficial [18–20] from two points-of-view: (i) allows one to understand the insight of the mechanism and (ii) allows one to do quantitative prediction of the effects of formulation and processing parameters on the resulting drug release kinetics. The major challenge in the development or optimization of automated drug delivery systems is to achieve optimal drug concentration at the site of action. In order to have the optimal concentration-time-profile at the site of action the release of the drug must be controlled as accurately as possible.

Pharmacokinetic/pharmacodynamics (PK/PD) models represents an important step in the process of drug development and this modeling tool also brought a significant contribution to anesthesia. PK/PD models are a set of mathematical

equations used to predict the drug effect in time. PK models describe what the body does to the drug in terms of ADME parameters (i.e. Absorption, Distribution, Metabolism and Elimination). PK modeling for analgesic, opioid and muscle relaxants drugs has been studied by several authors. In its classical version, compartmental analysis is based on mathematical models, typically in the form of systems of ordinary differential equations (see equations (5.1)-(5.4)) that are widely used to characterize the uptake, distribution and elimination of a drug into the body.

$$\dot{q}_1(t) = K_{21}q_2(t) + K_{31}q_3(t) - K_{12}q_1(t) - K_{13}q_1(t) - K_{10}q_1(t) - K_{1e}q_1(t) + U(t) \tag{5.1}$$

$$\dot{q}_2(t) = K_{12}q_1(t) - K_{21}q_2(t) - K_{20}q_2(t) \tag{5.2}$$

$$\dot{q}_3(t) = K_{13}q_1(t) - K_{31}q_3(t) - K_{30}q_3(t) \tag{5.3}$$

$$\dot{q}_e(t) = K_{1e}q_1(t) - K_{0e}q_e(t) \tag{5.4}$$

where: q_1, q_2 and q_3 [mg] denotes the amount of drug in the three compartments and V_1, V_2 and V_3 represents the volume in the three compartments. The drug concentration in the blood is expressed by q_1/V_1, respectively q_2/V_2 and q_3/V_3 for compartment 2 and 3. The peripheral compartments 2 (muscle) and 3 (fat) represents the drug exchange of the blood with well and poorly diffused body tissues. The parameters K_{ij} denote the drug transfer frequency from the $i-th$ to the $j-th$ compartment and $U(t)$ [mg/s] is the infusion rate of the drug into the first compartment. The parameters K_{ij} of the PK models depend on age, weight, height and gender and can be calculated for Propofol as follows: V_3 represents the volume of fat and is calculated using equation (5.5), while V_1 and V_2 are known (V_1=4.27 (L) and V_3=2.38 (L)).

$$V_2 = 18.9 - 0.391(age - 53) \tag{5.5}$$

Clearance is calculated as follows:

$$Cl_1 = 1.89 + 0.456(weight - 77) - 0.0681(lbm - 59) + 0.0264(height - 177) \tag{5.6}$$

$$Cl_2 = 1.29 + 0.024(age - 53) \tag{5.7}$$

and $Cl_3 = 0.836\ (l/min)$. where Cl_1 is the rate at which the drug is cleared from the body, and Cl_2 and Cl_3 are the rates at which the drug is removed from the central compartment to the other two compartments by distribution.

The lean body mass (lbm) for men and women has the following expressions:

$$\begin{aligned} bm_{man} &= 1.1 * weight - 128\frac{weight^2}{height^2} \\ lbm_{women} &= 1.07 * weight - 148\frac{weight^2}{height^2} \end{aligned} \tag{5.8}$$

A schematic representation of a three compartmental model is presented in Figure 5.1.

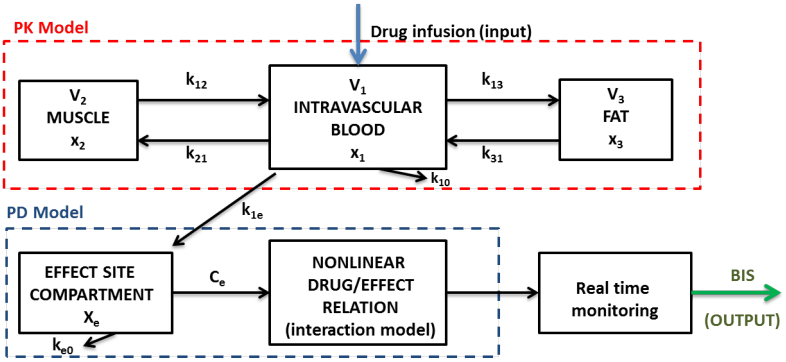

Figure 5.1: General compartmental model of the patient, where PK denotes the pharmacokinetic model and PD denotes the pharmacodynamic model of an infused drug.

An additional hypothetical effect compartment was proposed to represent the lag between plasma drug concentration and drug response. The amount of drug in this compartment is represented by q_e. The effect compartment receives drug from the central compartment by a first-order process and it is regarded as a virtual additional compartment. Therefore, the drug transfer frequency for Propofol from the central compartment to the effect site-compartment is equal to the frequency of drug removal from the effect-site compartment $k_{e0} = k_{1e} = 0.456[min^{-1}]$ and we have that:

$$\dot{C}_e(t) = K_{e0}(C_e(t) - C_p(t)) \tag{5.9}$$

with $C_e = q_e/V_1$ called the effect-site compartment concentration, and $C_p = q_1/V_1$ called the plasma concentration in the first compartment. The relation between the effect site concentration C_e and BIS is given by a nonlinear sigmoid Hill curve [129]:

$$Effect = E_0 - E_{max}\frac{C_e(t)^\gamma}{C_e(t)^\gamma + C_{50}^\gamma} \tag{5.10}$$

where E_0 is the value of the effect before the surgery (i.e. when the patient is awake), E_{max} is the maximum effect that can be achieved by the infusion of Propofol, C_{50} is the Propofol concentration at half of the maximum effect, and γ is a parameter which together with the C_{50} determines the patient sensitivity to the drug.

There are many assumptions regarding the modeling approach. Marsh et al. [130] considered weight as the only variable which covariates. A few years later

Kataria et al. [131] also included parameters such as age and gender as covariates. Later on, a linear relationship between the PK of the drug and the rate of infusion has been developed [132]. The conclusion of some other researches was that elderly patient are more sensitive to analgesic drugs than younger patients [133]. In the work of Vuyk et al. [134] a more accurate three compartmental PK model which takes into account age and weight parameters as significant covariates is described.

Fractional pharmacokinetics was first introduced by Dokoumetzidis and Macheas [12]. Their work presents the application of fractional calculus for a simple one compartmental model. Later on, this approach has been extended to a multi-compartmental model [15]. Popovic et al. [15] generalized the classical first order compartmental model by replacing the left hand side of the equation with fractional derivatives. Standard arguments imply that the equations which are determined by the mass balance in compartments have the following form [9].

$$\tau_1^{n_1-1} D^{n_1} q_1(t) = K_{21} q_2(t) + K_{31} q_3(t) - K_{12} q_1(t) - K_{13} q_1(t) - K_{1e} q_1(t) - K_{10} q_1(t) + U(t) \tag{5.11}$$

$$\tau_2^{n_2-1} D^{n_2} q_2(t) = K_{12} q_1(t) - K_{21} q_2(t) - K_{20} q_2(t) \tag{5.12}$$

$$\tau_3^{n_3-1} D^{n_3} q_3(t) = K_{13} q_1(t) - K_{31} q_3(t) - K_{30} q_3(t) \tag{5.13}$$

$$\tau_e^{n_e-1} D^{n_e} q_e(t) = K_{1e} q_1(t) - K_{0e} q_e(t) \tag{5.14}$$

where: τ_i represents the characteristic time of the $i-th$ compartment, expressed in seconds, $i = 1, ..., n$ and K_{ij}, for $i, j = 1, ..., n$ are standard diffusion coefficients having the dimension 1/s. The introduction of τ_i leads to the dimensional homogeneity of fractional rate equations. Dividing equations (5.11)-(5.14) by $\tau_i^{n_i}$ and redefining the constants we obtain the following fractional order differential equations.

$$D^{n_1} q_1(t) = k_{21} q_2(t) + k_{31} q_3(t) - k_{12} q_1(t) - k_{13} q_1(t) - k_{1e} q_1(t) - k_{10} q_1(t) + U(t) \tag{5.15}$$

$$D^{n_2} q_2(t) = k_{12} q_1(t) - k_{21} q_2(t) - k_{20} q_2(t) \tag{5.16}$$

$$D^{n_3} q_3(t) = k_{13} q_1(t) - k_{31} q_3(t) - k_{30} q_3(t) \tag{5.17}$$

$$D^{n_e} q_e(t) = k_{1e} q_1(t) - k_{0e} q_e(t) \tag{5.18}$$

with $n_1 = n_2 = n_3 = n$ and the constants were redefined according to relation (5.19).

$$k_{ij} = \frac{K_{ij}}{\tau_i^{n_1-1}} \tag{5.19}$$

where k_{ij} are the constants depending on the rate of absorption, elimination, tissue take up, characteristic and inactivation of drug. One of the characteristic of fractional derivatives is the "memory effect" term. It is well known that the state of many systems (biological, electrochemical, viscoelastic, etc.) at a given time depends of their configuration at previous time [135].

For compartmental models a general numerical solution of the fractional differential equation $D_t^n y(t) = f(y(t), t)$ can be expressed as:

$$y(t_k) = f(y(t_k), t_k)h^n - \sum_{j=1}^{k} c_j^n y(t_{k-j}) \tag{5.20}$$

where: $t_k = kh$, for $k = 1, 2, 3....N$ samples and h is the sampling time. For our case the numerical solution is obtained by applying equation (5.20) on equations (5.15)-(5.18) and it has the following form:

$$\begin{aligned} q_1(t_k) = (k_{21}q_2(t_k) + k_{31}q_3(t_k) - k_{12}q_1(t_k) - k_{13}q_1(t_k) - \\ k_{0e}q_e(t_k) - k_{10}q_1(t_k - 1))h^n - \sum_{j=1}^{k} c_j^n q_1(t_{k-j}) \end{aligned} \tag{5.21}$$

$$q_2(t_k) = (k_{12}q_1(t_k) - k_{21}q_2(t_k) - k_{20}q_2(t_{k-1}))h^n - \sum_{j=i}^{k} c_j^n q_2(t_{k-j}) \tag{5.22}$$

$$q_3(t_k) = (k_{13}q_1(t_k) - k_{31}q_3(t_k) - k_{30}q_3(t_{k-1}))h^n - \sum_{j=i}^{k} c_j^n q_3(t_{k-j}) \tag{5.23}$$

$$q_e(t_k) = (k_{1e}q_1(t_k) - k_{0e}q_e(t_{k-1}))h^n - \sum_{j=i}^{k} c_j^n q_3(t_{k-j}) \tag{5.24}$$

PD model describes the relationship between drug concentration and its clinical effect. Similar to PK modeling the influence of parameters such as gender or age were also investigated. Regarding the gender influence on the PD of analgesic drugs has been studied [136] and the conclusion was that there are significant differences between male and female patients on the response to analgesia. Drugs pharmacodynamics are described by an additional effect-site compartment (see Figure 5.1) and a non-linear relationship between drug concentration and drug effect. This relationship is often modeled by a sigmoid function [129]. The PD model relates the concentration provided by the PK model to the observed effect. Due to its nonlinearity PD models represent the challenging part of PK/PD models. To deal with this nonlinearity Hill equation is widely used. Hill equation has been extensively used to analyze quantitative drug-receptor relationship. Moreover, Hill equation is used in PK/PD modeling to describe the nonlinear drug dose response relationship. The basic expression is given by equation (5.10).

5.2 Pharmacodynamic model (interaction model)

The relation between the amount of drug administered and the entity of its effect, referred to as pharmacodynamics, is often modeled by a sigmoid function [129]. A sigmoid curve can be adopted to describe drug pharmacodynamics. The PD model relates the concentration provided by the PK model to the observed effect. The classic and most commonly used PD models is the sigmoid pharmacodynamic relation where the parameters are functions of the drug ratio (θ) [129]. For one drug, the model can be represented by equation (5.10), also known as Hill equation:

When a combination of two drugs A and B is used, equation (5.10) becomes equation (5.25) and a ratio (θ) of their normalized concentrations is defined.

$$Effect = E_{max}(\theta)\frac{\frac{U_A+U_B}{U_{50}(\theta)}}{1+\frac{U_A+U_B}{U_{50}(\theta)}} \tag{5.25}$$

$$\theta = \frac{U_B}{U_A+U_B} \tag{5.26}$$

$$U_A = \frac{C_A}{EC_50A}; U_B = \frac{C_B}{EC_50B} \tag{5.27}$$

$$E_{max}(\theta) = E_{maxA} + (E_{maxB} - E_{maxA} - \beta_{Emax}) * \theta + \beta_{Emax} * \theta^2 \tag{5.28}$$

$$\gamma(\theta) = \gamma_A + (\gamma_B - \gamma_A - \beta_\gamma) * \theta + \beta_\gamma * \theta^2 \tag{5.29}$$

$$U_{50}(\theta) = U_{50A} + (U_{50B} - U_{50A} - \beta_{U50}) * \theta + \beta_{U50} * \theta^2 \tag{5.30}$$

and considering that $U_{50A} = U_{50}(\theta = 1) = 1$ and $U_{50B} = U_{50}(\theta = 0) = 1$, equation (5.29) simplifies to:

$$U_{50}(\theta) = 1 - \beta_{U50}) * \theta + \beta_{U50} * \theta^2 \tag{5.31}$$

where:

- $U_{50}(\theta)$ represents the potency of the drug combination relative to the normalized potency of each drug by itself;
- E_{max}, U_{50}, and γ are expressed as functions of the drug ratio (θ), see equations (5.28)-(5.31);
- U_A and U_B are the normalized concentrations of drugs A and B;

- E_{maxA}, γ_A, U_{50A}, and $E_{maxB,}$, γ_B, U_{50B} are the pharmacodynamic parameters for the two drugs A and B;
- β_{Emax}, β_γ, and $U_{50}(\theta)$ represent the interaction parameters;
- $E_{max}(\theta)$, $\gamma(\theta)$ and $U_{50}(\theta)$ are the corresponding pharmacodynamic parameters for the sigmoid curve.

Figure 5.2 shows the block diagram of the BIS model. The objective is to describe the relationship between the drugs effect concentrations and its effect. Bruhn et al. [137] used an interaction model to relate the electroencephalographic parameter values (including BIS) to the effect concentrations of hypnotic and opioid drugs. This model model has been proposed by Minto et al. in a previous study [129].

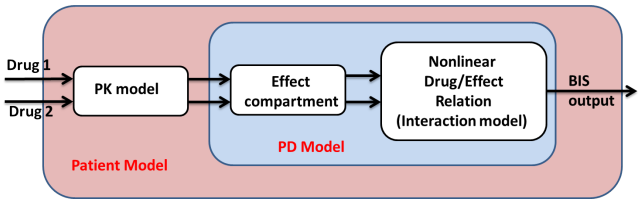

Figure 5.2: Block diagram of BIS model.

In the case of combined administration of two or more drugs, the potential interactions must be considered. Different approaches to drug interaction modeling have been developed. A common approach [129] is based on the use of response surfaces, where a combination of drugs is regarded as being a new drug with its own sigmoid pharmacodynamic concentration effect relation. In Figure 5.3 the global effect as a result of simultaneous administration of drugs 1 and 2 is given.

As a conclusion one may say that PK-PD data and the link between them can be model in two ways: either simultaneously, either separately [138]. In most situations PK models are better understood and defined than PD model and therefore an intermediate step is preferred. In this way, the pitfall due to poor PD data or wrong model selection can be avoided. However, for both mechanism-based and descriptive models, only rigorous validation procedures can ensure dose- and time-independence of PD parameters as E_{max} and EC_{50}. Using equations (5.21)-(5.24) one obtains the results presented in Figures 5.4 and 5.5.

A detailed description regarding the model parameters is given in [126, 127]. From Figure 5.4, it can be concluded that the order of the derivatives n determines the decay of the numerical solution. Notice that for $n < 1$, the decrease of the

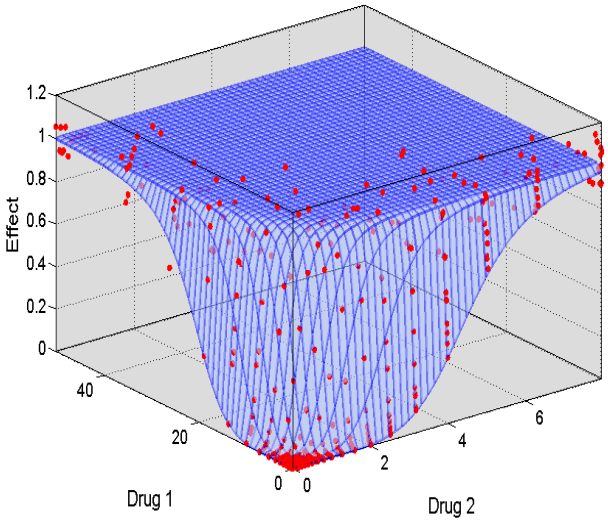

Figure 5.3: Example of response surface for the combined effect of two drugs.

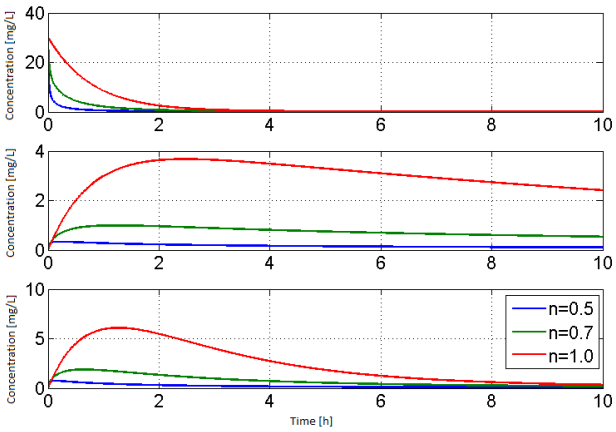

Figure 5.4: Drug concentration profile in compartment blood, muscle and fat.

amount in compartment 1 (plasma) is faster than in the integer order model ($n = 1.0$). This is a very important property of the fractional-order model that can be used to capture inter-patient variability.

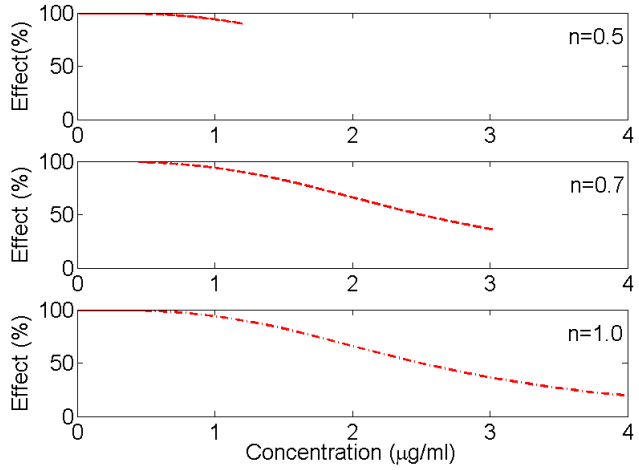

Figure 5.5: Drug concentration profile in compartment blood, muscle and fat.

5.3 Anomalous Kinetics

The PK literature is dominated by compartmental models of drug dynamics in human body, for a wide range of medical application or treatment [12, 139]. The mamillary compartmental model with single compartment seems to be the simplest representation of drug uptake and clearance, with the amount of a drug defined by a simple ordinary differential equation (ODE) relation:

$$\frac{dA(t)}{dt} = -k_{10}A(t) \tag{5.32}$$

with $A(0)$ the dose of bolus intake and K_{10} is the clearance rate constant. The solution, $A(t) = A(0) \cdot e^{-k_{10}t}$. However, usually 2-3 compartments are taken into account and as to specify the heterogeneity between the blood, muscle and fat tissue dynamics. It turns out that characterization as a function of time implies a negative power function derived from plasma drug concentration profiles [13]. Nevertheless, triexponentials with power and gamma functions were successfully fitted to power law data and results for several drug pharmacokinetics reported in literature [13]. An important decision at that time was to make observations on log-log plots with y- data and x-time axis. A limitation of the data intervals led to the use of gamma functions, assuming homogeneous distribution of drug into the compartmental volume. The necessity of several exponential terms to fit the data in linear regression algorithms seemed at the time unavoidable.

Later on, the necessity of a recirculation mechanism was to account for observed fluctuations in the time decay of a drug PK [140, 141]. The assumption

that compartmental models were homogeneous no longer fit the observed data. However, since the tools used to model the dynamical variability were ODEs, augmenting the model with a residence time information was a solution at hand. However, care must be taken when considering transient and residence times, since the two notions are different in PK specifications [140]. As stated in [140], classical compartmental models fail to explain the effect of different sampling sites, due to concentration differences across the various biological tissues. The units of the PK compartmental models are confined to exponentially distributed transit times. By contrast, recirculatory models may be characterized by any parametric or non-parametric class of drug transit time distributions. The choice of the model type is thus important, and it greatly depends on the objective it may serve.

In an effort to circumvent the choice of the model type, non-Markovian compartmental models were proposed [142]. Random particle distribution and transfer based on retention times seem adequate in capturing heterogeneous dynamic effects. The authors provide an adapted view of the models from Weiss in assuming a three compartmental PK model whereas one compartment is seen as a distribution of pseudo-compartments with different retention times. Clearly this is a more realistic approach since it enables phenomenological observations of drug accumulation and/or late recirculation loops. Still, oscillatory behaviour in drug concentration profiles for a single bolus intake are ignored. A conceptual view of such model representation is given in Figure 5.6. Tissue trapping was addressed

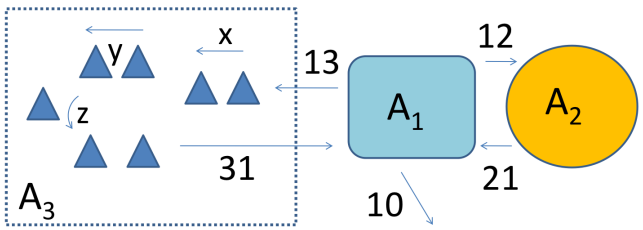

Figure 5.6: Distributed compartmental PK models. A three-compartmental scheme is given with classical two compartments on the right side combined with a distributed drug retention times compartment on the left side. Notice that intermediate drug profiles x,y,z may vary locally due to tissue trapping. Note that all drug fluxes denoted by arrows may have different dynamics (FDEs) as opposed to classical ODEs.

by Weiss later in [21], by proposing a non-classical PK model describing well the persistently increasing plasma concentration time curve during long term treatment and the washout curve following terminal therapy. The long tailed tissue residence time distribution is incorporated by means of a recirculatory model. Weiss [21] also acknowledges the anomalous kinetics and the fractal scaling property in char-

acterizing amiodarone drug dynamics. A conceptual schematic of such distribution is given in Figure 5.7.

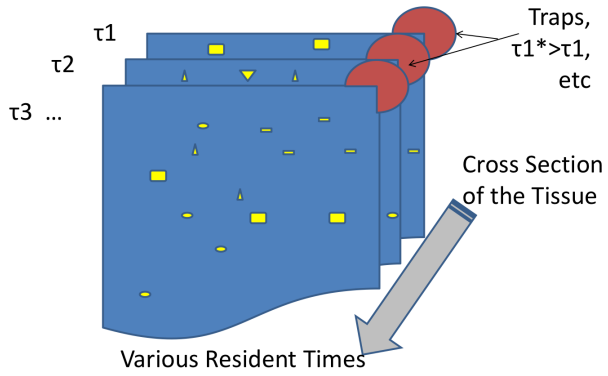

Figure 5.7: A conceptual view of distribution of tissue dynamics with various residence times and drug trapping areas.

A decade later, emerging tools from fractional calculus enabled a new wave of PK compartmental modelling theories, indicating some important flaws in the classical PK models. For example, multi-compartmental kinetics with fractional differential equations (FDEs) following consistent physiological mass balance rationale have been reported in [11]. Numerical methods to efficiently compute these equations are largely available to the community and simulations no longer pose tedious implementations. The great revelation of these numerical studies was that the presence of a transfer rate of fractional order produces a non-exponential terminal phase, while multiple dose and constant infusion systems never reach steady-state, resulting in drug accumulation. The latter is a life-threatening issue for the patient and imposes a critical observation on the usefulness of previous PK compartmental model definitions. Deep tissue trapping may account for observed secondary effects days, weeks and months in patients who undergone surgery with general anaesthesia, or following cancer treatment therapies. These new theoretical concepts and PK models may enable a different, novel perspective of drug drug kinetics. Such models more accurately predict the observed drug profiles and can provide an new basis for optimizing treatment.

Drug tissue trapping has been addressed also in [143] using fractional kinetics and data on amiodarone from [21]. Significant differences in linear or logarithmic drug intake profiles have been observed in numerical simulations, suggesting drug accumulation and inherent side affects in patient well-being. The paper from [143] proposes a dosing regime to stabilise the plasma concentration of amio-

darone when fractional PK models are used. .

Still, among all the previous works related to introducing anomalous kinetics and fractional PK compartmental models one cannot but notice the fact that some effects of drug trapping and releasing are yet unaccounted for.

Anomalous subdiffusion is represented by:

$$< X^2(t) > \approx t^n \tag{5.33}$$

with $0 < n < 1$. Subdiffusion could be used to model molecules of drug trapped in deep tissue for long times. The subdiffusive fractional Fokker-Planck equation can be employed as from [144]. Let $p(x,t)$ be the density function for finding the particle in the interval $(x, x+dx)$ at the time instant t; then

$$\frac{\partial p}{\partial t} = -\frac{\partial (v_n(x) D_t^{1-n} p)}{\partial x} + \frac{\partial^2 (D_\mu(x) D_t^{1-n} p)}{\partial x^2} \tag{5.34}$$

in which $D_n(x)$ is the fractional diffusion and $v_n(x)$ is the drift, with $n < 1$, and the Riemann-Liouville derivative is defined as

$$D_t^{1-n} p(x,t) = \frac{1}{\Gamma(n)} \frac{\partial}{\partial t} \int_0^t \frac{p(x,u)du}{(t-u)^{1-n}} \tag{5.35}$$

where we see the difference between the standard Fokker-Planck equation and the its fractional version by means of the rate of relaxation

$$p(x,t) \longrightarrow p_{st}(x) \tag{5.36}$$

When using this equation to extract residence times, on the long term, as $t \longrightarrow \infty$ the non-homogeneous variations of the parameter μ as a function of space should be carefully checked. Recent studies by [144–146] reported that the diffusion coefficient is a nonlinear function of the nonlinear reaction rate. In this model [146] the escape rate $\mathcal{T}$ of a particle from a position is modeled as a decreasing function of density $\rho(x,t)$:

$$\mathcal{T}(\tau, \rho) = \frac{n(\tau)}{1 + A\rho(x,t)} \tag{5.37}$$

which describes the phenomenon of con-specific attraction: the rate at which individual molecules or particles of drug emigrate from the point x is reduced due to the presence of many other con-specifics. The rate parameter $\mu(\tau)$ is a decreasing function of the residence time:

$$n(\tau) = \frac{n_0}{\tau_0 + \tau} \tag{5.38}$$

where n_0 and τ_0 are positive parameters. This particular choice of the rate has been motivated by non-Markovian crowding: the longer the particles stay in a particular site, the smaller the escape probability to another site (e.g. fat).

5.4 Revisited FDE PK Model

It has been suggested that instead of combining power law and exponential functions to account for anomalous kinetics, it is more efficient to use the Mittag-Leffler function [11]. This function has the capability to follow the stretched exponential for small times and the power function for long times, thus it is appropriate for characterizing both the short and the long time scales of drug concentration profiles. A classical two-compartmental model is given by the following ODEs:

$$\begin{array}{l} \frac{dA_1(t)}{dt} = -k_{12}A_1(t) + k_{21}A_2(t) - k_{10}A_1(t) \\ \frac{dA_2(t)}{dt} = k_{12}A_1(t) - k_{21}A_2(t) - k_{20}A_2(t) \end{array} \tag{5.39}$$

The correct fractionalisation of equation (6.29) maintaining mass balance, is given by:

$$\begin{array}{rcl} \frac{dA_1(t)}{dt} & = & -k_{12}{}_0^C D_t^{1-n_1} A_1(t) + k_{21}{}_0^C D_t^{1-n_2} A_2(t) - k_{10}{}_0^C D_t^{1-n_3} A_1(t) \\ \frac{dA_2(t)}{dt} & = & k_{12}{}_0^C D_t^{1-n_1} A_1(t) - k_{21}{}_0^C D_t^{1-n_2} A_2(t) - k_{20}{}_0^C D_t^{1-n_3} A_2(t) \end{array} \tag{5.40}$$

with k_{ij} rate constants and initial conditions $A_1(0) = dose$, $A_2(0) = 0$ which account for bolus injection and no initial amount in peripheral compartment. Here, the fractional order of the Caputo fractional derivative represents the heterogeneity of the diffusion dynamics [5].

Take for instance the two-compartmental PK model from Figure 5.8. Clearance and diffusion from 1-2 is considered as a classical (ODE) whereas diffusion 2-1 is fractional (FDE), with $n < 1$ to account for deep tissue trapping of the drug. The model can be described by the following set of equations:

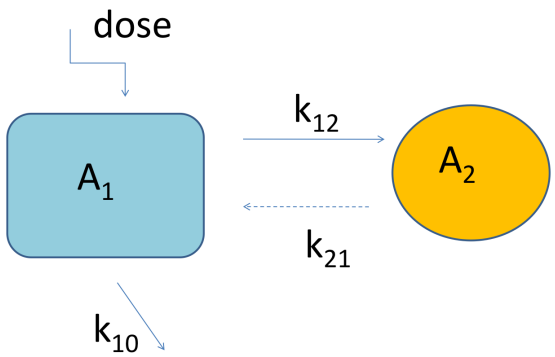

Figure 5.8: Two-compartmental PK model representation. The continuous arrows denote ODEs, whereas dashed arrows denote FDEs.

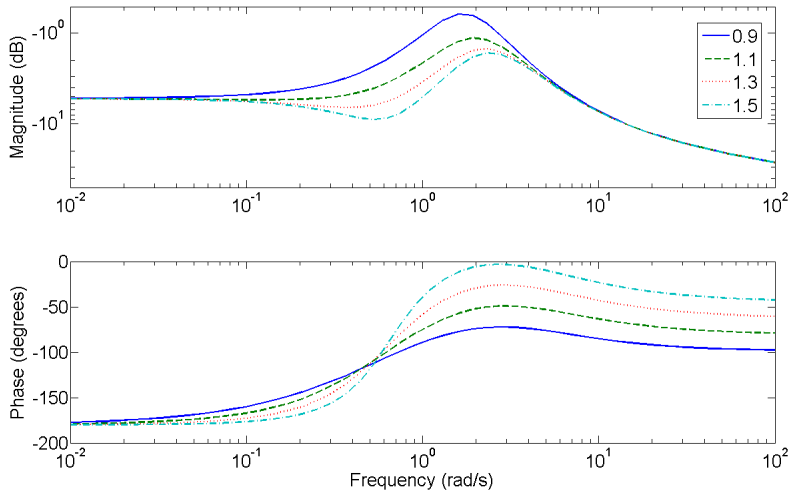

Figure 5.9: Frequency response of (5.42) for various values of n.

$$\begin{aligned} \frac{dA_1(t)}{dt} &= -(k_{12}+k_{10})A_1(t) + k_{21}\,{}_0^C D_t^{1-n} A_2(t) \\ \frac{dA_2(t)}{dt} &= k_{12}A_1(t) - k_{21}\,{}_0^C D_t^{1-n} A_2(t) \end{aligned} \tag{5.41}$$

The model has been transformed to the Laplace domain and solved for A_1 using a numerical inverse Laplace transform program in Matlab as described in [11]. The solution is given by:

$$A_1(s) = \frac{dose(s^n + k_{21})}{(s + k_{12} + k_{10})(s^n + k_{21}) - k_{12}k_{21}} \tag{5.42}$$

For values $n < 1$ the solution behaves essentially as a first order system, i.e. two poles of which one is cancelled by a zero at high frequencies. Suppose now that the values of na may increase above 1. The Bode plot of the transfer function is given in Figure 5.9 for various values of n, simulated with parameters as in table 5.1. From an engineering point of view, this non-rational transfer function changes dynamic behaviour from a first order to a second order system. In order to verify the time response of these transfer functions, it is necessary to use an inverse Laplace transform for non-rational polynomial representations. A numerical algorithm in Matlab has been proposed in [11], and it is used to simulate the results reported in this paper as well. The time domain simulations are given in Figure 5.10.

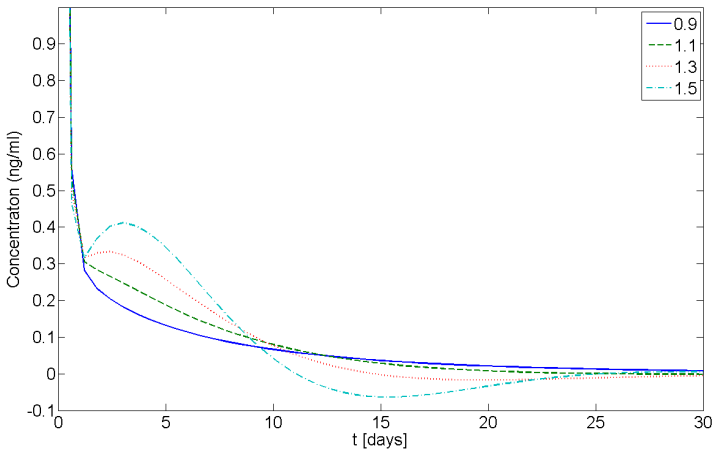

Figure 5.10: Time domain behaviour of the transfer function from (5.42) for various values of n.

5.5 Illustrative Example

A dynamic concentration profile (see Figure 5.10) for the drug Amiodarone taken from [21] has been mimicked for simulation purposes. The model from (5.42) has been identified to fit data which poses characteristics observed in real concentration values reported in literature. Of particular importance are the oscillatory dynamics which relate to recirculation effects as discussed above.

Using the nonlinear least squares algorithm in Matlab provided by the function `lsqnonlin` the parameters have been identified as in table 5.2.

The potential of increasing $\alpha > 1$ is observed in capturing possible variations in the concentration profiles, when compared to the result for $\alpha < 1$ sketched in

Parameter	Value
k_{10} (days^{-1})	1.49
k_{12} (days^{-1})	2.95
k_{21} (days$^{-\alpha}$)	0.48
α (-)	(0.5,1.5)
dose/V (ng/ml)	4.72

Table 5.1: Estimated model parameters used in simulation, with k the transfer rates between the compartments and clearance rate, and V the volume of the central compartment.

Figure 5.11.

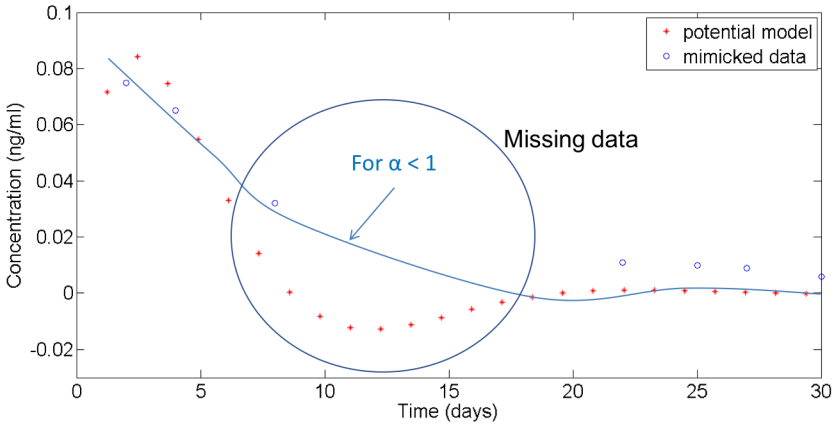

Figure 5.11: Variations obtained with sub- and supra- unitary values of α.

From this analysis, we were expecting to see oscillation (due to drug accumulation) but given the missing data in literature we could not reach to this conclusion and the results presented here are at this moment speculations. Of course, the model may be further tuned on real data profiles. It should be also noted that the amount of variability as a function of time differs from one patient to another, hence the model parameters could be fit in an individualised PK model framework.

The model with the solution given in (5.42) has some limitations in capturing all oscillatory dynamic profiles. This is due to the fact that only two compartments have been used, without recirculation, and without taking into account heterogeneity in the tissue. The distributed parameter compartmental models, as depicted in Figure 5.6, may potentially be employed to circumvent this limitation.

Parameter	Value
k_{10} (days^{-1})	1.7
k_{12} (days^{-1})	2.5
k_{21} (days$^{-\alpha}$)	0.6
α (-)	1.5

Table 5.2: Identified model parameters used in simulation from (5.42) for a fixed dose of 4.7268 (ng/ml).

5.6 Discussion and Perspectives

Naturally, tissue porosity, molecular binding and permeability vary within the organ, within the system and within the assumed compartment. Taking tissue specificity into account when modelling PK dynamic profiles may lead to increased model complexity. A trade-off between the usefulness and computational efficiency of such models must be made when evaluating the model objectives. If prediction for treatment optimisation is envisaged, then one may include as many details as possible to account for a personalised healthcare plan. If mere evaluation of dosing profiles and observational studies are involved, tissue specificity may be limited to the strictly necessary number of details (e.g. Occam's Razor approach). Obviously, large population data sets will be necessary to provide some reference baseline values for initial start-up. However, if data is available, data driven modelling/identification may be performed and model parameters tuned to fit the specificity of the case.

Applications of augmented PK models with FDEs are numerous and not limited in the number of turns. One may freely consider their application to modelling any drug PK dynamics. Multiples types of dosing intake may be assumed, either as a single type, or as combinations hereof: single dose, bolus, multiple dose, continuous infusion. When using FDEs in PK models, care must be taken for intake profiles may lead to drug accumulation and possibly over-dosing in some time intervals. Linear or power-law dosing profiles may be investigated to optimally use the dynamic model properties.

As such, time FDEs have been considered hitherto. However, tissue heterogeneity is also structural, geometric, and not only present in dynamic fluctuations. It may be worth considering introducing a time-space mathematical formulation (e.g. by employing fractional order space derivatives) to account for drug intake whereas time and location may be specified. This is of great importance in pathology cases, where changes in tissue structure and morphology affects directly the dynamic profiles of drug diffusion, permeability and molecular binding. Specific structural changes with disease may also reveal various paths of deep tissue trapping of drug and latency nodes which could explain effects observed in long-tailed observations.

5.7 Summary

In this chapter the existing compartmental modelling approaches have been revisited and their usefulness has been extended by employing emerging tools from fractional calculus . Undoubtedly, the fractional kinetics approach outperforms the classical ODE models while maintaining the link to physiological phenomena. It is worth mentioning that the assumption of a homogeneous compartment representa-

tion is no longer limiting in view of modelling objectives. Instead, tissue trapping and heterogeneous resident times may be taken into account by using distributed compartmental models with various diffusion rates. The combination of classical PK models and with fractional PK models is then the natural next step in the quest to improve their ability to mimic complex observed physiological phenomena.

6

Proposed Models and Their Validation

In this chapter the proposed models to characterize the nociceptor pathways are presented. These models have been validated (in vitro and in vivo) and have the potential to unlock the current state of art in this specific area of applications.

The main publications where this work has been presented are:

1. **D. Copot**, R. De Keyser, J. Juchem, C. Ionescu, Fractional order impedance model to estimate glucose concentration: in vitro analysis. Acta Polytechnica Hungarica, 14(1), 207-220, 2017.

2. **D. Copot**, C. Muresan, R. De Keyser, C. Ionescu, Fractional order modeling of diffusion processes: a new approach for glucose concentration estimation, International Conference on Automation, Quality and Testing, Robotics, Cluj-Napoca, Romania, 19-21 May, 407-712, 2016.

3. **D. Copot**, R. De Keyser, C. Ionescu, In vitro glucose concentration estimation by means of fractional order impedance models, IEEE International Conference on Systems, Man, and Cybernetics (SMC), 9-12 October, Budapest, Hungary, 2711-2716, 2016.

6.1 Introduction

Nociceptor pathway: relation between potassium channels and pain signalling
Potassium is one of the most common cation in the body and the principal intracellular cation. Approximately 3500 mmol of potassium are present in the body. The distribution of Na^+ and K+ can be thought of as opposite: one is in high concentration and the other is at low concentration. Sodium is the most prevalent cation in the extracellular fluid (ECF), with a normal level of around 140 mmol/L, but has a typical intracellular concentration of around 10 mmol/L. In contrast, potassium is the most prevalent cation in the intracellular uid, with a concentration around 150 mmol/L and about 5 mmol/L in the ECF [81, 147]. Because the intracellular space is the largest fluid compartment in the body, this makes it the most abundant cation overall. Hence, Na^+ and K^+ can only cross where specific carrier proteins allow them to do so. Excitable cells can change their permeability to allow the in flux and efflux of ions that constitute an action potential. At rest, the large concentration gradients for Na^+ and K^+ are maintained by the action of Na^+/K^+ pump [147]. This also maintains the net negative resting membrane potential, since it involves a net transfer of one positive charge out of the cell on each cycle [148, 149].

The observed increase in potassium concentration in the ECF varies between 0.1 and 10.0 mmol/L and depends on stimulation frequency, intensity, and duration [150]. An increase of 0.1-0.5 mmol/L has been found after a single electrical stimulus applied to the dorsal root, to peripheral nerve, or after a single adequate stimulus (light touch or pinch) applied to the skin. Repeated stimulation leads to summation of responses. For example, an increase of about 6-7 mmol/L was found in spinal cord after 15 seconds of high-frequency electrical stimulation (100 Hz) of peripheral nerves. When stimulation is continued, no greater changes in potassium concentration are found because a steady state is established, which is the result of concurrent release and clearance of K^+. This so called "ceiling level" can be exceeded only during epileptic seizures, anoxia or spreading depression, when K^+ can reach levels as high as 20-50 mmol/L [147, 149]. Because of the threshold, the action potential can be likened to a digital event, i.e. it either happens or it does not. If the threshold is not reached, then no action potential occurs. Action potentials are based on *all or nothing law*: either the membrane reaches the threshold and everything occurs as described or the membrane does not reach the threshold and nothing else happens.

While an action potential is in progress, another one cannot be initiated. That effect is referred to as the refractory period. There are two phases of the refractory period: the absolute refractory period and the relative refractory period. During the absolute phase, another action potential will not start. This is because of the inactivation gate of the voltage-gated Na^+ channel. Once that channel is back to

its resting conformation (i.e. less than -55 mV), a new action potential could be started, but only by a stronger stimulus than the one that initiated the current action potential. This is because of the flow of K^+ out of the cell. Because that ion is rushing out, any Na^+ that tries to enter will not depolarize the cell, but will only keep the cell from hyperpolarizing [150, 151].

6.2 Cole Cole model

Biological tissues are complex structures characterized by dynamic processes occurring at different lengths and time scales. Simple exponential relaxation models cannot adequately describe the behavior of such materials, as they do not consider the interactions among various relaxing phenomena and memory effects [152]. Non-integer formulations of the Debye relaxation models [153] are often necessary to account for slower and faster molecular rearrangements that take place within the microscopic, mesoscopic and macroscopic organization of the phenomena [152]. Therefore, to characterize such complex structures, electrical impedance spectroscopy and more specifically Cole-Cole models seem to be a good candidate.

The Cole-Cole generalize the Debye equation [152,154,155] and these models can be described in term of fractional order-differential equations [8, 119, 156, 157] often refereed to fractional calculus. Fractional calculus denotes the branch of calculus that extend the concepts of integrals and derivatives to non-integer and complex orders. This filed dates back to year 1695 and it has been during recent decades that FC was found to play a fundamental role in modeling several important physical phenomena. As a result, this emerged as an important tool which have been adopted in a wide range of topics, from dynamics of biological structures up to mechanical and electrical systems [14, 158].

The mathematical model of electrical properties of cell membranes, based on impedance measurements at multi frequency alternative current, was firstly formulated by Cole in 1940 [159]. Magin [119] derived and generalized Cole equation using fractional calculus. His model comprises three hypothetical circuit elements: a low frequency resistor R_0, a high-frequency resistor R_∞ and CPE_n. This circuit can be visualized as two serial connected elements, where the first one is R and the second one is $(R_0 - R_\infty)||CPE_\infty$. We denote the second element as the reduced Cole type element. The complex impedance described by Cole model is given by the following equation [159].

$$Z_\alpha(\omega) = R_\infty + \frac{R_0 + R_{inf}}{1 + (j\omega\tau_n)^n} \tag{6.1}$$

with the characteristic relaxation time, according to Magin, positive constant:

$$\tau_\alpha = \sqrt[n]{C_n(R_0 - R_n)} \tag{6.2}$$

where all coefficient are material constants independent of frequency.

Applied alternating voltage to the system is:

$$V(t) = V_0 exp(j\omega t + \theta) \tag{6.3}$$

with V_0 the voltage amplitude, θ is the phase angle between the voltage and the current, current passing through the system is $i(t) = i_0 exp(j\omega t)$. The Impedance of the system is given by $V(t) = Z_\alpha(\omega)i(t)$ with the relations describing the system with fractional Weyl derivative $D^n(j\omega)^n\}$:

$$1 + (\tau_n)^\alpha D^n)V(t) = (R_\infty(\tau_n)D^n + R_0)i(t) \tag{6.4}$$

If one takes into account geometrical properties of the physical system, such as surface of electrode and distance between them, complex dielectric constant becomes complex capacitance (C). Note that the in the theory of alternative current the admittance Y is described by formula $Y = j\omega C$. Therefore, the equation above describes frequency dispersion of complex resistivity in the case when geometry is not taken into account.

Formal replacement in equation above is done by:

$$(\tau_\alpha)^\alpha D^\alpha \rightarrow (\tau_{\alpha^*;\beta} K)^{\alpha^*;\beta} \tag{6.5}$$

where $n^*;\beta$ denote the real and imaginary parts of the fractional operator respectively. Notice that for $n^* = na$ and $\beta = 0$, this notation becomes the fractional order of real numbers (i.e. classical fractional calculus). Furthermore, for integer values of , we have then classical integer order calculus theory. By introducing new parameters for resistance in complex plane R_0^*, R_∞^* we can rewrite in general form the equation as:

$$(1 + (\tau_{n^*} K)^{n^*;\beta})V(t) = (R_\beta^*(\tau_{n^*;\beta} K)^{\alpha^*;\beta} + R_0^*)i(t) \tag{6.6}$$

and using the following change of notation $Z_\alpha(\omega) \rightarrow Z_{\alpha^*;\beta}(\omega)$ the following equation is obtained:

$$Z_{n^*;\beta}(\omega) = R_\infty^* + \frac{R_0^* - R_\infty^*}{1 + (j\omega\tau_{n^*;\beta})^{n^*\beta log(j\omega\tau_{n^*;\beta})}} \tag{6.7}$$

and this equation represents the new generalized Cole model. This model has five physical and phenomenological parameters: $n^*, \beta, \tau_{n^*;\beta}, R_0^*, R_\infty^*$. The meaning of the β parameter describes the relaxation properties of dielectric phenomena of the medium; the constant R_0^* and R_∞^* are the corresponding resistances, hence $\lim \beta \rightarrow R_0^* = R_0$; $\lim \beta \rightarrow R_\infty^* = R_\infty$. and thus we can note that for small values of β we have that $\alpha^* \approx \alpha, R_0^* \approx R_0, R_\infty^* \approx R_\infty$. Notice that in the complex plane paradigm, the meaning of R_0^* and R_∞^* are different since the members $\beta log(j\omega\tau_{n^*;\beta})$ and thus $Z_{n^*;\beta}(\omega)$ have different asymptotic behaviour when

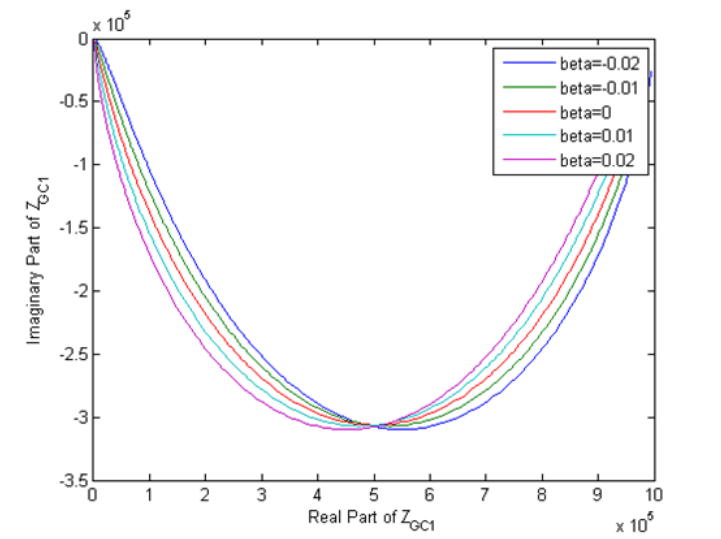

Figure 6.1: Elipsoid form of polar plot indicates existence of remnant memory (nonlinear effects).

$\omega \to \infty$ or $\omega \to 0$. In terms of Cole diagram, for values of $\beta \neq 0$, changes in $Z_{n^*;\beta}(\omega)$ are not circular (Figure 6.1), hence it exhibits a nonlinear dispersion of impedance.

The assumption that the change in conductive properties of electrical circuits is only in CPE leads to the following equation (generalized CPE):

$$Z_{CPE_\alpha}(\omega) = \frac{1}{C_\alpha (j\omega)^\alpha} \to Z_{GCPE_{\alpha^*;\beta}(\omega)} = \frac{1}{C_{\alpha^*;\beta}(\omega)(j\omega)^{\alpha^* + \beta log(j\omega\tau_{\alpha^*;\beta})}} \tag{6.8}$$

where we clearly see the nonlinear scaling of frequency for dispersion of impedance. Moreover, if α^*, β vary, then this implies further non-linearization with non-constant parameters. Hence, this model has significant advantages for capturing time varying changes in the skin impedance. Equation (6.8) introduces the generalisation of CPE (GCPE). The electrical circuit comprising of the element R^*_∞ in serial connection with the elements R^*_0 - R^*_∞ and $Z_{GCPE\alpha^*;\beta}(\omega)$ which depends on the element R^*_0 - R^*_∞.

Impedance measurements of the samples were performed with a Solatron ModulabXm impedance analyzer (Solatron Analytical, UK), see Figure 6.2. The impedance cell consisted of a plastic cylindrical tank with an inner diameter of 20 mm and a length of 30 mm. Several artificial samples at different potassium concentration have been prepared (considering the baseline concentration in the human body). In normal physiological conditions potassium concentration in the extracel-

lular fluid is about 4-5 mmol/L. Deionised water and potassium chloride was used to prepare the samples. Through the Solatron analyzer a 100 mV r.m.s. sinusoidal voltage has been applied to the outer couple of electrodes of the measurement probe which was immersed into the glass tube containing the analyzed sample. Impedance of the samples has been analyzed in the 1Hz-0.1MHz frequency range.

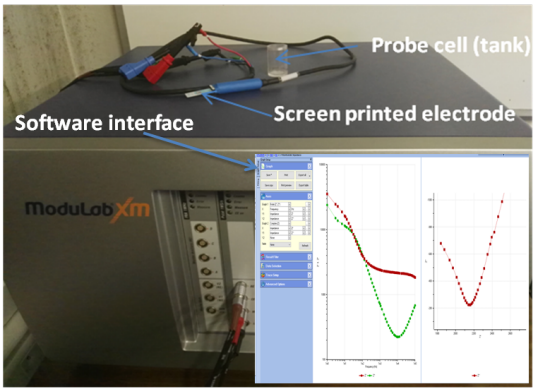

Figure 6.2: Solatron ModulabXm impedance analyzer.

ModuLab XM ECS is an Xtreme Measurement electrochemical test system that is capable of measuring ultra-low, micro-ohm impedance cells (latest generation batteries and fuel cells, for example), while able to accurately characterize ultra-high impedance corrosion coatings at the other extreme. The system uses a unique AC calibration method that ensures ultimate accuracy in all cases.

The results obtained using the Cole-Cole model (6.7) are given in Figure 6.3.

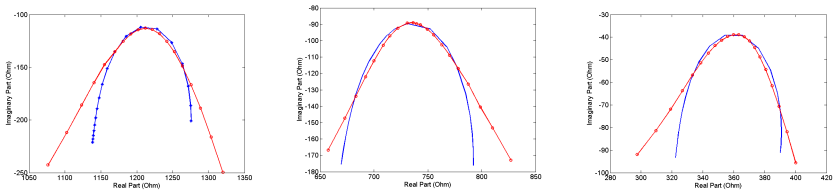

(a) (b) (c)

Figure 6.3: Cole-Cole model (blue line) and measured data (red line) for different potassium concentrations (a) 3.2 mmol/L; b) 4.9 mmol/L and c) 7.5mmol/L). The analysis has been performed in the frequency interval 1Hz - 0.1 MHz

6.3 Non-parametric Impedance model

The ANSPEC-PRO device records the voltage $V(t)$ (V) and current $I(t)$ (A) signals measured in the hand palm of the subject. The device is depicted in Figure 6.4 and a detailed description is presented in Appendix A.

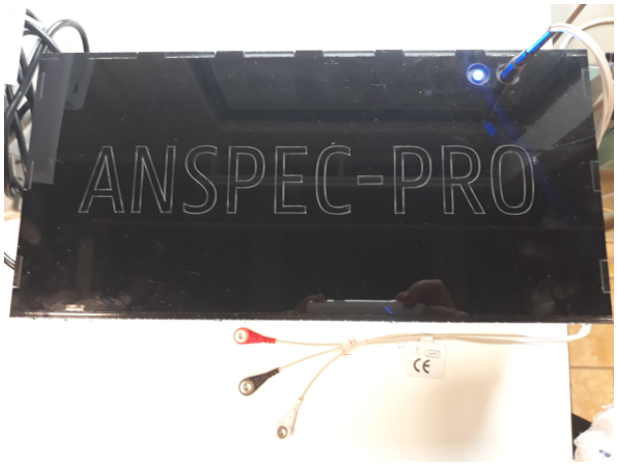

Figure 6.4: The developed prototype to enable a model of the nociceptor pathway.

To the measured signals non-parametric identification methods can be applied to extract the cross-spectral power density of the input and the output of the system. Given the input is of sinusoidal type ($A\sin(\omega t)$), the impedance is a frequency dependent complex variable evaluated as [14]:

$$Z(j\omega) = \frac{S_{UU}(j\omega)}{S_{UY}(j\omega)} \tag{6.9}$$

where $S_{XY}(j\omega)$ denotes the cross-correlation spectra between the various input-output signals, $\omega = 2\pi f$ is the angular frequency and $j = \sqrt{-1}$, the result being a complex variable. The derivation of (6.9) from the measured signals is detailed in [14].

The procedure followed for measurements and the preliminary results are presented hereafter. Following the measurement protocol described in Table 6.1 three different study cases have been investigated.

- Case 1 - Perform two consecutive measurements to investigate the device repeatability and if pain persists. Sensors are placed on the right hand and the pain stimulus is applied at the same location (i.e. same hand).
- Case 2 - Perform one measurement on a different day at the same time as the first case to investigate if the initial conditions have changed. The same location for the sensors and pain stimulus is used.

- Case 3 - Perform one measurement on a different day to investigate the location. In this case the sensors are placed on the right hand palm but the pain stimulus is applied on the left hand.

Minute	Nociceptor stimulation
0-2	Absent (NP)
2-3	Present (P)
3-6	Absent (NP)
6-7	Present (P)
7-10	Absent (NP)

Table 6.1: The consecutive steps in the 10 minute pain protocol

The measurement requires three electrode: two current-carrying electrodes and one pick-up electrode. The latter is an electrode picking up the voltage without carrying any currents, hence, no polarization occurs. All electrodes were placed on the palmar side of the hand (see Figure 6.5).

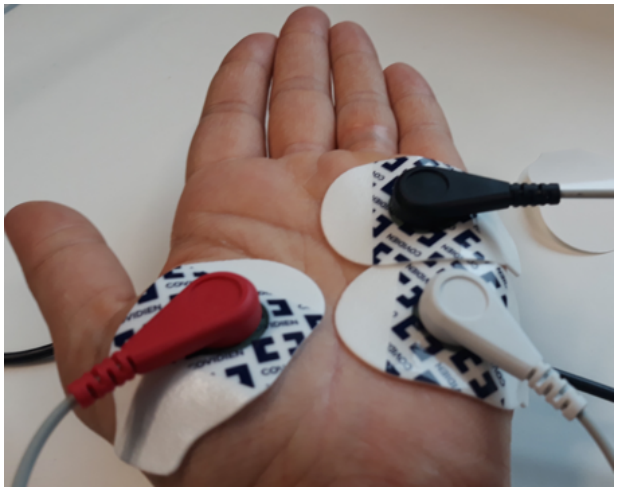

Figure 6.5: Placement of the electrodes during proof-of-concept measurements; two current-carrying electrodes (white, red) and one pick-up electrode (black)

The excitation signal is a multisine signal with 29 components in the frequency interval 100-1500 Hz, with step interval of 50Hz. This signal is send to the patient and the corresponding output is acquired. The sampling frequency is 15 KHz. The multisine signal is send with an amplitude of 0.2mA, still a factor 5 below the maximum allowed for patient safety [160].

The above described case studies have been investigated on a group of 10 volunteers. The biometric parameters (average) of the investigated subjects are: Age

(30 years); Height (1.73); Weight (73) and BMI (24). In Figures 6.6 - 6.7 the results obtained for one volunteer are presented. The results obtained for the other volunteers can be found in Appendix B.

The measured signals are filtered for noise prior to apply non-parametric identification methods [161]. Given the input is of sinusoidal type ($A\sin(\omega t)$) impedance is a frequency dependent complex variable evaluated as described in (6.9). Classical periodogram filtering technique has been applied with no overlapping interval, with windowing function Blackman implemented in Matlab environment [161]. The impedance is then evaluated every minute from online data streaming and plotted against frequency. This is then a frequency response either in complex form (Real and Imaginary Parts), either in Bode plot form (Magnitude and Phase).

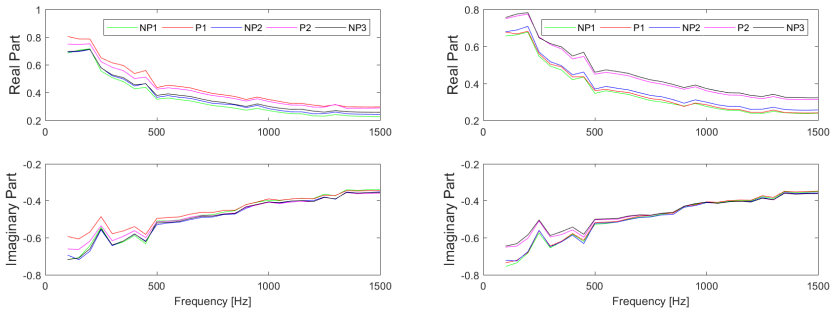

Figure 6.6: Impedance in its complex representation for the first study case (left: first measurement; right: second measurements).

In Figure 6.6-left the results for the first case study (first measurement) are shown. From here it can be noticed that the no pain (NP) situations are significantly different in amplitude than the pain (P) situations. This indicates that the impedance changes when a pain stimulus is applied. In Figure 6.6-right the results obtained after the second (consecutive) measurement are presented. Here we can notice that the NP and P situation are no longer separated. This indicates that pain persists from the first measurement (i.e. memory effect!). This is a remarkable finding to justify the use of fractional order impedance models. In Figure 6.7-left the results for the second study case are presented. Also in this case there is no significant difference between NP and P situations which indicated that the initial conditions in comparison with the previous day have changed (research is currently ongoing to investigate this hypothesis). Although we may tend to draw the same conclusions as for Figure 6.6-left (i.e. pain memory), this cannot be the case since the volunteer received no pain stimulus before.

In Figure 6.7-right the results for the third case study are presented. In this case, when the applied stimulus is on a different location that the sensor placement, we may draw the same conclusions as for the first case study (first measurement).

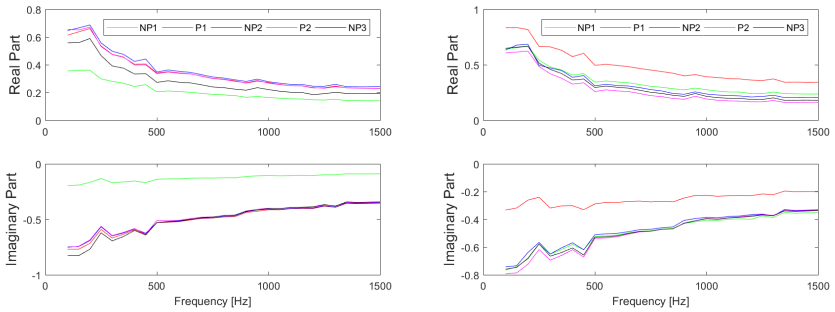

Figure 6.7: Impedance in its complex representation for the second (left) and third (right) study cases.

This means that the sensor location is not crucial (ongoing research investigates this hypothesis). However, in this particular case it can be noticed that the first pain stimulus has an impedance higher than for the NP situations (as expected) but for the second pain stimulus the impedance is lower than for the NP situations.

Next, only the pain situations for each case study are presented in Figures 6.8 - 6.9. For the first measurement (Figure 6.8-left) it can be seen that the first pain stimulus is higher in amplitude than the second pain stimulus. This indicates that pain persists from one stimulus to the other (i.e. memory). However, when a second consecutive measurement is applied the opposite is valid (i.e. the first stimulus is lower in amplitude than the second stimulus).

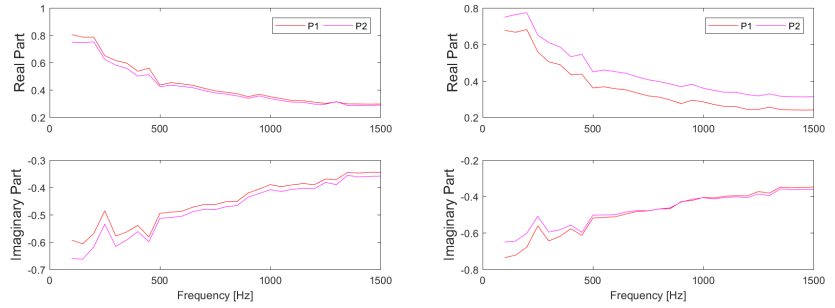

Figure 6.8: Impedance in its complex representation for the first study case (left: first measurement; right: second measurements) for pain situations only.

The impedance has been estimated by means of (6.9) and depicted by its complex impedance. The confidence intervals for each study case are presented in table 6.2.

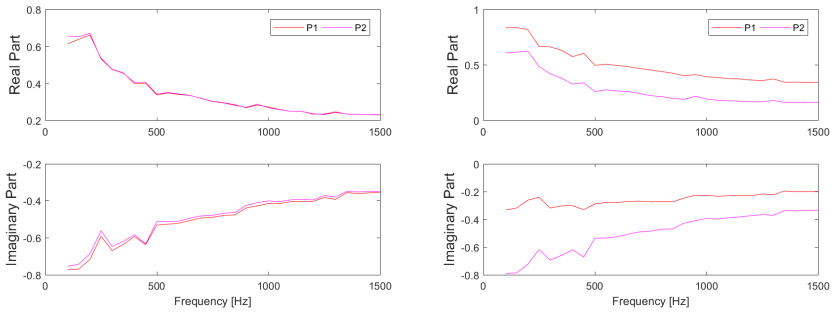

Figure 6.9: Impedance in its complex representation for the second (left) and third (right) study cases for pain situations only.

Case study	Mean	Min	Max	Std
1 (first measurement)	0.4536	0.3291	1.5060	0.1309
1 (second measurement)	0.4512	0.3369	1.4432	0.1180
2	0.2050	0.1085	0.7003	0.0635
3	0.3421	0.2447	1.1924	0.1114

Table 6.2: Confidence interval for the investigated case studies. Std denotes the standard deviation.

An analysis on the sum of absolute values of the frequency response complex impedance in terms of boxplot representation for all volunteers has been performed. It can be noticed that for each study case a different number of participants have been evaluated. This is due to the fact that one volunteer has failed the repetition test. However, for the proof-of-concept of the method and device the

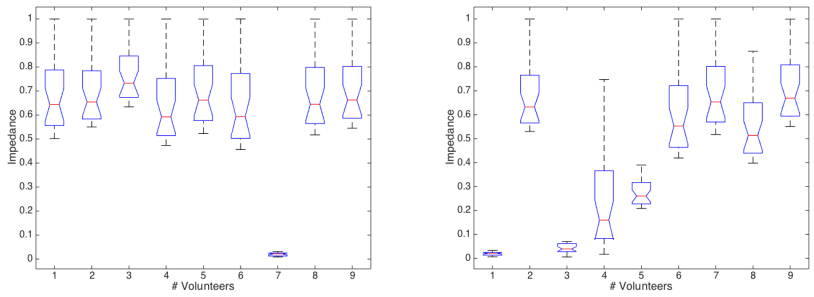

Figure 6.10: Case study 1: Boxplot analysis of the absolute values of the frequency response complex impedance in all individuals. Left: first nociception stimuli; Right: second nociception stimuli.

performed analysis is sufficient. In Figure 6.10 the results for the first case study (first and second pain stimuli) are presented.

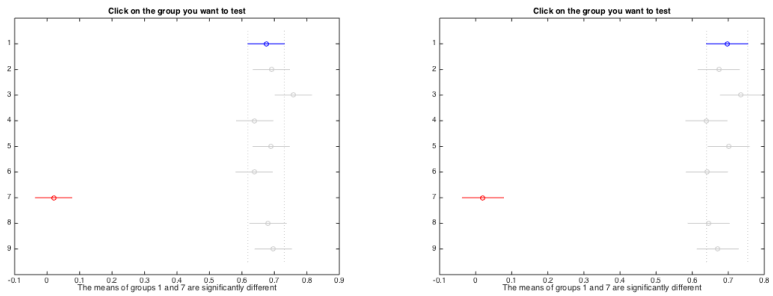

Figure 6.11: Case study 1: Multiple comparison test among individual absolute values of impedances during first nociception stimuli (left) and second nociception stimuli (right).

It can be noticed that eight subjects are in the same range of magnitude while one subjects has a significantly lower impedance. This volunteer is a pregnant women (in 6 months). One might consider that such a difference is normal since the amount of liquid in the body is higher in pregnant womens that in not pregnant womens. During pregnancy changes of the circulatory system, respiratory, metabolic, hormonal, etc. are occurring. All these changes may also contribute on

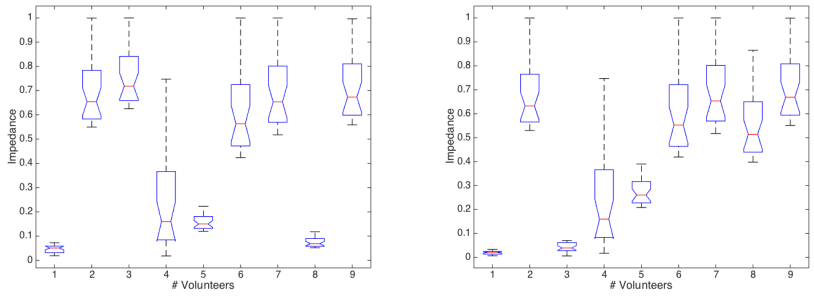

Figure 6.12: Case study 2: Boxplot analysis of the absolute values of the frequency response complex impedance in all individuals. Left: first nociception stimuli; Right: second nociception stimuli.

pain perception. In the case of the second stimuli (Figure 6.10-right) a difference in impedance is observed in all patients. This indicated that each volunteer has a pain memory effect (i.e. not fully recovered from the first pain stimulus applied). From here one may conclude that: there is a trend of impedance when a mechanical stim-

ulus is applied; the developed prototype can detect the changes in impedance and meaningful measurements can be performed. Additional, multiple comparison of means has been performed to see differences between the impedance absolute values of the two nociceptor stimulation interval during the first case study. Results are given in Figure 6.11.

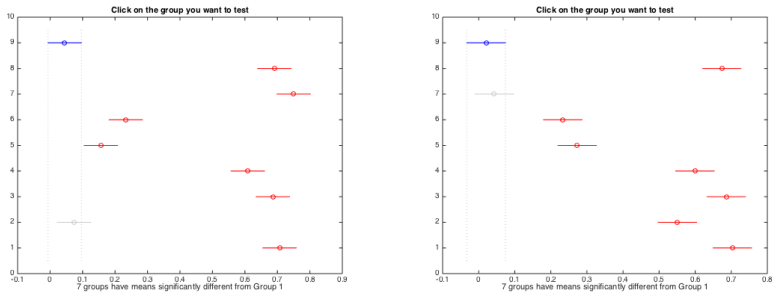

Figure 6.13: Case study 2: Multiple comparison test among individual absolute values of impedances during first nociception stimuli (left) and second nociception stimuli (right).

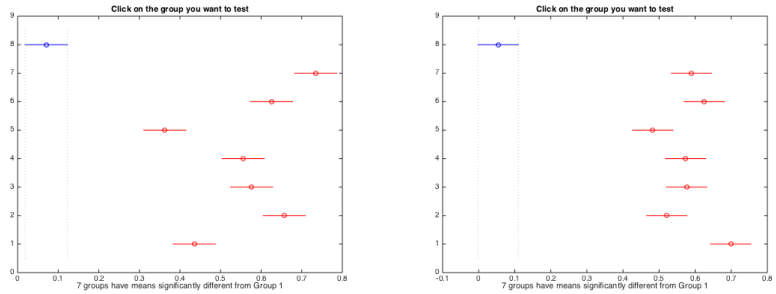

Figure 6.14: Case study 3: Multiple comparison test among individual absolute values of impedances during first nociception stimuli (left) and second nociception stimuli (right).

Same analysis has been performed for case study 2 and 3 and the results are given in Figures 6.12-6.14. One may notice that the results obtained for the third investigated case is significantly different from the others. Third case study consists of performing the same measurement protocol as in first and second case but on a different day. It is important to be mentioned that each participant has been measured in the same period of the day as for previous case. This is important in order to have consistency in the state of the participant. The difference observed in the third case might indicate that the initial conditions have changed but this

hypothesis needs further investigation.

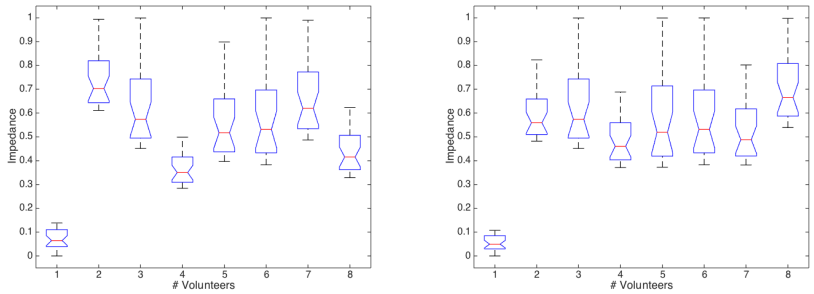

Figure 6.15: Case study 3: Boxplot analysis of the absolute values of the frequency response complex impedance in all individuals. Left: first nociception stimuli; Right: second nociception stimuli.

To analyse the variability within individual among the three study cases, the frequency response obtained using (6.9) has been used. For this analysis, the absolute values of the frequency response complex impedance per excited frequency point has been used. The results are given in Figures 6.16-6.17. From these figures it can be noticed that for most of the volunteers there is a difference within individual per protocol.

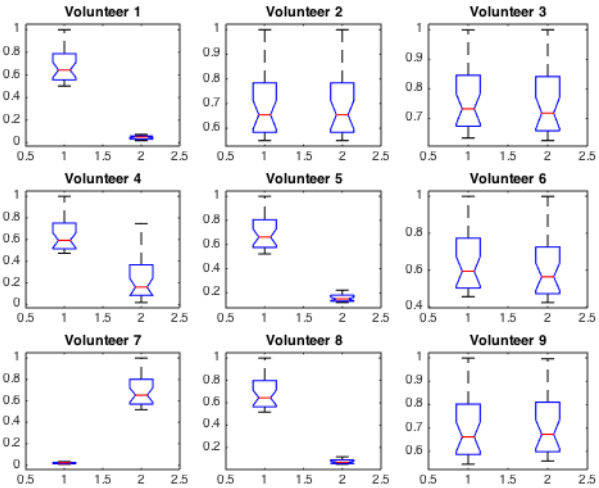

Figure 6.16: Comparison between case study 1 and case study 2.

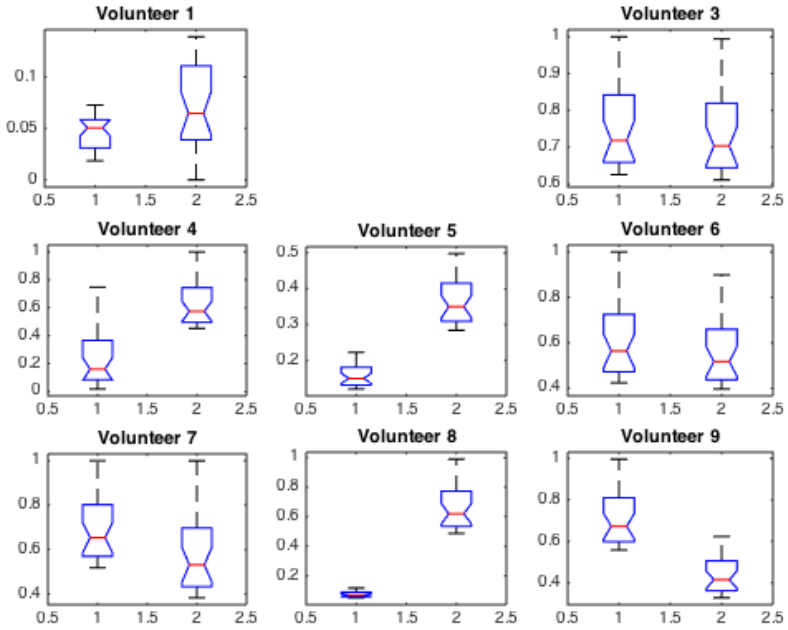

Figure 6.17: Comparison between case study 2 and case study 3.

6.4 Interlaced zero-pole impedance model

The transfer function provides a basis for determining important system response characteristics without solving the complete differential equation. As defined, the transfer function is a rational function in the complex variable $s = \sigma + j\omega$, that is:

$$H(s) = \frac{b_m s^m + b_m s^{m-1} + \cdots + b_1 s + b_0}{a_n s^n + a_{n-1} s^{n-1} + \cdots + a_1 s + a_0} \tag{6.10}$$

It is often convenient to factor the polynomials in the numerator and denominator, and to write the transfer function in terms of those factors:

$$H(s) = \frac{N(s)}{D(s)} = K \frac{(s - z_1)(s - z_2) \ldots (s - z_{n-1})(s - z_m)}{(s - p_1)(s - p_2) \ldots (s - p_{n-1})(s - p_n)} \tag{6.11}$$

where the numerator and denominator polynomials, $N(s)$ and $D(s)$, have real coefficients defined by the system's differential equation and $K = b_m/a_n$. As written in (6.11) the z_i's are the roots of the equation when $N(s) = 0$ and are defined to be the system $zeros$. The p_i's are the roots of the equations when $D(s) = 0$ and are defined to be the system $poles$. All of the coefficients of polynomials $N(S)$ and $D(s)$ are real, therefore the poles and zeros must be either purely real, or appear in complex conjugate pairs

In Figures 6.18-6.25 the measured impedance and the estimated impedance using the zero-pole interlacing method are shown. In these figures the results for one volunteer for all three study cases are presented. From these results we may conclude that there is a good correlation between measured and estimated impedance.

This is due to the advantages represented by this method. More specifically, given these zero-pole interlacing the model can capture the "fluctuations" in the measured impedance. However, this model has 13 parameters to be estimated, i.e. a complex model. For the results presented in this thesis the `lsqnonlin` method has been used to estimate the model parameters. Given its complexity further research has been conducted and a lumped fractional order impedance model has been derived. The model and the results obtained are presented in section 6.5.

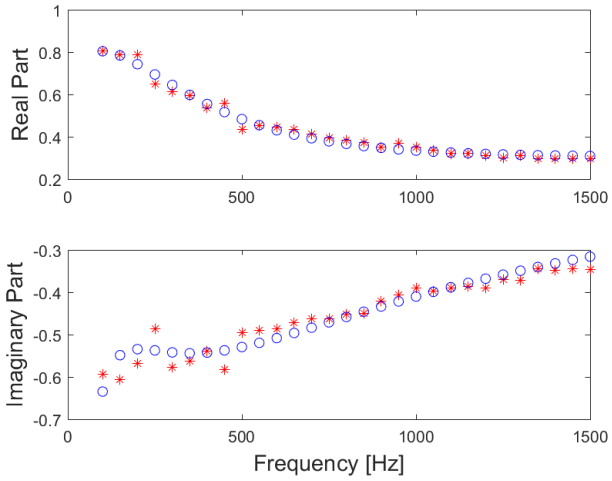

Figure 6.18: First pain stimuli: Impedance in its complex representation for first case study (first measurement). '$*$' denote measured impedance and 'o' denote the estimated impedance.

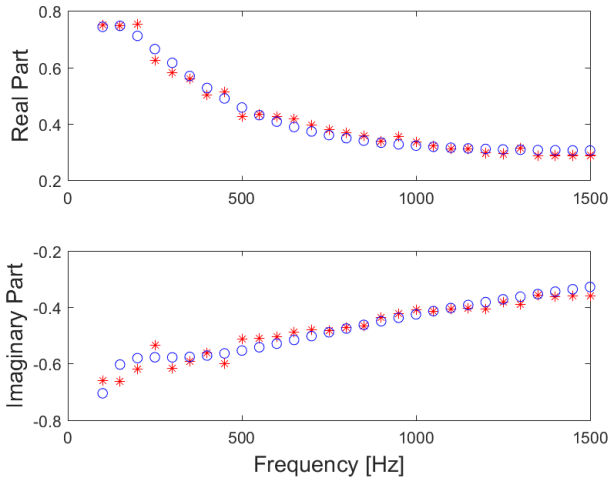

Figure 6.19: Second pain stimuli: Impedance in its complex representation for first case study (first measurement). '$*$' denote measured impedance and 'o' denote the estimated impedance.

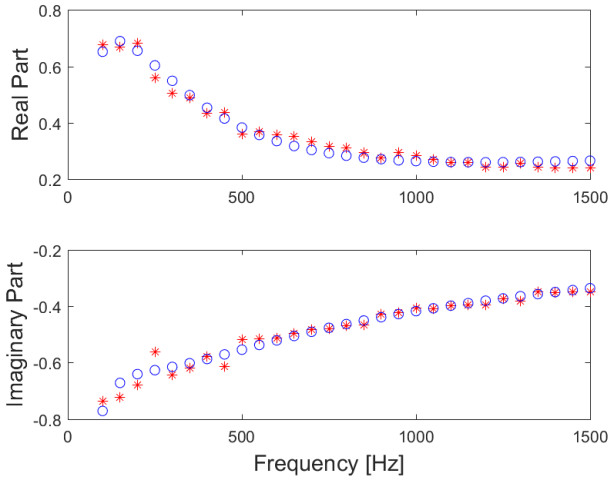

Figure 6.20: First pain stimuli: Impedance in its complex representation for first case study (second measurement). $'*'$ denote measured impedance and 'o' denote the estimated impedance.

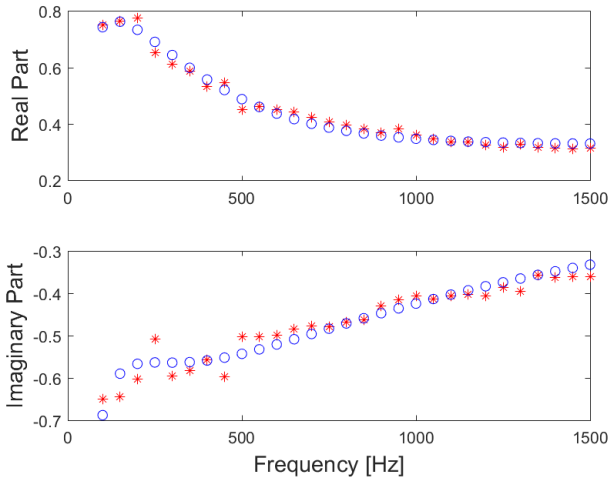

Figure 6.21: Second pain stimuli: Impedance in its complex representation for first case study (second measurement). $'*'$ denote measured impedance and 'o' denote the estimated impedance.

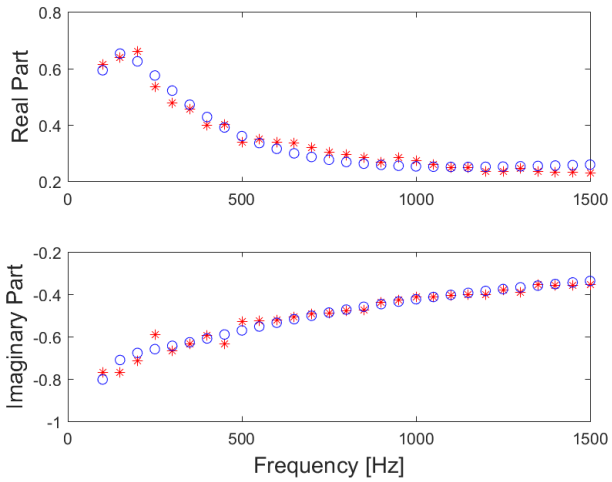

Figure 6.22: First pain stimuli: Impedance in its complex representation for second case study. '$*$' denote measured impedance and 'o' denote the estimated impedance.

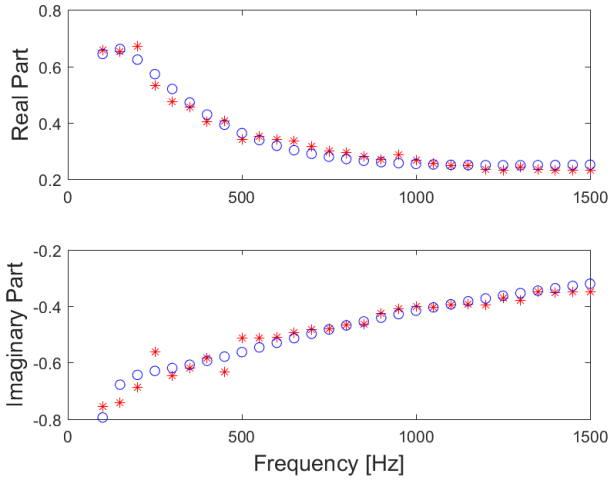

Figure 6.23: Second pain stimuli: Impedance in its complex representation for second case study. '$*$' denote measured impedance and 'o' denote the estimated impedance.

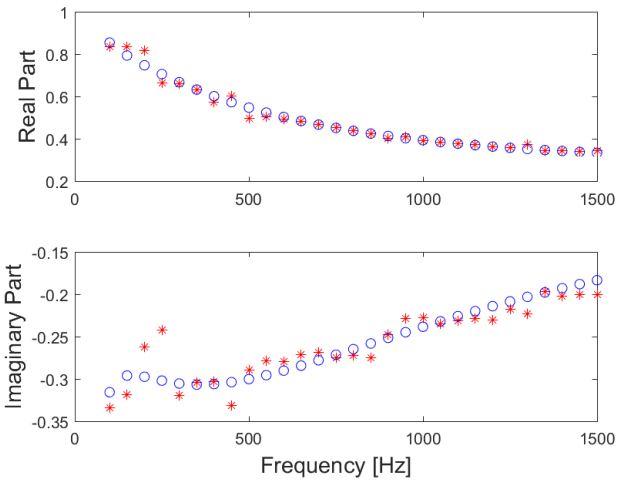

Figure 6.24: First pain stimuli: Impedance in its complex representation for third case study. '$*$' denote measured impedance and 'o' denote the estimated impedance.

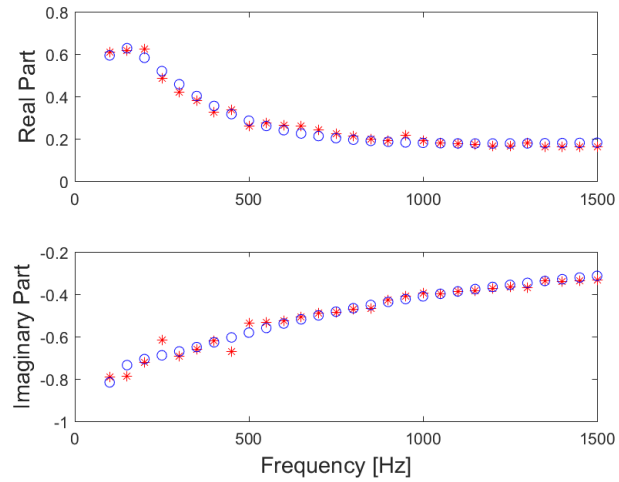

Figure 6.25: Second pain stimuli: Impedance in its complex representation for third case study. '$*$' denote measured impedance and 'o' denote the estimated impedance.

6.5 Lumped multiscale model

In general, drug regulatory loops are becoming popular in clinical practice, with prevalence in computer controlled anesthesia. There is evidence to support that closed loop control of drug dosing systems for anaesthesia perform better than manual control [162]. These control systems rely on the availability of a patient model [163, 164]. Within the anesthesia regulation paradigm, detecting and quantifying pain with an objective measure by means of a mathematical model is still a missing piece in the puzzle. As such, pain is a complex process, involving a manifold of chemical, physical and electrical sub-processes all sequenced in a systemic context. A manifold of papers report on initiatives to characterize pain levels from combinations of other featured signals available to the medical specialist. Hypnotic and opioid side-effects mark changes in other bio-signals as heart rate, respiratory rate, mean arterial pressure, gas in- and ex-piratory percentages, body temperature, etc. Hence, methods from artificial intelligence and data mining domains have proven to be useful tools, e.g. multivariate analysis [165], fuzzy logic [166, 167], neural networks [168, 169] etc.

The physiological pathway of pain can be described to four main processes [170]:

- transduction - when a stimulus is applied to the skin, the nociceptors located there trigger action potentials by converting the physical energy from a noxious thermal, mechanical or chemical stimulus into electrochemical energy,
- transmission - the signals are subsequently transmitted in the form of action potentials (similar to pulse trains) via nerve fibres from the site of transduction (periphery) to the dorsal root ganglion, which then activates the interneuron,
- perception - the appreciation of signals arriving in specified areas in the cerebral cortex as pain, and
- modulation - descending inhibitor and facilitator input from the brainstem that influences (modulates) nociceptive transmission from the spinal cord.

A linear input-output based model was identified by performing thermal cold stimuli into dental nerves and measuring resulted electrical activity correlated to pain [171]. The model was a simple second order transfer function with damping factor and impulse response corresponding to measured electrical activity in interdental nerves. This crude model was further improved to better approximate the intra-patient variability and plasticity of pain sensation after repeated stimuli [172]. Further in vivo tests indicated that modulation is present in the electrical activity when pain is perceived by the subject, suggesting thus that a frequency

dependence is necessary. Nonlinear terms in sine and cosine functions have been introduced in [173] to predict this nonlinear effect.

Somewhat later, a review of multi-scale processes involved in nociception and pain sensation has been made, summarizing all steps from thermal stimuli [174]. Although the review makes an excellent overview, it concludes that the mechanistic processes are far from being well understood and that engineering tools need to be further employed for delivering useful models for assessing pain in man. A model for electrical activity aroused from thermal nociceptor detection and transmission at neuronal level is then given. The model captures in part the pain pathway and thus is limited in its use to the anesthesia regulation paradigm. Later studies on thermal pain indicated the presence of adaptability and variability in pain sensation as a result of noxious stimulus intensity degree and pattern of stimulation [175]. In engineering terms, this is due to variability of disturbance profiles (i.e. stimuli) and thus the excitatory input to the measured response variation provides a spatio-temporal change in the path pathway. Simple linear models of classical system engineering theory can no longer capture such changes without increasing the complexity of the problem formulation.

In this chapter we present a view from system engineering standpoint making use of multi-scale models to obtain a lumped minimal parameter characterisation of nociception and pain pathways. We employ tools from mathematics, physics and chemistry to equivalent electrical circuit analogues beyond classical linear system theory. Fractional calculus and diffusion in heterogeneous medium is a key ingredient in this paper. The originality of the approach is in the integrative manner in which all sequences of nociception and pain related pathways are modelled, to maintain a minimal number of parameters to be later identified from experimental data. The tools used in this model derivation are borrowed from mathematics, i.e. fractional calculus, since they are a generalization of the classical linear system theory known in systems engineering. To the author's knowledge, a mathematical model based on such systematic derivation does not yet exist in literature.

Gate Control Theory:

The gate control theory (GCT) is a successful way to explain important features of the pain process [150]. This theory says that the small fibres ($A\delta$ and C) that carry the information about noxious stimuli, while the larger (L) fibres ($A\beta$) carry information about less-intense mechanical stimuli. As the signal from the small fibres is routed through substantia gelatinosa (SG) to the central transmission cells (T-cell) and onwards, the double inhibition (indicated by the minus signs) strengthens the signal, resulting that the sensation of pain is more easily evoked. However, the signal from A-fibres activates the inhibitory function of *substantia gelatinosa*, which will reduce the firing to transmission cells and suppress the pain in the end. This theory was modified later in that it included excitatory (indicated by the plus

signs) and inhibitory links from *substantia gelatinosa* to central transmission cells, as well as descending inhibitory control from some structures in the brainstem. The neuromatrix theory proposed by Melzak in 1999 [176], integrates multiple inputs to produce the output patterns that evokes pain. The body-self neuromatrix comprises a widely distributed neural network that includes somatosensory, limbic and thalamo-cortical components. A schematic representation of the gate control theory is given in Figure 6.26.

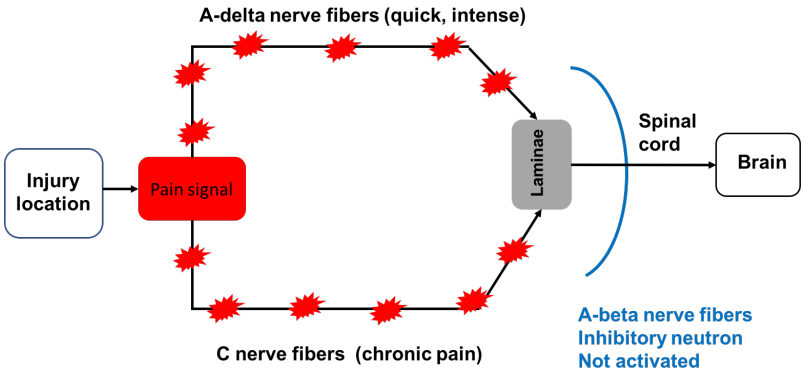

Figure 6.26: Schematic representation of gate control theory for signal transmission.

During consciousness, using MRI, it is possible to identify those brain areas directly related to pain [119, 150]. Such a stimulus reliably leads to activation of multiple brain areas, termed as the pain matrix. Different areas represent different aspects of pain. The primary and secondary somatosensory cortices are activated to discriminate the location and intensity of a painful stimulus. The anterior cingulate cortex, frontal cortex and anterior insula regions may be related the cognitive and emotional components. The problem is that these areas show significant modulation depending on the context of the stimulus, e.g. degree of attention, anxiety, expectation, depression and analgesic drug treatment.

To conclude this introductory description, the modelling of the pain pathway can be summarized as follows: i) stimulus effect; ii) transduction; iii) transmission; iv) modulation and v) perception. All these segments will be described in the remainder of the document by means of multi-scale modelling approach.

Multi-Scale Modelling Approach:

From Stimulus to Nociception Receptor Model:

Consider a semi-infinite medium with two spatial components: a source (S) component and a tissue (T) compartment. Assume the S compartment is distributed source of diffusing species without degradation and the T compartment is characterized by first order degradation without production. Introduce the term

c_s as the accumulated concentration of the S compartment (i.e. as a result of the stimulus) and c_f the concentration in the T compartment. The overall solution is the sum of the two terms

$$c(x) = c_s(x) + c_f(x) \tag{6.12}$$

with the two domains assumed to be orthogonal, i.e. $c_s(x) = 0$, in the distal compartment $x > L$ and $c_f(x) = 0$ in the proximal compartment $x < L$, with L the depth of the tissue layers. A continuous and smooth solution implies the equilibrium conditions:

$$c_s(x)|_{x=L-} = c_f(x)|_{x=L+} \tag{6.13}$$

$$\frac{\partial c_s}{\partial x}(x)|_{x=L-} = \frac{\partial c_f}{\partial x}(x)|_{x=L+} \tag{6.14}$$

and boundary conditions $c(0) = 0; c(\infty) = 0$.

The amount of extracellular space (ECS) varies as a function of tissue structure, function, and geometry within a system or an organ, i.e liver, arteries, heart, lungs, brain, muscle, fat, etc. Impeded diffusion can be thus modelled either by using classical diffusion laws, or by anomalous laws following fractional calculus tools.

Classical diffusion considers that the medium imposes only a spatial impediment on the diffusing species and does not change the diffusion law. For example, in [177] the densely packed cells of the brain and their interstitial spaces resemble a porous medium with two phases, i.e. an intra- and an extra- cellular phase. Diffusion in the permeable phase of the porous media is analogous to the diffusion in the narrow spaces between brain cells, i.e. the ECS. In our case, we consider the permeable phase as that being with fast time constants, i.e. the fat cells and other mediums without fast electrical conductivity are thus representing the ECS.

Volume transport of species having concentration c is governed by rescaled reaction-diffusion equation:

$$\frac{\partial c}{\partial} t = \frac{\overline{D}}{\lambda^2}\nabla^2 c + \frac{\overline{s}}{\alpha} - \kappa c, \text{ with } \lambda = \sqrt{\frac{\overline{D}}{D}} \tag{6.15}$$

where the stimulus source term is denoted by s, the clearance term by $k(c) = \kappa c$ is assumed to be first order decay and D is the diffusion coefficient (i.e. defined as $length^2/time$). Additionally, we have the dimensionless parameters of tortuosity λ and porosity α, and the clearance rate κ (1/time). Tortuosity can be considered as the linear correction for the anomalous diffusion in a complex medium [178].

Rename $D = \frac{\overline{D}}{\lambda^2}$ and $s = \frac{\overline{s}}{\alpha}$ and the transport equation can be redefined using fractional calculus as

$$\frac{\partial c}{\partial t} = D\nabla\nabla^\beta c + s - \kappa c \tag{6.16}$$

where ∇^β denotes the fractional order Fick's law, i.e. the fractional flux in the medium. This form of diffusion naturally implies spatial non-locality and can be derived rigorously using spatial averaging theorems [179, 180].

Introducing the Caputo definition of an differ-integral as [5]:

$$\mathcal{D}_a^\beta f(x) = \frac{1}{\Lambda(1-\beta)} \int_a^x \frac{f'(t)}{(x-t)^\beta} dt \tag{6.17}$$

where Λ is the Euler gamma function and reducing the system of coordinates to the axial variable it follows that diffusion is given by $-D\mathcal{D}_a^\beta c$, as following from the derivation presented in [181]. Introducing a mass conservation law for the particle concentrations it follows that

$$\frac{\partial c}{\partial t} = D \frac{\partial}{\partial x} \mathcal{D}_0^\beta c + s + \kappa c \tag{6.18}$$

whose explicit solutions have been given in [181].

Hence, we have that the model from stimulus to nociceptor receptor is governed by a diffusion equation in heterogeneous medium depending on time along single linear spatial dimension. At this point we can describe the contact surface of the stimulus as an ultracapacitor whose impedance can be formulated as a function of the porous nature of medium [182].

The Impedance Model:

Signalling pathways is limited by ionic diffusion and electrical cellular stimulation above a minimal threshold value. Geometry dependent diffusion impedances have been derived in [16,17] for several particle geometries: planar, cylindrical and spherical. In our case, the specific geometry is due to that localization of noxious stimuli on different types of tissue structures, e.g. skin (planar), muscle (cylindrical) or organ (spherical). Sufficiently low frequencies it appeared that impedances behave as a resistor in series with a capacitor with specific terms according to geometrical features. The electrochemical impedance of the Na^+/K^+ pump for signalling pathways of nociceptor stimulus involves activation of material particles and can be considered as a charge transfer process. At high frequencies (i.e. above 1 Hz in most ultracapacitor cases) the overall impedance does not depend on geometrical features and follows the frequency dependence of its complex values as in a modified circuit:

$$Z(s) = R + \frac{R_c}{1+\tau_c s} + Z_m(s) \tag{6.19}$$

where R is a threshold value (i.e. the gate control theory on-off signalising condition), R_c and τ_c values related to the overall cellular impedance and Z_m the bounded diffusion impedance from molecular level dependent on anomalous diffusion geometry. The charge transfer characteristic pulsation frequency is then $\omega_c = \frac{1}{\tau_c}$.

The fractional differ-integral operator can be expressed as a continuous integer order system approximating the fractional term in a limited bandwidth, synthesized

by cascading elementary phase-delay filters within the bandwidth [183]. This approximated filter is truncated at low and at high frequency boundaries. When considering the asymptotic behaviour of bounded diffusion impedance models at low and high frequencies, it can be observed that they behave as a classical integrator and an integrator of non-integer order n=1/2. The blocking diffusive behaviour is thus modelled by a gain b_0 and a fractional integrator $\mathcal{I}$:

$$Z_m(s) = \frac{b_0}{s} + b_1 \mathcal{I}(\omega_b, s) \tag{6.20}$$

The asymptotic behaviour at low frequencies (i.e. $\omega \ll w_b$) is

$$Z_m|\omega_b = \frac{b_0}{s} + b_1 \omega_b^{-n} \tag{6.21}$$

with n the fractional order which for homogeneously diffusion patterns is close to the value of 0.5. It follows thus the overall fractional impedance model as

$$Z(s) = R + \frac{R_c}{1 + \tau_c s} + \frac{b_0}{s} + b_1 \mathcal{I}(\omega_b, s) \tag{6.22}$$

The Signalling Pathway Model:

Typical dynamic processes observed in the neuron include diffusion phenomena [184, 185], electrochemisty [186] and bistability [187]. Each of these features has been shown previously to be captured by power law models or fractional order derivatives [119]. A typical feature of the fractional order dynamics is a phase constancy observed over a limited frequency range. Intuitively, one expects that the lumped simplification of the complex dynamics governing the neuronal mechanisms would also exhibit a phase constancy. Our previous results confirm this expectation and the ladder network model presented in [188] can be employed with complex elements to capture specific neural structures (e.g. visual cortex, hippocampus, corpus callosum, etc).

The further use of the cable theory and consequently the equivalent recurrent ladder network for information transmission of nociceptor activity implies knowledge of some time-space dependent features. The geometrical and morphological features of the neural structure for propagating pathway determine the global dynamic behaviour of the transmission network. By changing the neuron interconnectivity (i.e. selective connectivity), the properties and dynamics of the structure may vary, hence adapt for various purposes. In this way, adaptability and variability in sensitivity can be captured.

The longitudinal and transversal impedances can be defined as a function of voltage and current:

$$Zl_m(s) = \frac{U_{m-1}(s) - U_m(s)}{I_{m-1}(s)} \tag{6.23}$$

and

$$Zt_m(s) = \frac{U_m(s)}{I_{m-1}(s) - I_m(s)} \tag{6.24}$$

from which we can use: $U_m(s) - U_{m+1}(s) = Zl_{m+1}(s)I_m(s)$, leading to:

$$\frac{I_m(s)}{U_m(s)} = \frac{1/Zl_{m+1}(s)}{1 + \frac{U_{m+1}(s)}{I_m(s)Zl_{m+1}(s)}} \tag{6.25}$$

and respectively $I_m(s) - I_{m+1}(s) = \frac{U_{m+1}(s)}{Zt_{m+1}(s)}$, leading to:

$$\frac{U_{m+1}(s)}{I_m(s)} = \frac{Zt_{m+1}(s)}{1 + Zt_{m+1}(s)\frac{I_{m+1}(s)}{U_{m+1}(s)}} \tag{6.26}$$

From (6.25)-(6.26), the total admittance of the ladder at level $m = 0$ is given by:

$$Y_1(s) = \frac{1/Zl_1(s)}{1 + \dfrac{Zt_1(s)/Zl_1(s)}{1 + Zt_1(s)\dfrac{I_1(s)}{U_1(s)}}} \tag{6.27}$$

If we calculate the total admittance until $m = 1$, we have that:

$$Y_2(s) = \frac{1/Zl_1(s)}{1 + \dfrac{Zt_1(s)/Zl_1(s)}{1 + \dfrac{Zt_1(s)/Zl_2(s)}{1 + \dfrac{U_2(s)}{I_1(s)Zl_2(s)}}}} \tag{6.28}$$

or, equivalently,

$$Y_2(s) = \frac{1/Zl_1(s)}{1 + \dfrac{Zt_1(s)/Zl_1(s)}{1 + \dfrac{Zt_1(s)/Zl_2(s)}{1 + \dfrac{Zt_2(s)/Zl_2(s)}{1 + Zt_2(s)\dfrac{I_2(s)}{U_2(s)}}}}} \tag{6.29}$$

From (6.27)-(6.29) one may generalize via recurrence the form of the total admittance with $m = N$ cells, for $N \to \infty$:

$$Y_N(s) = \frac{1/Zl_1(s)}{1 + \dfrac{Zt_1(s)/Zl_1(s)}{1 + \dfrac{Zt_1(s)/Zl_2(s)}{1 + \dfrac{Zt_2(s)/Zl_2(s)}{\cdots \dfrac{\cdots}{1 + \dfrac{Zt_{N-1}(s)/Zl_N(s)}{1 + Zt_N(s)/Zl_N(s)}}}}}} \tag{6.30}$$

which is, in fact, a continued fraction expansion. If in this network, we can express each compartment as a recurrent function of the first compartment, then the total impedance of such a network exhibits a phase–constancy [189]. This phase constancy can be positive or negative, depending on the values of Zt and Zl as a function of the frequency. We shall make use of such generalized network model to determine the neuron network impedance model.

Considering any combination of cellular composition it follows the general form of this continuous fraction expansion:

$$Y_N(s) = \cfrac{W'(s)}{1+\cfrac{W(s)}{1+\cfrac{W(s)/\alpha}{1+\cfrac{W(s)/\alpha\eta}{1+\cfrac{W(s)/\alpha^2\eta}{\cdots\cfrac{\cdots}{1+\cfrac{W(s)/\alpha^{N-1}\eta^{N-2}}{1+W(s)/\alpha^{N-1}\eta^{N-1}}}}}}} \tag{6.31}$$

which is a generally valid form, irrespective of the definitions of $W(s)$ and $W'(s)$. For any $|W(s)| > 1$, this general form (6.31) can be approximated by a lumped admittance whose form depend on the functions $W(s)$ and $W'(s)$ in which exists at least one term in fractional-order given by:

$$\gamma = \frac{\log(\alpha)}{\log(\alpha)+\log(\eta)} \tag{6.32}$$

The frequency interval where the convergence to this form is valid, hence the constant-phase behavior in the frequency response of such a ladder network, is given by the condition imposed via $|W(s)| > 1$.

In [190], an early study on fractional dynamics for distributed relaxation processes in sensory adaptation, the authors found that the fractional derivative and its Fourier transform $s^\alpha = j\omega^\alpha$ were able to capture the wide dynamic range of sensory adaptations. Distributed relaxation processes are common in cells and tissues, involving electrochemical reactions. The latter have been shown to be well characterized by the fractional order circuit element $Z = Z_0\omega^{-\alpha} \times e^{(jatg(\frac{\pi\alpha}{2}))}$ which exhibits constant phase dynamics [119]. The link from the frequency domain to time domain of such a fractional order element can be derived by means of the fractional derivative definition. Suppose the impedance written in Laplace domain:

$$z(s) = \frac{v(s)}{i(s)} = R + \frac{1}{s^\alpha C(s)} \tag{6.33}$$

then the transient voltage response to a step in the applied current is described in time domain by

$$V(t) = I_0 R + \frac{I_0 t^\alpha}{C\Gamma(\alpha+1)} \tag{6.34}$$

which gives a power law response. This shows that there must exist a link between the fractal dimension observed in the time domain EEG signals and the frequency response fractional order dynamics. The current knowledge on structural arrangements of neural networks and their dynamics is not yet mature to fully account the complex dynamics observed in the EEG.

Fractional order dynamic models of complex, multiscale systems such as the brain, account for anomalous behavior through a simple extension of the order of the algebraic operations from integer to fractional. In the time domain, this extension is manifested through incorporation of a variable degree of system memory through convolution with a power law kernel exhibiting fading memory of the past [119]. In system engineering terminology this is also known as a forgetting factor, a weight on the past data between 0-1, whereas fractions closer to 0 indicate the past is not important.

Pain Perception Model:

The perception model based on exponential and power law combined functions seems to be a good candidate for capturing essential electrical activity modulated in brain [191]. Plasticity in synaptic variance is introduced in a layer-based sensory area in cortex by reverse node engineering modelling. In the case of pain perception, the combined effect can be obtained by using the Mittag-Leffler function, which is well-known to capture hybrid exponential and power-law behaviour in biological tissues [119].

Diffusion of perception sensory activity in brain using Mittag Leffler function in time domain corresponds to a non-integer order derivative easily expressed in frequency domain [22]. Layered activity can be represented by ladder networks with serial connection of RC-cells. To account for plasticity, the RC cells are not identical, instead they behave as a memristor with unbalanced dynamics. For instance, first pain perception is more intense than the second, given the latency of the delayed pain stimulus (i.e. sharp first increase followed by slowly decaying tail).

Assuming the brain-cortex area as a porous tissue whose porosity varies (i.e intra- and extra- cellular space tissue with different densities), one can model the changes in viscosity as a function of this porous density. It has been shown that fractional order derivatives are natural solutions to anomalous diffusion equations [12, 15]. Time variations of information flow profiles in time-dependent viscous fluids have been also characterized with the same Mittag-Leffler function [192]. The use and physical interpretation of this very useful fractional calculus tool has been discussed in several works, e.g. [7, 193–195]. The advantage of using the Mittag-Lefler function is that it allows introducing memory formalism [196], therefore taking into account the tissue rheology. The mixed area in brain tissue will introduce a dynamic viscosity and thus a dynamic perception of

nociceptor induced pain.

To characterize this dynamic formalism, we make use of the Mittag Leffler function. Let the Riemann-Liouville fractional integral defined in [197] be given by:

$$J_t^\beta f(t) = \frac{1}{\Gamma(\beta)} \int_0^t (t-\tau)^{\beta-1} f(\tau) d\tau \tag{6.35}$$

for positive values of β and time t over integration step $d\tau$. Assuming uni-directional information flow and piecewise constant density, we have that stress and strain relation in local tissue areas is generalized to:

$$\tau_{ij} = 2\mu_0 J_t^\alpha e_{ij} \tag{6.36}$$

with τ_{ij} the stress tensor, μ is the dynamic viscosity, e_{ij} is the strain tensor, $0 < \alpha < 1$ and positive time t. The Laplace transform of the fractional integral is given by:

$$L(J_t^\alpha u(y,t))(s) = s^{-\alpha} \tilde{u}(y,s) \tag{6.37}$$

We also have that:

$$\int_0^\infty e^{-st} t^{\mu-1} E_{\nu,\mu}(at^\nu) dt = \frac{s^{\nu-\mu}}{s^\nu - a} \tag{6.38}$$

where we make use of the Mittag-Leffler function:

$$E_{\nu,\mu} = \sum_{r=0}^{\infty} \frac{s^r}{\Gamma(\nu r + \mu)} \tag{6.39}$$

Solutions for bounded domains fractional diffusion equations can be found using the Mittag-Lefler function. We have the following initial/boundary value problem:

$$\begin{cases} \partial_t u = \mu_0 \partial_{yy} J_t^\alpha u, \text{for } \alpha \in (0,1) \\ u(0,t) = u(2r,t) = 0, \text{for } t \leq 0 \\ u(y,0) = U_0 = ct, \text{for } 0 \leq y \leq h \end{cases}$$

In this problem assume a constant initial velocity field $u(y,0) = U_0$ in a determined plane, with null boundary conditions. Using the exact solution in a boundary domain given in [192], information signal velocity profiles are given as a function of (6.39):

$$\begin{array}{l} u(y,t) = U_0 \frac{2}{\pi} \sum_{n=1}^{\infty} E_{\alpha+1} \\ (-\sqrt{\mu_0} a^2 n^2 t^{\alpha+1}) \frac{\sin(ayn)}{n} (1 - \cos(n\pi)) \end{array} \tag{6.40}$$

with $1 < (\alpha + 1) < 2$, n the wave number, and $a = \pi/2r$ with $2r$ the diameter of a sphere denoting the stimulated area.

The result of memory effects due to time variability of the viscosity coefficient is an anomalous fractional Mittag-Leffler oscillation function. This indicates that

fractional order impedance models may be a good instrument to describe global and local damping due to local time variability of the viscosity coefficient, linked to levels of consciousness [198].

The multi-scale lumped model:

Given the processes characterized hitherto, we can now proceed to approximate them with lumped terms. The stimulus effect to nociception reception is enabled essentially by diffusion characterised by an ultracapacitor. The gate control theory acts at lower frequencies as a resistance and at high frequencies as a ultracapacitor. The signalling pathway model is reduced to a fractional order integro-derivative function (depending on the sign of the fractional order) - this term essentially captures whether or not the information is taken up to the brain. The pain perception model is also an integro-derivative function capturing levels of perception of noxious stimuli in the brain.

It follows that the complete mathematical model expressed as an impedance in Laplace variable s is given by

$$Z_{tot}(s) = R + \frac{D}{s_1^\alpha} + \frac{S}{s_2^\alpha} + P s_3^\alpha \tag{6.41}$$

where $0 < \alpha_{1,2,3} < 1$ and R, D, S, P are real numbers. Not all terms in this model are necessary at all times, as some of the physiological processes may be impaired in some applications (e.g. analgesia will put zero the effect of the perception term in P). The units are arbitrary, as the model is defined as a difference to the initial state of the patient - due to the use of fractional derivatives - and not as absolute values. This enables patient specificity since no generic model is assumed to be valid and thus broadcasts a new light upon the interpretation of such models.

Model Validation:

Apart from the non-parametric identification performed with (6.9) and the zero-pole interlacing method, a parametric identification has been performed using the fractional order model from (6.41). The results obtained using the fractional order model impedance (6.41) are presented in Figures 6.27-6.34. In this part of the thesis only the results for one volunteer for all study cases are presented. The results for the other participants are included in Appendix C.

From the results presented in this section a good correlation between the measured impedance and the estimated impedance using (6.41) can be observed. One may argument that the fitting with the zero-pole interlacing method gave better results (for more subjects) than the lumped fractional order impedance model. This might be indeed the case, but it has to be taken into account that the zero-pole interlacing model has 13 parameters to be estimated while for the lumped fractional model we have only 7.

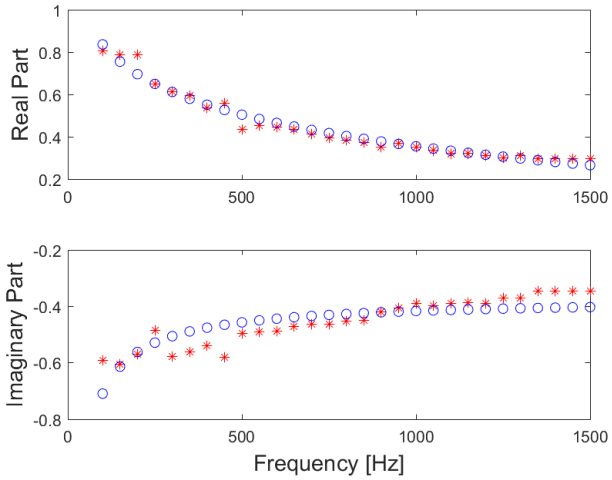

Figure 6.27: First pain stimuli: Impedance in its complex representation for first case study (first measurement). '∗' denote measured impedance and 'o' denote the estimated impedance.

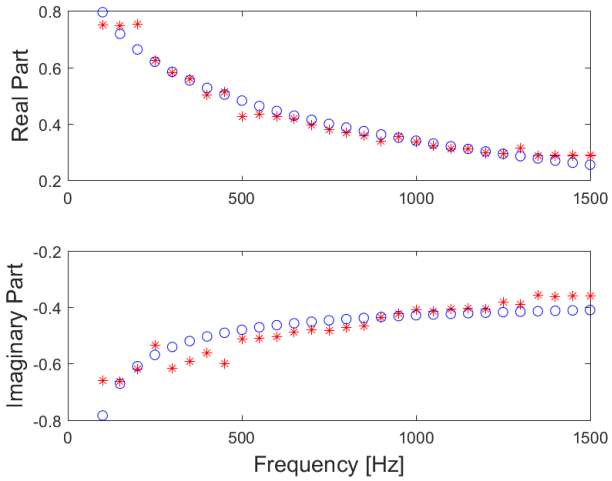

Figure 6.28: Second pain stimuli: Impedance in its complex representation for first case study (first measurement). '∗' denote measured impedance and 'o' denote the estimated impedance.

The next challenge is to identify the physiological meaning of each of these parameters. For this, further research, beyond this thesis, will be performed. A clinical study, for which the ethical committee EC/2017/1517 has been already

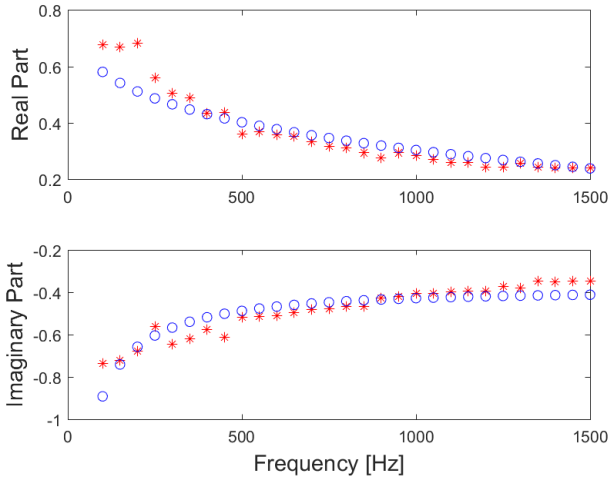

Figure 6.29: First pain stimuli: Impedance in its complex representation for first case study (second measurement). $'*'$ denote measured impedance and 'o' denote the estimated impedance.

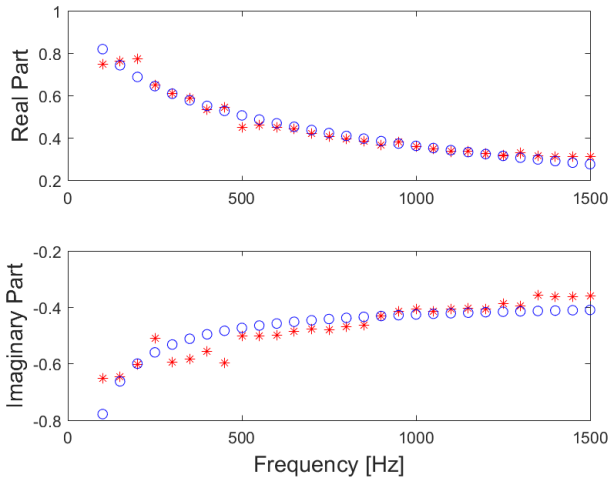

Figure 6.30: Second pain stimuli: Impedance in its complex representation for first case study (second measurement). $'*'$ denote measured impedance and 'o' denoted the estimated impedance.

submitted, will be conducted at Ghent University Hospital. This study will take place in the first half of 2019. In parallel the necessary steps to apply for an observational study at the hospital in Brescia (via prof. Antonio Visioli, Brescia

University) have been taken. During these observational studies patients in the post-operative care unit will be monitored with the ANSPEC-PRO device.

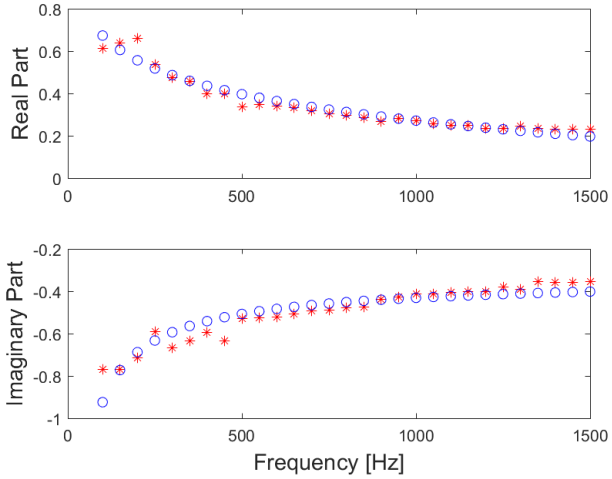

Figure 6.31: First pain stimuli: Impedance in its complex representation for second case study. $'*'$ denote measured impedance and 'o' denote the estimated impedance.

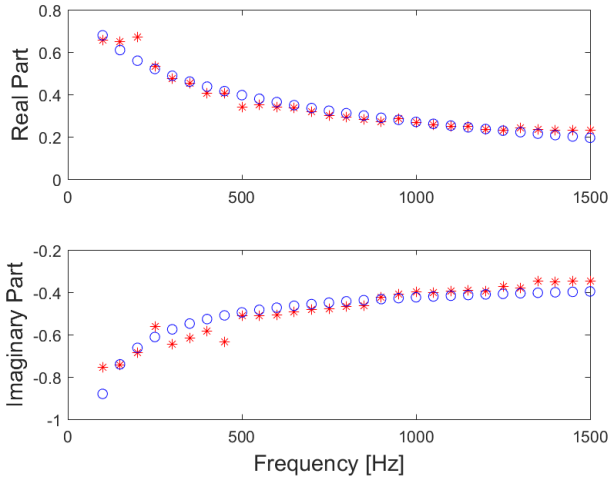

Figure 6.32: Second pain stimuli: Impedance in its complex representation for second case study. $'*'$ denote measured impedance and 'o' denote the estimated impedance.

During the clinical trials impedance will be recorded but also additional information such as: NRS score (given by the patients), heart rate, cardiac output,

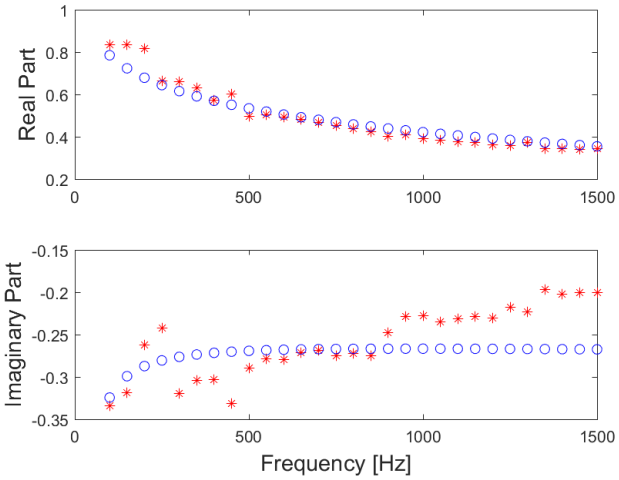

Figure 6.33: First pain stimuli: Impedance in its complex representation for third case study. '$*$' denote measured impedance and 'o' denote the estimated impedance.

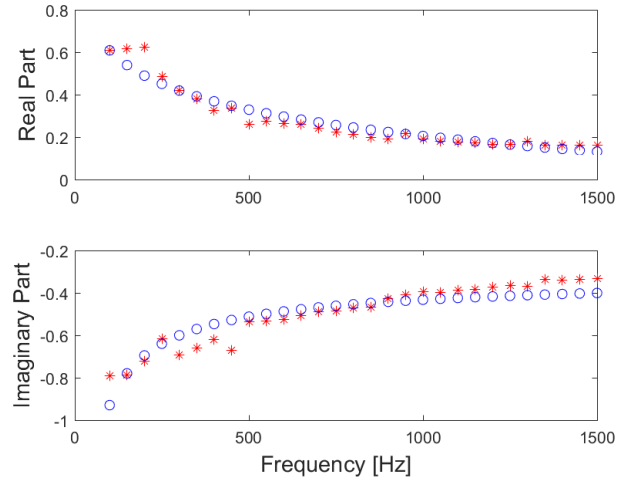

Figure 6.34: Second pain stimuli: Impedance in its complex representation for third case study. '$*$' denote measured impedance and 'o' denote the estimated impedance.

etc. will be registered. From the data available after this observational study, a rigorous analysis will be performed. Given the additional information available and the patient biometric parameters a correlation between model parameters and their physiological meaning will be derived. The identification values of the model parameters are presented in table 6.3. Although the identification results are satis-

factory and we have noticed that there are differences in model parameters between the investigated case studies a more in depth analysis is needed. Therefore, further research with respect to the fractional order model parameters will be conducted. Also, an analysis between fractional order model parameter and the biometric parameters has been conducted in order to identify if there is any correlation between them. From this analysis no clear conclusion could be taken. We have noticed that for some of the fractional order parameter there is a correlation for others not. Therefore, these results have not been included in this chapter of the thesis but in Appendix A. Further research with respect to this particular item will be performed after this thesis when also a higher number of subjects will be investigated such that statistically significant conclusions can be taken.

Table 6.3: Standard deviation (SD) of the lumped FO model parameters.

SD	R	D	S	P	α_1	α_2	α_3
Case 1 (1st meas.) 1st Pain stimuli	1.13	6.14*10^4	1.22*10^5	1.24	0.99	1.38	0.024
Case 1 (1st meas.) 2nd Pain stimuli	17.35	3.09*10^4	6.40*10^4	17.52	0.96	1.46	0.07
Case 1 (2nd meas.) 1st Pain stimuli	8.64	5.16	2.56*10^5	8.70	0.07	5.26	0.075
Case 1 (2nd meas.) 2nd Pain stimuli	1.47	6.7*10^4	2.59*10^5	1.02 0.87	9.67	0.048	
Case 2 1st Pain stimuli	6.51	-8.13*10^2	1.23*10^5	97.90	0.78	1.28	0.43
Case 2 2nd Pain stimuli	2.36	2.03*10^3	2.47*10^5	2.01	1.10	1.14	0.23
Case 3 1st Pain stimuli	1.88	3.24	6.17*10^4	10.74	0.33	7.01	0.34
Case 3 2nd Pain stimuli	2.40	3.77	1.39*10^3	1.91	0.41	241	0.10

6.6 Summary

In this Chapter the proposed model and their validation are presented. Four models have been investigated: Cole-Cole model, non-parametric impedance model, zero-pole interlacing model and lumped fractional order impedance model. All these models have been validated on real data and the outcome of this chapter is that the fractional order impedance model can capture the changes in impedance when a pain stimulus is applied. Although the obtained results are satisfactory further research is needed and the following tasks need to be performed:

- measurements on larger number of participants to enable statistical meaningful conclusions;
- a clinical study where patients are standardly treated for pain (i.e. not a controllable environment, pain is already present);
- perform a rigorous analysis of these measurements to extract the required information for a physisological interpretation of each parameter in the model;
- an index needs to be derived to indicate the level of pain;

All these tasks are beyond the scope of this thesis.

7 Conclusions

In this Chapter the conclusions of the work presented in this thesis are addressed. The main contributions and further work are emphasized. The conclusions are drawn from two perspectives: diffusion model of gas exchange in the lungs and a model to characterize the nociceptor pathways.

Diffusion of gas in the lungs is a passive physical process that exchanges oxygen and carbon dioxide between the alveoli and the blood (in the lungs) and between the blood an the cells (in the periphery). Based on the theory presented in Chapter 2 and the results given in Chapter 3 we have shown that the complex phenomenon of gas exchange in the lungs can be approximated with a fractional order model. In this thesis, the importance of diffusion in patients with COPD disease has been investigated. Measurement of the diffusion factor might be of importance in (early) detection of COPD disease. The single breath method became the most generally accepted method. In this thesis emerging tools from fractional calculus have been used to capture changes in COPD disease and to understand their effect on the model parameters.

The results presented in this thesis indicate a direct link relation between the T index and the heterogeneity in COPD lungs. Although the results obtained are promising there are still challenges to be solved. The model presented in this thesis is an approximation based on analogy, hence the theoretical link between diffusion in the lungs and the model presented in Chapter 2 will be further investigated. Moreover, in this thesis a relatively small study in a somewhat heterogeneous group of COPD patients has been performed.

According to the literature, detection and parameterization of nociceptor activity is of crucial importance for treatment in chronic pain patients, in post-surgery patients, rehabilitation and follow up studies of new medication development. The lack of system engineering tools to capture the most important multi-scale processes involved in the reception, transmission and perception of pain has kept on a slow pace the potential development of pain management services. A specific domain of application where such models are greatly needed is the depth of anesthesia regulatory paradigm. As such, the model presented in this thesis enables new horizons and has the potential to unlock the current state of art in this specific area of application.

Patient specificity implies the ability to characterise changes in the various process dynamics involved in nociceptor pathways and perception. The proposed parametric model is unique in its formalism and systems engineering approach. The lumped model provides the most versatile features to capture changes in dynamic responses, with the minimal number of parameter values. This keeps the numerical complexity to a low level, enabling deployment on real-time platforms and fast computation rates for identification from real-life data.

The proposed model considers a time-frequency mathematical formulation. It has been shown that many biomedical signals may benefit from time-frequency analysis. Since the frequency content of many biomedical signals can fast with time (i.e. changes in impedance when a pain stimulus is applied are very fast), the time-frequency analysis allows us to capture these changes. This is of great importance in pathology cases, where changes in tissue structure and morphology affects directly the dynamic profiles of drug diffusion, permeability and molecular binding. Specific structural changes with disease may also reveal various paths of deep tissue trapping of drug and latency nodes which could explain effects observed in long-tailed observations. This work enables a mapping of the various components of the pain pathways. The description follows the micro- and macro-structural elements. The end result is an innovative and original methodology to capture the signalling pathways and deliver an objective, independent and useful measure for pain.

In this thesis, the first steps towards a sensor to measure the pain level in an objective manner and a model of nociception pathway have been made. The result is the ANSPEC-PRO monitor, non-invasively measuring pain by means of skin impedance. The prototype has been validated at this moment only in awake volunteers with self-induced nociceptor excitation (i.e. mechanical pain stimuli). Given the low subjects number and the controlled environment in which the device has been tested, an ethical committee application (EC/2017/1517) has been submitted for measurements at the University Hospital Ghent. In parallel, the necessary steps for submitting an ethical committee application at Brescia University Hospital have been taken. The aim of these observational studies is to observe patients

in the post-operative care unit. These patients are treated for pain following the standard procedure (i.e. based on NRS scale).

7.1 Future perspectives

Anesthesia paradigm consists of three main components: hypnosis, neuromuscular blockade and analgesia. The first two components are well now mature for integration in a single environment. Hence, the missing piece is analgesia. The results of this thesis will enable the next steps towards a complete regulatory dynamic system for controlling general anesthesia by means of its all three components. However, the proposed model cannot be yet used in closed loop and a further development is required. More specifically, a correlation with drug concentration needs to be made. This aspect has not been addressed in this thesis. A possibility to measure drug concentration is using blood sample. However, to include this information in closed loop continuous measurement of drug concentration is necessary. Given the technological advances nowadays a non-invasive or minimally invasive measurement of drug concentration would be ideal. This is not yet available and a first hypothesis to be investigated is similar to continuous measurement of glucose concentration. More specifically, a thing wire sensor is inserted under the skin and measures the glucose concentration in the interstitial fluid. Studies have shown that there is no significant time lag among the interstitial fluid, capillary and venous glucose levels. At this moment the model can be used as disturbance. For instance if we know the surgery profile we can used the developed model as a disturbance to predict that an increase in the nociception level will occur.

The aim beyond this doctoral thesis is to develop a bullet-proof analysis of a complete regulatory dynamic system for controlling general anesthesia by means of all its three components: hypnosis, analgesia and neuromuscular blockade. To date, nowhere worldwide exist such a complete system in simulation studies, let alone in practice. This system will feature multiple input and multiple output variable analysis, model development and adaptation and robust, stable, adaptive control algorithms. Safety loops will be mimicked into the system, as well as surgical disturbances and noxious stimulation profiles. All these independent features are available in their single regulatory loop. Their combination and the effect of their combination on the patient state profiles is yet unknown.

The longer term objective will be to implement a clinical onset for this complete regulatory system following EC advise and policies at Ghent University Hospital. This is a challenging and unconventional research which requires the collaboration and acceptance from the medical practitioners. Given our long-standing collaboration with Ghent University Hospital and other hospitals in Europe (i.e. Breascia University) ethical committee files will be submitted to validate the developed automated anesthesia system.

A

ANSPEC-PRO Device

In this Appendix the development of a measurement device for continuous monitoring of changes in skin impedance as a function of an applied stimulus is presented. This proof of concept device has been developed starting from the perspective that a pain stimulus can be detected from a change in skin impedance as a function of time and frequency. The skin is a black box and in order to obtain the impedance the skin is excited with a known voltage and simultaneous measuring the current flowing through the skin. The relation between this input voltage $V(s)$ and output current $I(s)$ is:

$$Z(s) = \frac{V(s)}{I(s)} \tag{A.1}$$

Notice that skin impedance $Z(s)$, input voltage $V(s)$ and output current $I(s)$ are in function of $s = j\omega$ and, thus, are dependent on frequency ($\omega = 2\pi f$) of the excitation signal [201]. To obtain a wide range of information on the behaviour of the skin impedance the skin is excited at different frequencies. For this identification method with multiple exciting frequencies a *multisine* signal is used [202]. This signal is a superposition of a number of sines with different frequencies. Using Non-Parametric Identification techniques the impedance $Z(s)$ can be estimated. As mentioned before, this transfer function $Z(s)$ will change in time, due to pain stimuli or other external influences [203]. This will increase the complexity of the Non-Parametric Identification as a time factor will be introduced.

The device will consist of the following subsystems that will work together: hardware, software and data analysis. Measuring current is not easy compared to voltages and therefore the signal is conditioned and the current is transformed to

a voltage which can be interpreted by the measuring device (see Figure A.1). A signal is designed off-line (a priori). This signal $v(t)$ is sampled and needs to be sent to an analogue output port, using zero-order hold, with a certain sampling frequency, f_s. Simultaneously, the current $i(t)$ coming from the skin needs to be measured. The voltage $v(t)$ and current $i(t)$ are saved in a file that is defined by the user.

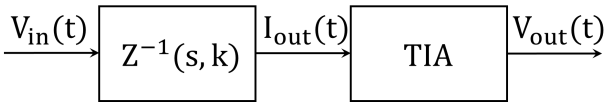

Figure A.1: Block diagram with the skin impedance $Z(s,k)$ as black box system; The bioimpedance is in function of the frequency and discretised time k.

General description of the investigational device and its components including materials used: The developed device is non-invasive, as electrodes are temporarily attached to the skin of the human body. The electrodes and electrode connectors are CE-marked (according to MDD93/42/EEC). The National Instruments CompactRIO that is used to measure the patient fulfills the following electrical equipment safety standards:

- IEC 61010-1, EN 61010-1
- UL 61010-1, CSA 61010-1
- EN 60079-0:2012, EN 60079-15:2010
- IEC 60079-0: Ed 6, IEC 60079-15, Ed 4
- UL 60079-0; Ed 5, UL 60079-15; Ed 3
- CSA 60079-0:2011, CSA 60079-15:2012

Regarding the electromagnetic compatibility the cRIO meets the requirements of the following EMC standards for electrical equipment:

- EN 61326 (IEC 61326): Class A emissions; Industrial immunity
- EN 55011 (CISPR 11): Group 1, Class A emissions
- AS/NZS CISPR 11: Group 1, Class A emissions
- FCC 47 CFR Part 15B: Class A emissions
- ICES-001: Class A emissions

The devices meets the essential requirements of applicable European Directives, and therefore receiving the CE Mark, as follows:

- 2014/35/EU; Low-Voltage Directive (safety)
- 2014/30/EU; Electromagnetic Compatibility Directive (EMC)
- 94/9/EC; Potentially Explosive Atmospheres (ATEX)

The device is built while taking into account the A.R.E.I. (Algemeen Reglement op de elektrische installaties) regulations, that provides rules of thumbs for safety of electrical equipment, regarding electrical shocks, safety, grounding, etc. The device consists of two hardware parts: a laptop and a data-acquisition circuit. The two parts are interconnected through Ethernet cables that links the two devices to a common network. The laptop is a standard laptop with the operating system Windows 7 Enterprise 64-bit and a INTEL(R) Core(TM) i7-6600U CPU@2.80GHz processor.

Data-acquisition circuit consists of two DC-converters with galvanic separators, step-down transformers, that will output 24 V DC and +/-15 V DC. The +/-15 V DC will supply the power to the electrodes. The power is 3.75 VA and the transformer is approved according to the ENEC 10 (VDE) legislations. The safety class of the transformer is class II, which indicates that it has a double insulation. The voltage is rectified and a voltage regulator provides a short-circuit protection in its package. A National Instruments (Texas, USA) device (cRIO9074 with NI9201- and NI9263-slots) is used to excite a part of the skin with an off-line designed voltage signal. This voltage will induce a current in the circuit related to the impedance of the human body. This current is captured and saved onto the laptop. A voltage buffer limits the supplied current to +/-20 mA.

The user interface has been developed in LabView and the main block diagrams behind figure A.2 are presented below. In this interface, the following numbers are depicted:

1. Load the input signal;
2. Set the sampling frequency in Hz;
3. Set the frequency resolution in Hz;
4. Set the amplitude of output signal. This is to control saturation of the input signal to the patient (see 10);
5. The number of seconds that are saved per data file.
6. After fields 1 to 5 and 7 are filled in, start acquiring by pressing 6 - Start acquisition;
7. Create the paths and file name where to save the data. Remark that the data is only saved when 9 - Save is selected;

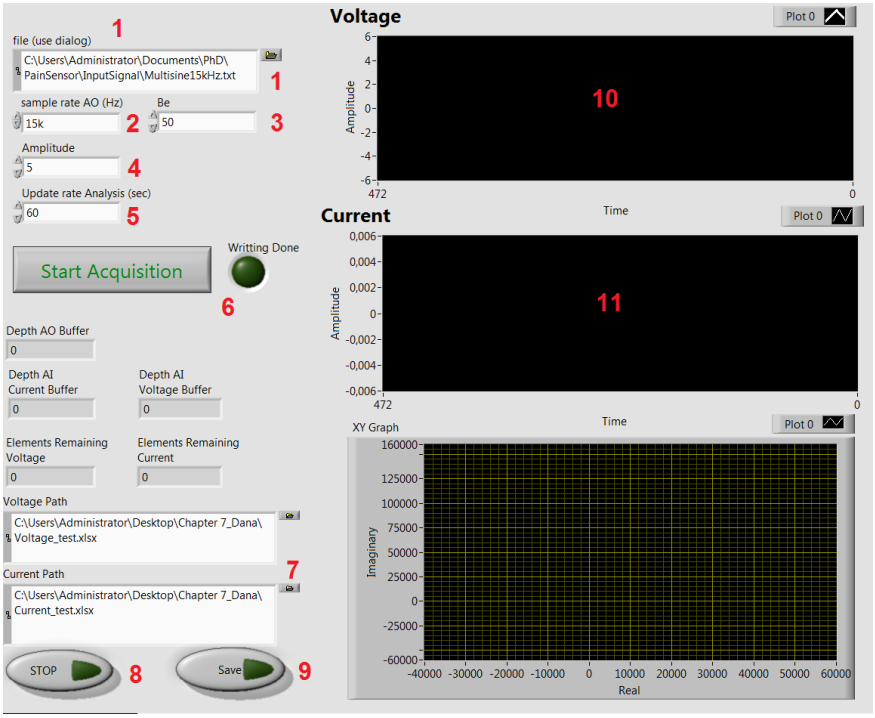

Figure A.2: The user interface on the laptop that controls the ANSPEC-PRO device

8. After acquiring press 8 - Stop to stop the acquisition;

9. The save-button should be highlighted to save data to the location indicated in 7;

In figure A.3 the block diagram for software initialization and parameters definition is shown, followed by the acquisition block diagram presented in figure A.4. The block diagrams for receiving and writing the data are presented in figures A.5 and A.6.

Table A.1 provides a list with all components used in the circuitry. The PCB (printed circuit board) is made of Laminates (resin material), copper-clad laminates, resin impreginated B-stage cloth (Pre-preg), and copper foil.

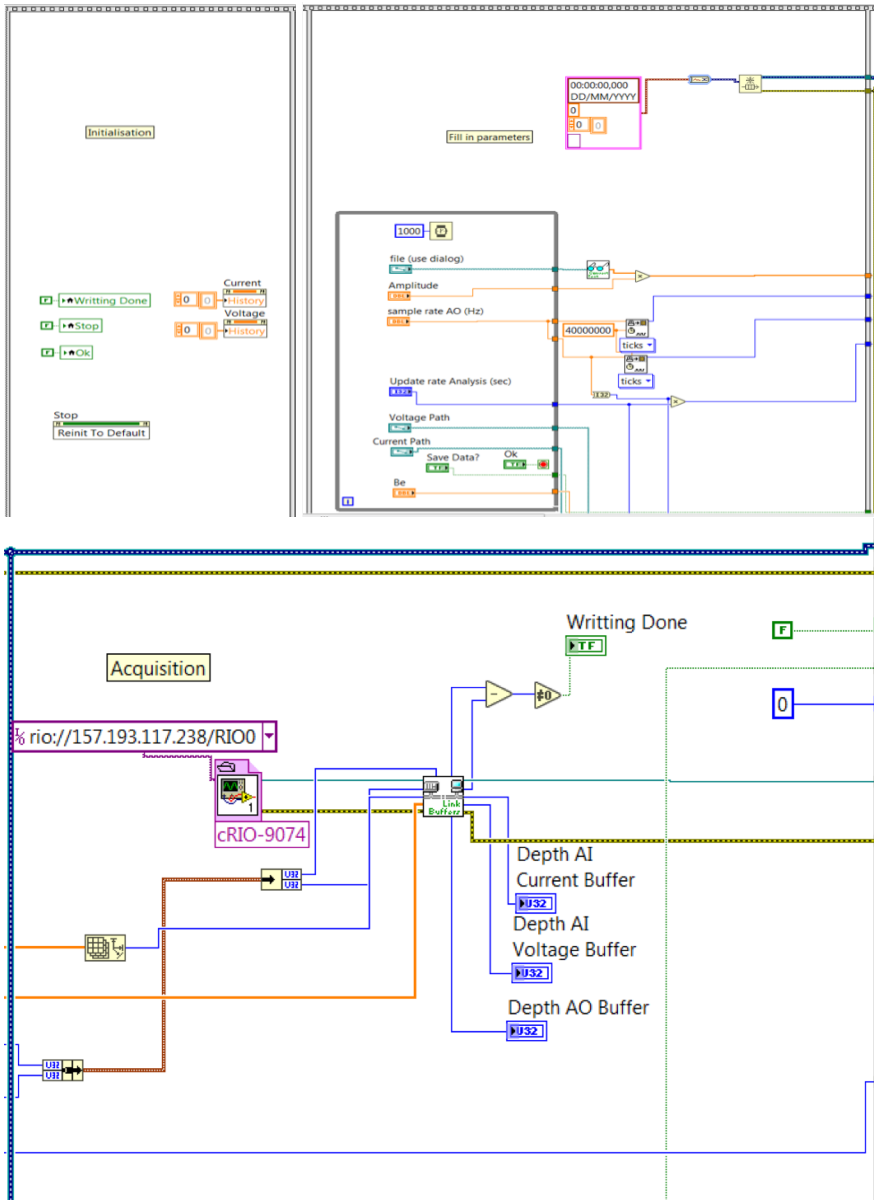

Figure A.4: Acquisition block diagram in LabView.

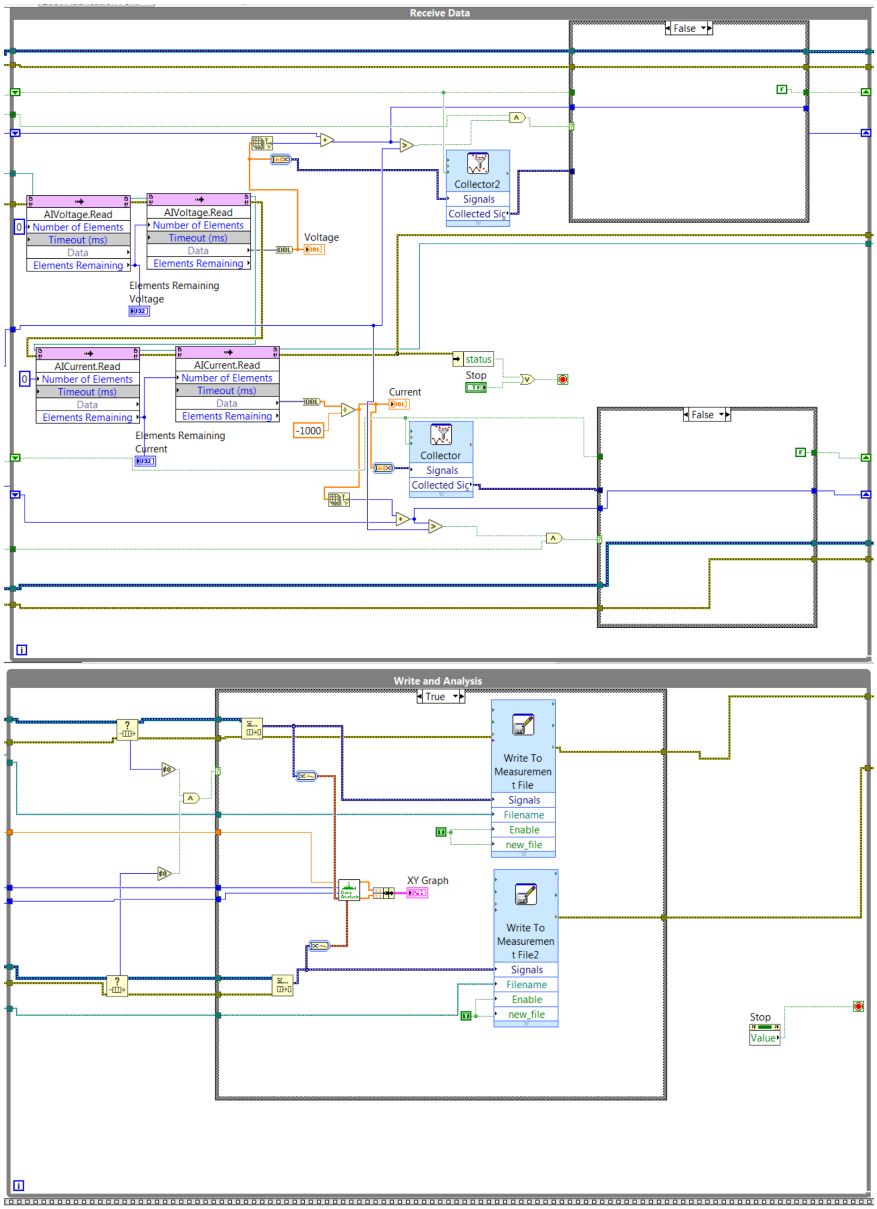

Figure A.6: Write block diagram in LabView.

Module	Name	Company
cRIO	cRIO-9074	National Instruments
cRIO	NI-9201	National Instruments
cRIO	NI-9263	National Instruments
cRIO	PS-125	National Instruments
cRIO	Ethernet cable (5E - patched)	/
S	PCB	EELAB
S	2way PCB Terminal Block	Phoenix
S	Transformer 15V -3.5VA	Block
S	Diodes - 400V	ON Semiconductor
S	Electrolytic Capacitor (3300nF-35V)	United Chemi-Con
S	Voltage Regulator (+12V/1A) (MC7812)	ON Semiconductor
S	Voltage Regulator (-12V/1A) (MC7912)	ON Semiconductor
S	Heat Sink TO-220	AAVID-Thermalloy
S/VB	3way PCB Terminal Block	Phoenix
VB	Op Amp MC1458P	Texas Instruments
VB	4way PCB Terminal Block	Phoenix
VB	Audio Connector (3 contacts, Jack 3.5)	Pro Signal
VB	Sensor Cable (3 electrodes, Jack 3.5)	/
VB	Foam, Hydrogel Electrode H92SG Kendall	Covidien
VB	Diaphoretic foam Monitoring Electrode 2230	3M
VB/TIA	PCB	Own Design
TIA	Op Amp ADA4077-2	Analog Devices
TIA	Resistance (1000Ω -5%)	Velleman
TIA	Ceramic Capacitor (10pF-50V)	Kemet

Table A.1: Electrical Components; (cRIO) National Instruments' compactRIO; (S) Op amp voltage source; (VB) Voltage Buffer; (TIA) Transimpedance Amplifier;

B

Measurement results

Results obtained using the non-parametric impedance model

In Figures B.1 - B.6 the measurement results obtained for the first case study are reported followed by the results for the second case study in Figures B.7 - B.9 and third case study in Figures B.10 - B.12. Next, the results only showing the pain intervals are presented in Figures B.13 - B.18 for the first case study followed by the results for the second case study in Figures B.19 - B.21 and for the third case study in Figures B.22 - B.24.

Case study 1 / All intervals (P-Pain/NP-No Pain)

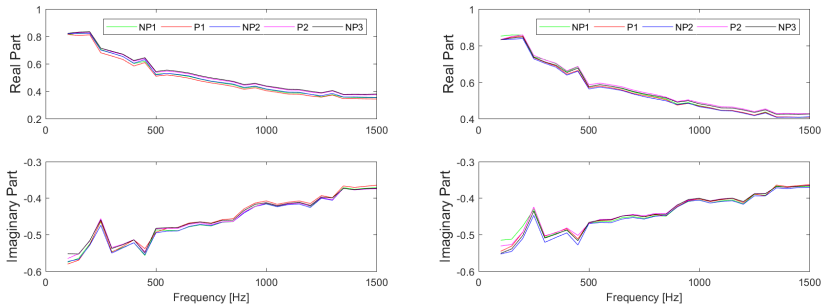

Figure B.1: Volunteer 2: Impedance in its complex representation for the first study case (left: first measurement; right: second measurements).

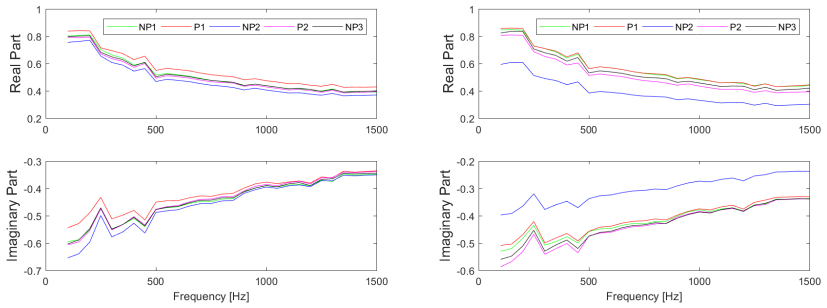

Figure B.2: Volunteer 3: Impedance in its complex representation for the first study case (left: first measurement; right: second measurements).

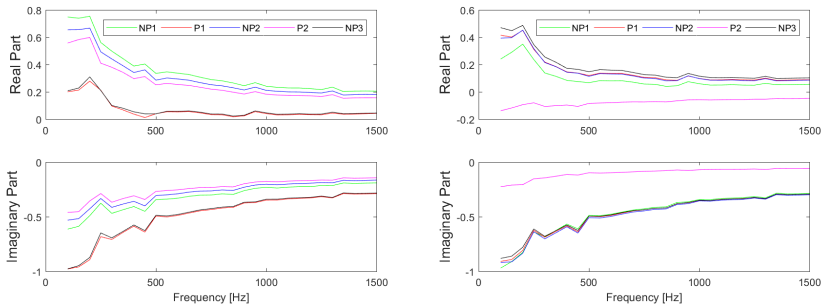

Figure B.3: Volunteer 4: Impedance in its complex representation for the first study case (left: first measurement; right: second measurements).

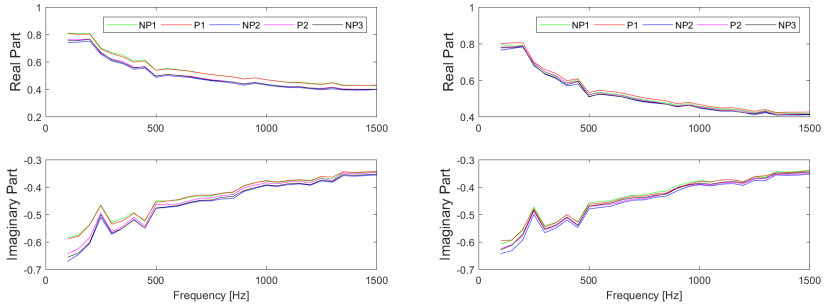

Figure B.4: Volunteer 5: Impedance in its complex representation for the first study case (left: first measurement; right: second measurements).

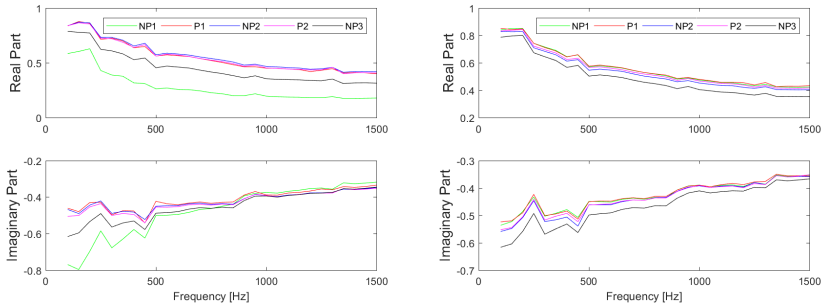

Figure B.5: Volunteer 6: Impedance in its complex representation for the first study case (left: first measurement; right: second measurements).

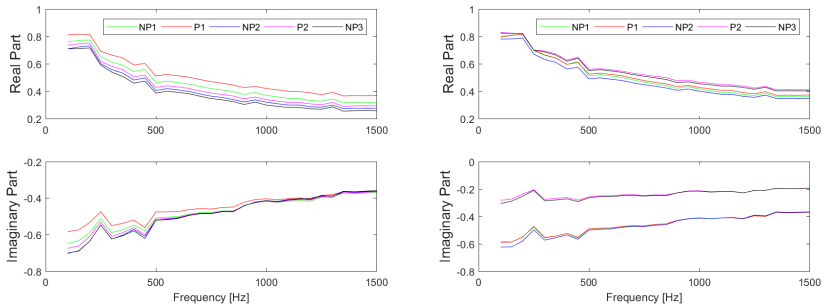

Figure B.6: Volunteer 7: Impedance in its complex representation for the first study case (left: first measurement; right: second measurements).

Case study 2 / All intervals (P-Pain/NP-No Pain)

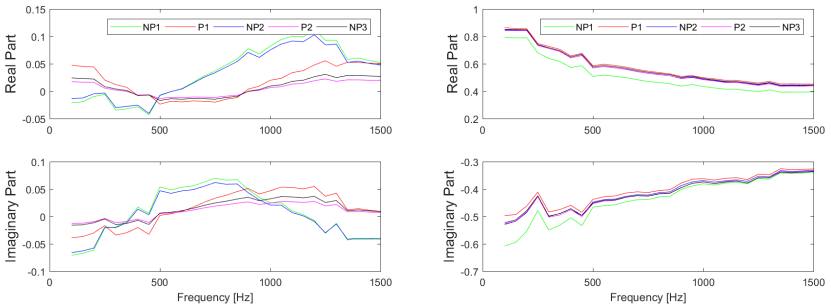

Figure B.7: Impedance in its complex representation for the second study case (left: volunteer 2; right: volunteer 3).

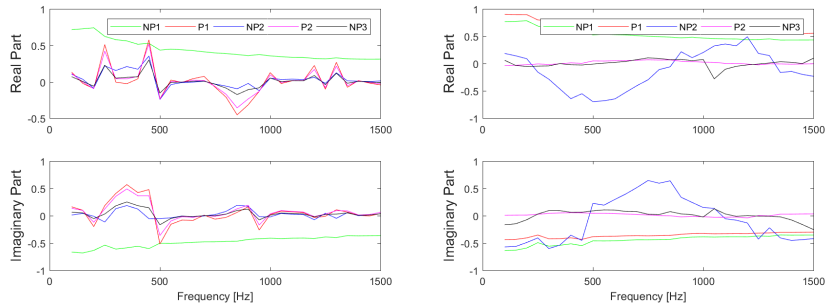

Figure B.8: Impedance in its complex representation for the second study case (left: volunteer 4; right: volunteer 5).

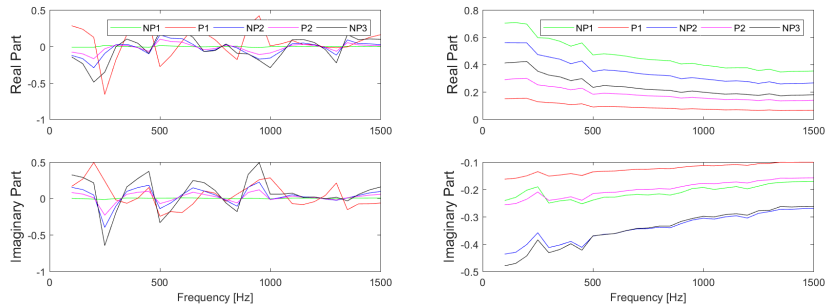

Figure B.9: Impedance in its complex representation for the second study case (left: volunteer 6; right: volunteer 7).

Case study 3 / All intervals (P-Pain/NP-No Pain)

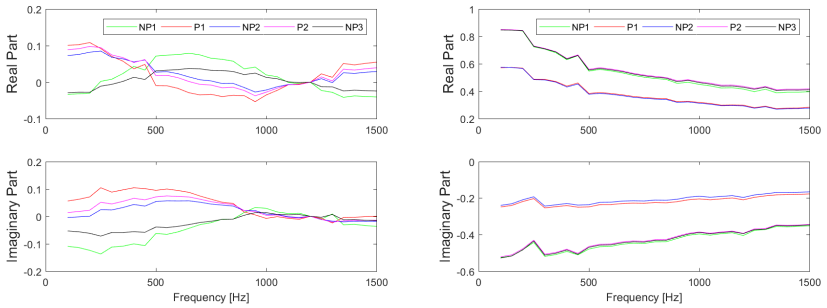

Figure B.10: Impedance in its complex representation for the third study case (left: volunteer 2; right: volunteer 3).

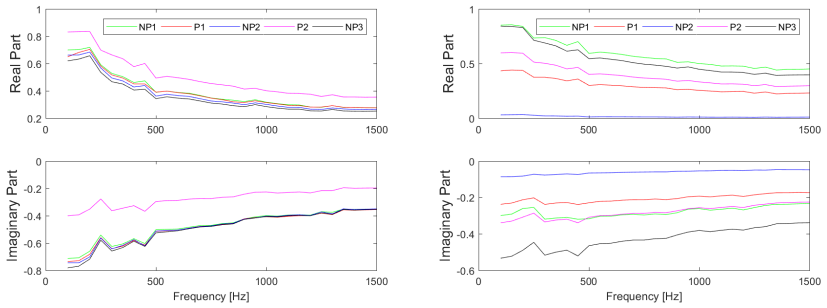

Figure B.11: Impedance in its complex representation for the third study case (left: volunteer 4; right: volunteer 5).

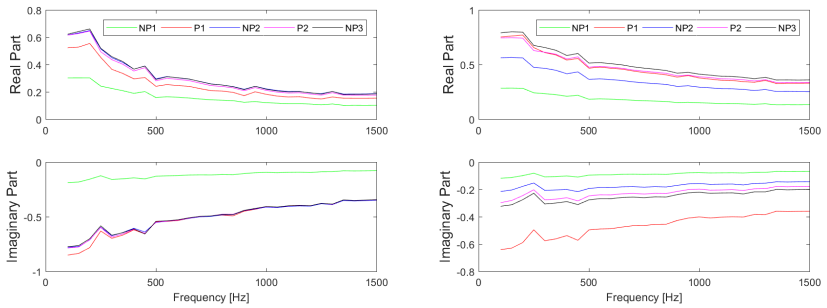

Figure B.12: Impedance in its complex representation for the third study case (left: volunteer 6; right: volunteer 7).

Case study 1 / Only pain intervals

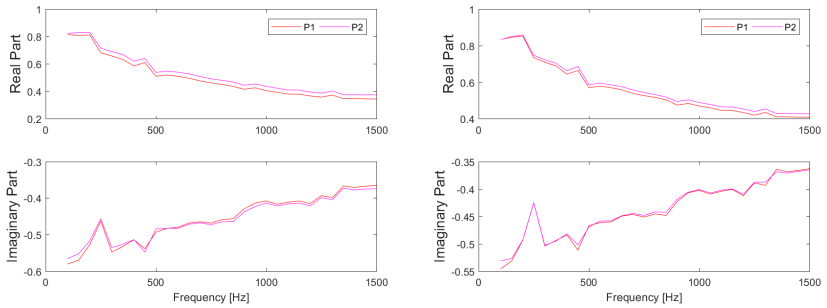

Figure B.13: Volunteer 2: Impedance in its complex representation for the first study case (left: first measurement; right: second measurements).

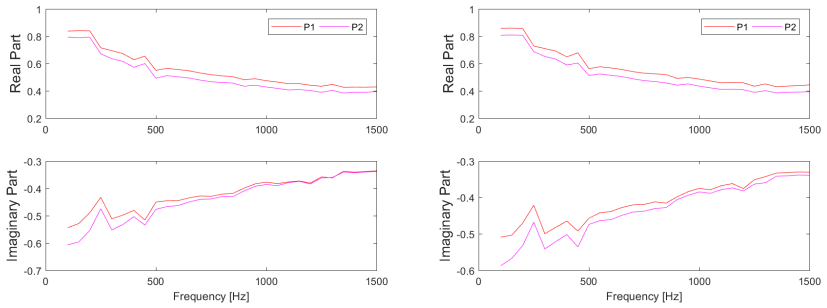

Figure B.14: Volunteer 3: Impedance in its complex representation for the first study case (left: first measurement; right: second measurements).

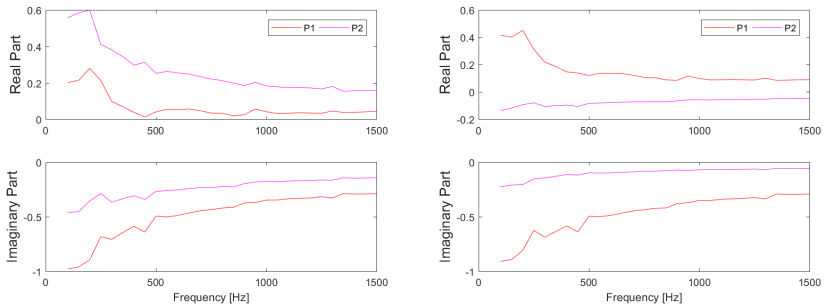

Figure B.15: Volunteer 4: Impedance in its complex representation for the first study case (left: first measurement; right: second measurements).

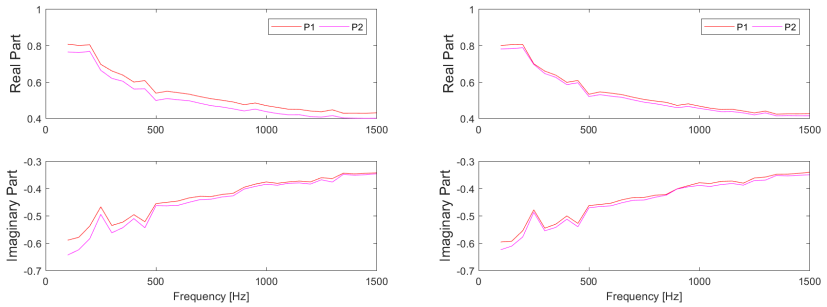

Figure B.16: Volunteer 5: Impedance in its complex representation for the first study case (left: first measurement; right: second measurements).

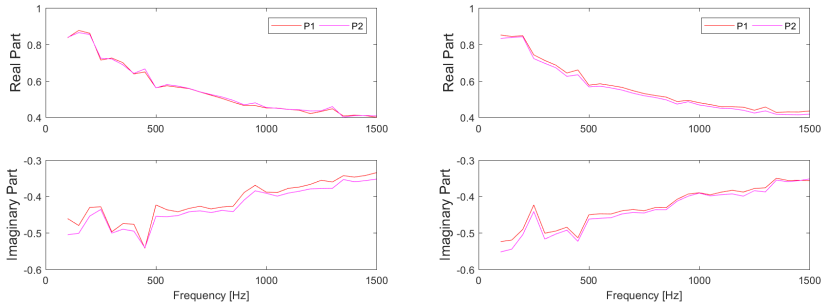

Figure B.17: Volunteer 6: Impedance in its complex representation for the first study case (left: first measurement; right: second measurements).

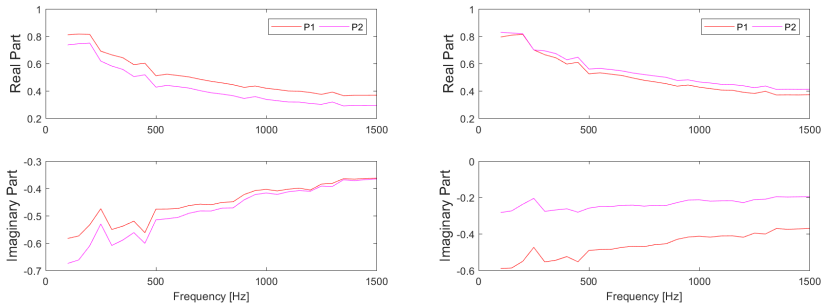

Figure B.18: Volunteer 7: Impedance in its complex representation for the first study case (left: first measurement; right: second measurements).

Case study 2 / Only pain intervals

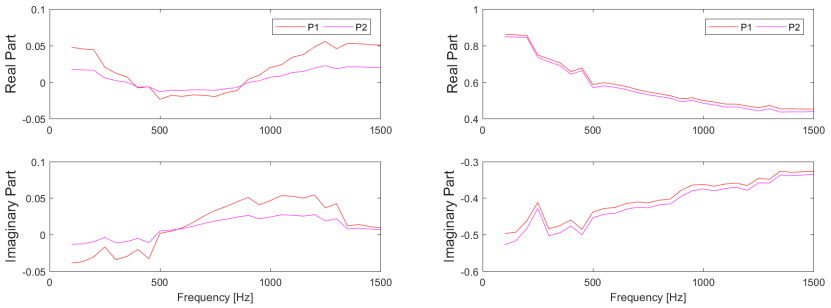

Figure B.19: Impedance in its complex representation for the second study case (left: volunteer 2; right: volunteer 3).

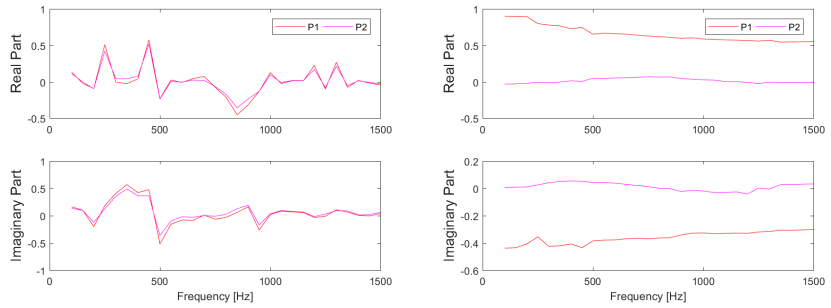

Figure B.20: Impedance in its complex representation for the second study case (left: volunteer 4; right: volunteer 5).

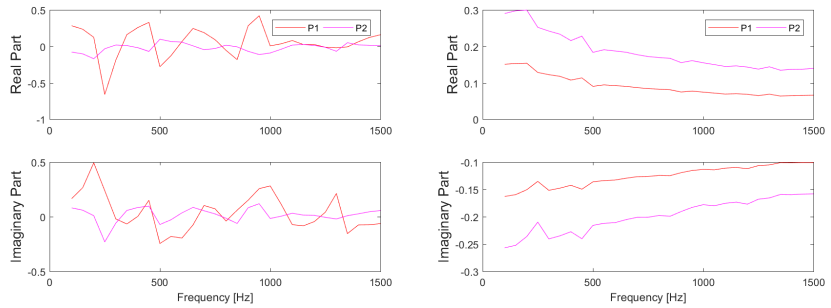

Figure B.21: Impedance in its complex representation for the second study case (left: volunteer 6; right: volunteer 7).

Case study 3 / Only pain intervals

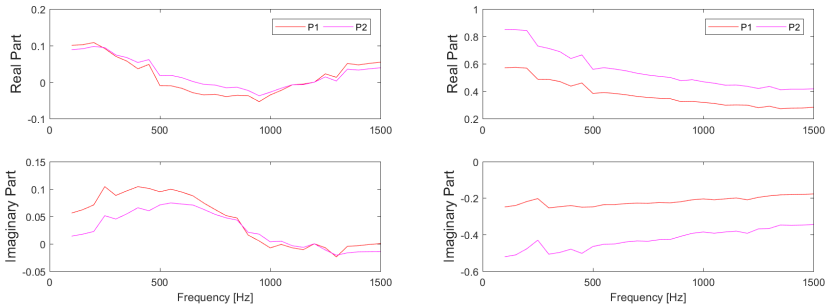

Figure B.22: Impedance in its complex representation for the third study case (left: volunteer 2; right: volunteer 3).

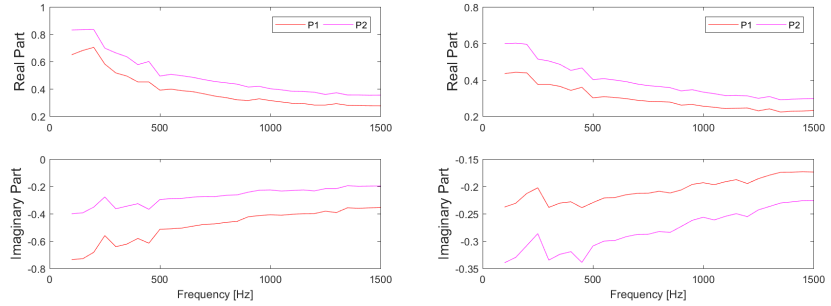

Figure B.23: Impedance in its complex representation for the third study case (left: volunteer 4; right: volunteer 5).

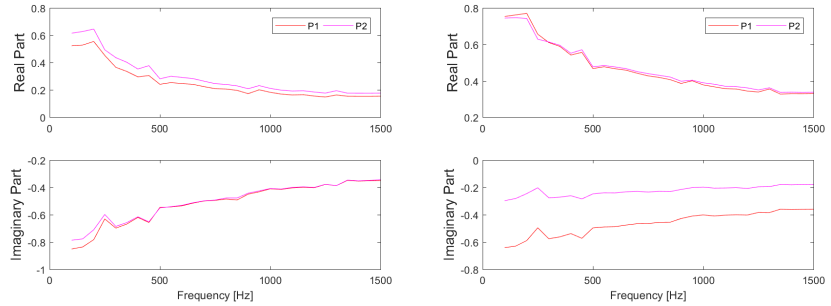

Figure B.24: Impedance in its complex representation for the third study case (left: volunteer 6; right: volunteer 7).

C

Identification results

In this appendix the results obtained for the zero pole model and the fractional order impedance model are presented. Both models have been validated on real data and the outcome of this chapter is that the fractional order impedance model can capture the changes in impedance when a pain stimulus is applied. An iterative identification procedure has been performed in order to fit the model to the measured data. Iteration has been performed to avoid local minimum and the number of iterations between the identified results varied between 2 and 4 in all data. The iteration stopped when the model parameters have changed less than 5%. As for the case of the non-iterative method, the using the iterative method the fitting of the model to the real data did not worked for all cases. From the analysis performed in this thesis we could not conclude is there is a correlation between the biometric data of the volunteers and model parameters. This can be due to the limited number of volunteers but also given the homogeneity of the group. This will be further investigated based on the data recorded during the clinical trial that will take place at the UZ Gent. In this case the variety of patient type (e.g. body mass index) will be more significant than in our group of volunteers and an analysis on the variability among patients can be performed.

FO model: Case study 1/First measurement/First pain stimuli

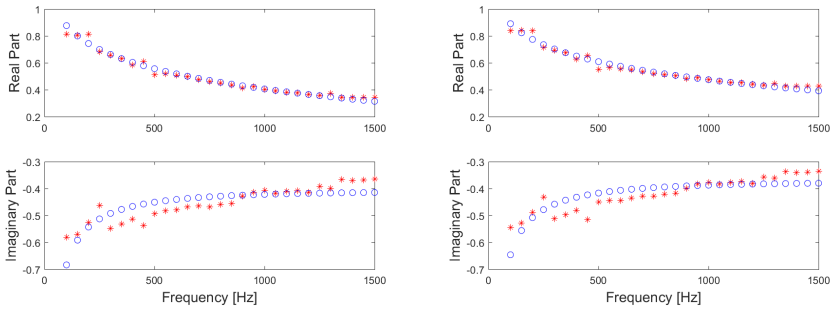

Figure C.1: Left: Volunteer 2; Right: Volunteer 3. Blue denotes the identified model and Red denotes the measured impedance.

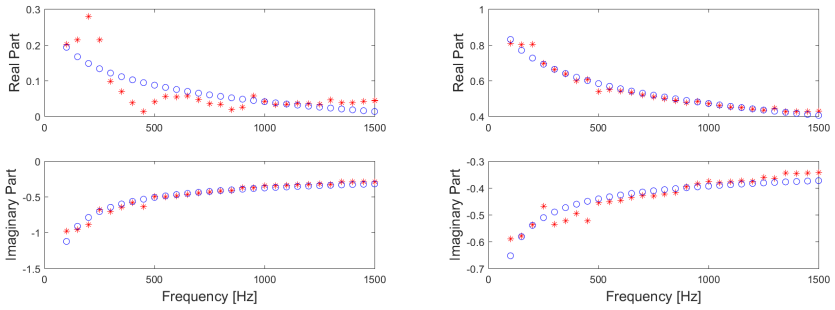

Figure C.2: Left: Volunteer 4; Right: Volunteer 5. Blue denotes the identified model and Red denotes the measured impedance.

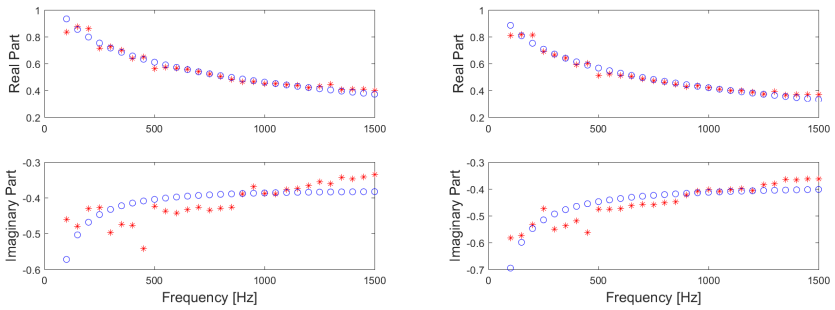

Figure C.3: Left: Volunteer 6; Right: Volunteer 7. Blue denotes the identified model and Red denotes the measured impedance.

Case study 1/First measurement/Second pain stimuli

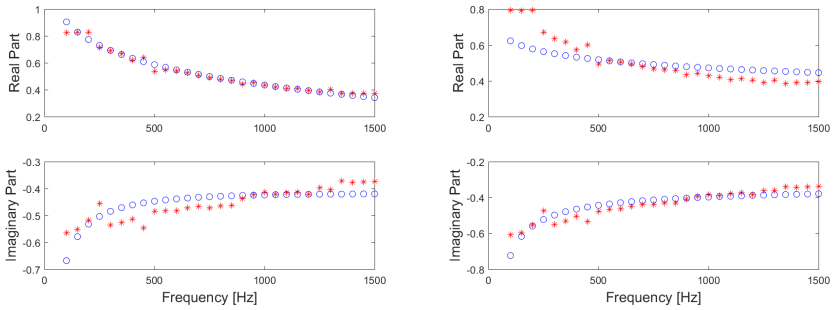

Figure C.4: Left: Volunteer 2; Right: Volunteer 3. Blue denotes the identified model and Red denotes the measured impedance.

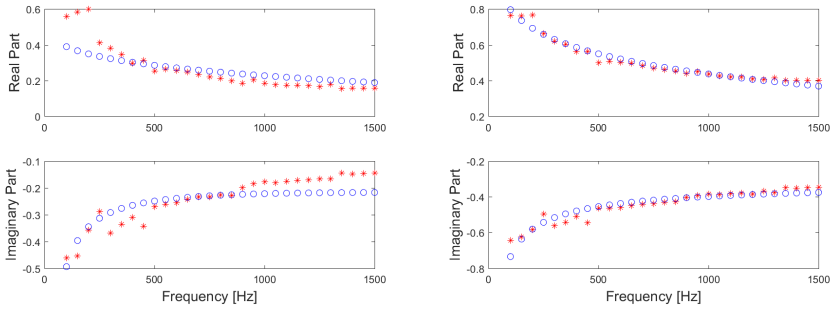

Figure C.5: Left: Volunteer 4; Right: Volunteer 5. Blue denotes the identified model and Red denotes the measured impedance.

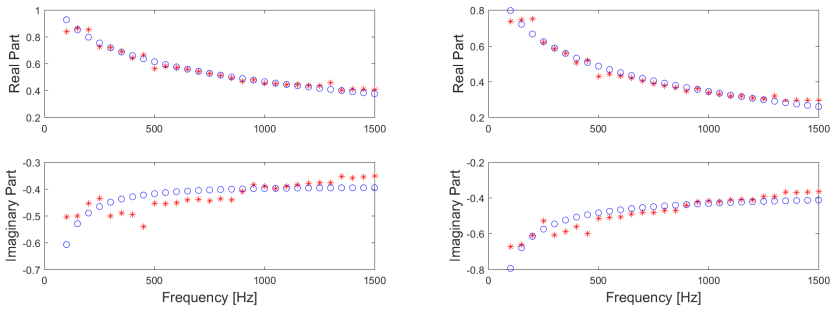

Figure C.6: Left: Volunteer 6; Right: Volunteer 7. Blue denotes the identified model and Red denotes the measured impedance.

Case study 1/Second measurement/First pain stimuli

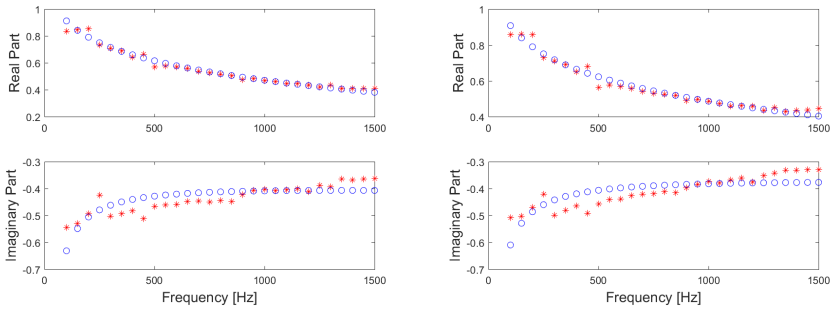

Figure C.7: Left: Volunteer 2; Right: Volunteer 3. Blue denotes the identified model and Red denotes the measured impedance.

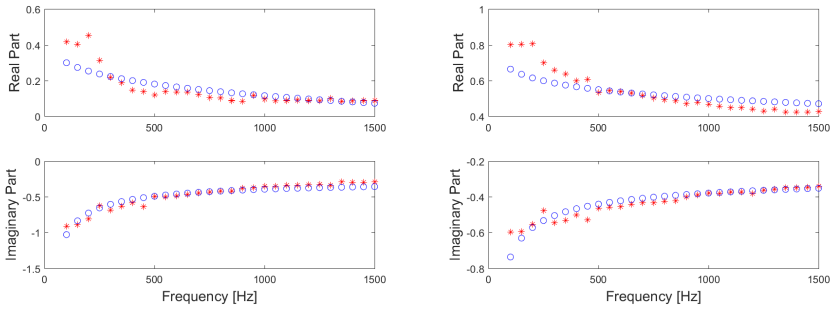

Figure C.8: Left: Volunteer 4; Right: Volunteer 5. Blue denotes the identified model and Red denotes the measured impedance.

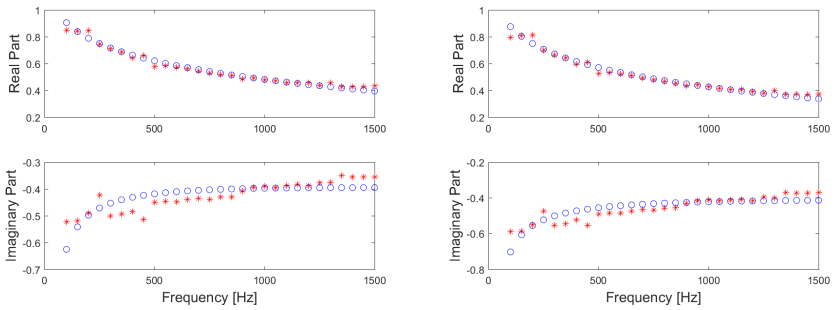

Figure C.9: Left: Volunteer 6; Right: Volunteer 7. Blue denotes the identified model and Red denotes the measured impedance.

Case study 1/Second measurement/Second pain stimuli

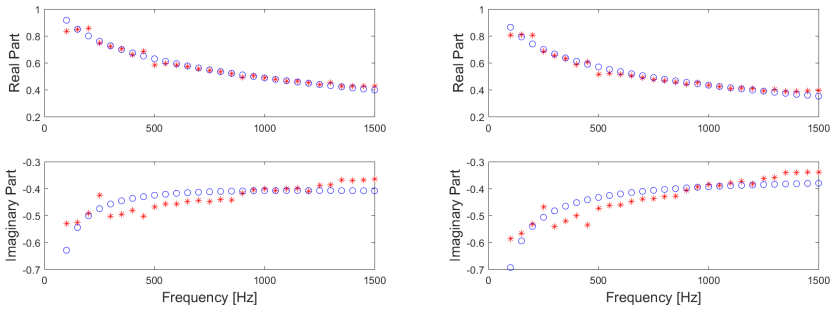

Figure C.10: Left: Volunteer 2; Right: Volunteer 3. Blue denotes the identified model and Red denotes the measured impedance.

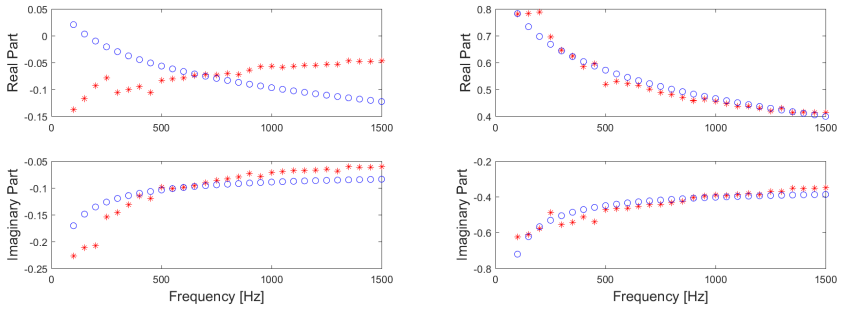

Figure C.11: tLeft: Volunteer 4; Right: Volunteer 5. Blue denotes the identified model and Red denotes the measured impedance.

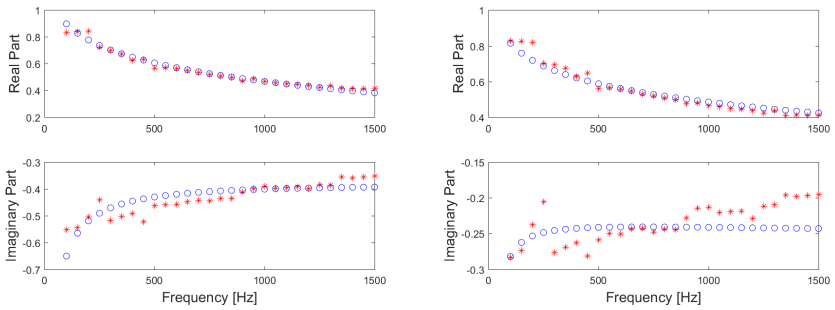

Figure C.12: Left: Volunteer 6; Right: Volunteer 7. Blue denotes the identified model and Red denotes the measured impedance.

Case study 2/First pain stimuli

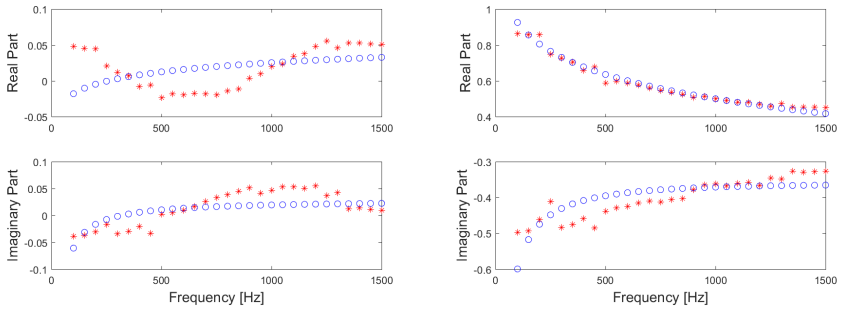

Figure C.13: Left: Volunteer 2; Right: Volunteer 3. Blue denotes the identified model and Red denotes the measured impedance.

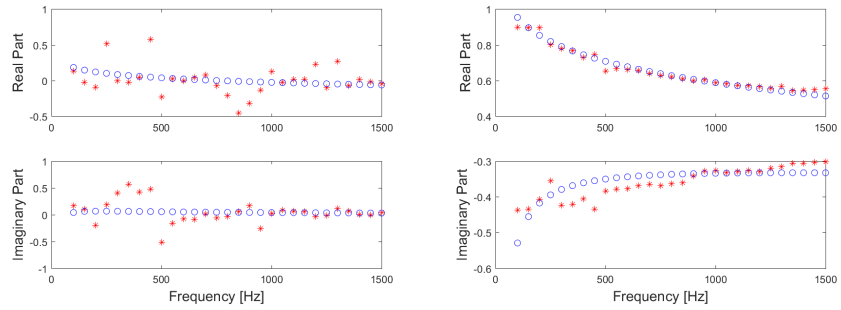

Figure C.14: Left: Volunteer 4; Right: Volunteer 5. Blue denotes the identified model and Red denotes the measured impedance.

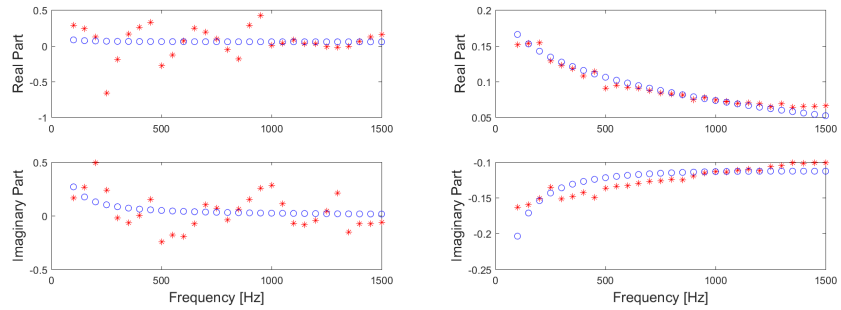

Figure C.15: Left: Volunteer 6; Right: Volunteer 7. Blue denotes the identified model and Red denotes the measured impedance.

Case study 2/Second pain stimuli

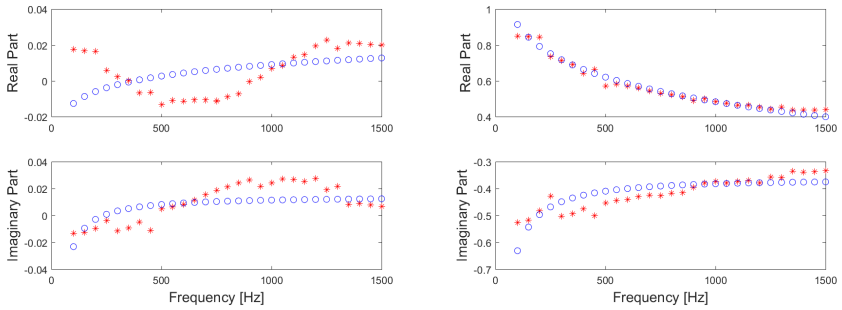

Figure C.16: Left: Volunteer 2; Right: Volunteer 3. Blue denotes the identified model and Red denotes the measured impedance.

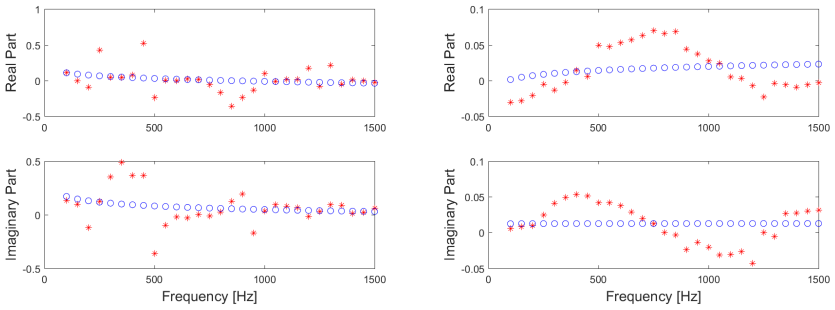

Figure C.17: Left: Volunteer 4; Right: Volunteer 5. Blue denotes the identified model and Red denotes the measured impedance.

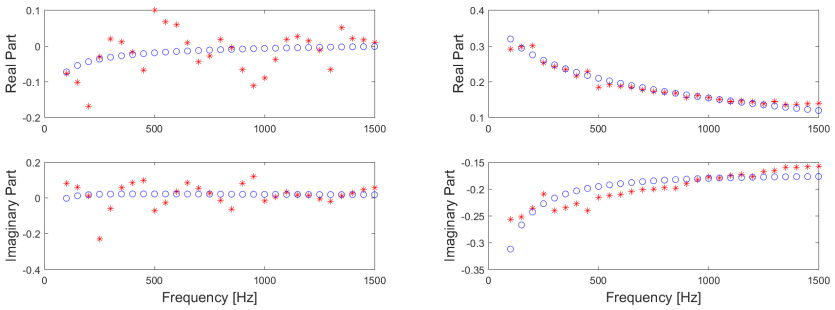

Figure C.18: Left: Volunteer 6; Right: Volunteer 7. Blue denotes the identified model and Red denotes the measured impedance.

Case study 3/First pain stimuli

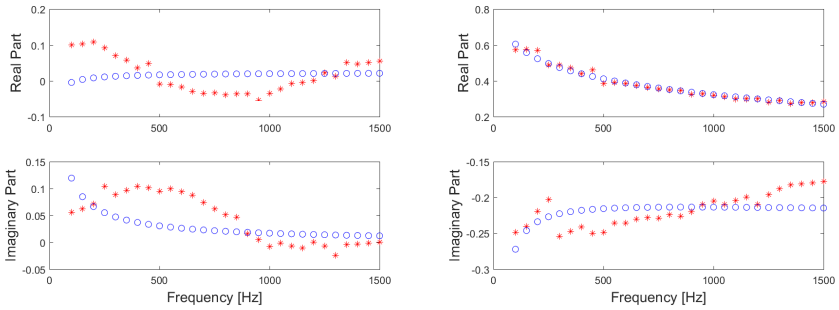

Figure C.19: Left: Volunteer 2; Right: Volunteer 3. Blue denotes the identified model and Red denotes the measured impedance.

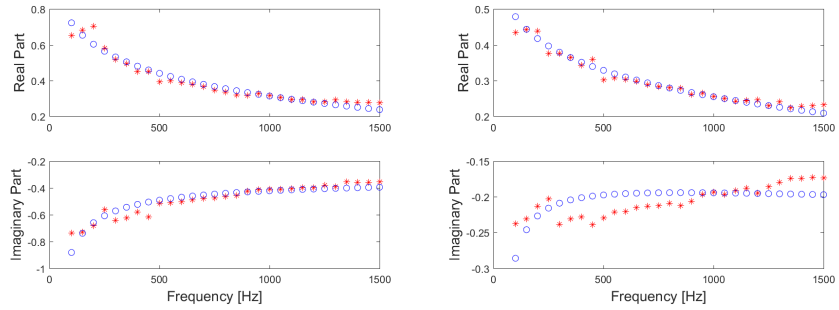

Figure C.20: Left: Volunteer 4; Right: Volunteer 5. Blue denotes the identified model and Red denotes the measured impedance.

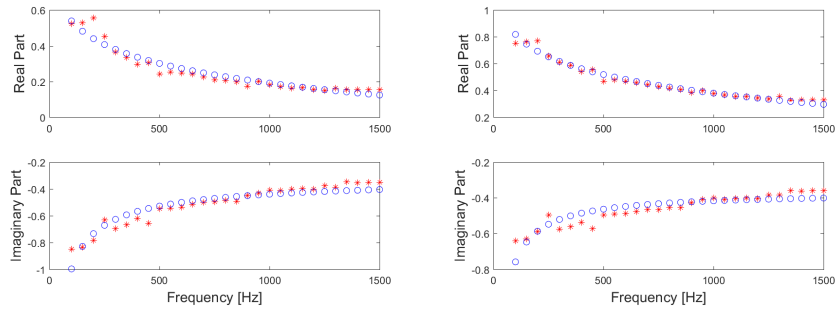

Figure C.21: Left: Volunteer 6; Right: Volunteer 7. Blue denotes the identified model and Red denotes the measured impedance.

Case study 3/Second pain stimuli

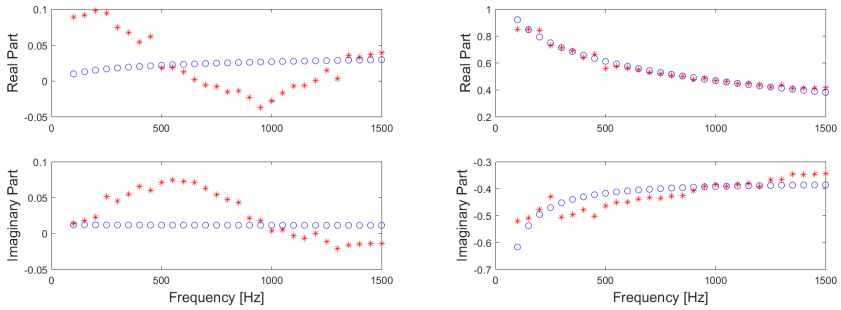

Figure C.22: Left: Volunteer 2; Right: Volunteer 3. Blue denotes the identified model and Red denotes the measured impedance.

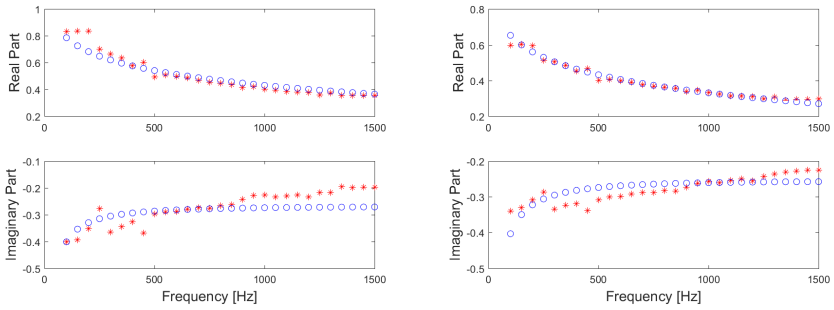

Figure C.23: Left: Volunteer 4; Right: Volunteer 5. Blue denotes the identified model and Red denotes the measured impedance.

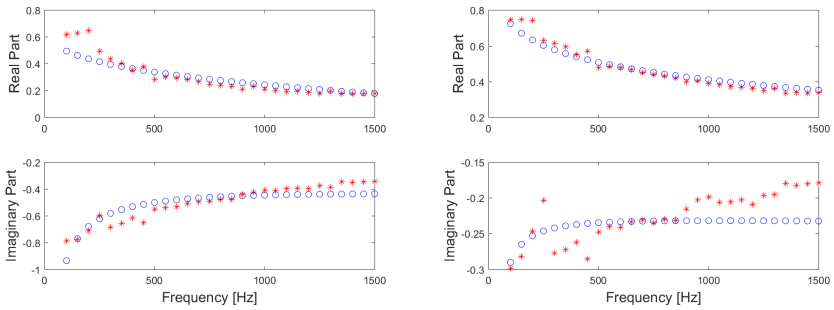

Figure C.24: Left: Volunteer 6; Right: Volunteer 7. Blue denotes the identified model and Red denotes the measured impedance.

Model parameter analysis as a function of biometric data for each study case.
Case study 1/First measurement

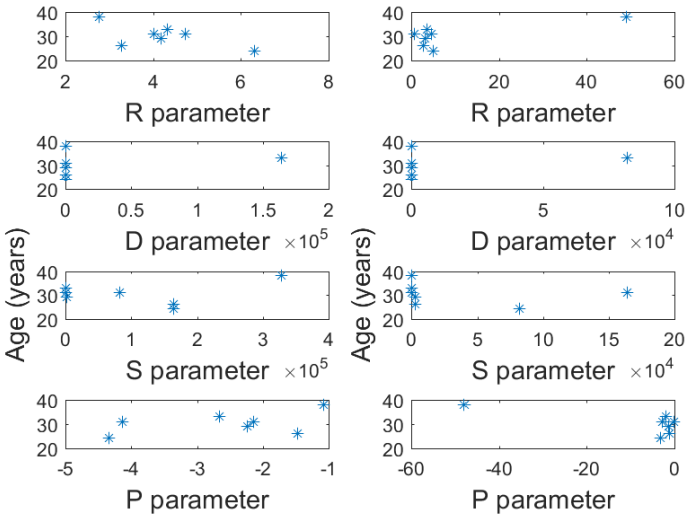

Figure C.25: Left: First pain stimulus; Right: Second Pain stimulus

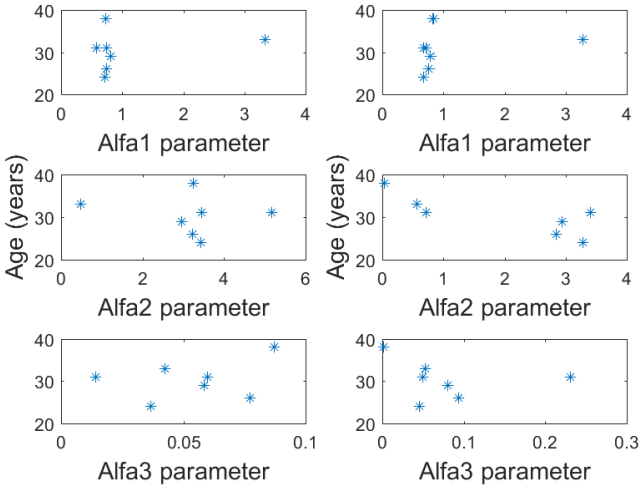

Figure C.26: Left: First pain stimulus; Right: Second Pain stimulus

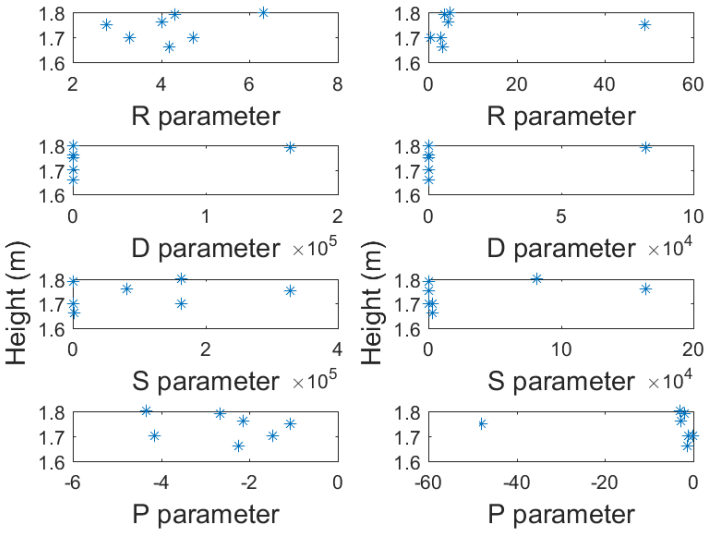

Figure C.27: Left: First pain stimulus; Right: Second Pain stimulus

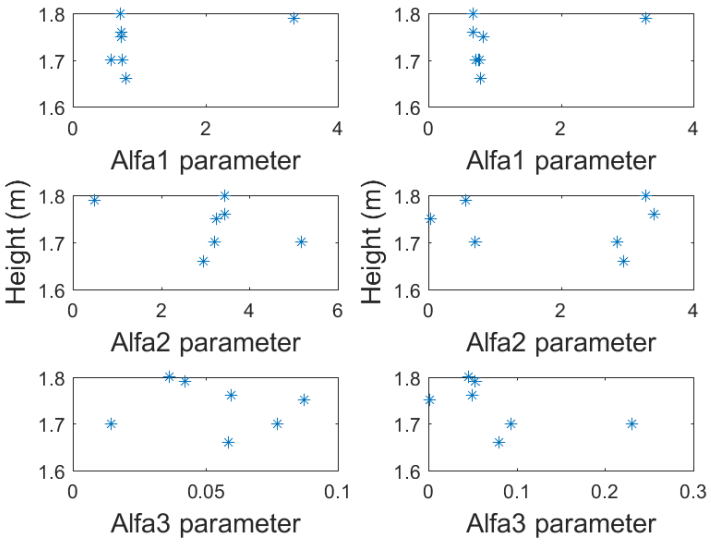

Figure C.28: Left: First pain stimulus; Right: Second Pain stimulus

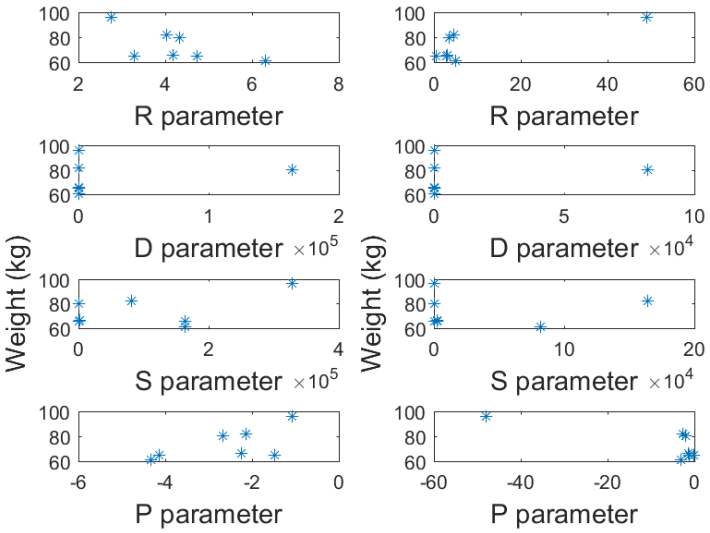

Figure C.29: Left: First pain stimulus; Right: Second Pain stimulus

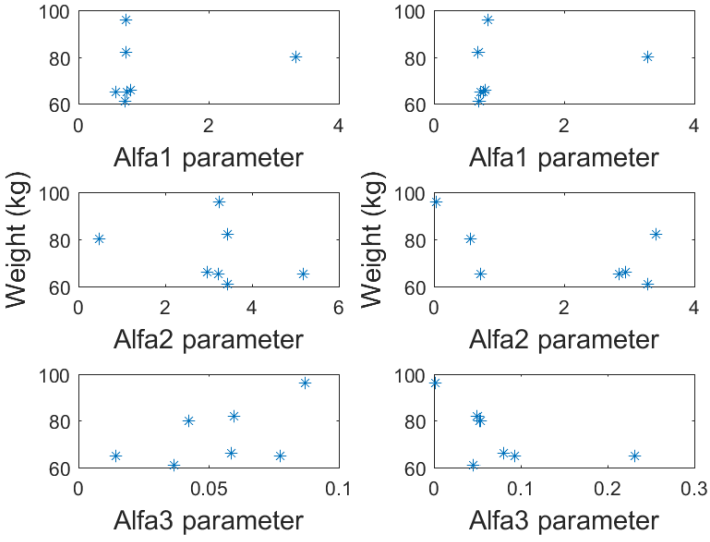

Figure C.30: Left: First pain stimulus; Right: Second Pain stimulus

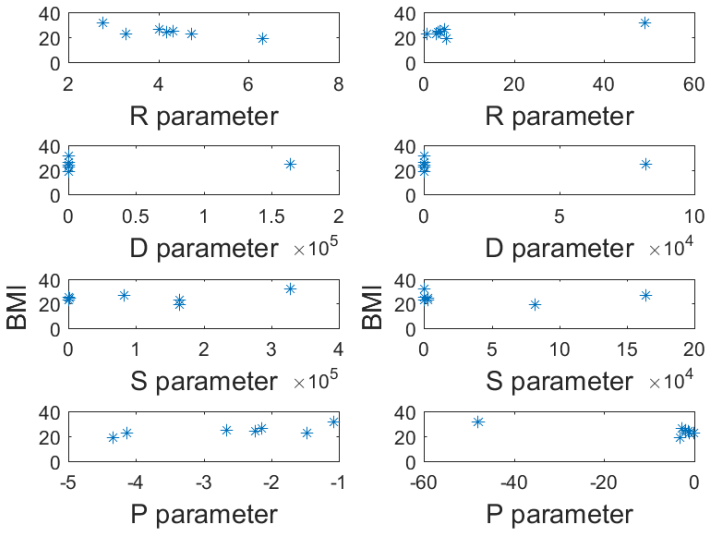

Figure C.31: Left: First pain stimulus; Right: Second Pain stimulus

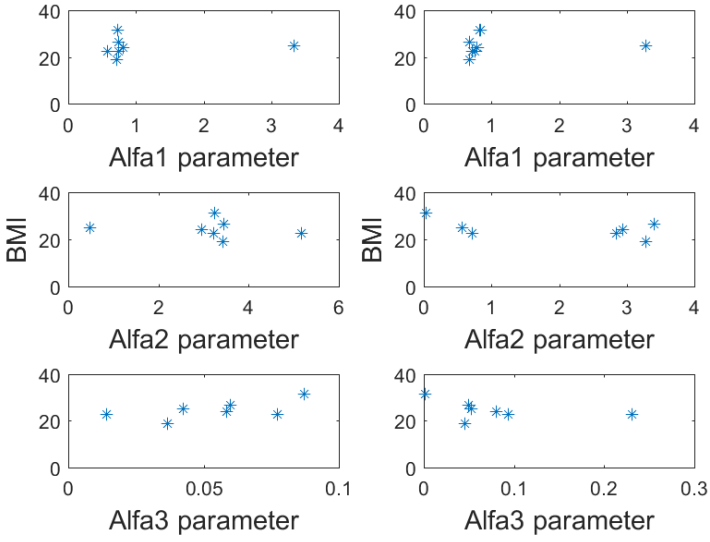

Figure C.32: Left: First pain stimulus; Right: Second Pain stimulus

Case study 1/Second measurement

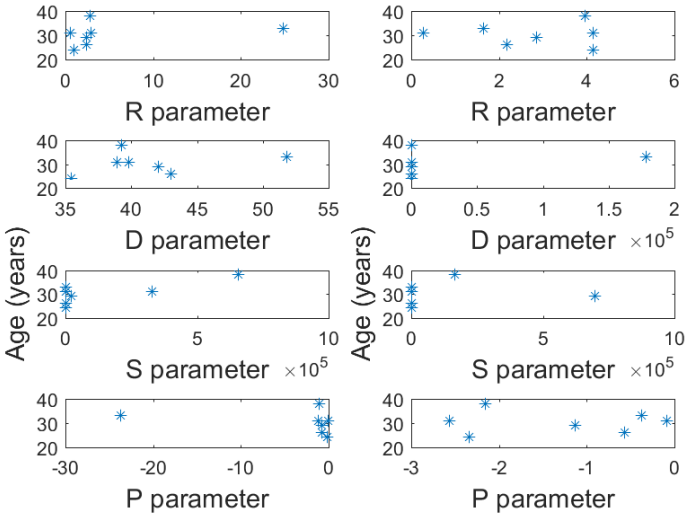

Figure C.33: Left: First pain stimulus; Right: Second Pain stimulus

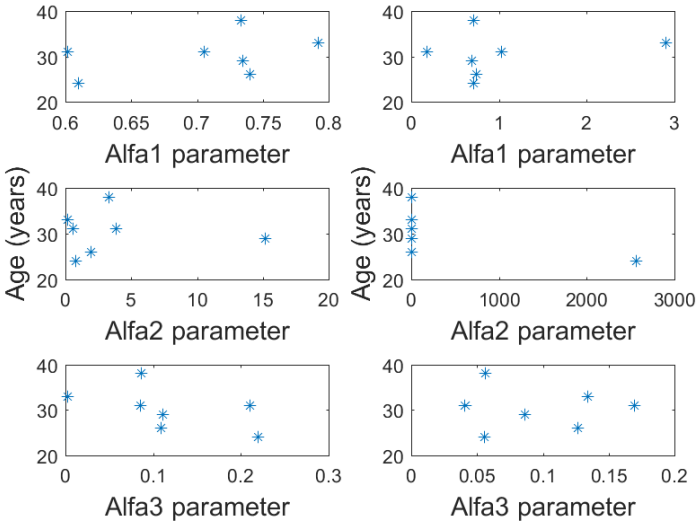

Figure C.34: Left: First pain stimulus; Right: Second Pain stimulus

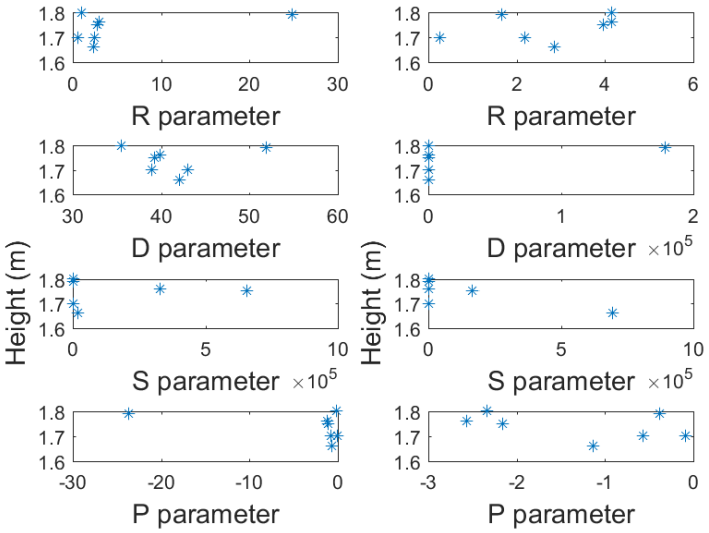

Figure C.35: Left: First pain stimulus; Right: Second Pain stimulus

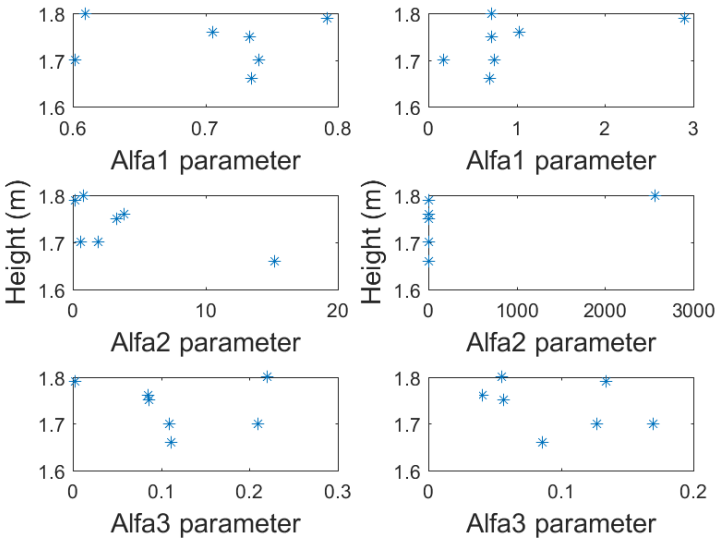

Figure C.36: Left: First pain stimulus; Right: Second Pain stimulus

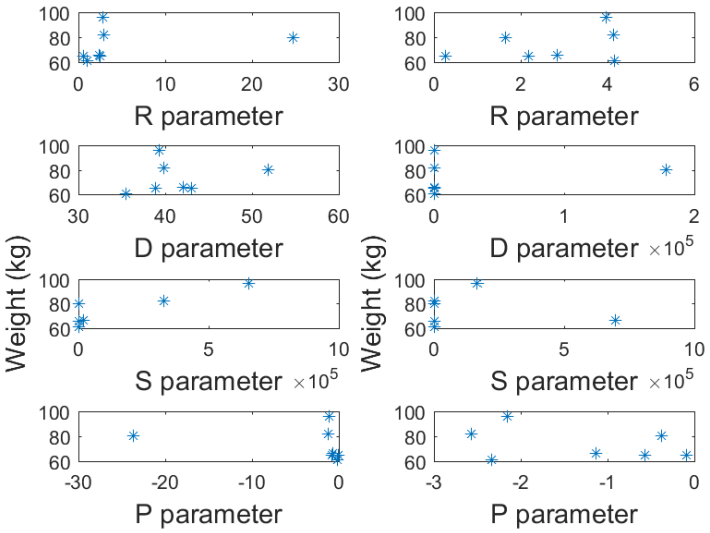

Figure C.37: Left: First pain stimulus; Right: Second Pain stimulus

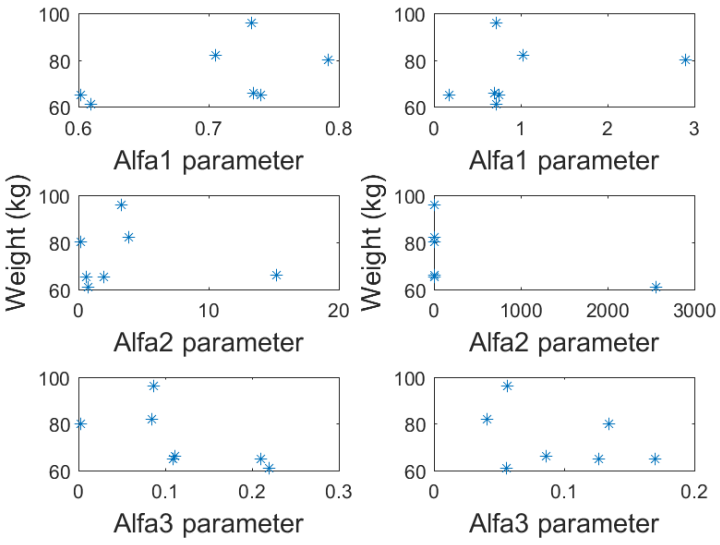

Figure C.38: Left: First pain stimulus; Right: Second Pain stimulus

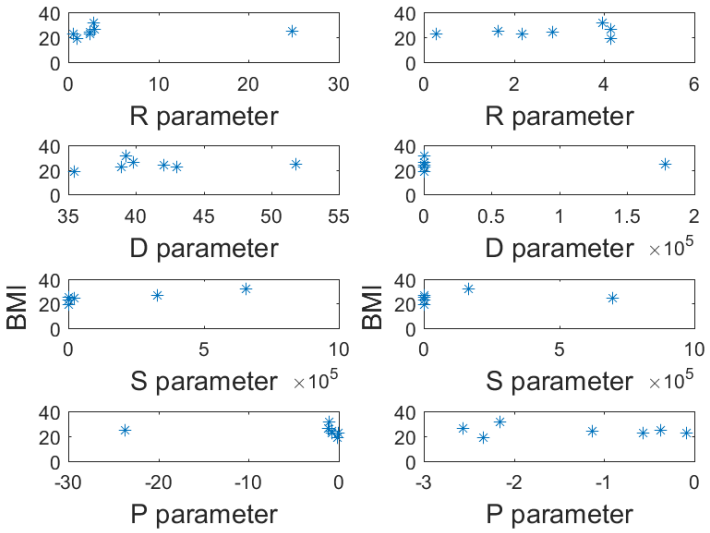

Figure C.39: Left: First pain stimulus; Right: Second Pain stimulus

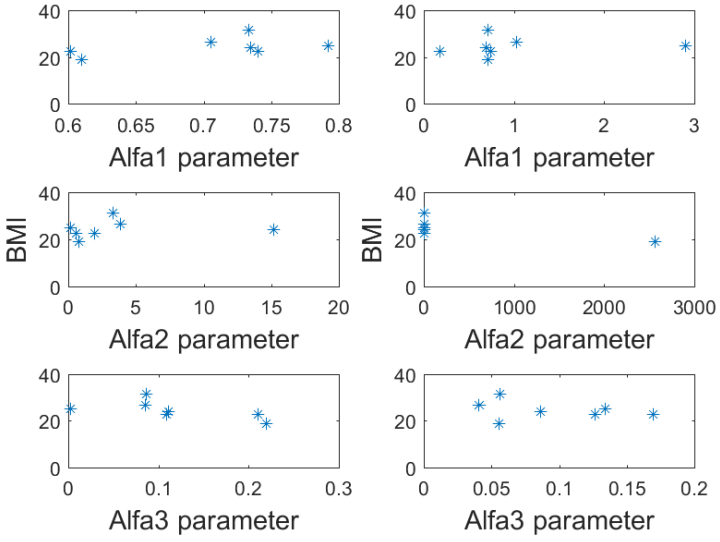

Figure C.40: Left: First pain stimulus; Right: Second Pain stimulus

Case study 2

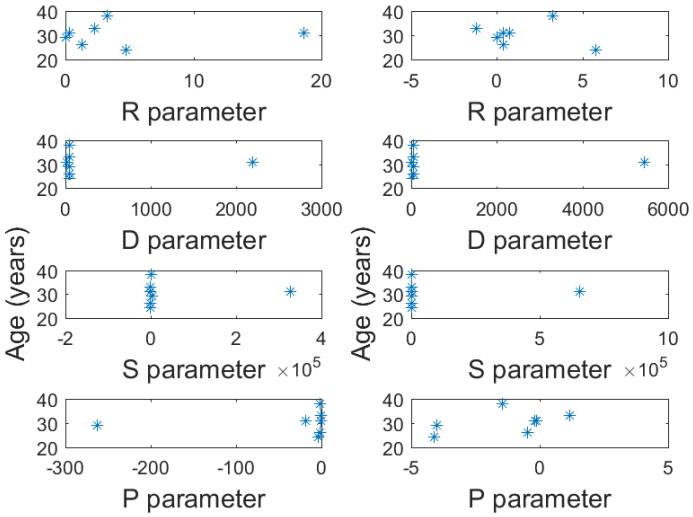

Figure C.41: Left: First pain stimulus; Right: Second Pain stimulus

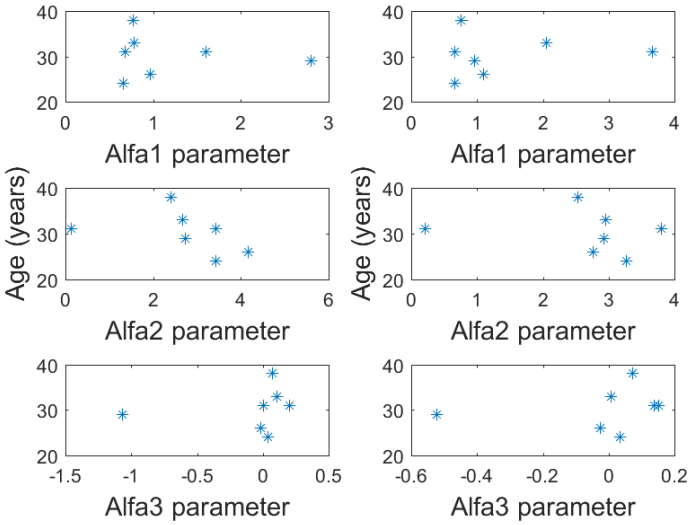

Figure C.42: Left: First pain stimulus; Right: Second Pain stimulus

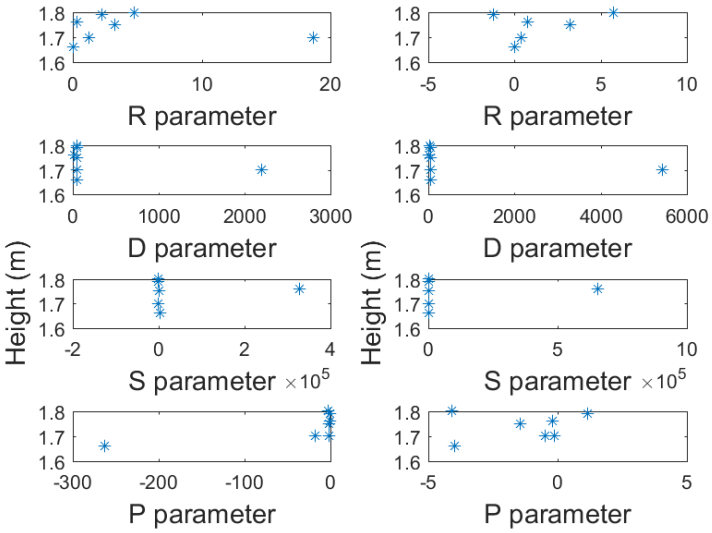

Figure C.43: Left: First pain stimulus; Right: Second Pain stimulus

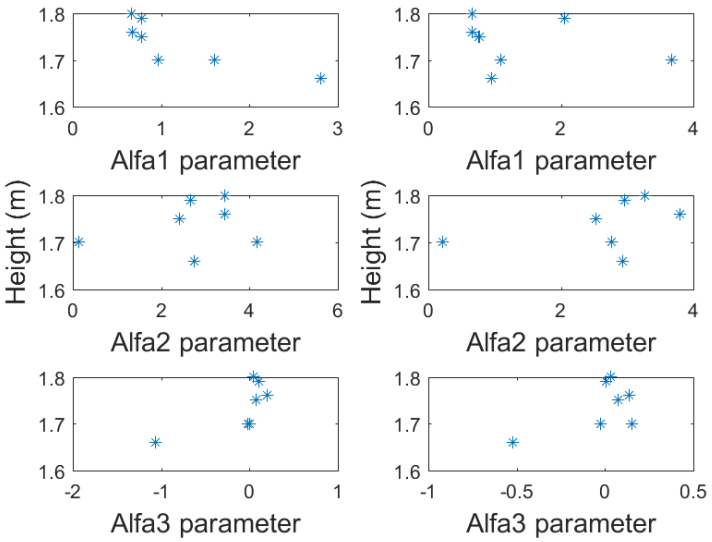

Figure C.44: Left: First pain stimulus; Right: Second Pain stimulus

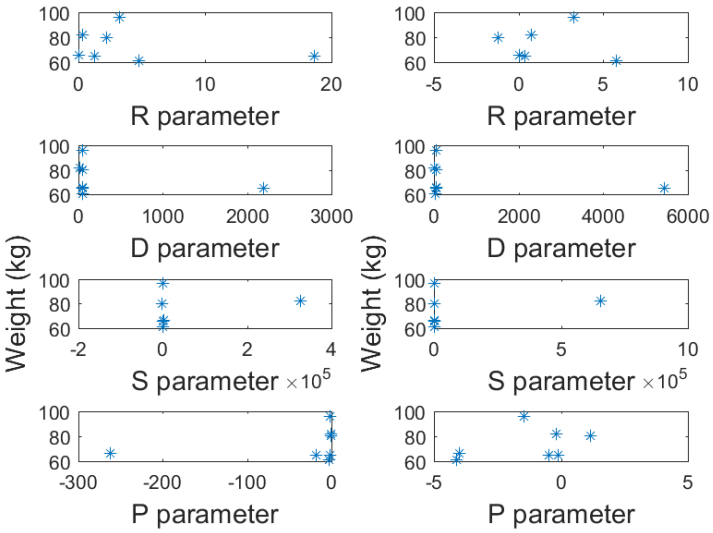

Figure C.45: Left: First pain stimulus; Right: Second Pain stimulus

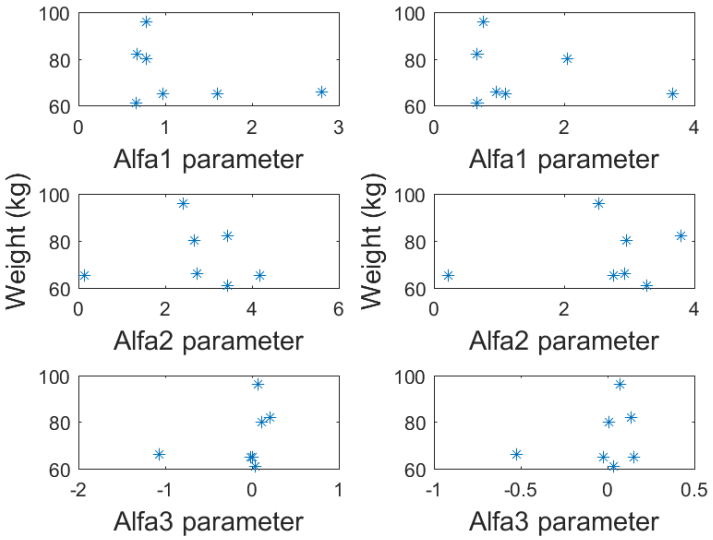

Figure C.46: Left: First pain stimulus; Right: Second Pain stimulus

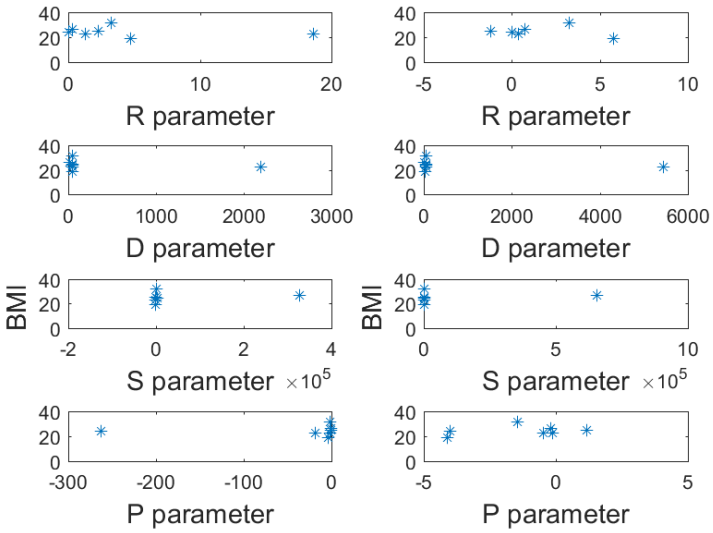

Figure C.47: Left: First pain stimulus; Right: Second Pain stimulus

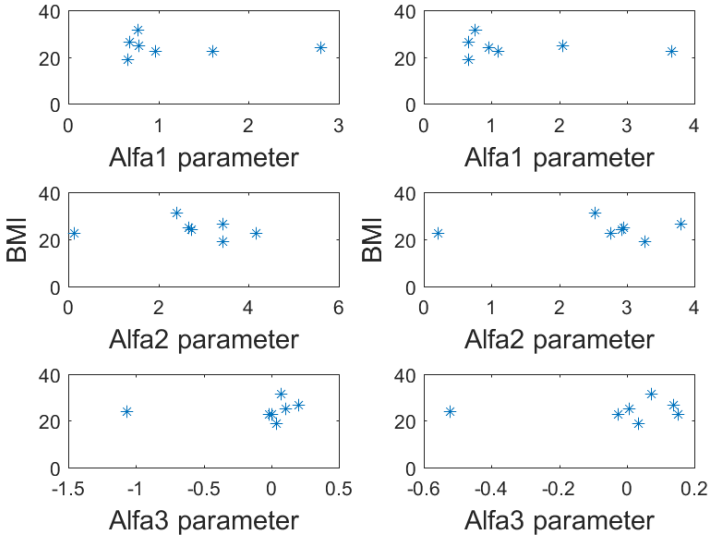

Figure C.48: Left: First pain stimulus; Right: Second Pain stimulus

Case study 3

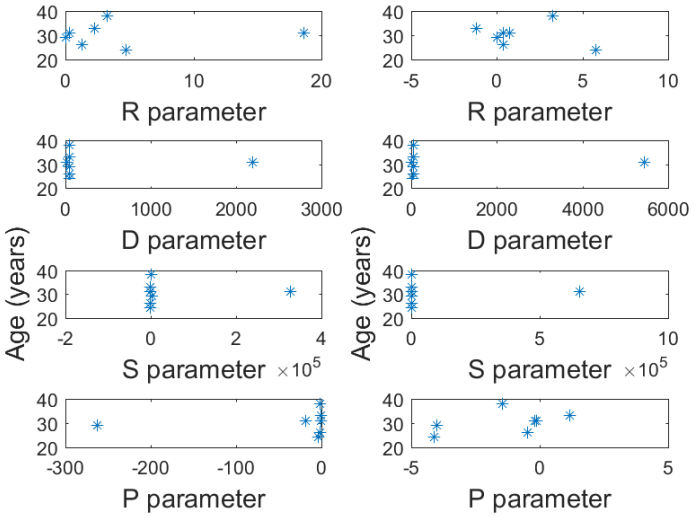

Figure C.49: Left: First pain stimulus; Right: Second Pain stimulus

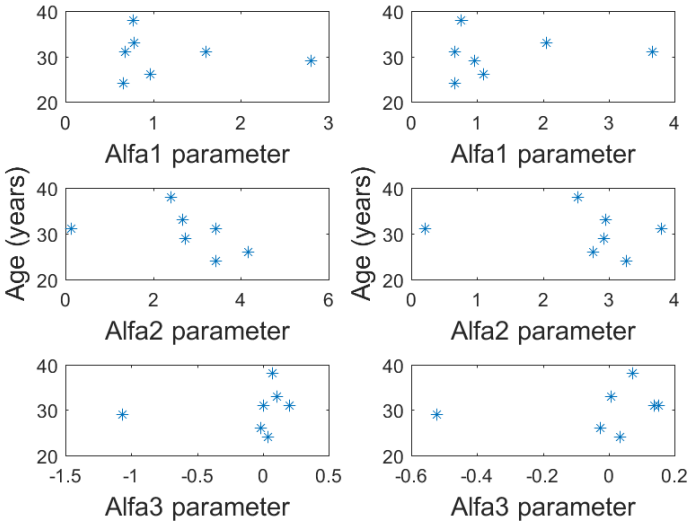

Figure C.50: Left: First pain stimulus; Right: Second Pain stimulus

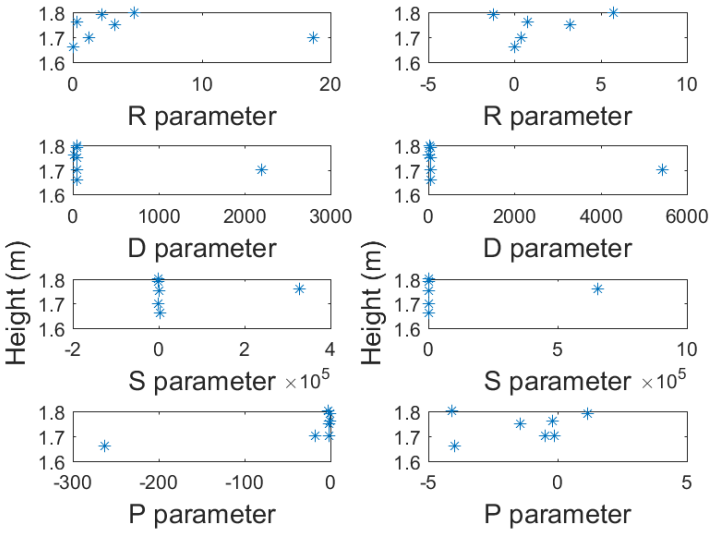

Figure C.51: Left: First pain stimulus; Right: Second Pain stimulus

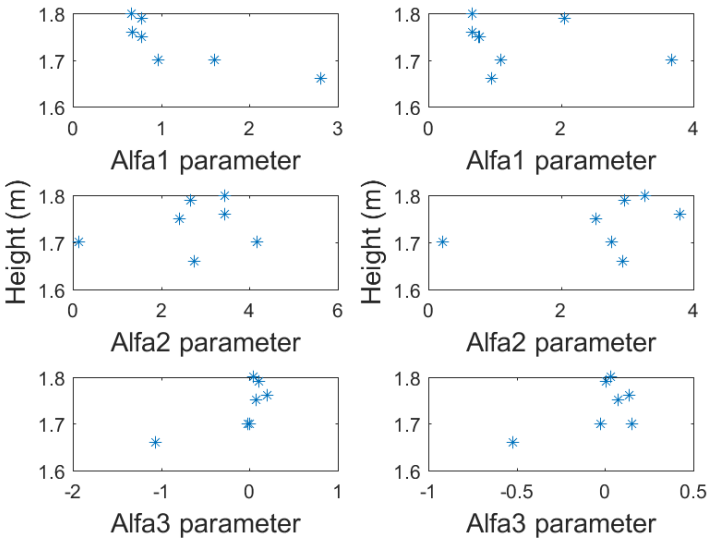

Figure C.52: Left: First pain stimulus; Right: Second Pain stimulus

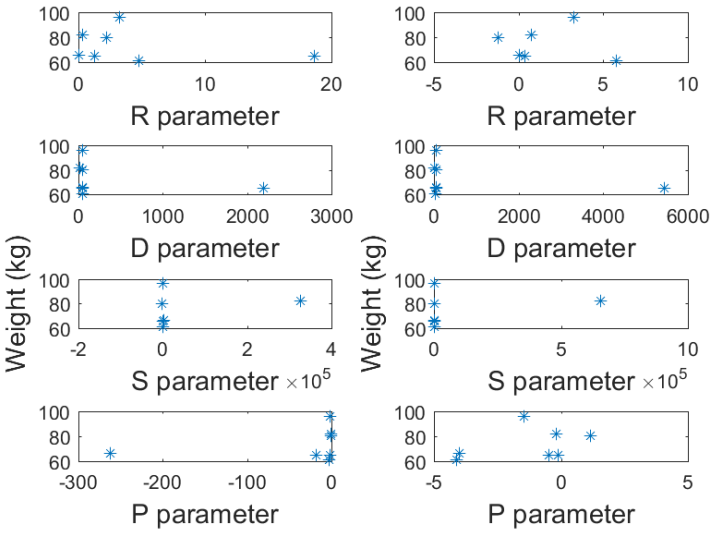

Figure C.53: Left: First pain stimulus; Right: Second Pain stimulus

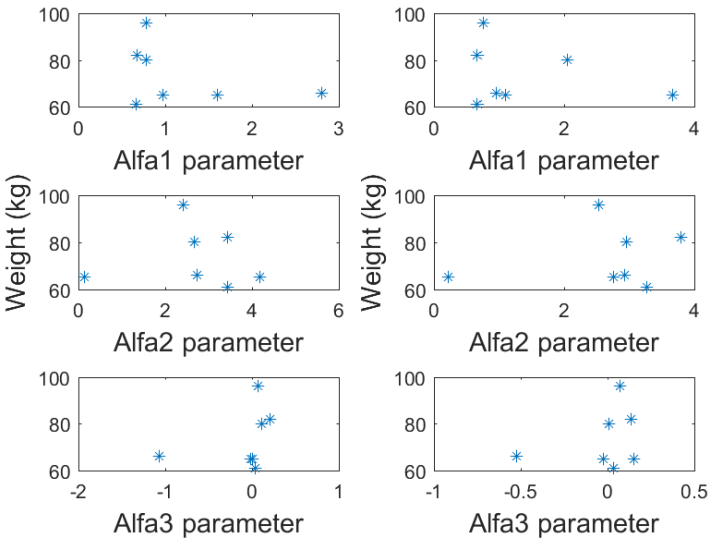

Figure C.54: Left: First pain stimulus; Right: Second Pain stimulus

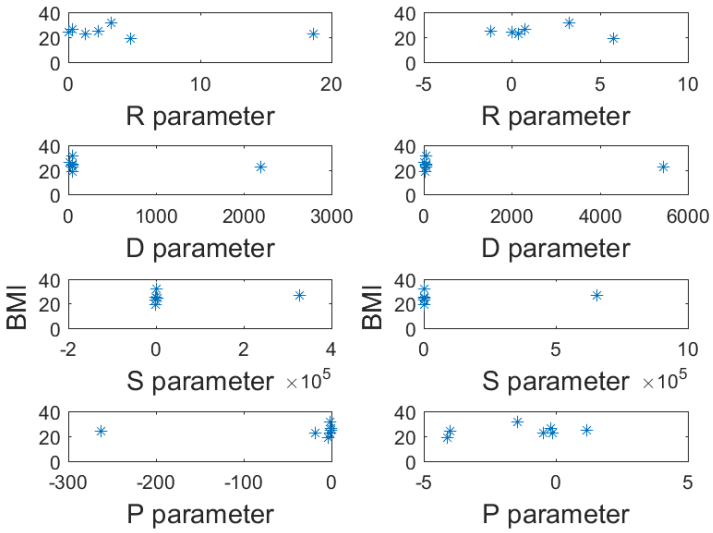

Figure C.55: Left: First pain stimulus; Right: Second Pain stimulus

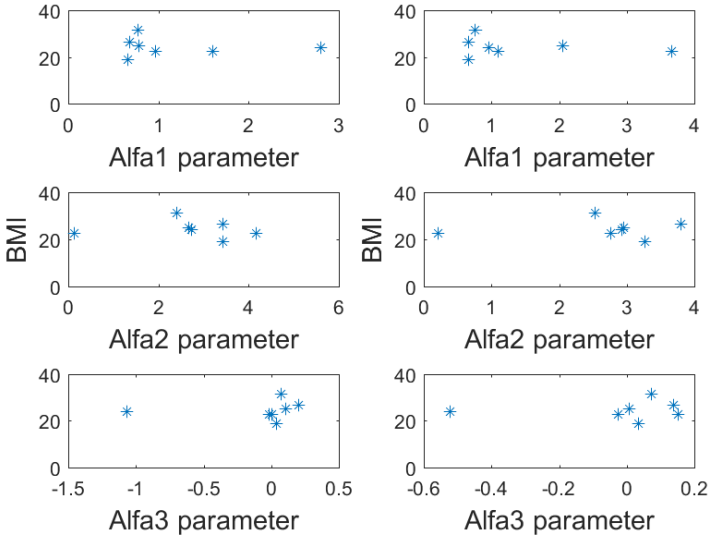

Figure C.56: Left: First pain stimulus; Right: Second Pain stimulus

Zero-pole interlacing model Case study 1/1st measurement/1st pain stimuli

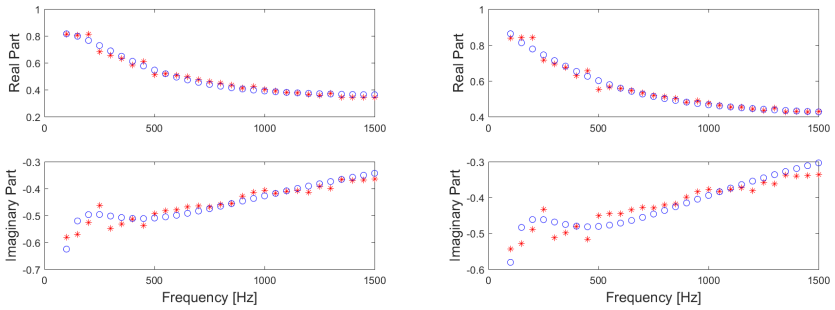

Figure C.57: Left: Volunteer 2; Right: Volunteer 3. Blue denotes the identified model and Red denotes the measured impedance.

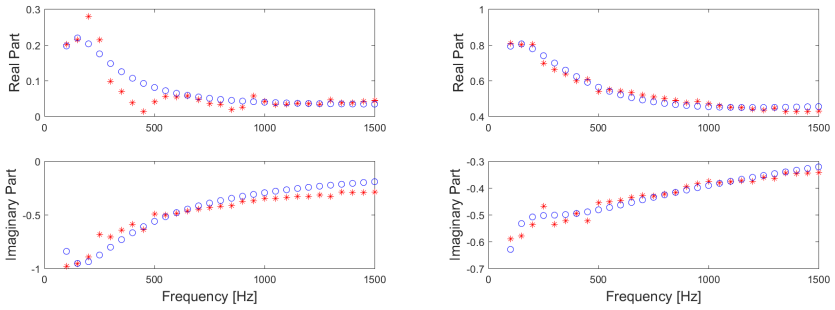

Figure C.58: Left: Volunteer 4; Right: Volunteer 5. Blue denotes the identified model and Red denotes the measured impedance.

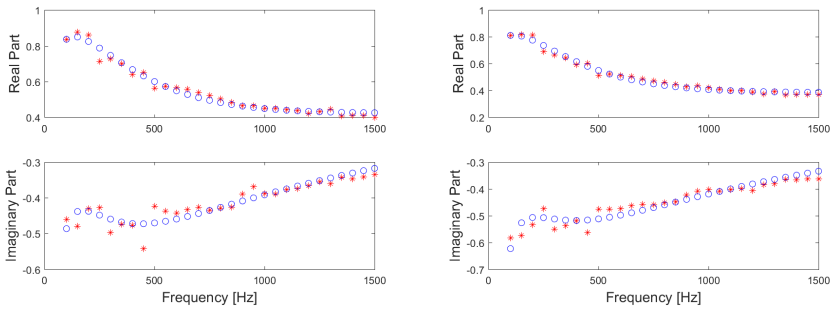

Figure C.59: Left: Volunteer 6; Right: Volunteer 7. Blue denotes the identified model and Red denotes the measured impedance.

Case study 1/First measurement/Second pain stimuli

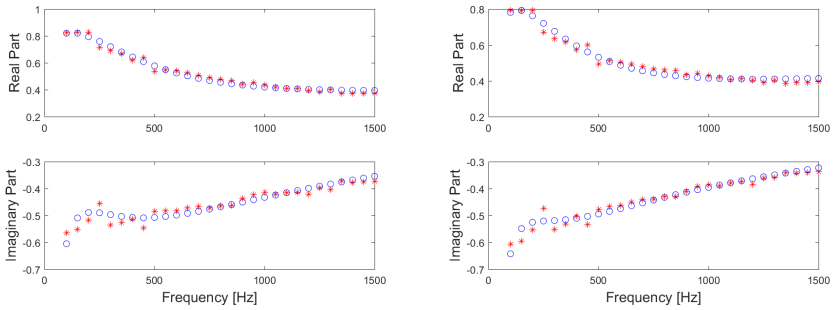

Figure C.60: Left: Volunteer 2; Right: Volunteer 3. Blue denotes the identified model and Red denotes the measured impedance.

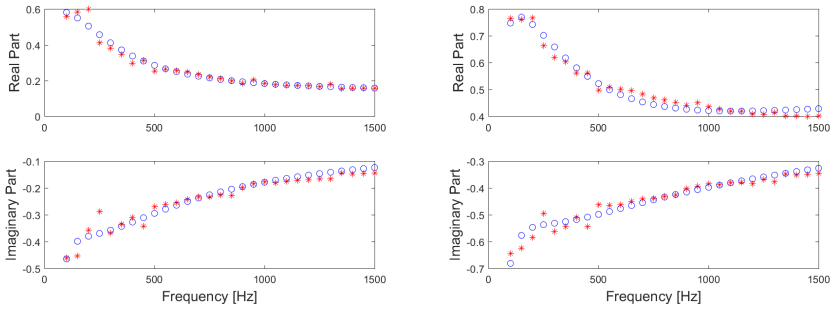

Figure C.61: Left: Volunteer 4; Right: Volunteer 5. Blue denotes the identified model and Red denotes the measured impedance.

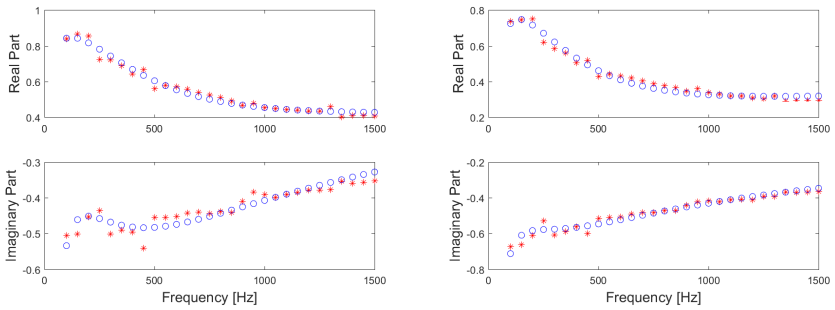

Figure C.62: Left: Volunteer 6; Right: Volunteer 7. Blue denotes the identified model and Red denotes the measured impedance.

Case study 1/Second measurement/First pain stimuli

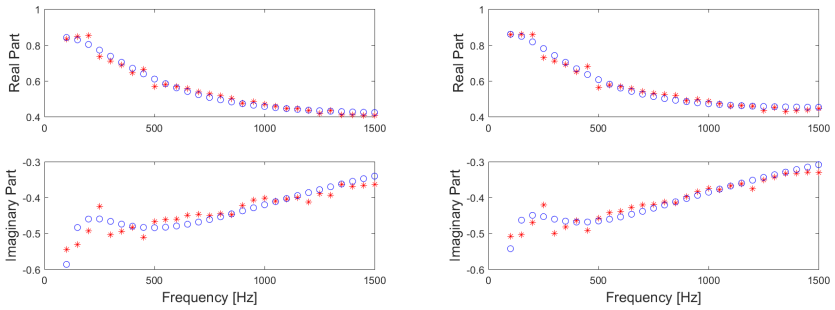

Figure C.63: Left: Volunteer 2; Right: Volunteer 3. Blue denotes the identified model and Red denotes the measured impedance.

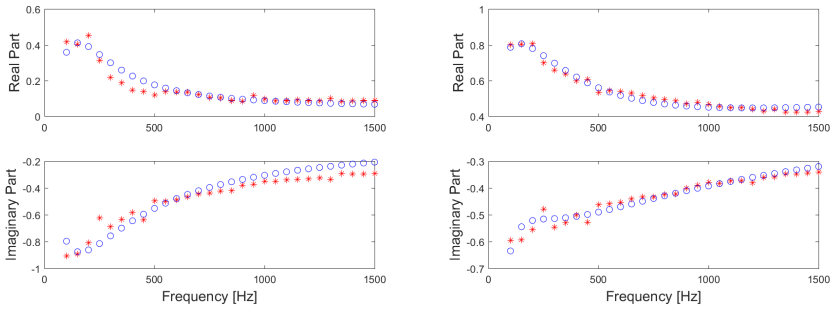

Figure C.64: Left: Volunteer 4; Right: Volunteer 5. Blue denotes the identified model and Red denotes the measured impedance.

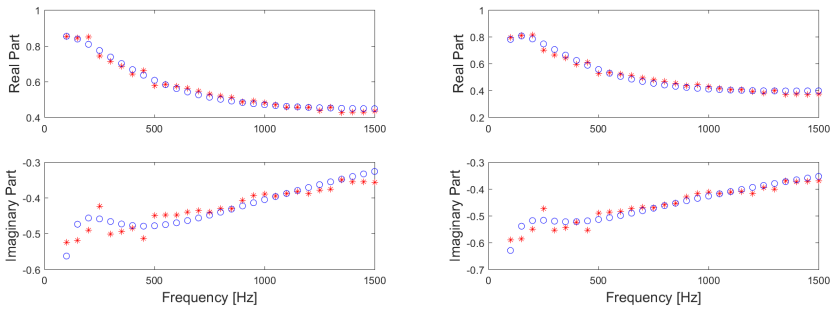

Figure C.65: Left: Volunteer 6; Right: Volunteer 7. Blue denotes the identified model and Red denotes the measured impedance.

Case study 1/Second measurement/Second pain stimuli

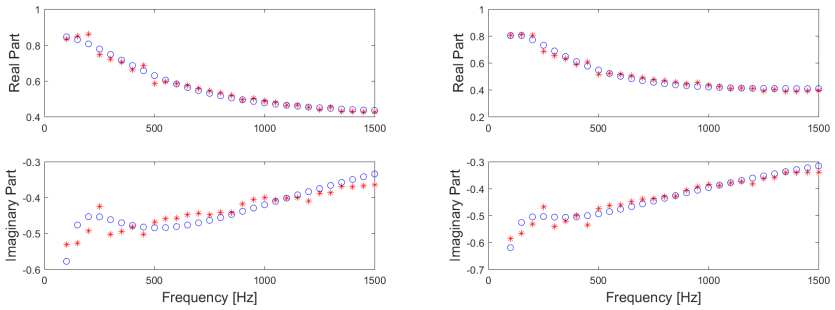

Figure C.66: Left: Volunteer 2; Right: Volunteer 3. Blue denotes the identified model and Red denotes the measured impedance.

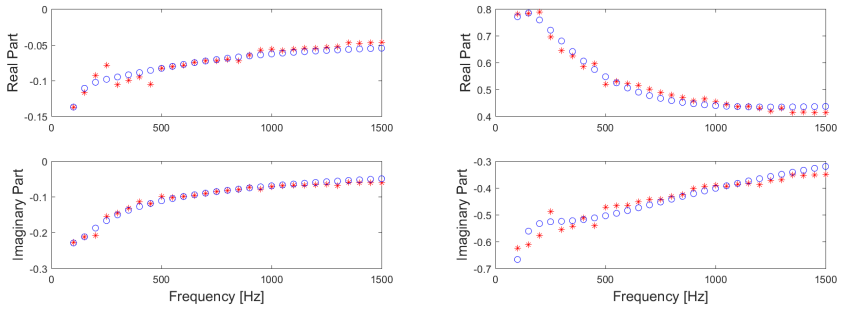

Figure C.67: tLeft: Volunteer 4; Right: Volunteer 5. Blue denotes the identified model and Red denotes the measured impedance.

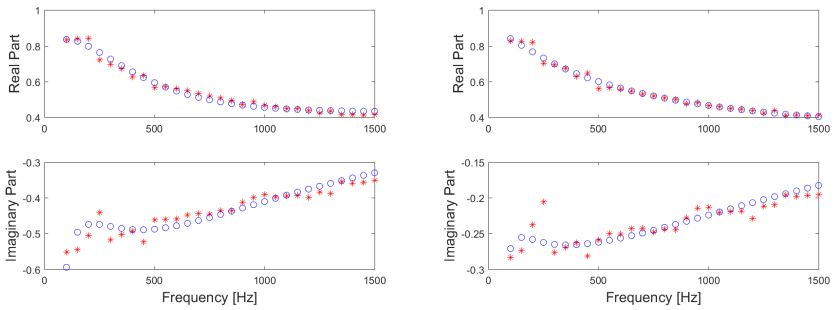

Figure C.68: Left: Volunteer 6; Right: Volunteer 7. Blue denotes the identified model and Red denotes the measured impedance.

Case study 2/First pain stimuli

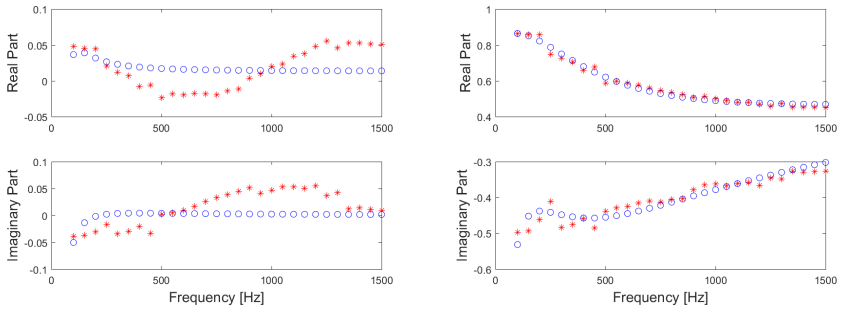

Figure C.69: Left: Volunteer 2; Right: Volunteer 3. Blue denotes the identified model and Red denotes the measured impedance.

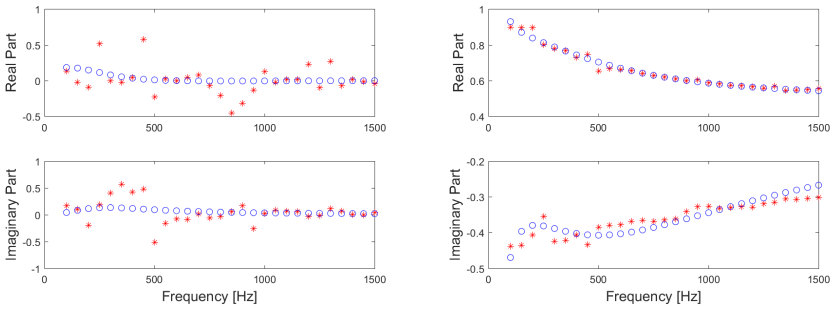

Figure C.70: Left: Volunteer 4; Right: Volunteer 5. Blue denotes the identified model and Red denotes the measured impedance.

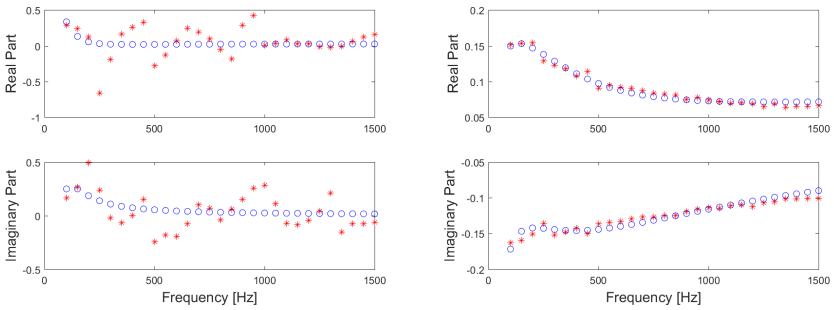

Figure C.71: Left: Volunteer 6; Right: Volunteer 7. Blue denotes the identified model and Red denotes the measured impedance.

Case study 2/Second pain stimuli

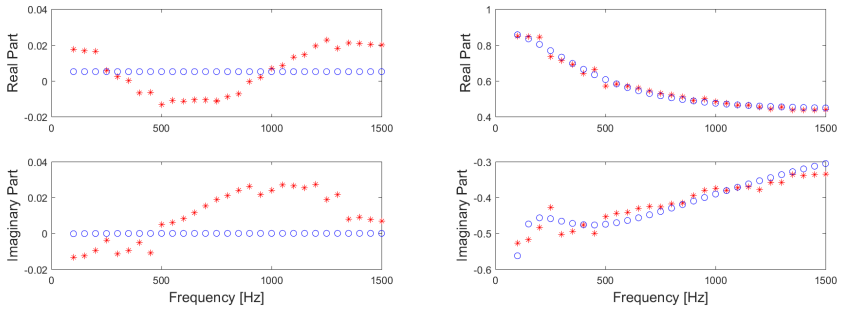

Figure C.72: Left: Volunteer 2; Right: Volunteer 3. Blue denotes the identified model and Red denotes the measured impedance.

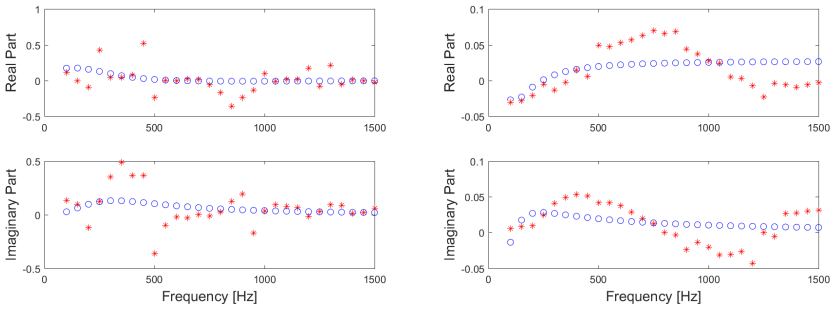

Figure C.73: Left: Volunteer 4; Right: Volunteer 5. Blue denotes the identified model and Red denotes the measured impedance.

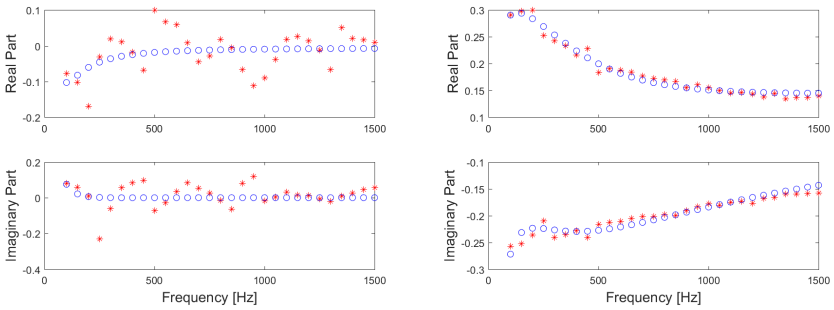

Figure C.74: Left: Volunteer 6; Right: Volunteer 7. Blue denotes the identified model and Red denotes the measured impedance.

Case study 3/First pain stimuli

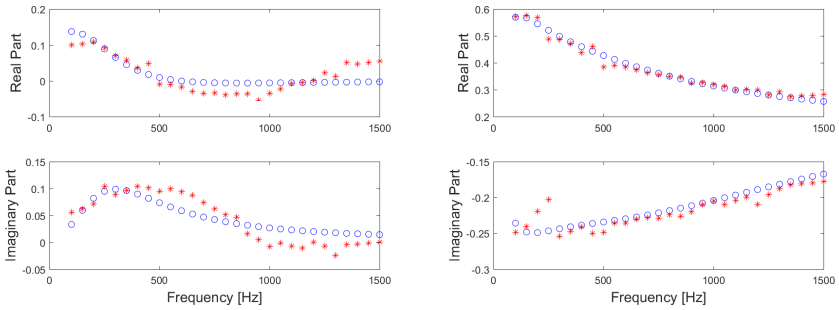

Figure C.75: Left: Volunteer 2; Right: Volunteer 3. Blue denotes the identified model and Red denotes the measured impedance.

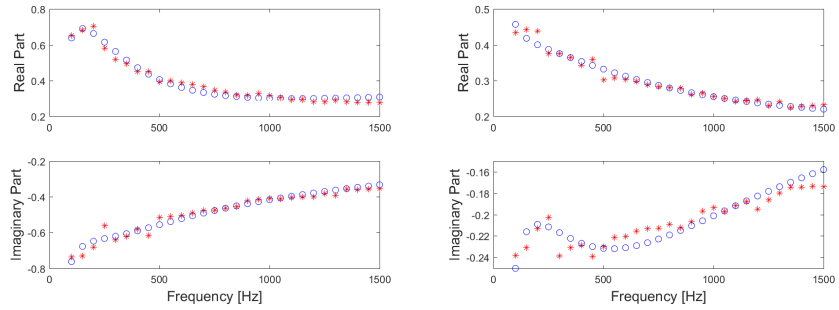

Figure C.76: Left: Volunteer 4; Right: Volunteer 5. Blue denotes the identified model and Red denotes the measured impedance.

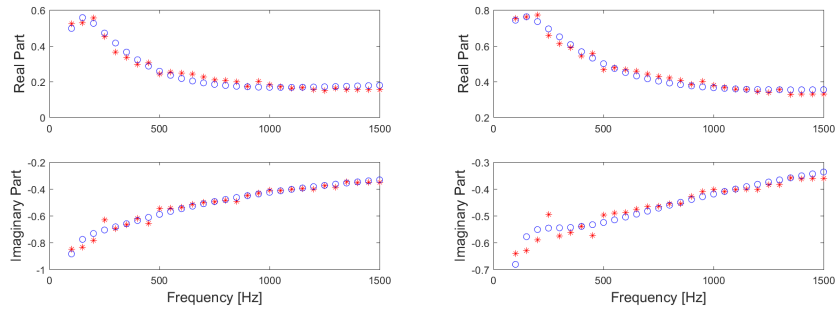

Figure C.77: Left: Volunteer 6; Right: Volunteer 7. Blue denotes the identified model and Red denotes the measured impedance.

Case study 3/Second pain stimuli

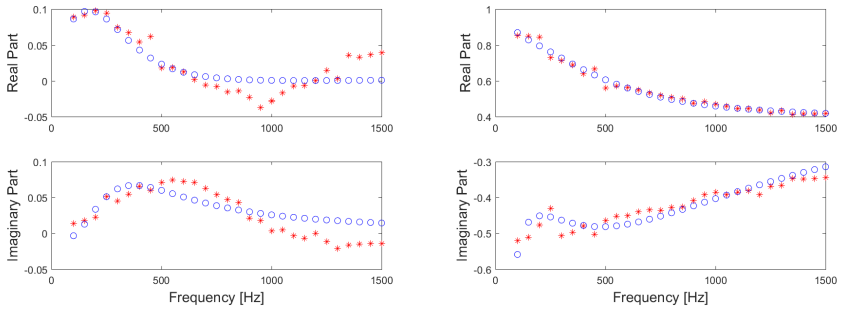

Figure C.78: Left: Volunteer 2; Right: Volunteer 3. Blue denotes the identified model and Red denotes the measured impedance.

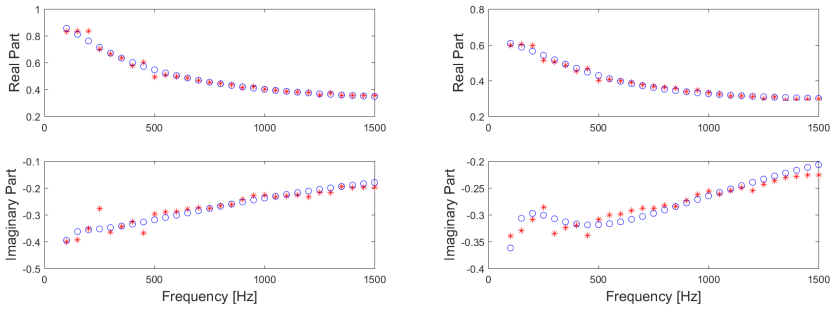

Figure C.79: Left: Volunteer 4; Right: Volunteer 5. Blue denotes the identified model and Red denotes the measured impedance.

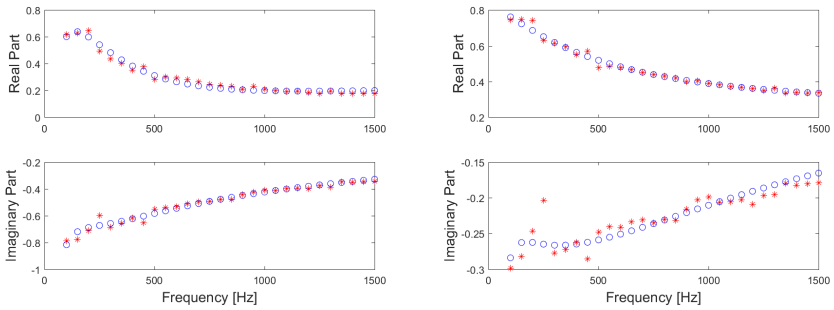

Figure C.80: Left: Volunteer 6; Right: Volunteer 7. Blue denotes the identified model and Red denotes the measured impedance.

D

List of additional publications

Publications in international journals (A1)

1. A. Maxim, **D. Copot**, C. Ionescu, Model predictive control with minimal process information for interacting sub-system, Journal of Process Control, in revision.

2. N. Nicolai, F. De Leersnyder, **D. Copot**, M. Stock, C. Ionescu, I. Nopens, T. De Beer, Development of a PAT-based advanced process control solution for continuous twin-screw wet granulation, AIChE Journal, in print.

Publications in international conferences (P1)

1. A. Chevalier, C. Copot, **D. Copot**, C.M. Ionescu, R. De Keyser. Fractional-order feedback control of a poorly damped system. 19th IEEE International Conference on Automation, QualityandTesting, Robotics, Cluj-Napoca, Romania, 22-24 May, 2014.

2. **D. Copot**, C. Ionescu, A. Hernandez, J. Thybaut, R. De Keyser, Development of a control strategy for efficient operation of a CSTR reactor. International Conference on System Theory Control and Computing, Sinaia, Romania, 14-17 October, 17-722, 2015.

3. Ionescu, C. Muresan, **D. Copot**, R. De Keyser, Constrained multivariable predictive control of a train of cryogenic 13C separation columns, 11th IFAC Symposium on Dynamics and Control of Process Systems, Trondheim, Norway, 6-8 June, 1103-1108, 2016.

4. **D. Copot**, A. Maxim, R. De Keyser, C. Ionescu, Multivariable control of sextuple tank system with non-minimum phase dynamics, International Conference on Automation, Quality and Testing, Robotics (AQTR), Cluj-Napoca, Romania, 19-21 May, 399-404, 2016.

5. **D. Copot**, C. Ionescu, I. Nascu, R. De Keyser, Online weight estimation in a robotic gripper arm, International Conference on Automation, Quality and Testing, Robotics (AQTR), Cluj-Napoca, Romania, 19-21 May, 151-156, 2016.

6. Clara Ionescu, Dana Copot, Anca Maxim, Eva Dulf, Robin De Keyser, Robust Autotuning MPC for chemical process applications, International Conference on Automation, Quality and Testing, Robotics (AQTR), Cluj-Napoca, Romania, 19-21 May, 369-374, 2016.

7. I. Birs, S. Folea, **D. Copot**, O. Prodan, C. Muresan, Comparative analysis and experimental results of advanced control strategies for vibration suppression in aircraft wings, European Workshop on Advanced Control and Diagnosis, Lille, France, 17-18 July, 2017.

8. A. Maxim, **D. Copot**, C.M. Ionescu, R. De Keyser, A methodology for control structure adaptation in presence of varying, unknown sub-system interaction degree, IEEE International Conference on Emerging Technologies and Factory Automation-ETFA, Limassol, Cyprus, 2-5 September, 2017.

9. C.M. Ionescu, N. Van Oevelen, D. Copot, B. Paijmans, R. De Keyser, Control of LPV Mechatronic Systems in Presence of Dynamic Uncertainties, IEEE International Conference on Intelligent Engineering Systems, Larnaca, Cyprus, 20-23 October, 125-130, 2017.

Publications in international conferences (C1)

1. **D. Copot**, C. Ionescu, T. Vannecke, E. Volcke, R. De Keyser, An approach towards multivariable control of anaerobic digestion using the EPSAC predictive control strategy, 11th IWA Conference on Control and Automation, 142-149, 2013.

2. A. Chevalier, **D. Copot**, C. Ionescu, R. De Keyser. A Theoretical Study on Modeling the Nonlinear Dynamics of a Knee Emulator, International Conference on Mathematical methods in engineering, July 22-26, Porto, Portugal, 142-149, 2013.

3. A. Chevalier, C. Copot, **D. Copot**, C. Ionescu, R. De Keyser, Fractional PID control of a poorly damped system based on a 3-parameter design method. International Conference on Systems and Signals, 1-3 October, Cluj-Napoca, Romania, 2015.

4. C. Ionescu, C. Copot, A. Chevalier, **D. Copot**, R. De Keyser, Adaptive sliding mode control with non-integer order reference function. International Conference on Systems and Signals, 1-3 October, Cluj-Napoca, Romania, 2015.

References

[1] K.B. Oldham and J. Spanier. *The Fractional Calculus*. IEEE Transactions on Parallel and Distributed Systems, 14:369–382, 2003.

[2] K.S. Miller and B. Ross. *An Introduction to the Fractional Calculus and Fractional Deferential Equations*. John Wiley and Sons Inc., New York, 1993.

[3] R. Gorenflo and S. Vessella. *Abel Integral Equations: Analysis and Applications, Lecture Notes in Mathematics*. Springer, Berlin Heidelberg, 1991.

[4] M. Lazarevic. *Advanced Topics on Application of Fractional Calculus on Control Problem, System Stability and Modeling*. WSEAS Press, 2012.

[5] M. Caputo. *Linear models of dissipation whose Q is almost frequency independent*. Journal of Royal Australian Society, 13:529–539, 1967.

[6] B. West. *Fractal physiology and the fractional calculus: a perspective*. 2010.

[7] Podlubny I. *Geometric and physical interpretation of fractional integration and fractional differentiation*. Fractional Calculus and Applied Analysis, 5(4):367–386, 2002.

[8] S. Samko, A. Kilbas, and O. Marichev. *Fractional Integrals and Derivatives - Theory and Applications*. Gordon and Breach Science Publishers, Amsterdam, 1993.

[9] R. Hilfer. *Applications of Fractional Calculus in Physics*. World Scientific Publishing Co., 2000.

[10] R. Magin, M. Ortigueira, I. Podlubny, and J. Trujillo. *On the fractional signals and systems*. Signal Processing, 91:350–371, 2011.

[11] A. Dokoumetzidis, R. Magin, and P. Macheras. *Fractional kinetics in multicompartmental systems*. Journal of Pharmacokinetics and Pharmacodynamics, 37:507–524, 2010.

[12] A. Dokoumetzidis and P. Macheras. *Fractional kinetics in drug absorption and disposition processes*. Journal of Pharmacokinetics and Pharmacodynamics, 36:165–178, 2009.

[13] M. Wise. *Negative Power Functions of Time in Pharmacokinetics and Their Implications*. Journal of Pharmacokinetics and Biopharmaceutics, 13(3):309–346, 1985.

[14] C. Ionescu. *The human respiratory system: an analysis of the interplay between anatomy, structure, breathing and fractal dynamics*. Springer, Series in BioEngineering, 2013.

[15] J. Popovic, M. Atanackovic, A. Pilipovic, M. Rapaic, and S. Pilipovic. *A new approach to the compartmental analysis in pharmacokinetics: fractional time evolution of diclofenac*. Journal of Pharmacokinetics and Pharmacodynamics, 37(4):119–138, 2010.

[16] J. Gabano and T. Poinot. *Fractional modelling and identification of thermal systems*. Signal Processing, 91:531–541, 2011.

[17] J. Gabano and T. Poinot. *Estimation of thermal parameters using fractional modelling*. Signal Processing, 91:938–948, 2011.

[18] J. Siepman and F. Siepmann. *Mathematical modeling of drug delivery,*. International Journal of Pharmaceutics, 364:328–343, 2008.

[19] J. Siepmann and A. Goepferich. *Mathematical modeling of bioerodible, polymeric drug delivery systems*. Advanced Drug Delivery Review, 48:229–247, 2001.

[20] R. Baker. *Controlled Release of Biologically Active Agents*. John Wiley & Sons, New York, 1987.

[21] M. Weiss. *The anomalous pharmacokinetics of amiodarone explained by nonexponential tissue trapping*. Journal of Pharmacokinetics and Biopharmaceutics, 27(4):383–396, 1999.

[22] X.J. Zhou, Q. Gao, O. Abdullah, and R.L. Magin. *Studies of anomalous diffusion in the human brain using fractional order calculus*. Magnetic Resonance in Medicine, 63(3):562–569, 2010.

[23] A. Benchellal, T. Poinot, and J. Trigeassou. *Approximation and identification of diffusive interfaces by fractional models*. Signal processing, 86:2712–2727, 2006.

[24] T. Poinot and J. Trigeassou. *Modelling and simulation of fractional systems*. In Workshop on fractional differetiation and its applications, pages 656–663, 2004.

[25] H. Wang, A. Degiovanni, and C. Moyne. *Periodic thermal contact: a quadrupole model and an experiment*. International Journal of Thermal Sciences, 41:125–135, 2002.

[26] G. Andrews, R. Askey, and R. Roy. *Encyclopedia of mathematics and its applications*. Cambridge University Press, 2001.

[27] D. Maillet, S. Andre, J. Batsale, A. Degiovanni, and C. Mayone. *Thermal quadrupoles: Solving the heat equation through integral transforms*. Wiley, 2000.

[28] A. Oustaloup. *Diversity and non-integer differentiation for system dynamics*. Wiley and Sons, 2014.

[29] A. Guyton and J. Hall. *Textbook of medical Physiology*. Elsevier, 2006.

[30] J. Hogg. *Pathophysiology of airflow limitation in chronic obstructive pulmonary disease*. Lancet, 364:709–721, 2004.

[31] P. Barnes. *Chronic Obstructive pulmonary disease*. New England Journal of Medicine: Medical Progress, 343:269–280, 2000.

[32] H. Parameswaran, A. Majumdar, S. Ito, A. Alencar, and B. Suki. *Quantitative characterization of airspace enlargement in emphysema*. Journal of Applied Physiology, 100:186–193, 2006.

[33] R. Lopes and N. Betrouni. *Fractal and multifractal analysis: A review*. Medical Image Analysis, 13:634–639, 2009.

[34] L. Sorensen and M. de Bruijne. *Dissimilarity representation in lung parenchyma classification*. In proceedings of the Spie digital library Conference, Medical Imaging, Computer-Aided Diagnosis, 2009.

[35] L. Sorensen, S. Shaker, and M. de Bruijne. *Quantitative analysis of pulmonary emphysema using local binary patterns*. IEEE Transactions on Medical Imaging, 29:559–569, 2010.

[36] S. Boser, H. Park, S. Perry, M. Menache, and F. Green. *Fractal geometry of airway remodeling in human asthma*. American Journal of respiratory and Critical Care Medicine, 172:817–823, 2005.

[37] G. Tourassi, E. Frederick, C. Floyd, and R. Coleman. *Multifractal texture analysis of perfusion lung scans as a potential diagnostic tool for acute pulmonary embolism*. Computers in Biology and Medicine, 31:15–25, 2001.

[38] E. Oostveen, D. Macleod, H. Lorino H, R. Farr, Z. Hantos Z, K. Desager, and F. Marchal. *The forced oscillation technique in clinical practice: Methodology, recommendations and future developments*. European Respiratory Journal, 22:1026–1041, 2003.

[39] C. Ionescu, P. Segers, and R. De Keyser. *Mechanical Properties of the Respiratory System Derived From Morphologic Insight*. IEEE Transaction on Biomedical Engineering, 56:949–959, 2009.

[40] E. Weibel. *Morphometry of the human lung*. Springer-Verlag, New York, 1963.

[41] E. Weibel. *Fractal geometry: a design principle for living organism*. American Journal of Physiology, 261:L361–L369, 1991.

[42] B. Mandelbrot. *The Fractal Geometry of Nature*. Freeman, New York, 1983.

[43] A. Oustaloup. *La derivation non entiere*. Hermes, Paris, 1995.

[44] Z. Hantos, B. Daroczy, B. Suki, G. Galgoczy, and T. Csendes. *Forced oscillatory impedance of the respiratory system at low frequencies*. Journal of Applied Physiology, 60:123–132, 1986.

[45] Z. Hantos and B. Suki. *Viscoelastic properties of the visceral pleura and its contribution to lung impedance*. Respiratory Physiology, 90:271–287, 1992.

[46] B. Suki B, A. Barabasi, Z. Hantos, F. Petak, and H. Stanley. *Avalanches and power law behaviour in lung inflation*. Nature, 368:615–618, 1994.

[47] C. Ionescu, D. Copot, and R. De Keyser. *A fractional order impedance model to capture the structural changes in lungs*. In 19th World Congress The International Federation of Automatic Control Cape Town, South Africa, pages 5362–5368, 2014.

[48] G. Irvin, J. Pak, and R. Martin. *Airway-parenchyma uncoupling in nocturnal asthma*. American Journal Respiratory and Critical Care Medicine, 161:50–56, 2000.

[49] F. Petak, G. Hall, and P. Sly. *Repeated measurements of airway and parenchymal mechanism in rats by using low frequency oscillation*. Journal of Applied Physiology, 84:1616–1625, 1998.

[50] C. Ionescu, J. Schoukens, and R. De Keyser. *Detecting and analyzing nonlinear effects in respiratory impedance measurements*. In American Control Conference, San Francisco, USA, pages 5412–5417, 2011.

[51] V. Mitic, V. Pavlovic, L. Kocic, V. Paunovic, and D. Mancic. *Applications of the intergranular impedance model in correlating microstructure and electrical properties of Doped $BaTiO_3$*. Science of Sintering, 41:247–256, 2009.

[52] J. Liou, C. Tsai, and J. Lin. *A microcontact model developed for sphere and cylinder based fractal bodies in contact with a rigid flat surface*. Wear, 268:431–442, 2010.

[53] R. Karimi, G. Tornling, H. Forsslund H, M. Mikko, A. Wheelock, and S. Nyren. *Lung density on high resolution computer tomography (HRCT) reflects degree of inflammation in smokers*. Respiratory Research, 15, 2014.

[54] E. Ponder. *The coefficient of thermal conductivity of blood and various tissues*. The Journal of General Physiology, 45:454–451, 1962.

[55] R. Magleby, A. Schallop, E. Schulman, and J. Sterling. *The effect of vascularization and tissue type on cryosurgical procedure*. Computer Aided Engineering: Applications to Biomedical Processes, 453:410–413, 2008.

[56] V.B. Mountcastle. *Medical Physiology*. C. V. Mosby Company, St. Louis, Missouri, 1980.

[57] R.A. Sternbach. *Pain: a Psychophysiological Analysis*. Academic Press Inc. (London) Ltd., New York, 1968.

[58] H. Marskey and N. Bogduk. *Classification of Chronic Pain: Descriptions of Chronic Pain Syndromes and Definitions of Pain Terms*. IASP Press, Seattle, Washington, 1994.

[59] T. Sokka. *Assessment of Pain in Rheumatic Diseases*. Clin Exp Rheumatol, 23:S77–S84, 2005.

[60] C.S. Rodriguez. *Pain Measurement in Elderly: A Review*. Pain Management Nursing, 2(2):38–46, 2001.

[61] P. Wall and R. Melzack. *The Challenge of Pain*. Penguin, London, United Kingdom, 1996.

[62] N. Desbiens, A. Wu, S. Broste, N. Wenger, A. Connors, J. Lynn, Y. Yasui, R.S. Phillips, and W. Fulkerson. *Pain and Satisfaction with Pain Control in seriously ill hospitalized Adults: findings from the SUPPORT research*

investigations. For the SUPPORT investigators. Study to understand Prognoses and Preferences for Outcomes and Risks of Treatment. Critical Care Medicine, 24(12):1953–1961, 1996.

[63] I.A Harris, J.M. Young, H. Rae, B.B. Jalaludin, and M.J. Solomon. *Factors associated with Back Pain after Physical Injury*. Spine, 32(14):1561–1565, 2007.

[64] M. Bates, W. Edwards, and K. Anderson. *Ethnocultural Influences on Variation in Chronic Pain Perception*. Pain, 52(1):101–112, 1993.

[65] I. Lund, T. Lundeberg, J. Kowalski, and E. Svensson. *Gender Differences in Electrical Pain Threshold Responses to Transcutaneous Electrical Nerve Stimulation (TENS)*. Neuroscience Letters, 375(2):75–80, 2005.

[66] K. Herr, K. Spratt, P. Mobily, and G. Richardson. *Pain Intensity assessment in older Adults: use of experimental Pain to compare Psychometric Properties and Usability of selected Pain Scales with younger Adults*. The Clinical Journal of Pain, 20(4):207–219, 2004.

[67] E. Flaherty. *Using Pain-Rating Scales with Older Adults*. American Journal of Nursing, 108(6):40–47, 2008.

[68] R. Hamill-Ruth and M. Marohn. *Evaluation of Pain in the Critically Ill Patient*. Critical Care Clinics, 15(1):35–54, 1999.

[69] K. Puntillo, D. Stannard, C. Miaskowski, K. Kehrle, and S. Gleeson. *Use of a Pain Assessment and Intervention Notation (P.A.I.N.) tool in critical Care Nursing Practice: Nurses' Evaluations*. Heart and Lung: the journal of Critical Care, 31(4):303–314, 2002.

[70] K. Puntillo, C. Miaskowski, K. Kehrle, D. Stannard, S. Gleeson, and P. Nye. *Relationship between Behavioral and Physiological Indicators of Pain, Critical Care Patients' Self-reports of Pain, and Opoid Administration*. Critical Care Medicine, 25(7):1159–1166, 1997.

[71] P. McArdle. *Intravenous Analgesia*. Critical Care Clinics, 15(1):89–104, 1999.

[72] J. Jacobi, G. Fraser, D. Coursin, R. Riker, D. Fountaine, E.T. Wittbrodt, D.B. Chalfin, M.F. Masica, H.S. Bjerke, W.M. Coplin, D.W. Crippen, B.D. Fuchs, R.M. Kelleher, P.E. Marik, S.A. Nasraway, M.J. Murray, W.T. Peruzzi, and P.D. Lumb. *Clinical Practice Guidlines for the Sustained use of Sedatives and Analgesics in the Critically Ill Adult*. Critical Care Medicine, 30(1):119–141, 2002.

[73] K. Herr, P. Coyne, T. Key, R. Manworren, M. McCaffery, S. Merkel, J. Pelosi, and L. Wild. *Pain Assessment in the Non-verbal Patient: Position Statement with Clinical Practice Recommendations*. Pain Management Nursing, 7(2):44–52, 2006.

[74] T. Hadjistavropoulos, D. Chapelle, H. Hadjistavropoulos, S. Green, and G. Asmundson. *Using Facial Expressions to assess Musculoskeletal Pain in older Persons*. European Journal of Pain, 6(3):179–187, 2002.

[75] United States. Agency for Health Care Policy, Research, and United States. Acute Pain Management Guideline Panel. *Acute Pain Management: Operative or Medical Procedures and Trauma*. U.S. Department of Health and Human Services, Public Health Service, Agency for Health Care Policy and Research, Acute Pain Management Guideline Panel, Washington DC, 1992.

[76] W.E. Fordyce, D.C. Turk, and R. Melzack. *Pain Measurement and Assessment*. Raven Press, New York, New York, 1983.

[77] S. Merkel. *Pain assessment in infants and young children: the finger span scale*. The American Journal of Nursing, 102:55–56, 2002.

[78] C. Pasero and M. McCaffery. *Pain in the critically ill*. The American Journal of Nursing, 102:59–60, 2002.

[79] C. Sessler, M. Grap, and G.Brophy. *Multidisciplinary management of sedation and analgesia in critical care*. Seminars in Respiratory and Critical Care Medicine, 22:211–225, 2001.

[80] J. Kress and J. Hall. *Sedation in the mechanically ventilated patient*. Critical Care Medicine, 22:2541–2546, 2006.

[81] M. Ocaña, C. Cendan, E. Cobos, J. Entrena, and J. Baeyens. *Potassium Channels and Pain: present Realities and future Opportunities*. European Journal of Pharmacology, 500(1–3):203–219, 2004.

[82] M.P. Jensen and C.A. McFarland. *Increasing the Reliability and Validity of Pain Intensity Measurement in Chronic Pain Patients*. Pain, 55(2):195–203, 1993.

[83] C. Hürny, J. Bernhard, A. Coates, H. Peterson, M. Castiglione-Gertsch, R.D. Gelber, C.M. Rudenstam, J. Collins, J. Lindtner, A. Goldhirsch, and H.J. Senn. *Responsiveness of a single-item Indicator versus a multi-item Scale: Assessment of emotional Well-being in an International Adjuvant Breast Cancer Trial*. Medical Care, 34(3):234–248, 1996.

[84] E. Breivik, G. Björnsson, and E. Skovlund. *A Comparison of Pain Rating Scales by Sampling from Clinical Trial Data*. The Clinical Journal of Pain, 16(1):22–28, 2000.

[85] I. McDowell. *Measuring Health: A Guide to Rating Scales and Questionnaires*. Oxford University Press, New York, New York, 2006.

[86] J.T. Farrar, R.K. Portenoy, J.A. Berlin, J.L. Kinman, and B.L. Strom. *Defining the clinically important Differences in Pain Outcome Measures*. Pain, 88(3):287–294, 2000.

[87] J.T. Farrar, J.P. Young, L. LaMoreaux, J.L. Werth, and R.M. Poole. *Clinical importance of Changes in Chronic Pain Intensity measured on an 11-point Numerical Pain Rating Scale*. Pain, 94(2):149–158, 2001.

[88] M.P. Jensen, P. Karoly, D.C. Turk, and R. Melzac. *Handbook of Pain Assessment*. Guilford Press, New York, 1992.

[89] J. Labus, F. Keefe, and M. Jensen. *Self-reports of pain intensity and direct observations of pain behavior: When are they correlated?* Journal of Pain, 102:109–124, 2003.

[90] J. Payen, O. Bru, J. Bosson, A. Lagrasta, I. Deschaux E. Novel, P. Lavagne, and C. Jacquot. *Assessing pain in critically ill sedated patients by using a behavioral pain scale*. Critical Care Medicine, 29:2258–2263, 2001.

[91] Y. Aissaoui, A. Zeggwagh, A. Zekraoui, K. Abidi, and R. Abouqal. *Validation of a behavioral pain scale in critically ill, sedated, and mechanically ventilated patients*. Anesthesia and Analgesia, 101:1470–1476, 2005.

[92] J. Young, J. Siffleet, S. Nikoletti, and T. Shaw. *Use of a behavioral pain scale to assess pain in ventilated, unconscious and/or sedated patients*. Intensive Critical Care Nursing, 22:32–39, 2006.

[93] C. Gelinas, L. Fillion, K. Puntillo, C. Viens, and M. Fortier. *Validation of the Critical-Care Pain Observation Tool in adult patients*. American Journal of Critical Care, 15:420–427, 2006.

[94] K. Puntillo, A. Morris, C. Thompson, J. Stanik-Hutt, C. White, and L. Wild. *Pain behaviors observed during six common procedures: Result form Thunder Project II.* Critical Care Medicine, 32:421–427, 2004.

[95] I. Roeggen, H. Storm, and D. Harrison. *Skin Conductance Variability between and within Hospitalised Infants at Rest*. Early Human Development, 87(1):37–42, 2011.

[96] K.E. Hagbarth, R.G. Hallin, A. Hongell, H.E. Torebjörk, and B.G. Wallin. *General Characteristics of Sympathetic Activity in Human Skin Nerves*. Acta Physiologica Scandinavica, 84(2):164–176, 1972.

[97] G.F. Goddard. *A pilot study of the Changes of Skin Electrical Conductance in Patients undergoing General Anaesthesia and Surgery*. Anaesthesia, 37(4):408–415, 1982.

[98] H. Storm. *Skin Conductance and the Stress Response from Heel Stick in Preterm Infants*. Archives of Disease in Chidlhood - Fetal and Neonatal Edition, 83(2):F143–F147, 2000.

[99] D. Harrison, S. Boyce, P. Loughnan, P. Dargaville, H. Storm, and L. Johnston. *Skin Conductance as a measure of Pain and Stress in Hospitalised Infants*. Early Human Development, 82(9):603–608, 2006.

[100] H. Storm. *The Capability of Skin Conductance to Monitor Pain Compared to Other Physiological Pain Assessment Tools in Children and Neonates*. Pediatrics and Therapeutics, 3(4):168–173, 2013.

[101] F. Savino, L. Vagliano, S. Ceratto, F. Viviani, R. Miniero, and F. Ricceri. *Pain Assessment in Children undergoing Venipuncture: the Wong-Baker Faces Scale versus Skin Conductance Fluctuations*. Early Human Development, 82(9):603–608, 2013.

[102] M.D. Larson, D.I. Sessler, D.E. Washington, B.R. Merrifield, J.A. Hynson, and J. McGuire. *Pupillary Response to Noxious Stimulation during Isoflurane and Propofol Anesthesia*. Anaesthesia and Analgesia, 76(5):1072–1078, 1993.

[103] I. Constant, M.C. Nghe, L. Boudet, J. Berniere, S. Schrayer, R. Seeman, and I. Murat. *Reflex Pupillary Dilatation in Response to Skin Incision and Alfentanil in Children Anaesthetized with Servoflurane: a more sensitive measure of Noxious Stimulation than the commonly used Variables*. British Journal of Anaesthesia, 96(5):614–619, 2006.

[104] M.D. Larson, P.D. Berry, J. May, A. Björksten, and D. Sessler. *Autonomic effects of Epidural and Intravenous Fentanyl*. British Journal of Anaesthesia, 98(2):263–269, 2007.

[105] S. Isnardon, M. Vinclair, C. Genty, A. Hebrard, P. Albaladejo, and J.F. Payen. *Pupillometry to detect Pain Response during general Anaesthesia following Unilateral Popliteal Sciatic Nerve Block*. European Journal of Anaesthesiology, 30(7):429–434, 2013.

[106] D. Li, C. Miaskowski, D. Burkhardt, and K. Puntillo. *Evaluations of Physiologic Reactivity and Reflexive Behaviors during Noxious Procedures in Sedated Critically Ill Patients*. Journal of Critical Care, 24(3):472.e9–472.e13, 2009.

[107] M. Aissou, A. Snauwaert, C. Dupuis, A. Atchabahian, F. Aubrun, and M. Beaussier. *Objective Assessment of the Immediate Postoperative Analgesia using Pupillary Reflex Measurements*. Anesthesiology, 116(5):1006–1012, 2012.

[108] N. Ben-Israel, M. Kliger, G. Zuckerman, Y. Katz, and R. Edry. *Monitoring the Nociception Level: a Multi-Parameter Approach*. Journal of Clinical Monitoring and Computing, 27(6):659–668, 2013.

[109] C.H. Martini, M. Boon, S.J. Broens, E.F. Hekkelman, L.A. Oudhoff, A.W. Buddeke, and A. Dahan. *Ability of the Nociception Level, a Multi-Parameter Composite of Autonomic Signals, to Detect Noxious Stimuli during Propofol-Remifentanil Anesthesia*. Anesthesiology, 123(3):524–534, 2015.

[110] R. Edry, V. Recea, Y. Dikust, and D. Sessler. *Preliminary Interoperative Validation of the Nociception Level Index*. Anesthesiology, 125(1):193–203, 2016.

[111] K. Godfrey. *Compartmental models and their applications*. Academic Press, London, 1983.

[112] L. Kovacs, B. Benyo, J. Bokor, and Z. Benyo. *Induced L 2-norm minimization of glucoseinsulin system for Type I diabetic patients*. Computer Methods and Programs in Biomedicine, 102(2):105–118, 2011.

[113] D. Drexler, L. Kovacs, J. Sapi, I. Harmati, and Z. Benyo. *Model-based analysis and synthesis of tumor growth under angiogenic inhibition: a case study*. IFAC Proceedings, 44(1):3753–3759, 2011.

[114] B. Kiss, J. Sapi, and L. Kovacs. *Imaging method for model-based control of tumor diseases*. Proceedings of the IEEE 11th International Symposium on Intelligent Systems and Informatics (SISY), -:271–275, 2013.

[115] D. Copot and C. Ionescu. *Drug delivery system for general anesthesia: Where are we?* Proceedings of the IEEE International Conference on Systems, Man, and Cybernetics (SMC), pages 2452–2457, 2014.

[116] J. K. Popovic, D.T. Spasic, J.Tovic, J.L. Kolarovic, R. Malti, I. M. Mitic, S. Pilipovic, and T.M. Atanackovic. *Fractional model for pharmacokinetics*

of high dose methotrexate in children with acute lymphoblastic leukaemia. Communications in Nonlinear Science and Numerical Simulation, 22:451–471, 2015.

[117] A. Churilov, A. Medvedev, and A. Shepeljavyi. *Mathematical model of non-basal testosterone regulation in the male by pulse modulated feedback*. Automatica, 45:78–85, 2009.

[118] G.A. Losa, D. Merlini, T.F. Nonnenmacher, and E.R. Weibel. *Fractals in Biology and Medicine*. Birkhauser, Berlin, 2002.

[119] R.L. Magin. *Fractional calculus in bioengineering*. Begell House, Connecticut, 2006.

[120] J. Machado, V. Kiryakova, and F. Mainardi. *Recent history of fractional calculus*. Communications in Nonlinear Science and Numerical Simulation, 16(3):1140–1153, 2011.

[121] J. Machado, V. Kiryakova, and F. Mainardi. *Que vadis?* Fractional Calculus Analysis and Applications, page in press, 2017.

[122] C. Ionescu, D. Copot, and R. De Keyser. *Modelling for control of depth of hypnosis: a patient friendly approach*. Proceedings of the IEEE International Conference on Systems, Man, and Cybernetics, pages 2653–2658, 2016.

[123] F. Padula, C. Ionescu, N. Latronico, M. Paltenghi, A. Visioli, and G. Vivacqua. *Inversion-based propofol dosing for intravenous induction of hypnosis*. Communications in Nonlinear Science and Numerical Simulation, 39:481–494, 2016.

[124] C. Ionescu, J. T. Machado, R. De Keyser, J. Decruyenaere, and M. MRF Struys. *Nonlinear dynamics of the patients response to drug effect during general anesthesia*. Communications in nonlinear science and numerical simulation, 20(3):914–926, 2015.

[125] C. Ionescu, I. Nascu, and R. De Keyser. *Lessons learned from closed loops in engineering: towards a multivariable approach regulating depth of anaesthesia*. Journal of clinical monitoring and computing, 28(6):537–546, 2014.

[126] D. Copot, A. Chevalier, C. Ionescu, and R. De Keyser. *A two-compartment fractional derivative model for propofol diffusion in anesthesia*. Proceedings of the 2013 IEEE International Conference on Control Applications (CCA), pages 264–269, 2013.

[127] D. Copot, R. De Keyser, and C. Ionescu. *Drug Interaction Between Propofol and Remifentanil in Individualised Drug Delivery Systems*. Proceedings of the IFAC-PapersOnLine, 48(20):64–69, 2015.

[128] G. Wilkinson. *The dynamics of drug absorption, distribution, and elimination*. New York, 2002.

[129] C. F. Minto, T. Schnider, T. G. Short, K. M. Gregg, A. Gentilini, and S. L. Shafer. *Response surface model for anesthetic drug interactions*. Anesthesiology, 92:1603–1616, 2000.

[130] B. Marsh, M. White, N. Morton, and G. N. Kenny. *Pharmacokinetic model driven infusion of Propofol in children*. British Journal of Anaesthesia, 67:41–48, 1991.

[131] B. Kataria, S. Ved, and H. Nicodemus. *The pharmacokinetics of propofol in children using three different data analysis approaches*. Anesthesiology, 80:104–1022, 1994.

[132] T. Schnider, C. Minto, and P. Gambus. *The influence of method of administration and covariates on the pharmacokinetics of propofol in adult volunteers*. Anesthesiology, 88:1170–1182, 1998.

[133] T. Schnider, C. Minto, and S. Shafer. *The influence of age on propofol pharmacodynamics*. Anesthesiology, 90:1502–1516, 1999.

[134] J. Vuyk J, T. Schnider, and F. Engbers. *Population pharmacokinetics of propofol for target-controlled infusion (TCI) in the elderly*. Anesthesiology, 93:1557–1558, 2000.

[135] D. Sierociuk, T. Skovranek, M. Macias, I. Podlubny, I. Petras, A. Dzielinski, and P. Ziubinski. *Diffusion process modeling by using fractional-order models*. Applied Mathematics and Computation, 257:2–11, 2015.

[136] M. Gandhi, F. Aweeka, R. Greenblatt, and T. Blaschke. *Sex differences in pharmacokinetics and pharmacodynamics*. Annual Review of Pharmacology and Toxicology, 44:499–523, 2004.

[137] J. Bruhn, T. Bouillon, L. Radulesco, A. Hoeft, E. Bertaccini, and S. Shafer. *Correlation of approximate entropy, bispectral index, and spectral edge frequency 95 (SEF95) with clinical signs of "Anesthetic Depth" during coadministration of propofol and remifentanil*. Anesthesiology, 98:621–627, 2003.

[138] N.H. Holford and L.B. Sheiner. *Pharmacokinetic and pharmacodynamic modeling in vivo*. CRC Critical Reviews in Bioengineering, 5:273–322, 1981.

[139] L.M. Pereira. *Fractal Pharmacokinetics*. Computational and Mathematical Methods in Medicine, 11(2):161–184, 2010.

[140] M. Weiss. *Commentary to "Pharmacokinetics from a dynamical system point of view"*. Journal of Pharmacokinetics and Pharmacodynamics, pages 393–397, 1989.

[141] M. Weiss. *Comparison of distributed and compartmental models of drug disposition: assessment of tissue uptake kinetics*. J. Pharmacokinetics and Pharmacodynamics, 43:505–512, 2016.

[142] J. Matis and T. Wehrly. *A general approach to non-markovian compartmental models*. Journal of Pharmacokinetics and Biopharmaceutics, 26(4):437–456, 1998.

[143] M. Hennion and E. Hanert. *How to avoid unbounded drug accumulation with fractional pharmacokinetics*. Journal of Pharmacokinetics and Pharmacodynamics, 40:691–700, 2013.

[144] S. Fedotov. *Subdiffusion, chemotaxis, and anomalous aggregation*. Physical Review E, 83:1–6, 2011.

[145] S. Fedotov and S. Falconer. *Subdiffusive master equation with space-dependent anomalous exponent and structural instability*. Physical Review E, 85:1–6, 2012.

[146] S. Fedotov, A. Tan, and A. Zubarev. *Persistent random walk of cells involving anomalous effects and random death*. Physical Review E, 91:1–6, 2015.

[147] C. Tsantoulas and McMahon X. *Opening paths to novel analgesics:the role of potassium channels in chronic pain*. Trends in Neurosciences, 37(3):146–158, 2014.

[148] M. Liu and J.N. Wood. *The roles of sodium channels in nociception: implications for mechanisms of neuropathic pain*. Pain Med., 12(3):S93–S99, 2011.

[149] E. Sykova. *Extracellular potassium accumulation in the central nervous system*. Progress in Biophysics and Molecular Biology, 42:135–189, 1983.

[150] S. McMahon, M. Koltzenburg, I. Tracey, and D Turk. *Wall and Melzack's Textbook of Pain*. Elsevier Saunders, 2013.

[151] C.M. Ionescu. *The phase constancy in neural dynamics*. IEEE Trans Syst Man Cyb, part A Systems and Humans, 42(6):1543–1551, 2012.

[152] Y. Feldman anf A. Puzenko and Y. Ryabov. *Non-Debye dielectric relaxation in complex materials*. Chemical Physics, 284:139–168, 2002.

[153] C. Bottcher, C. Van Belle, P. Bordewijk, A. Rip, and D. Yue. *Theory of electric polarization*. Journal of the Electrochemical Society, 121:211C, 1974.

[154] A. Elwakil and B. Maundy. *Extracting the Cole-Cole impedance model parameters without direct impedance measurement*. Electronics Letters, 46:1367–1368, 2010.

[155] S. Emmert, M. Wolf, R. Gulich, S. Krohns, S. Kastner, P. Lunkenheimer, and A. Loidl. *Electrode polarization effects in broadband dielectric spectroscopy*. The European Physical Journal B, 83:157–165, 2011.

[156] K. Diethelm. *The analysis of fractional differential equations*. Springer, 2010.

[157] F. Mainardi. *Fractional calculus and waves in linear viscoelasticity: an introduction to mathematical models*. Imperial College Press, 2010.

[158] R. Nigmatulin. *Fractional kinetic equation and universal decoupling of a memory function in mesoscale region*. Physica A: Statistical Mechanics and its Applications, 363:299–313, 2006.

[159] K. Cole. *Permeability and impermeability of cell membranes for ions*. Cold Spring Harbor Symposium Quantum Biology, 8:110–122, 1940.

[160] R. Fish and L. Geddes. *Conduction of electrical current to and through the human body: a review*. OA J of Plastic Surgery, 9:407–421, 2009.

[161] R.Pintelon and J.Schoukens. *System Identification: a frequency domain approach*. 2001.

[162] M. Neckebroek, T. De Smet, and M. Struys. *Automated drug delivery in anesthesia*. Curr Anesthesiol Rep, 3:18–26, 2013.

[163] C. Ionescu, R. De Keyser, B. Claure-Torrico, T. De Smet, M.M.R.F. Struys, and J.E. Normey-Rico. *Robust predictive control strategy applied for Propofol using BIS as a controlled variable during Anesthesias*. IEEE Transactions on Biomedical Engineering, 55(9):2161–2170, 2008.

[164] C. Ionescu, J.A.T. Machado, R. De Keyser, J. Decruyenaere, and M.M.R.F. Struys. *Nonlinear dynamics of the patient's response to drug effect during general anesthesia*. Communications in Nonlinear Science and Numerical Simulation, 20(3):914–926, 2015.

[165] I. Caroll, R. Gaeta, and S. Mackey. *Multivariate Analysis of Chronic Pain Patients Undergoing Lidocaine Infusions: Increasing Pain Severity and Advancing Age Predict Likelihood of Clinically Meaningful Analgesia*. Clinical Journal of Pain, 28(3):702–706, 2007.

[166] J.S. Shieh, M. Fu, S.J. Huang, and M.C. Kao. *Comparison of the applicability of rule-based and self-organizing fuzzy logic controllers for sedation control of intracranial pressure pattern in a neurosurgical intensive care unit*. IEEE Transactions on Biomedical Engineering, 53(8):1700–1705, 2006.

[167] J.S. Shieh, D.A. Linkens, and A.J. Ashbury. *A hierarchical system of on-line advisory for monitoring and controlling the depth of anaesthesia using self-organizing fuzzy logic*. Engineering Applications of Artificial Intelligence, 18:307–316, 2005.

[168] R. Allen and D. Smith. *Neuro-fuzzy closed-loop control of depth of anaesthesia*. Artificial Intelligence in Medicine, 21:185–191, 2001.

[169] W.M. Haddad, J.M. bailey, T. Hayakawa, and N. Hovakimyan. *Neural Network Adaptive Output Feedback Control for Intensive Care Unit Sedation and Intraoperative Anesthesia*. IEEE Trans Neural Networks, 18(4):1049 – 1066, 2007.

[170] J. Schuttler and H. Schwilden. *Modern Anesthetics*. Springer: Berlin Heidelberg, 2008.

[171] U.G.H. Fors, M.L. Ahlquist, R. Skagerwall, G.A. L. Edwall, and G.A.T. Haegerstam. *Relation between intradentall nerve activity and estimated pain in man - a mathematical model*. Pain, 18:397–408, 1984.

[172] U.G.H. Fors, M.L. Ahlquist, G.A. L. Edwall, and G.A.T. Haegerstam. *Evaluation of a mathematical model analysing the relation between intradental nerve impulse activity and perceived pain in man*. International Journal of Bio-Medical Computing, 19:261–277, 1986.

[173] U.G.H. Fors, G.A. L. Edwall, and G.A.T. Haegerstam. *The ability of a mathematical model to evaluate the effects of two pain modulating procedures on pulpal pain in man*. Pain, 33:253–264, 1988.

[174] Y.J. Zhu and T.J. Lu. *A multi-scale view of skin thermal pain: from nociception to pain sensation*. Philosophical Transactions of the Royal Society of London A, 368:521–559, 2010.

[175] C.D. Morch, K.S. Frahm, R.C. Coghill, L. Arendt-Nielsen, and O.K. Andersen. *Distinct temporal filtering mechanisms are engaged during dynamic increases and decreases of noxious stimulus intensity*. Pain, 156:1906–1912, 2015.

[176] R. Melzack. *From the gate to the neuromatrix*. Pain, 82:S121–S126, 1999.

[177] C. Nicholson, P. Kamali-Zare, and L. Tao. *Brain extracellular space as a diffusion barrier*. Computing and Visualization in Science, 14(7):309–325, 2011.

[178] C. Nicholson. *Diffusion and related transport properties in brain tissue*. Reports on Progress in Physics, 64:815–884, 2001.

[179] M.M. Meerschaert, J. Mortensen, and S.W. Wheatcraft. *Fractional vector calculus for fractional advection-dispersion*. Physica A: Statistical Mechanics and its Applications, 367:181–190, 2006.

[180] S.W. Wheatcraft and M.M. Meerschaert. *Fractional conservation of mass*. Advances in Water Resources, 31(10):1377–1381, 2008.

[181] D. Prodanov and J. Delbeke. *A model of space-fractional-order diffusion in the gliar scar*. Journal of Theoretical Biology, 403:97–109, 2016.

[182] J. Gabano, T. Poinot, and H. Kanoun. *LPV Continuous fractional modelling applied to ultracapacitor impedance identification*. Control Engineering Practice, 45:89–97, 2015.

[183] R. De Keyser, C. Muresan, and C. Ionescu. *An efficient algorithm for low-order direct discrete-time implementation of fractional order transfer functions*. ISA Transactions, -:–, in review.

[184] D.N. Wheatley. *Diffusion theory, the cell and the synapse*. BioSystems, 45:151–163, 1998.

[185] S. Fedotov, H. Al-Shamsi, AL. Ivanov, and A. Zubarev. *Anomalous transport and nonlinear reactions in spiny dendrites*. Physical Review, E-82:041103, 2010.

[186] B. Rigaud, L. Hamzaoui, M. Frikha, N. Chauveau, and J. Morucci. *In vitro tissue characterization and modelling using electrical impedance measurements in the 100 Hz-10 MHz frequency range*. Physiological Measurement, 16, 1995.

[187] S. Kalitzin, B.W. van Dijk, and H. Spekreijse. *Self-organized dynamics in plastic neural networks: bistability and coherencee*. Biological Cybernetics, 83:139–150, 2000.

[188] C. Ionescu, J.A.T Machado, and R. De Keyser. *Modeling of the Lung Impedance Using a Fractional-Order Ladder Network With Constant Phase Elements*. IEEE Transaction on Biomedical Circuits and Systems, 5(1):83–89, 2011.

[189] C. Ionescu, I. Muntean, J. Machado, R. De Keyser, and M. Abrudean. *A theoretical study on modelling the respiratory tract with ladder networks by means of intrinsic fractal geometry*. IEEE Transactions on Biomedical Engineering, 57(2):246–253, 2010.

[190] J. Thorson and M. Biederman-Thorson. *Distributed relaxation processes in sensory adaptation*. Science, 183:161–172, 1974.

[191] R. Bogacz. *A tutorial on the free-energy framework for modelling perception and learning*. Journal of Mathematical Psychology, 76:198–211, 2017.

[192] Garra R. and Polito F. *Fractional calculus modelling for unsteady unidirectional flow of incompressible fluids with time-dependent viscosity*. Commun Nonlinear Sci Numer Simulat, 17:5073–507, 2012.

[193] Li Y, Chen Y-Q, and Podlubny I. *MittagLeffler stability of fractional order nonlinear dynamic systems*. Automatica, 45(8):1965–1969, 2009.

[194] Li Y, Chen Y-Q, and Podlubny I. *Stability of fractional-order nonlinear dynamic systems: Lyapunov direct method and generalized MittagLeffler stability*. Computers & Mathematics with Applications, 59(5):1810–1821, 2010.

[195] C.M. Ionescu. *A memory-based model for blood viscozity*. Communications on Nonlinear Science and Numerical Simulation, 45:29–34, 2017.

[196] J. Trujillo. *Fractional models: Sub and super-diffusives, and undifferentiable solutions*. Innovation in Engineering Computational Technology, -:371–401, 2006.

[197] Heymans N. and Podlubny I. *Physical interpretation of initial conditions for fractional differential equations with Riemann-Liouville fractional derivatives*. Rheologica Acta, 45(5):765–771, 2006.

[198] G. Tononi. *An information integration theory of consciousness*. BMC Neurosci, 5:42, 2004.

[199] F. Padula, C. Ionescu, N. Lantronico, M. Paltenghi, A. Visioli, and G. Vivacqua. *Optimized PID control of depth of hypnosis in anesthesia*. Computer Methods and Programs in Biomedicine, 144:21–35, 2017.

[200] T. Mendoca, J. Lemos, H. Magahales, P. Rocha, and S. Esteves. *Drug delivery for neuromuscular blockade with supervised multimodal adaptive control*. IEEE Transactions on Control System Technology, 17:1237–1244, 2009.

[201] D. Lykken. *Square-wave analysis of Skin Impedance*. Psychophysiology, 7(2):262–275, September 1970.

[202] Y. Yang, F. Zhang, K. Tao, L. Wang, H. Wen, and Z. Teng. *Multi-frequency simultaneous measurement of Bioimpedance Spectroscopy based on low crest factor Multisine excitation*. Physiological Measurement, 36(3):489–501, February 2015.

[203] A. Hodgkin and A. Huxley. *A quantitative description of membrane current and its application to conduction and excitation in nerve*. The Journal of Physiology, 117(4):500–544, 1952.